Controlled Drug Release From Oriented Biodegradable Polymers

Rohan AMBARDEKAR

Submitted for the Degree of

Doctor of Philosophy

Faculty of Life Sciences

University of Bradford

2015

Abstract

Rohan Ambardekar

Controlled drug release from oriented biodegradable polymers

Keywords: controlled release, directional release, solid-state orientation, biaxial orientation, die drawing, biodegradable, implantable

This research is the first systematic investigation of solid-state orientation as a novel method for controlling drug release from biodegradable polymers. The effect of various degrees of polymer orientation was studied in oriented Poly (L-lactic acid) (PLA) films containing curcumin and theophylline as model drugs. Additionally, direction specific drug release was studied from oriented PLA rods containing paracetamol.

The films oriented to 2X uniaxial constant width (UCW) or 2X2Y biaxial draw ratio showed retardation of drug release, when their nematic structure was stabilised by the presence of crystalline theophylline. Contrarily, the same films when contained solid solution of curcumin, shrunk in the release medium and exhibited a release profile similar to the un-oriented films. All films oriented to the UCW draw ratio ≥ 3X contained α crystalline form of PLA and showed acceleration of drug release proportionate to the draw ratio. According to the proposed mechanism augmented formation of water filled channels in these films was responsible for faster drug release.

Similarly, the paracetamol loaded PLA rods die-drawn to uniaxial draw ratios ≥ 3X exhibited enhancement of drug release. Importantly, the amount of drug released along the oriented chain axis was significantly larger than that in the perpendicular direction. Drug release from the die-drawn rods was accelerated by a greater degree than that observed from the oriented films. This can be correlated to the differences in their size, geometry and the crystalline form of PLA.

In conclusion, the current study provided substantial evidence that solid-state orientation can offer a control over drug release from PLA.

Acknowledgements

Millions of men have lived to fight, build palaces and boundaries, shape destinies and societies; but the compelling force of all times has been the force of originality and creation profoundly affecting the roots of human spirit. The same forces of originality compelled me to enter the area of scientific research; and this report arose in part out of diligent lab work as well as intellectual and practical inputs from various people. Therefore, writing this humble acknowledgement to them that I owe my deepest gratitude.

In the first place, I would like to record my profound gratitude and venerable regards to my esteemed research supervisors, Prof. AR Paradkar, Prof. PD Coates, Dr. AL Kelly and Dr. PD Caton-Rose for their cherished guidance, vital encouragement, incisive criticism and dynamic assistance. I am indeed indebted by them for inspiring me and enriching my growth.

It gives me immense pleasure to express my sincere gratitude towards Mr. John Wyborn, Mr. Glen Thompson, Prof. Yongfeng Men, Dr. Guruswami Kumaraswami, Dr. Richard Telford, Dr. Christina-LuminitaTuinea-Bobe, Dr. Ben Whiteside and Dr. Tim Gough for their valuable advice and practical help. I am grateful to Mr. Amit Sonawane, Mr. Hrushikesh Karandikar and rest of the fellow PhD students who immensely helped me in completion of this thesis.

I feel a deep sense of gratitude for my family who formed part of my vision and taught me the good things that really matter in life. They are the one who transformed my dream of becoming a pharmaceutical researcher in to reality. They are my strongest source of motivation and have buttressed my confidence. I would forever be indebted and hence dedicate this work to them.

Finally, I would like to thank everybody who was important to the successful realization of thesis, as well as expressing my apology that I could not mention personally one by one.

Table of contents

List of Figures

List of Tables

Glossary

PLA: Poly (lactic acid)

PLLA: Poly (L-Lactic acid)

CPLA: Curcumin loaded PLA

TPLA: Theophylline loaded PLA

PPLA: Paracetamol loaded PLA

PLDA: Poly (DL-lactic acid)

PLGA: Poly (lactic-glycolic acid)

PEO: Poly (ethylene oxide)

UCW: Uniaxial Constant Width stretching

SB: Simultaneous Biaxial stretching

SEQ: Sequential Biaxial stretching

RAD: Row Nuclei Associated Domains

DSC: Differential Scanning Calorimetry

MDSC: Modulated Differential Scanning Calorimetry

XRD: X-ray Diffraction

WAXD: Wide Angle X-ray Diffraction

TGA: Thermo- Gravimetric Analysis

FTIR: Fourier Transform Infra-Red

ATR: Attenuated Total Reflectance

GC/MS: Gas Chromatography/ Mass Spectroscopy

HPLC: High Performance Liquid Chromatography

GPC: Gel Permeation Chromatography

Mw: Weight average molecular weight (g/mol)

Mn: Number average molecular weight (g/mol)

PD: Polydispersity

MP: Melting point (^{o}C)

Tg: Glass transition temperature (^{o}C)

λ : Draw ratio

G' : Storage modulus (Pa)

G" : Loss modulus (Pa)

ω : Angular frequency (rad/sec)

η^* : Complex viscosity (Pa.s)

η_0 : Zero shear viscosity (Pa.s)

m/z : Mass to charge ratio

F_h: Herman's orientation function

γ_L^D: Dispersive surface tension (liquid) (mJ/m^2)

γ_L^P: Polar surface tension (liquid) (mJ/m^2)

γ_f^D: Dispersive surface energy (solid) (mJ/m^2)

γ_f^P : Polar surface energy (solid) (mJ/m^2)

δ_t : Hansen's total solubility parameter(J$^{1/2}$. M$^{-3/2}$)

R_t : Retention time in a chromatography

E: Young's modulus or modulus of elasticity (N/m^2)

1. Introduction

1.1. The hypothesis

The research reported in this thesis aims to test the hypothesis that structuring the morphological domains within a polymer matrix by solid-state polymer orientation will offer control over drug release from that matrix.

1.1.1. Introduction to the hypothesis

Spatial and temporal control over the release of a drug, in order to meet the specific delivery challenges associated with a particular disease is both attractive and challenging. Controlled drug delivery can be achieved through a simple dosage form such as tablets or complex nano-formulations, or even biomedical devices, e.g. drug loaded biomedical screws. Polymers play a critical role in such systems by facilitating (1) the selective release of a drug near the target organ, in order to increase bioavailability or to reduce toxicity, e.g. implants; (2) the release of a drug in response to a biological stimuli, e.g. release of Insulin only when the blood glucose levels are elevated; or importantly (3) a rate controlled release necessary to maintain constant drug levels in the blood plasma, e.g. in the treatment of chronic diseases such as arthritis. Despite the great potential, there are practical and commercial limitations on the number of new polymers synthesised, owing to the laboriousness of the process. Similar to drugs, an important barrier preventing large investment in search of new biomedical polymers is fear of regulatory noncompliance. Such situations can be addressed by exploring the technology to modify existing polymers such that the desired properties can be obtained without altering their chemical identity.

Thermal, physical, and mechanical properties of polymers essentially depend on their structural features (Brostow, 2007; Ward and Sweeney, 2012). Polymers are long chain molecules. Few with stereo-regularity can undergo regular chain folding in order to achieve a lower energy state. On the most

fundamental level the folded region is referred as lamellar crystals, which are connected by amorphous segments. The lamellar crystals are further organised into more complex superstructures of different length scales. Such organisation provides a platform for increased intramolecular interactions and hence bulk properties of a semicrystalline polymer vary according to percentage crystallinity and crystal morphology. Owing to the same reason, semicrystalline polymers offer a broader margin for altering the polymer properties by changing the morphological features. Therefore, this work is focused on orientation of semicrystalline polymers for controlled drug delivery applications.

Solid-state orientation (Coates and Ward, 1981; De Vries *et al.*, 1977) of semicrystalline polymers has a significant effect on polymer properties, by virtue of its ability to structure the morphological domains within a polymer matrix. The term 'orientation', in the case of semicrystalline polymers relates to alignment of amorphous and crystalline regions, resulting in development of strong anisotropic properties such as enhanced mechanical strength, gas/vapour barrier and reduced biodegradability. Such changes may also affect the drug release properties of the polymeric matrices. In this work, the effect of polymer orientation on drug release has been evaluated.

The literature survey suggested that there have been no reported systematic studies on solid-state orientation, which examine the effect of different degrees of orientation on drug release. Moreover, the role played by the nature of a drug in influencing polymer orientation and the consequent release profile has not been studied. Importantly, orientation of polymers results in development of anisotropic properties and hence the rate of drug release in the direction parallel to orientation is expected to be different from that in the perpendicular direction. Previous reports on drug releasing oriented materials have failed to characterise this phenomenon. This work attempts to address these gaps and construct a mechanistic understanding of drug release from oriented matrices.

The effect of the degree and the nature of polymer orientation (e.g. uniaxial, biaxial) on drug release was systematically studied here using a simple two dimensional geometry, i.e. films (figure 1.1). Poly (lactic acid) – (PLA) films loaded with a polymer soluble or a suspended drug were made by melt extrusion. They were oriented using a biaxial stretcher. These films also allowed investigation of the effect of the physical state of a drug on the release profile exhibited by the oriented matrices. The possibility of obtaining anisotropic drug release from oriented matrices was studied from a three dimensional cylindrical geometry. PLA rods containing a model drug were melt-extruded, followed by orientation using the die drawing method. Drug release from the lateral (curved) surface and the cross section (base) was studied separately (figure 1.2).

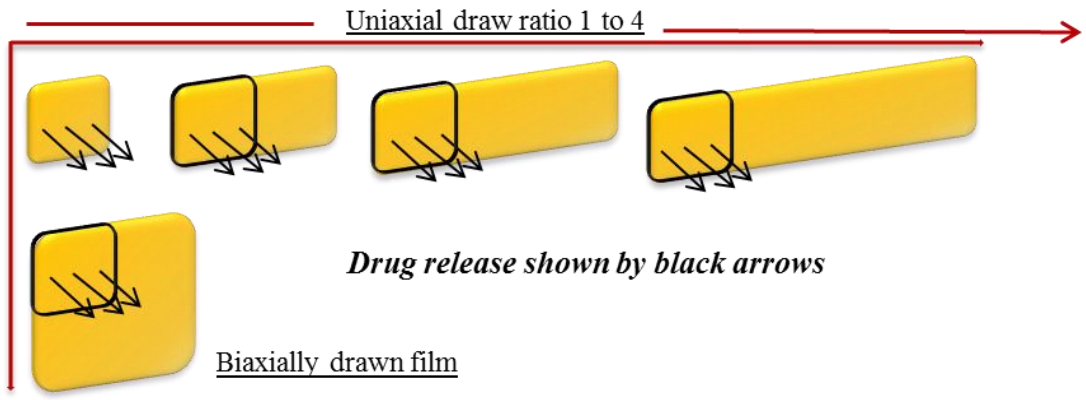

Figure 1.1: *Schematic representation of drug release from the oriented films*

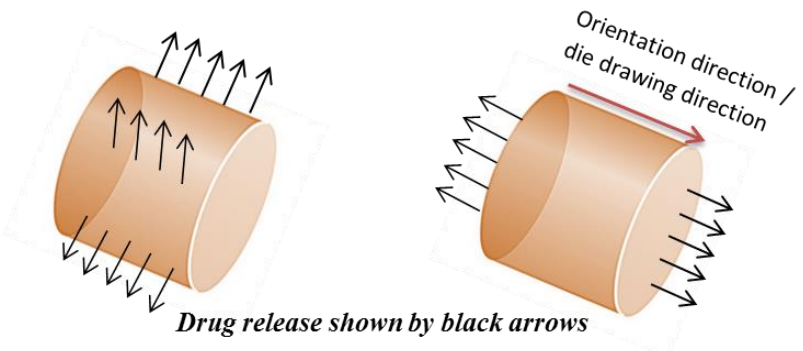

Figure 1.2: *Anisotropic drug release from an oriented 3D geometry*

1.2 Significance of controlled drug release from oriented polymers

In recent years there has been an increasing interest to use bioresorbable polymers in the preparation of implantable medical devices. Hydrolytic or enzymatic degradation of these polymers generate by-products which are harmless to the human body. Therefore implantable devices made from bioresorbable polymers do not require surgical removal. Additionally, they are more biocompatible and smoothly transfer the function to the human body as they are eroded. For example, a fractured bone that has been fixated with a metallic implant bears minimal load in presence of the implant. Consequently, there is a risk of re-fracture upon removal of the implant. Contrarily, biodegradation of polymeric implant smoothly transfers the load to the healing bone and makes it stronger.

Several researchers have utilised polymer orientation techniques such as die-drawing, biaxial drawing for production of self-reinforced polymeric implants (Mikkonen *et al*., 2009; Waris *et al*., 2003; Ylikontiola *et al*., 2004). Addition of a therapeutic agent to such devices combines the advantages of increased mechanical strength and bioresorbability with localised drug delivery. For example, Mikkonen *et al*. (2009) added an anti-proliferative agent to self-reinforced braided stents, in order to prevent formation of cellular plaque around the stent, thereby delaying the requirement for restenosis. Similarly Veiranto *et al*. (2002) added an antibiotic to a die-drawn bone fixation screw, which may aid prevention of infections associated with surgical implantation of the screw. Despite great potential there is a paucity of research on the effect of polymer orientation on drug release from self-reinforced biomedical devices.

This research attempts to generate a fundamental understanding of the effect of various degrees (draw ratio) and nature (uniaxial/ biaxial) of polymer orientation on drug release rate. This knowledge will enable creation of a design rule by which mechanical properties and drug release rate from a self-reinforced implant can be balanced by manipulation of polymer orientation. Based on the

outcomes of this research, polymer orientation can be utilised as a novel method for controlling drug release from a variety of pharmaceutical polymers. Preparation of drug eluting transdermal or wound-care membranes, ocular or sub-dermal implants already utilise techniques such as melt-extrusion (Crowley *et al*., 2007), injection moulding (Rothen-Weinhold *et al*., 1999) , electro spinning (Luong-Van *et al*., 2006) etc. Incidental polymer orientation caused by these manufacturing methods may influence the drug release rate to different extents. However, this factor has not received considerable attention. The results of the current research will highlight the importance of polymer chain organisation in affecting drug release.

It is known that unidirectional polymer orientation leads to generation of anisotropic properties (Coates and Ward, 1979; Ward and Sweeney, 2012). The research described in this thesis attempts to verify if this correlation also applies to drug elution. The outcome of this research will generate a fundamental understanding of the influence of anisotropic chain organisation on the directionality of drug diffusion. Nevertheless, it may highlight the anisotropic percolation of the bathing medium into the oriented polymeric device. Importantly, the results will establish if uniaxially oriented materials have an isotropic drug release rate or if the observed rate is a combination of two anisotropic release rates. This knowledge will provide further insight and control over drug release from oriented materials. Based on this information, a novel drug delivery system can be designed, where the rate of drug release can be simply altered by changing the surface that is exposed to the biological fluid. Such drug delivery systems can include cylindrical implants made from uniaxially oriented biodegradable polymers; e.g. PLA/ PLGA. Alternatively, simple tablets can be generated from a die-drawn billet consisting of fast dissolving semicrystalline polymers such as PVA.

1.3 Introduction to the thesis

This research involves a novel approach to control drug release from biodegradable polymers. It attempts to present a fundamental understanding of the structure evolution in the drug loaded polymeric matrices, when subjected to solid-state orientation and its effect on drug release.

This introduction is followed by the aims and objectives of the work (chapter 2). The background and literature review chapter (Chapter 3) presents an overview of the fundamental knowledge of controlled drug release methods, kinetics and the polymers involved. It further discusses various morphological features in a semi-crystalline polymer, changes associated with polymer orientation and methods of polymer orientation. Biocompatible polymers and active agents which are related to this thesis are briefly introduced in this chapter. Importantly, existing knowledge about the role of a polymeric microstructure in controlling drug release is reviewed and the limitations of the reported studies are identified.

The next part of the thesis is organised such that each chapter represents a key stage in the exploration of the hypothesis. Chapter 4 includes discussion of the methods used for preparation and solid-state orientation of the drug loaded PLA matrices, along with supporting characterisation techniques. Precisely, melt compounding of the drug-polymer systems, film extrusion and solid-state orientation of the films using a biaxial stretcher, extrusion moulding of the drug loaded PLA billets and their die drawing is discussed.

Chapter 5 reports the findings that formed a basis for the selection of the model drug - polymer systems studied further in this thesis. Poly (L-lactic acid) (PLA) was selected as a candidate polymer based on the literature survey, material availability and initial studies carried out to understand the processing suitability. Since biomedical devices made from PLA exploit various polymer orientation processes for achieving higher mechanical strength, it was considered a good candidate for studying the anisotropic drug release after

being subjected to solid-state orientation. Curcumin, theophylline and paracetamol were selected as thermostable and inert model drugs. Curcumin and paracetamol with PLA represents a solid solution system; whereas theophylline represents a model drug that remains in a suspension form.

The drug loaded PLA matrices utilised in this work were prepared by melt extrusion. Rheological studies were used for defining optimum melt processing conditions. Changes in the polymorphic state of the experimental materials and their degradation during melt extrusion can potential affect solid-state orientation process and the resultant drug release profile. Therefore, thermal stability of the selected materials and changes in their polymorphic state when subjected to melt processing were assessed by various techniques. The results of these studies are described in chapter 5.

The work discussed in chapter 6, included solid-state orientation of the films and studying drug release from the same. The crystalline structure developed during solid-state orientation of the films was investigated by techniques such as WAXD, DSC and surface energy measurement. Moreover, the changes in the molecular weight, crystallinity and morphology of the oriented films were monitored during drug release studies. A mechanistic understanding of the effect of solid-state orientation on drug release was generated by correlating these findings with the drug release profile.

Chapter 7 relates to evaluation of anisotropic or direction specific drug release from an oriented three dimensional geometry, i.e. rods. The chapter reports characterisation of the anisotropic structure of the die-drawn billets by WAXD and DSC. Finally, the data obtained from drug release studies is discussed in an attempt to understand the role of anisotropic polymer structure in shaping the direction specific drug release.

Chapter 8 presents the conclusions. Additionally, the future work is suggested in chapter 9 based on the achievement of set milestones and newly identified goals.

2. Aims and objectives

The aim of this work was to investigate the effect of polymer orientation on drug release. This ultimate aim was divided into sub-objectives (figure 2.1). First, the variation in polymer properties that accompanies solid-state orientation was studied. The changes in the oriented matrices during drug release were examined in order to comprehend the mechanism of drug release. Initially, a mechanistic understanding of the effect of different degrees of orientation on drug release was generated, using a two-dimensional geometry, i.e. films. The knowledge obtained from these studies was extrapolated to assessment of anisotropic drug release from an oriented cylindrical geometry.

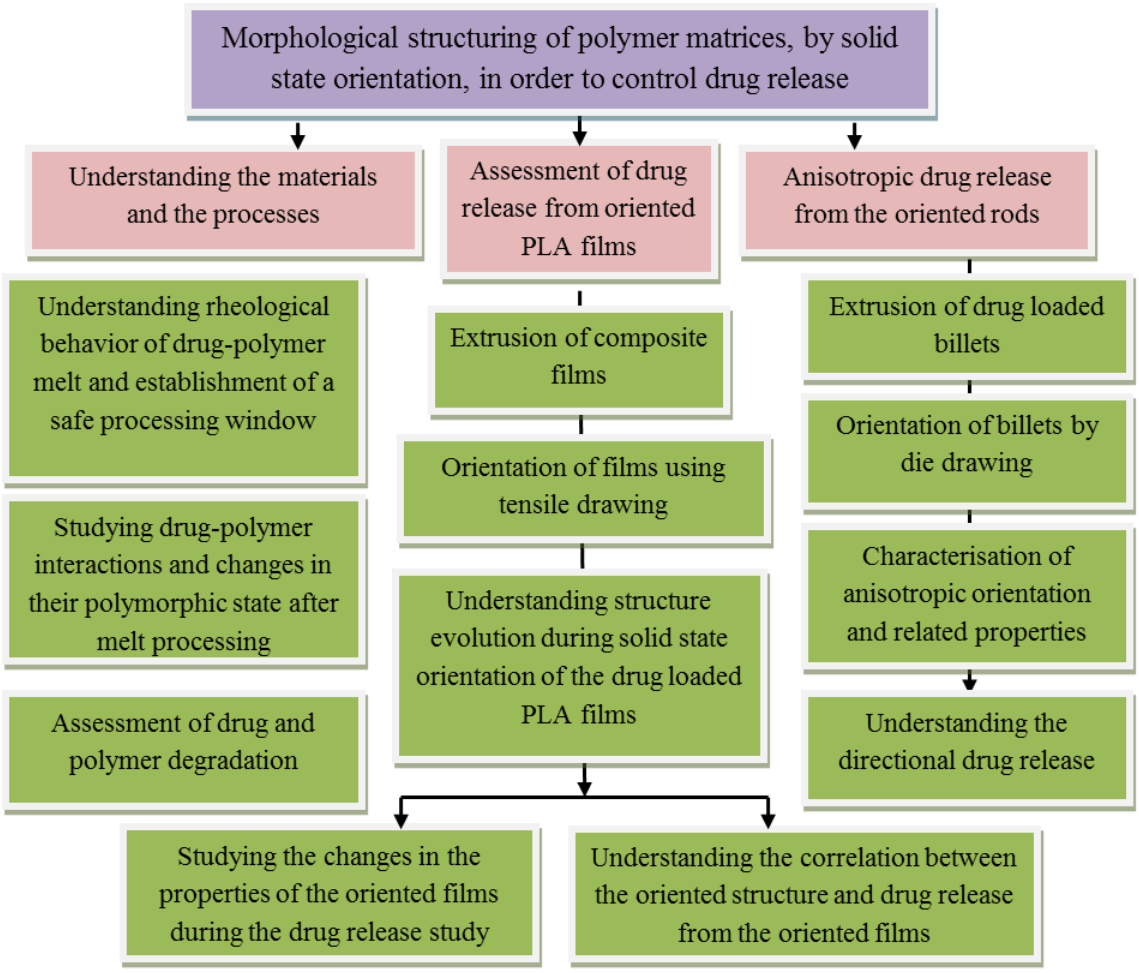

Figure 2.1: *Objectives of the research*

3. Background and literature survey

This chapter presents an overview of the fundamental knowledge about controlled drug release systems and polymer orientation. The existing knowledge about the role of polymeric microstructure in controlling drug release is reviewed. Moreover, the biodegradable polymers and the active agents related to this research are briefly introduced in this chapter.

3.1. Introduction to the materials

3.1.1. Poly (lactic acid) PLA

PLA is a semisynthetic thermoplastic polymer with a large number of applications in the biomedical industry. It can undergo hydrolytic degradation within the body and does not require enzymatic catalysis. The hydrolytic products generated, being part of the natural metabolism, attribute bioresorbability to PLA. It is usually obtained by polycondensation of lactic acid (Maharana *et al.*, 2009) or from ring opening polymerisation of a cyclic dimer of lactic acid, i.e. lactide (Okada, 2002)

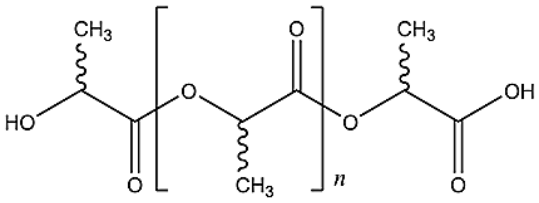

Figure 3.1: *Chemical structure of PLA*

The chemical structure of PLA is depicted in figure 3.1. The presence of methyl side groups contributes to the hydrophobicity of PLA due to steric factors (Vroman and Tighzert, 2009). The glass transition and the melting temperature for PLA homopolymers ranges between 55-65 °C and 170–180 °C respectively (Sodergard and Stolt, 2002). It is a hygroscopic polymer and undergoes degradation above 200 °C, by hydrolysis, lactide formation or oxidative chain scission (Jamshidi *et al.*, 1988). The narrow processing window of PLA puts

major limitations on its applicability. The processing window for PLA can be broadened by addition of plasticizer or D-isomer, which lowers its melting temperature (Blackburn *et al.*, 2006). PLA is soluble in chlorinated solvents, tetrahydrofuran, dioxane and hot benzene, while it is insoluble in acetonitrile and swells in acetone (Garlotta, 2001).

Lactic acid exists in two optically active isomers. Controlled polymerisation of L- and D- isomers may lead to a certain degree of racemisation in the end polymer. The stereological makeup of the end polymer dictates its crystallisation behaviour, mechanical properties as well as biodegradability. Commercially utilised PLA is a poly (L-lactic acid) variety with different D-isomer content.

PLA shows two distinct types of crystal habits. The α Form has a pseudo-orthorhombic unit cell with dimensions a = 10.7 Å, *b* = 6.126 Å and, and *c* = 28.939 Å. On the other hand, the β Form has orthorhombic unit cell having dimensions as follows: a = 10.31 Å, b = 18.21 Å, c = 9.0 Å (Hoogsteen *et al.*, 1990). It was observed that the β Form is associated with a fibrillar morphology, while the α crystals signify the presence of lamellar stacks. In a tensile drawing process, crystallisation occurs as a bilateral event. When processed at lower drawing temperature, formation of α Form is favoured; while the β crystals are generated only near the melting temperature, or at significantly higher draw ratios (Hoogsteen *et al.*, 1990).

3.1.2. Curcumin ($C_{21}H_{20}O_6$ | Mol. wt. 368.38 g/mol)

Curcumin is a yellow pigment found in the dietary spice turmeric (*Curcuma longa*). Chemically it is a linear diphenylheptanoid or specifically (1*E*, 6*E*)-1,7-Bis (4-hydroxy-3-methoxyphenyl)-1,6-heptadiene-3,5-dione. Curcumin exists in two tautomeric forms (figure 3.2). The keto form exists in acidic solutions, whereas the enol form exists at alkaline pH. Curcumin undergoes photo-degradation as well as hydrolytic degradation in alkaline pH. Products of hydrolytic degradation include feruloyl methane, ferulic acid and vanillin, which can be easily detected by HPLC.

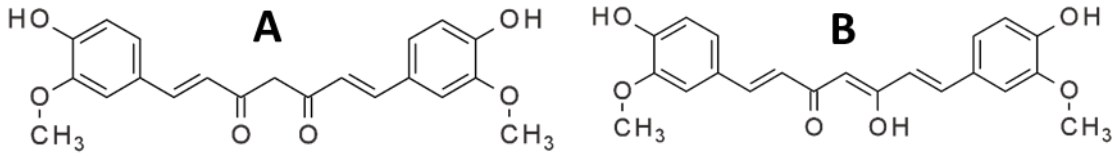

Figure 3.2: *Chemical structure of curcumin* ***(A)*** *The keto form,* ***(B)*** *The enol form of curcumin.*

Curcumin is practically insoluble in water at acidic and neutral pH; it is soluble in acetone, methanol, ethanol, DMSO and chlorinated solvents such as dichloroethane (Stankovic, 2004). It is a crystalline solid and exhibits three different crystal habits (Sanphui *et al.*, 2011). Form I, which is most stable has a melting point at 181 °C. Forms II and III are both metastable and their melting points are 175 °C and 172 °C respectively. When cooled rapidly from the melt, curcumin remains in a glassy amorphous state. Its ability to remain in amorphous state after melting and compatibility with PLA formed the basis for its selection as a model drug in the current studies.

3.1.3. Theophylline ($C_7H_8N_4O_2$ | Mol. wt. 180.164 g/mol)

Theophylline is a bronchodilator and a smooth muscle relaxant, used in the treatment of chronic obstructive pulmonary disease and asthma and infant apnoea. It is a methyl xanthine derivative with IUPAC name 1,3-dimethyl-7H-purine-2,6-dione (figure 3.3).

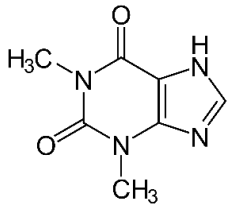

Figure 3.3: *Chemical structure of theophylline*

Theophylline melts at approximately 270 °C. It is slightly soluble in water and sparingly soluble in ethanol, ether. Theophylline exists in a monohydrate form and four anhydrous polymorphs (Khamar *et al.*, 2011). The monohydrate form converts to Form II in low humidity conditions or above 80 °C. The Form

IV is the most stable followed by Form II. Form I is stable at high temperatures, whereas Form III is highly unstable and converts rapidly to Form II.

Ease of quantification and its non-reactive nature has deemed theophylline an excellent model for studying drug release (Bodmeier and Chen, 1988; Kader and Jalil, 1998; Vargas and Ghaly, 1999; Zhang and McGinity, 2000). It was selected as a model drug in this study, based on the experimental evidence that it remains suspended in the PLA matrix, owing to its lower solubility in PLA melt and a significantly high melting point.

3.1.4. Paracetamol ($C_8H_9NO_2$ | Mol. wt. 151.2 g/mol)

Paracetamol, also known as acetaminophen is a popular over-the-counter analgesic, antipyretic. It is chemically named as N-acetyl-p-aminophenol and has the structure represented in figure 3.4. It is a polar molecule owing to presence of a hydroxyl and amide group along with the pi cloud of the benzene ring (Bales *et al*., 1985). Paracetamol exhibits two polymorphs, namely the more stable, monoclinic Form I and the orthorhombic Form II. (Espeau *et al*., 2005). Quench cooling the paracetamol melt forms an amorphous state, which when exposed to temperatures above Tg (22-25 °C), crystallises into Form II (Di Martino *et al*., 2000).

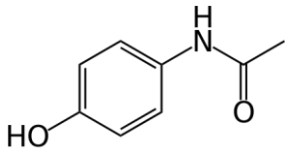

Figure 3.4: *Chemical structure of paracetamol*

Paracetamol is a weak acid with Pka 9.38 at 25 °C (Dasmalchi *et al.*, 1995). Its water solubility is reported to be 17.38 g/ litre. It is practically insoluble in nonpolar solvents, but has higher solubility in alcohols and polar solvents due to hydrogen bonding (Granberg and Rasmuson, 1999). It melts at 169 °C (Form I). A match between the melting temperatures of PLA and paracetamol, coupled with the literature reports on successful molecular dispersion after melt

extrusion of the paracetamol with PLA (Maniruzzaman *et al.*, 2012; Yang *et al.*, 2010), formed basis for its selection as a model drug in the current research.

3.2. Introduction to controlled release drug delivery systems

The past two and half decades have evidenced an exponential rise in applications of synthetic and natural-based polymers in the pharmaceutical and biomedical industry. Polymers have been used for making innovative drug delivery systems that offer spatiotemporal control on release. Controlled release systems can maintain a steady therapeutic level of a drug in the plasma for extended duration. This approach prevents therapeutic failure and minimises side effects. Moreover, it reduces the frequency of dosing, improves bioavailability and prevents dose dumping. Controlled release systems are extremely benevolent in the treatment of chronic diseases such as arthritis, where a single administration can deliver a dose for long duration. They are also promising in the case of paediatric or geriatric patients having difficulty in taking normal dosage, or to avoid dose skipping. Considering these factors, controlled release systems have demonstrated a greater patient compliance and are therefore considered as a better treatment option.

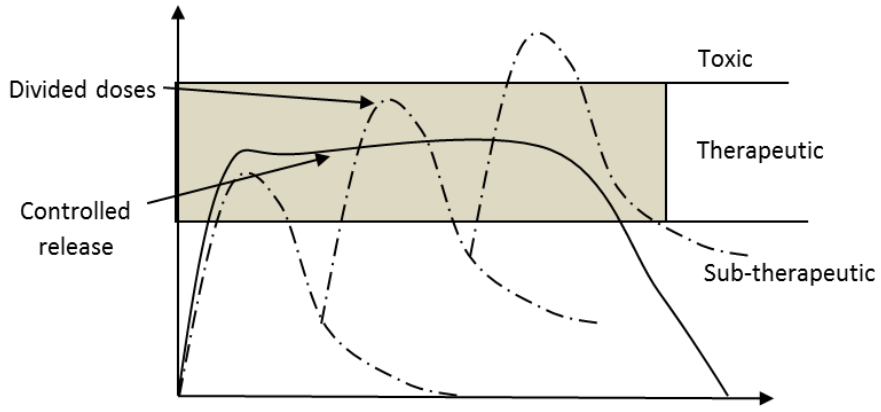

Figure 3.5: *Plasma concentration Vs. time profile for conventional and controlled release systems.*

A conventional drug treatment involves multiple dosing of the therapeutic agent in order to achieve a desired concentration in the plasma for extended duration. A typical plasma profile after successive administration of the conventional dosage form is represented by the dashed lines in figure 3.5. It suggests that the plasma drug concentration in such cases rarely remains constant. Moreover, there is always a possibility of drug concentration exceeding the maximum safe level or falling below the therapeutic level. Either of the events is unwanted but unavoidable in the case of conventional dosage forms. Controlled release systems can maintain a steady plasma drug concentration, by controlling the rate at which drug becomes available for absorption or to the systemic circulation. The solid line in figure 3.5, depicts a distinctive blood plasma profile from the controlled release systems. In order to achieve such a plasma profile, numerous approaches based on physico-chemical properties of the drug or a polymer, have been tried.

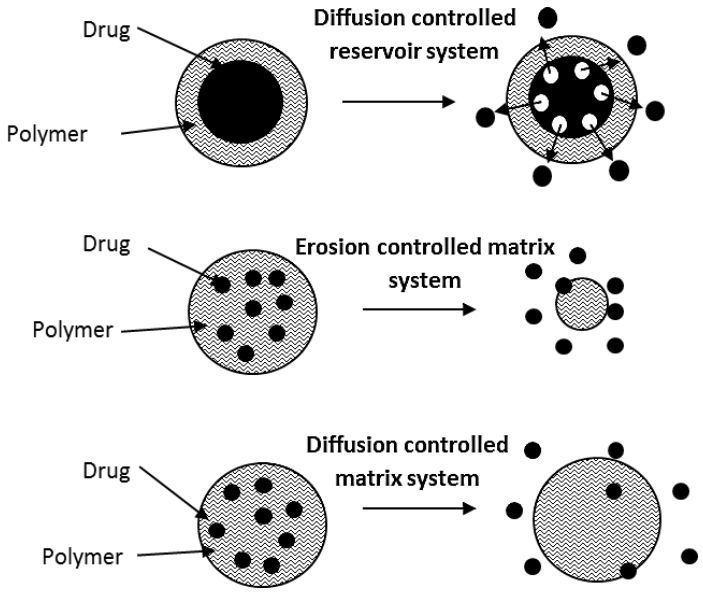

Figure 3.6: *Mechanisms of controlled drug release.*

A controlled release system can be fabricated either by coating a drug core by a suitable polymer or by suspending the drug uniformly within a polymer matrix. The former is known as the reservoir approach, whereas the latter

systems are referred to as matrix/ monolithic carriers. Polymers play a central role in controlling drug release by modulating the rate at which they dissolve (erosion controlled) or by controlling the rate at which drug diffuses out from the polymer matrix (diffusion controlled). A pictorial representation of controlled release systems is given in figure 3.6 Reservoir systems

Ocusert® – a pilocarpine containing polymeric eye implant (Zaffaroni, 1980) was one of the early reservoir based controlled release systems, used clinically. In this system, a water soluble polymer matrix containing pilocarpine is sandwiched between a non-erodible rate controlling membrane and an impermeable polymer membrane, in order to achieve a unidirectional controlled release. Under 'steady-state' conditions, the drug release from such a device can be explained by Fick's first law of diffusion. According to this, the rate of drug diffusion is defined by the concentration gradient across the rate controlling polymer membrane (equation 3.1).

$$\mathrm{J} = -\mathrm{D}\frac{\partial \mathrm{C}}{\mathrm{H}} \qquad \textbf{(Equation 3.1)}$$

Where, **J** is the diffusion flux in dimensions of [(moles of a substance) length^{-2} time^{-1}]
D is the diffusion coefficient or diffusivity in dimensions of [length^{2} time^{-1}]
H is the thickness of the polymer membrane.

In non-steady state conditions, where diffusion of the drug causes a change in the concentration gradient with time, drug release (∂C/∂t) is more appropriately explained by Fick's second law (equation 3.2).

$$\frac{\partial \mathrm{C}}{\partial t} = \mathrm{D}\frac{\partial^2 \mathrm{C}}{\partial \mathrm{h}^2} \qquad \textbf{(Equation 3.2)}$$

Reservoir systems further include delayed release systems, which are made by coating the drug core with an impermeable but erodible polymer. The time required for erosion, and consequent delay in the drug release can be adjusted by using appropriate polymers or their combination.

Examples of polymers used in the reservoir systems include water insoluble polymers such as, poly (ethylenevinyl acetate) (EVA), ethyl cellulose, silicone and polyacrylates, etc. EVA membranes were popularly used as a rate controlling layer in the pilocarpine ocular inserts (Zaffaroni, 1980). Moreover, their utility in the transdermal delivery of a variety of drugs (Chen and Lostritto, 1996; Shin and Lee, 2002) or steroids (Shin and Byun, 1996) has been reported. Higuchi *et al.* (1973a) attempted to reduce the permeability of EVA membranes by subjecting them to solid-state orientation.

3.3. Matrix systems

Matrix systems are composed of a homogenous dispersion of a drug in a non-erodible (diffusion controlled) or an erodible (erosion controlled) polymer matrix. Drug release from 'bioerodible' systems is shaped by both polymer erosion and drug diffusion in a complex way. Matrix systems are generally preferred over reservoir systems, since they are easier to manufacture and importantly a desired release profile can be easily tuned in such systems without involving the risk of dose dumping due to membrane rupture.

Depending upon the manufacturing method and physicochemical properties of the drug and the polymer, matrix systems may have a suspension of drug particles in the polymer matrix, a molecular dispersion or a solution. The physical form of the drug within the polymer matrix affects the nature and the degree of interactions between the drug and the polymer, consequently affecting its release profile.

3.3.1. Diffusion controlled matrix systems

Kinetics of the drug release from a diffusion controlled matrix system were explained by Higuchi (1963), based on following assumptions.

- Sink conditions are maintained.

- Drug release from the matrix occurs in a pseudo-steady state manner, where diffusion coefficients for the drug and the polymer remain constant throughout.
- Drug particles must travel distances marginally larger than their particle diameter and there is no interaction between the drug and the polymer.

Bioerodible diffusion controlled matrices may invalidate the second assumption. Therefore, to simplify the understanding, diffusion controlled matrix systems are defined as those made from non-erodible polymers, and where the release occurs by drug diffusion as the only mechanism. Drug release from such a matrix system was assumed to be a layer by layer diffusion phenomenon. On contact with a biological fluid, the drug contained in the outermost layer of the matrix diffuses uncontrollably. Following that, drug release is regulated by diffusion of the drug contained in each theoretical plane of the device, through several drug depleted planes before it reaches the surface of the device. The kinetic contribution from such drug depleted layers towards the overall drug release rate was explained by Roseman and Higuchi (1970).

If the drug is present in the dissolved state, its release from a film geometry can be described by the approximation given in equations 3.3 and 3.4 (Roseman and Higuchi, 1970).

$$\frac{\partial M}{\partial t} = 2M_0 \left(\frac{D}{\pi L^2}\right)^{0.5}$$, for the initial 60% of the release **(Equation 3.3)**

$$\frac{\partial M}{\partial t} = 4 \left(\frac{8DM_0}{L^2}\right) e^{-\frac{\pi^2 Dt}{L^2}}$$, for the final portion of the release **(Equation 3.4)**

Where, $\frac{\partial M}{\partial t}$ = rate of drug release/ amount of drug released as a function of time.

M_0 = total amount of drug present in the matrix system.

D = diffusivity of the drug.

L = thickness of the film.

Ritger *et al.* (1987) suggested that these equations apply only to the thin films, where the assumption of one dimensional diffusion of the drug under perfect sink conditions would follow Fick's second law perfectly. For non-planar geometries, Fick's law must be modified to incorporate deviations from one dimensional diffusion and changes in the boundary conditions, due to geometric considerations. A mathematical description of drug release from cylindrical and spherical geometries based on the Fick' law modification was deduced by Ritger *et al.* (1987).

When a drug is present as a suspension in the polymer matrix, drug release kinetics vary according to the level of drug loading. For less than 5% w/w drug loading, release occurs mainly by dissolution of the drug into the polymer matrix, diffusion of the dissolved drug towards the surface and subsequent release into the biological fluid (Higuchi, 1963). For a film geometry having homogenous distribution of a drug, the total amount of drug released under sink conditions is given by the Higuchi model (equation 3.5).

$$Q_t = \sqrt{Dt\,(2Q_0 - C_s)C_s} \qquad \textbf{(Equation 3.5)}$$

Where, $\mathbf{Q_t}$ = amount of drug release per unit surface area in time 't'.

D = diffusivity of drug in the polymer.

$\mathbf{C_s}$ = saturation solubility of the drug in the polymer matrix.

$\mathbf{Q_0}$ = total amount of drug present in the polymer matrix.

The term $(2Q_0 – C_S)$ can be reduced to $2Q_0$, in the equation 3.5, since the saturation solubility of the suspended drug in the polymer matrix is significantly lower in comparison to the total drug loading. It was reported that the cumulative amount of drug released is inversely proportional to the square root of time over the initial 60% release of the drug (Ritger and Peppas, 1987). In the later stages, release rate is largely independent of time.

When the amount of suspended drug exceeds 5% w/w, the physical state of the drug – polymer matrix changes from a molecularly mixed to a granular

state. Release from such matrices is significantly faster, since it involves leaching of the biological fluid through pores, cracks and inter-granular spaces. This fluid dissolves the drug and carries it to the external sink. Moreover, dissolution of the drug leads to generation of fluid filled pores, which further increase the permeability of the matrix. When the drug loading exceeds 15% w/w of the polymer, the density of the drug is significant enough to cause a particle-particle contact. In such a case, a phenomenon referred as contact dissolution takes place; i.e. drug particles in contact with each other dissolve when one of them is approached by the leaching fluid. This enhances the porosity of the matrix even faster. A mathematical description of the drug release kinetics from a granular matrix is given by equation 3.6.

$$Q_t = \sqrt{\left(\frac{D\varepsilon}{\tau}(2Q_0 - \epsilon C_S)C_S t\right)}, \text{ for 5\% w/w} \leq A \leq \text{15\%w/w} \qquad \textbf{(Equation 3.6)}$$

In addition to the previously mentioned parameters, equation 3.6 takes into consideration ε and τ, which are the porosity index and the tortuosity index of the polymer matrix respectively.

3.3.2. Polymers for diffusion controlled matrix systems

A preliminary requirement for all diffusion controlled systems is that the polymer is non-erodible so that release of a drug is strictly governed by the diffusion mechanism. The commonly used polymers include ethyl cellulose (Friedman and Golomb, 1982), polyacrylates (Chiang and Tenzel, 1991; Cleary, 1990; Di Colo and Zambito, 2002) and polyurethanes (Schierholz *et al.*, 1997). Ethyl cellulose is extensively used for making diffusion controlled drug delivery systems. Ethyl cellulose solvent cast films containing 5, 10 and 20% of chlorhexidine diacetate exhibited drug release coherent with the Higuchi model discussed previously (Friedman and Golomb, 1982). The influence of morphology of the solvent casted ethyl cellulose matrix on drug diffusion was described by Jones *et al.* (1995). They postulated that a good solvent or a

solvent having the solubility parameter matching that of the polymer generates a dense, homogeneous network of the interpenetrating polymer chains, as the solvent is evaporated. Contrastingly, a poor solvent would not fully extend the polymer coils, resulting in a heterogeneous matrix with poor intermolecular interaction and presence of micro-voids. Release of chlorhexidine was augmented as the proportion of the poor solvent in the solvent mixtures increased. An extremely slow release was obtained when drug containing ethyl cellulose matrices were melt extruded (Brabander de *et al.*, 2003). Melt extrusion leads to densification of the polymer chains to the extent that extruded material has practically zero porosity (Crowley *et al.*, 2004b).

Drug release from non-erodible matrices is also shaped by the nature of the association between a drug and the polymer. At the same level of drug loading, gentamycin and flucloxacillin remained homogenously distributed in the polyurethane matrices; whereas, ciprofloxacin and fosfomycin matrices exhibited a granular structure. This was reciprocated as slow continuous release behaviour for the prior two and fast initial release for the latter pair (Schierholz *et al.*, 1997).

3.3.3. Dissolution controlled matrix system

Dissolution controlled systems derive their name from the fact that release of a drug from such matrices is governed by dissolution of the polymer. A demarcation between bioerodible and dissolution controlled systems is that the latter are formulated from water soluble polymers such as poly (ethylene oxide) – (PEO), polysaccharides, and therefore the erosion mechanism does not involve any chemical change in the polymer. The loss of the polymer bulk takes place in two steps. First the medium leaches into the matrix, which is followed by chain disentanglement. The free drug can subsequently dissolve in the surrounding medium and mix with the bulk sink (Narasimhan and Peppas, 1997).

3.3.4. Polymers for dissolution controlled matrix systems

Poly (ethylene glycol)s (PEG) and their higher molecular weight derivatives, referred to as poly (ethylene oxide)s (PEO) are extensively used for making dissolution controlled matrices of various geometries (Crowley *et al.*, 2004a; Prodduturi *et al.*, 2005; Zhang and McGinity, 1999). For lower molecular weight PEO (200 – 900kDa), the rate of chain disentanglement marginally exceeds the rate of swelling after water uptake. Therefore, drug release follows the dissolution controlled mechanism. As the molecular weight increases, the rate of swelling increases; while the rate of disentanglement decreases due to longer chain reptation time. Consequently, matrices made from PEO having molecular weight 2000 kDa or over exhibit an initial diffusion mediated release, followed by an erosion phase (Apicella *et al.*, 1993; Colo di *et al.*, 2001).Since PEO can be polymerised into a range of molecular weights, their combination can be used for balancing the rate of erosion and the rate of swelling, so that a constant drug release rate is obtained (Wu *et al.*, 2005).

Similar to PEO, the water soluble nature of poly (vinyl alcohol) (PVA) and polysaccharides makes them suitable for fabrication of dissolution controlled matrices (Guohua *et al.*, 2006; Tsukada *et al.*, 1994). The semicrystalline nature of PVA offers control over polymer erosion and resultant drug release by manipulation of the polymer's crystallinity. Wan *et al.* (1992) observed a reduction in drug release rate following heat treatment of PVA films above their glass transition temperature (Tg).

3.4. Biodegradable matrix systems

3.4.1. The concept

Biodegradable systems are most commonly erodible matrix systems consisting of a water insoluble polymer. Erosion mechanism can be as simple as hydrolysis, or it may involve polymer degradation by cellular or enzymatic pathways. If the degradation products are small molecules normally found in the physiological processes, the systems are referred to as 'bio-resorbable'.

Depending upon the diffusivity of the water into the polymer matrix, susceptibility of the polymer's functional group to degradation and matrix dimensions, the erosion can be sub-classified as 'surface erosion' or 'bulk erosion' figure 3.7

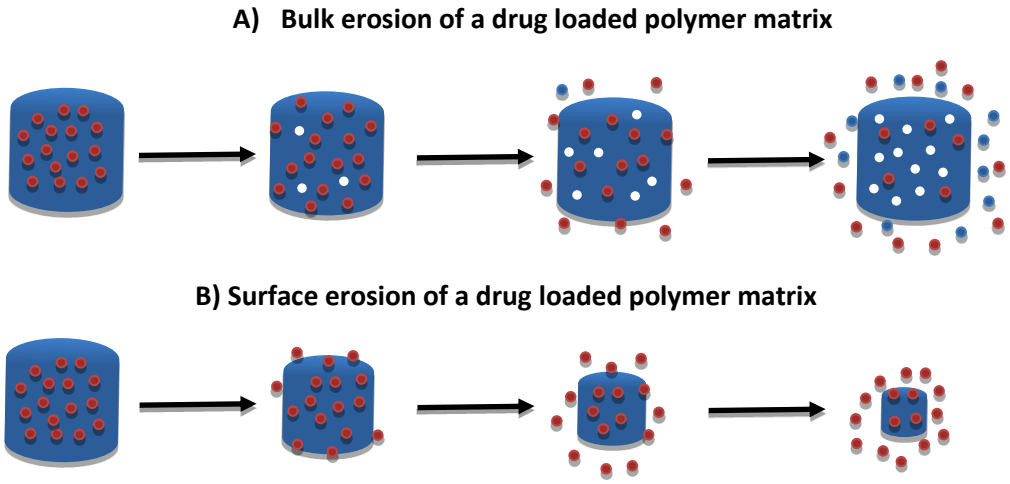

Figure 3.7: *Polymer erosion mechanisms*

Generally bulk erosion takes place when the rate of water permeation is significantly higher than the rate of polymer degradation. Consequently, hydrolysis takes place simultaneously throughout the matrix. Hydrolytic susceptibility of the bond decreases in order from anhydrides, ortho-esters, esters to amides, due to steric factors (Gopferich, 1996). As a result of this, a matrix with a constant geometry will exhibit surface erosion if it is made from poly-anhydrides or poly-ortho-esters; whereas, it will undergo bulk erosion if it has ester or amide linkages. Most biodegradable polymers erode by both mechanisms; however, the contribution from each varies depending on the chemical structure of the polymer, matrix microstructure, crystallinity, porosity, pH of the medium, drug distribution and the level of drug loading, etc. Importantly, certain polymers such as poly (lactic acid) undergo crystallisation during bulk degradation, which substantially changes the degradation kinetics (Wada *et al.*, 1991). A detailed information on these mechanisms can be found in the review by Gopferich A. (1996).

From a drug delivery point of view, surface eroding matrices are preferred over bulk eroding ones for the following reasons. Namely, the rate of drug release is uniform and predictable, the release rate can be tailored by simply varying the geometry of the matrix and importantly, water labile drugs are protected from degradation until they are actually released (Uhrich *et al.*, 1999).

In reality, drug release from bioerodible devices occurs by drug diffusion as well as polymer erosion. If the rate of diffusion through such matrices significantly exceeds the rate of erosion, the kinetics can be defined by the Higuchi model for diffusion controlled non-erodible matrices (equation 3.5). Under such circumstances, it is assumed that the change in the diffusivity of the polymer due to erosion process is small enough to be ignored. On the contrary, if the diffusion rate is equivalent to the erosion rate or if it exceeds the erosion rate only by a small margin, The Higuchi equation must be modified to include the contribution from polymer erosion (equation 3.7).

$$\mathrm{Q}_t = \sqrt{2\mathrm{D}Q_0\mathrm{e}^{\mathrm{kt}}\mathrm{C}_\mathrm{s}\mathrm{t}} \qquad \textbf{(Equation 3.7)}$$

Where, $\mathbf{Q_t}$ = amount of drug release per unit surface area in time 't'.

D = diffusivity of drug in the polymer.

$\mathbf{Q_0}$ = total amount of drug present in the polymer matrix.

$\mathbf{C_s}$ = saturation solubility of the drug in the polymer matrix.

$\mathbf{e^{kt}}$ = factor considering the polymer degradation rate.

When the polymer erosion rate significantly exceeds the diffusion rate, the matrix is referred as an 'erosion controlled' system. Drug release from an erosion controlled system may vary depending on the nature of erosion (surface erosion / bulk erosion), and the geometry / surface area of the matrix. There are several mathematical models reported to describe the kinetics of drug release from erosion controlled systems. These models were reviewed by Fu *et al.* (2010). Hopfenberg (1976) described the release rate of the drug from surface eroding polymers, using the following equations (3.8, 3.9).

For a film having initial thickness '2a', the fraction of the drug released ($\frac{M_t}{M_\infty}$) is given by,

$$\frac{\mathrm{M_t}}{\mathrm{M_\infty}} = \frac{(\mathrm{K_0 t})}{(\mathrm{Ca})} \qquad \textbf{(Equation 3.8)}$$

For a cylinder having initial radius 'a', the fraction of drug released ($\frac{M_t}{M_\infty}$) is given by,

$$\frac{\mathrm{M_t}}{\mathrm{M_\infty}} = 1 - \left(1 - \frac{\mathrm{K_0 t}}{\mathrm{Ca}}\right)^2 \qquad \textbf{(Equation 3.9)}$$

Where, $\mathbf{K_0}$ = erosion rate constant

C = initial drug loading

The model by Hofenberg did not confirm the experimental results for drug release from a cylindrical geometry, since it did not consider the differential erosion rates from radial and axial surfaces (Karasulu *et al.*, 2000). A modified equation (eqn. 3.10) was suggested to account for this phenomenon.

$$\frac{\mathrm{M_t}}{\mathrm{M_\infty}} = 1 - \left(1 - \frac{\mathrm{K_a t}}{\mathrm{Ca}}\right)^2 \left(1 - \frac{2\mathrm{K_b t}}{\mathrm{Cb}}\right)^1 \qquad \textbf{(Equation 3.10)}$$

Where, $\mathbf{K_a}$ = radial erosion rate constant

$\mathbf{K_b}$ = axial erosion rate constant

C = initial drug loading

a = initial radius of the cylinder

b = initial thickness of the cylinder

Due to the heterogeneous nature of bulk erosion, few attempts have been made to describe such matrices mathematically. A broader model that can be applied to surface eroding, bulk eroding or even intermediate systems was reported by Rothstein *et al.* (2009). The model divided the process of drug release into three prominent stages. In the first stage, water diffuses into the

polymeric matrix and causes hydrolysis of the matrix. The rate of this process is dictated by the hydrolysis rate as well as the diffusion gradient for water. Following diffusion of the water, water that was not used in the hydrolysis dissolves the free drug. Therefore the rate limiting factors in the second stage are concentration of the drug, saturation solubility of the drug and the amount of dissolution media available. The third stage involves diffusion of the dissolved drug out of the matrix. This process depends on the porosity and the diffusion path availed by the matrix undergoing degradation. A mathematical derivation for drug release kinetics, based on these variables reads as follows (equation 3.11):

$$\frac{\partial C_A}{\partial t} = \nabla(D_{eff}\nabla C_A) + K_{dis}C_{Sn}C_{An}C_{Wn} \qquad \textbf{(Equation 3.11)}$$

Where, $\mathbf{C_A}$ = concentration of the dissolved drug.

$\mathbf{K_{dis}}$ = intrinsic dissolution rate constant.

$\mathbf{C_{Sn}}$ = normalized concentration of solid drug in the polymer matrix.

$\mathbf{C_{An}}$= difference between the aqueous drug concentration and its saturation solubility.

$\mathbf{C_{Wn}}$ = normalized concentration of water in the polymer matrix.

$\mathbf{D_{eff}}$ = effective diffusivity term.

3.4.2. Polymers for bioerodible matrix systems

The four prominent groups of bioerodible/ biodegradable polymers include poly (anhydrides) (PAH), poly (ortho-esters) (POE), Poly (esters) of lactic (PLA) / glycolic acid (PGA) and poly (amides) (PA) (Uhrich *et al.*, 1999). Based on the erosion mechanism, the prior two are classified as surface eroding polymers, whereas the latter are referred to as bulk eroding polymers. Since drug release from surface eroding matrices can be easily tailored by changing the geometry, PAH and POE have been comprehensively used in controlled drug delivery systems. The primary application of bulk eroding polymers involves implantable biomedical devices (bone fixation screws, stents), where the bulk erosion mechanism allows mechanical strength as well as the shape of the matrix to be

maintained for an extended duration. Considering the scope of this report only the poly-esters of lactic and glycolic acid are discussed here.

3.4.2.1. Drug release from poly-esters of lactic and glycolic acid

Polyesters of α–hydroxy acids have been widely used in the production of high strength, high modulus biomedical devices, owing to their semicrystalline and bioresorbable nature. Such devices can be designed to release a drug at a local site of application for longer durations. Initial approaches to couple a therapeutic agent with a biomedical device involved coating the device with a drug loaded bioresorbable polymer. Stenberg *et al.* (2007) utilised this approach for coating metallic stents with a PLA matrix containing an anti-proliferative agent. In another study, extruded PLA fibres were subjected to tensile drawing and then hot compacted to create braided stents (Mikkonen *et al.*, 2009). A drug was incorporated by solution coating with an additional polymer layer. Drug release in either case followed first order kinetics, where the release rate was dependent on the drug loading and the hydrophobicity of the drug.

In general, matrices made from PLA show a sigmoidal release pattern with an initial lag phase followed by a faster release phase, finally reaching a plateau (Miyajima *et al.*, 1997). This is attributed to the fact that the initial stages in the bulk erosion of PLA are characterised by water penetration and loss of mechanical strength, but no actual erosion takes place. In this stage the drug is released mainly by diffusion, according to the Higuchi model (equation 3.5). Miyajima *et al.* (1997) confirmed through DSC and SEM studies that on exposure to water an amorphous PLA matrix underwent a transformation into a porous semicrystalline structure. These pores contain crystal defects in the form of hydrophilic chain ends, which promote water penetration; consequently leading to enhanced drug release. Teupe *et al.* (1992) obtained a similar three phase release pattern for ciprofloxacin from melt extruded PLA cylinders. The release profile, however, was evaluated by conducting microbiological inhibition assays instead of chemical/ spectroscopic measurement.

Similar to PLA, poly (glycolic acid) (PGA) and their lactic acid copolymers (PLGA) have witnessed a plethora of applications in controlled release drug delivery systems (Grayson *et al.*, 2003; Schmitt and Polistina, 1976; Singh *et al.*, 2004). Biodegradation of PGA homopolymer is 6-7 times faster than that of PLA. Therefore, copolymerisation of lactic and glycolic acids in different ratios yields polymers with a desired biodegradation rate as well as mechanical strength (Lewis, 1990). In several independent studies (Li, 1999; Naraharisetti *et al.*, 2006), the proportion of the glycolic acid in the oligomer was systematically varied, with a common observation that a higher glycolic acid content accelerated drug release. Quantitative Nuclear Magnetic Resonance (NMR) studies provided further insight into the degradation of PLA/PGA matrices; suggesting significantly slower hydrolysis of the PLA backbone, it being sterically hindered by the methyl side group (Alexis *et al.*, 2006)

The drug delivery matrices composed of PGA display a triphasic release pattern similar to PLA (Shah *et al.*, 1992). A mechanism for polymer degradation and drug release from PGA matrices was explored by Hurrel *et al.* (2001a; 2001b). They evidenced a sigmoidal release pattern, overlapping with a four-phase bulk degradation pattern. In the short first stage, a small amount of water diffuses into the sample and reaches an equilibrium concentration within the polymer. This is followed by the stage II, which is characterised by the hydrolysis reaction. The polymer chains become increasingly mobile as the molecular weight falls and water plasticises the sample. The mobile chains undergo insertion crystallisation. A critical molecular weight is reached at the beginning of stage III, and oligomers start to leach out. Water molecules diffuse into the space created by the removal of the oligomers, which in turn encourage more oligomers to diffuse out. At stage IV, the whole sample is porous and highly crystalline. Degradation proceeds homogeneously and more slowly in this stage.

3.4.2.2. Factors affecting drug release from PLA/ PLGA

Hydrolytic degradation and drug release from PLA/ PLGA depends on their enantiomeric composition, crystallinity and molecular weight, etc. (Alexis, 2005). The **enantiomeric composition** plays a vital role, owing to higher susceptibility of the L-isomer of the lactic acid to hydrolysis than the D-isomer (Li *et al.*, 2000). Moreover, the enantiomeric composition shapes the crystallinity of PLA, which further influences the release of a bioactive agent. The effect of **crystallinity** and the crystalline morphology of PLA on drug release is discussed at length, later in this chapter.

A higher **molecular weight** indicates higher diffusional resistance or slower erosion. Therefore, drug release from the polyesters of alpha hydroxy acids exhibits an inverse relationship with their molecular weight (Omelczuk and McGinity, 1992; Park, 1994). Contrasting results were obtained by few researchers (Cam *et al.*, 1995; Wu and Wang, 2001). They attributed this to the lower crystallisation tendency of higher molecular weight PLA, which enhances its biodegradation.

Drug release from PLA/ PLGA matrices is also governed by **the nature and solubility of the drug**, and importantly **the size** of the matrix. Witt *et al.* (2001) observed the degradation rate decreasing in order from tablets, rods, films to microspheres. Although, larger matrices hydrolyse faster, existence of a bulk degradation mechanism may restrict the ability of the drug and the degraded oligomers to leach out, resulting into heterogeneous drug release (Lu *et al.*, 1999; Witt and Kissel, 2001).

Higher **drug loading** accelerates the overall drug release with a higher initial burst (Sampath *et al.*, 1992; Wada *et al.*, 1990). Moreover, an **acidic or a basic nature of the compounded drug** plays a key role in shaping polymer degradation and consequently drug release. Miyajima *et al.* (1998) reported a rise in the Tg of the PLGA rods when they were compounded with basic drugs. This was linked to a probable interaction between the basic drug and the

carboxyl groups of the polymer, which reduced drug release. Moreover, such an interaction may attenuate the autocatalytic effect of the acidic chain ends, resulting into slower polymer erosion (Mauduit *et al.*, 1993). Contrastingly, several groups observed higher polymer erosion when a basic drug was incorporated. They attributed it to the base catalysed hydrolysis of the ester linkages (Cha and Pitt, 1989; Li *et al.*, 1996). Alexis *et al.* (2006) suggested that neutralisation of carboxylic groups by basic drug may occur when the molecular weight of the polymer is low enough to have plenty of end groups. In the case of a higher molecular weight PLA, they found base catalysed hydrolysis to be the predominant mechanism.

Apart from a drug, other **additives such as plasticisers** can enhance drug release, either by reducing the Tg of the matrix or by creating fluid filled channels, following their solubilisation (Andreopoulos, 1994; Kranz *et al.*, 2000). Moreover, a change in the ***in vitro*** **experimental conditions** may be reflected into the drug release profile. Extreme acidic and alkaline **pH** of the release medium accelerates the hydrolysis by acid catalysis and base catalysis respectively (Belbella *et al.*, 1996; Makino *et al.*, 1986). The degradation mechanism shows a strong **temperature** dependence, with temperatures above Tg showing a drastic augmentation of degradation (Aso *et al.*, 1994; Hakkarainen *et al.*, 1996). Arm *et al.* (1997) observed faster release of bovine albumin from PLGA (50/50) rods when they were subjected to a cyclic bending load. **Applied stress** leads to elongation of pores into wider cracks, which further enhances the release. *In vivo*, this might correlate to drug release from a biomedical device (such a bone fixation screw), which is constantly subjected to a stress.

In summary, it is safer to state that drug release from PLA/ PLGA matrices is simultaneously controlled by several factors. A thorough understanding of all these factors is necessary before the observed change in release patterns can be attributed to a particular one.

3.5. Controlled drug release models

Translation of the drug release data into a mathematical function facilitates a quantitative interpretation of the underlying mass transport mechanism. Several mathematical models that describe controlled drug release are reported in the literature (Costa and Sousa Lobo, 2001). Few are derived by a theoretical analysis of the release process, e.g. zero order kinetics; while, the most are empirical and correspond to the known release mechanisms, such as diffusion, swelling, and erosion. The relevant models are summarised in the table 3.1. The drug release data is usually plotted into the mathematical format corresponding to the individual model and the best model is selected by statistical analysis such as regression or analysis of variance (ANOVA).

Table 3.1: *Mathematical models describing controlled drug release*

The model	Mathematical expression	Applicable if the following is linear	Significance
First order kinetics	$Q_t = Q_0 + e^{-kt}$ **Q_t =** Cumulative release **Q_0 =** Original amount of drug **K =** proportionality constant **t=** time	**Y-axis:** $\mathrm{Log}(Q_0 - Q_t)$ **X-axis:** time	Drug release rate dependent on the concentration of drug available
Zero order kinetics	$Q_t = Q_0 + Kt$	**Y-axis:** Q_t **X-axis:** time	A constant drug release rate
Higuchi Model (1963)	$Q_t = \sqrt{\frac{D\varepsilon}{\tau}(2Q_0 - \varepsilon C_S)C_S\, t}$ **D =** diffusivity, **ε =** porosity **τ =** tortuosity of the diffusion path **C_S =**saturation solubility of the drug in the release medium	**Y-axis:** Q_t **X-axis:** $\sqrt{\text{time}}$	Describes drug release by diffusion through the polymer and the water filled pores. Drug release follows the Fick's diffusion law.
Hixson–Crowell (1931)	$Q_0^{1/3} - Q_t^{1/3} = K_S\, t$ **K_S** is a constant accounting for the change in the geometry	**Y-axis:** $Q_0^{1/3} - Q_t^{1/3}$ **X-axis:** time	Describes drug release limited by erosion of the matrix. Accounts for the change in the geometry of the matrix as it is eroded.
Korsmeyer–Peppas model (1983)	$\frac{Q_t}{Q_0} = Kt^n$ **'n'** is the release exponent predicting the release mechanism	**Y-axis:** $\mathrm{Log}(Q_t/Q_0)$ **X-axis:** $\log(\text{time})$	**n ≤ 0.5:** Fickian diffusion. **0.5 < n < 1:** Non-Fickian transport. **n = 1:** Case II transport responsible for the zero order release. **n ≥ 1:** Super case II transport.

3.6. Orientation of polymers

The volume and prospects of research related to oriented polymers are continuously growing particularly since the last decade. Examples of polymer orientation encountered in day-to-day-life are silk, cobwebs etc. (Christopher, 1997; Termonia, 1994). Frenkel S (2008) has divided routes of formation of oriented structures, principally into three categories. The natural process of spinning silk is categorised under 'direct generation'. The second mode of orientation involves assemblage of microstructures into a macrostructure, where the macrostructure essentially has a similar morphology to that of its fundamental units. The phenomenon can be understood through the process of organisation of collagen fibres from a solution of tropocollagen or even primary gelatine. Assemblage simply involves organisation of existing microstructure and hence virtually no energy is required for this thermodynamic event. The third mode of orientation in contrast to assemblage requires a great deal of energy and is referred to as 'rearrangement'. The existing structure decides the statistical possibility of different configurations and the energy barrier involved in a jump from one to another. Rearrangement of polymer structure on tensile drawing is an example of such a process. To understand the phenomena of orientation in synthetic semicrystalline polymers, it is important to know the structural/ morphological features present within such polymers. This understanding can then be extrapolated to comprehend the changes in oriented drug – polymer composites and its implications on drug release.

3.7. Morphological structures within a semicrystalline polymer

Ordinarily, polymer chains exhibit an entangled mesh due to secondary forces of attraction such as Van der Waal's forces, hydrogen bonds, etc. In the case of semicrystalline polymers, stereological constraints imposed by covalent bonds within the chain structure give rise to supramolecular structures of different dimensions and shapes. In other words, semicrystalline polymers co-exhibit a randomised chain structure along with some highly ordered regions,

commonly referred to as amorphous and crystalline domains respectively. The spatial and numeric distribution of these regions depends primarily on the average molecular weight, structural features and process history of the polymer (Tung and Buckser, 1958). In a molten state, polymer chains are randomly distributed. Ideally, if this mass is quenched rapidly, the random distribution is frozen in its isotropic state and hence the polymer exhibits an amorphous morphology. On the other hand, if the polymer is allowed to cool slowly, it provides sufficient time for crystal growth. (Mandelkern, 2002). The percentage crystallinity, as well as morphology and organisation of the crystalline regions play a vital role in shaping polymer properties. Thus, manipulation of polymer morphology offers an enormous potential for tailoring its properties according to the designated application.

3.7.1. Morphology of the amorphous section

The amorphous region within a polymer can most conveniently be simulated by a random mesh of spaghetti. Amorphous segments act as chains that tie and hold together the crystallites, hence are sometimes referred to as tie molecules. Configuration of amorphous chains depends on the nature of the crystalline region. If the polymer has long needle like crystals, then amorphous chains are typically present as overgrowths from either ends of the needle (Wenderoth *et al.*, 1985). However if the polymer exhibit lamellar geometry, then amorphous chains act as intra-lamellar and inter-lamellar connecting molecules (Men *et al.*, 2003). These interconnecting links within the polymer structure reduce brittleness and bestow pliability, extensibility and ability to recover the structure.

3.7.2. Morphology of the crystalline section

The process of crystallisation signifies attempts by the atomic units to achieve the lowest possible free energy state. Long polymer chains can achieve a lower free energy state by folding upon themselves. Such folding continues simultaneously in different regions, leading to several lamellar crystals being

spanned by a single polymer chain. The model suggested by Keller (1992) explained the folding to be sharp with adjacent re-entry of polymer chains (figure 3.8 - A). The previous model considered chain folding to be random (Flory, 1962) and was called the switchboard or irregular re-entry model (figure 3.8 - B).

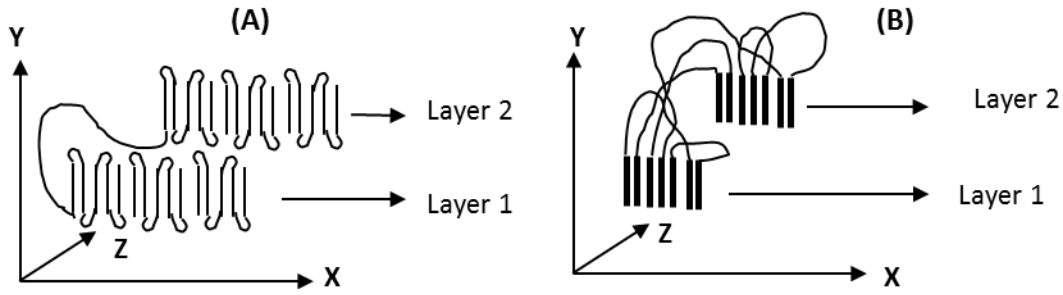

Figure 3.8: *Lamellar folding models.* ***A)*** *Adjacent re-entry,* ***B)*** *Switchboard model*

3.7.3. Spherulites, shish-kebab and fibre like superstructures

3.7.3.1. Spherulite

A spherulite is a spherical aggregate of polymer crystals (figure 3.9 - A). Formation of this birefringent entity can be easily observed in solidifying melt of poly (ethylene oxide) (Cheng *et al*., 1990; Price and Kilb, 1962). A spherulite is essentially a high-density packing of lamellae. The presence of a temperature gradient in the direction perpendicular to the molecular chain leads to stacking of a lamellar arrangement. Whenever such a gradient is absent, lamellar growth can occur radially emerging from a single point, hence giving rise to a spherulitic structure. In early growth stages, a rod like structure is developed, which undergoes branching and expansion to a double inverted umbrella, ultimately leading to a sphere (Price, 1961). Formation of spherulites is dependent on nucleation density, molecular weight and cooling rate (Barnes *et al*., 1961; Godovsky *et al*., 1972). Therefore, size of the spherulites vary largely from 1µM to 1cm (Silvestre C *et al*., 2000).

3.7.3.2. Shish-Kebab structure

Many processing methods such as injection moulding and fibre spinning involve application of high shear to the polymer melt and induce extensional flow. Consequently, a unique anisotropic microstructure called 'Shish Kebab' can be formed (Schultz *et al*., 2000; Wang *et al*., 2004). Fundamentally, the Shish-Kebab structure is composed of central fibrillar bundles oriented in the flow direction with a regular, transverse growth of lamellae, perpendicular to chain direction (figure 3.9 - B). The prior is called ‘Shish’ and the latter ‘Kebabs’. Such a structure was first investigated and modelled by Penning (1967). The shish bundles were thought to be made up of extended polymer chains organised in the direction of melt flow. Whereas, the secondary nuclei attached to the extended chains give rise to lamellar folding in the perpendicular direction (Somani *et al*., 2005). It has been observed that the presence of the shish-kebab morphology markedly enhances tensile strength, barrier properties and thermal stability of polymers (Pornnimit and Ehrenstein, 1991; Vasile, 2002).

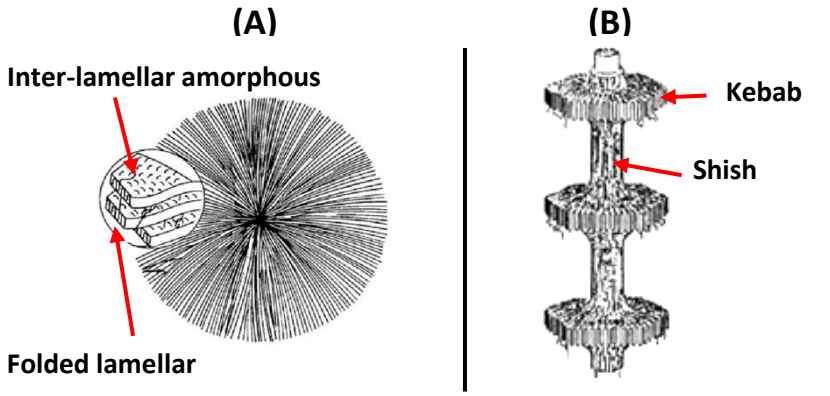

Figure 3.9: *Schematic representation of* ***A)*** *the spherulitic crystals and* ***B)*** *the shish-kebab crystals in a semi-crystalline polymer.*

[adapted from (Somani *et al*., 2005) originally from (Meijer-Han, 1997)].

3.7.3.3. Fibrils

Fibrillar crystal structure is a very important morphology developed in highly oriented polymers. Fortisan, an ultra-oriented cellulose as well as Nylon 6 show fibrillar units. Fibrils in Nylon 6 are made up of lamellar folding where the

polymer chains lie at right angles to the fibril length. Contrarily, the fortisan chains are aligned roughly parallel to the long axis of the fibre. During melt crystallisation, if an extended set of nuclei are confined to a plane surface it leads to generation of fibrils that does not further develop into spherulites (Sharples, 1966). Similarly, tensile drawing of PLA to a significantly higher strain and/or near the melting temperature generates a beta crystalline form, having fibrillar morphology.

3.8. Methods to achieve orientation

Deliberate orientation can be produced through a variety of methods, classified as solid-state and fluid-state orientation processes. Important ones are reviewed in figure 3.10.

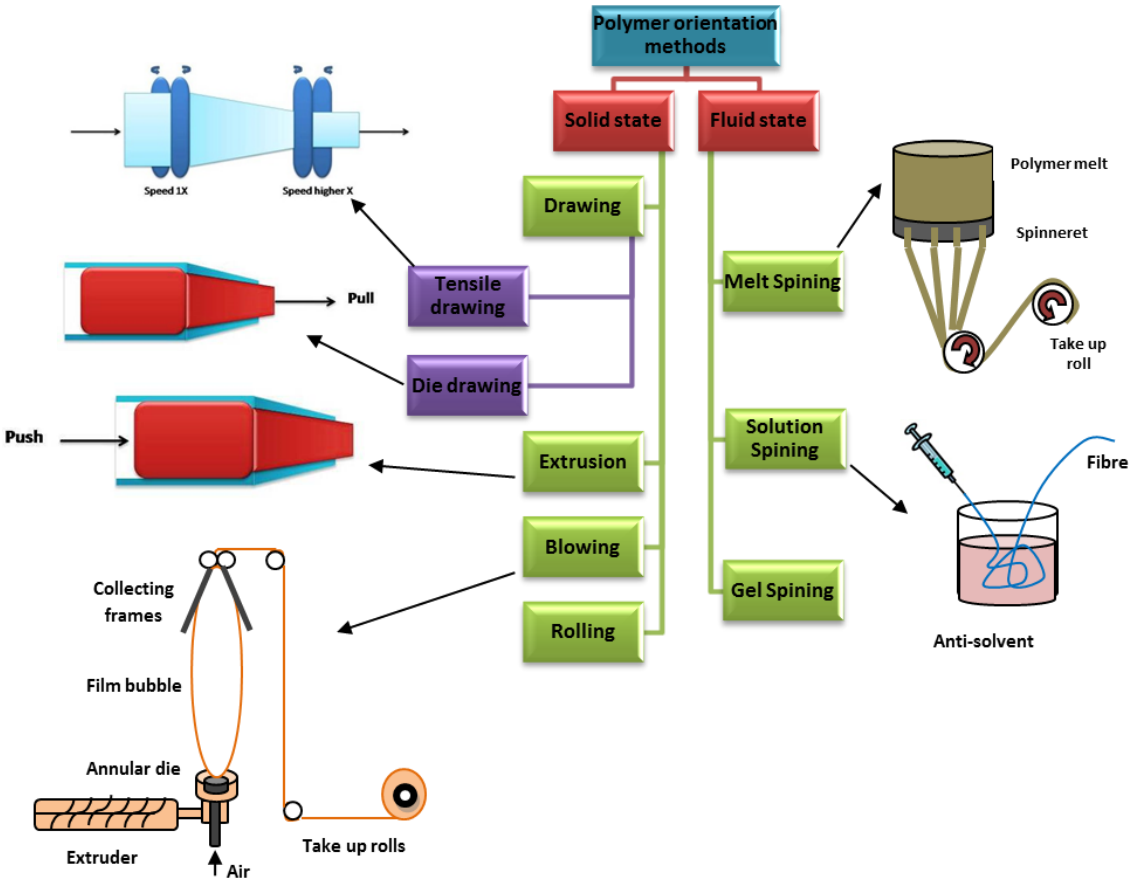

Figure 3.10: *Polymer orientation methods.*

3.8.1. Solid-state processes

The term solid-state orientation signifies orientation of a polymer above its glass transition but below the melting. The solid-state processes are categorised under drawing (tensile/ die drawing), extrusion (ram/ hydrostatic), blowing and rolling. Of these, tensile drawing and die drawing will be utilised in the current research.

3.8.1.1. Tensile drawing

The tensile drawing process for a film like geometry can be easily visualised through the simple tensile test, where the sample is clamped at either ends and extended, keeping one end fixed. When stretching a film using a tensometer, necking may lead to a decrease in the width of the film. In order to keep the width constant, equipment such as a biaxial stretcher is used. Generally a square film is clamped at multiple positions along all four sides and then extended along a single axis. Alternatively, the film can be oriented along both of the axes to the same or different extents, either simultaneously or in succession. These processes are referred to as Uniaxial Constant Width (UCW) orientation and biaxial orientation respectively. The biaxial stretcher is usually provided with an oven and can operate at various strain rates. However, such an instrument is useful only at a laboratory scale. At an industrial scale, the process has to be continuous and therefore a roller system is used in line with a film extruder. To achieve uniaxial orientation the extruded film is passed between two rollers, the latter rotates at higher speed than the previous. The draw ratio (the final length divided by the original length) depends on the ratio of the speeds of two rollers. Orientation can also be induced with a single roller, if its speed is higher than the exit velocity of the polymeric film, from the melt extruder die. In such cases, the draw ratio is the ratio of the chilled roller velocity and the exit velocity of the film (Sreenivas *et al.*, 2011b). For producing biaxial orientation, a tentering frame is used sideways, along with a roller

system. Clamps within the frames grab the film on its lateral edges and gradually stretch it to the final width.

Owing to the methodical variations, entirely different structures are formed during various tensile drawing processes (figure 3.12). Uniaxial drawing involves deformation of spherulitic or stratified lamellae into an extended chain structure (Peterlin, 1965). In simultaneous biax, molecular chains are pulled in either direction simultaneously; hence, poor overall orientation is developed (figure 3.12). On the contrary, sequential-biax involves development of a strong orientation in the primary drawing direction, followed by rotation of crystallites and amorphous chains towards the second drawing direction (figure 3.12) (Hinrichsen *et al*., 1981b; Ou and Cakmak, 2008). The uniaxial drawing leads to generation of unidirectional anisotropic properties, whereas biaxial orientation enhances the film properties in the longitudinal as well as the transverse direction (Ajji *et al*., 1997; Lee *et al*., 2000; Ng *et al*., 2000; Penel-Pierron *et al*., 2001)

3.8.1.2. Die drawing

The ‘die drawing’ process was originally invented by Coates and Ward (1980; 1979; 1981), as an energy efficient method, that could significantly enhance mechanical properties by reaching a higher draw ratio. In this process, the sample is heated within an oven, by dielectric means or by a brief localised contact with a heated plate (Kamezawa *et al.*, 1979). The softened sample is then pulled through a conical die, leading to orientation of polymer chains in the drawing direction. The sample can assume various shapes such as rods, tubes, sheets or monofilament, depending on the initial geometry of the sample and the die geometry.

To begin with the die-drawing of rods, a billet is machined into a conical shape that fits the die and a tag that protrudes through the die exit. The very first reported die drawing process (Coates and Ward, 1979) used a die housed in an aluminium heating block. The die housing was drawn upwards using the

tensile test equipment, keeping the tag of the billet attached to the fixed grips. This assembly was later modified into stationary die housing, which had a tubular heating chamber. The billet was drawn by pulling the tag end. The latter method allowed design of a continuous process (Morath *et al.*, 1993).

Coates *et al.* (1979; 1981) described the advantages of die drawing over conventional processes as follows:

1. A rise in the polymer density due to initial compression inside the die followed by a slow drop in the density, paralleled with the drawing process ensures that the polymer can be drawn to a significantly higher draw ratio.
2. A higher draw ratio results into a greater production rate.
3. Lower loads are needed to pull the material through a die than pushing it, as in the case of hydrostatic extrusion.
4. The process can be adapted to a bigger scale, nevertheless can made continuous.

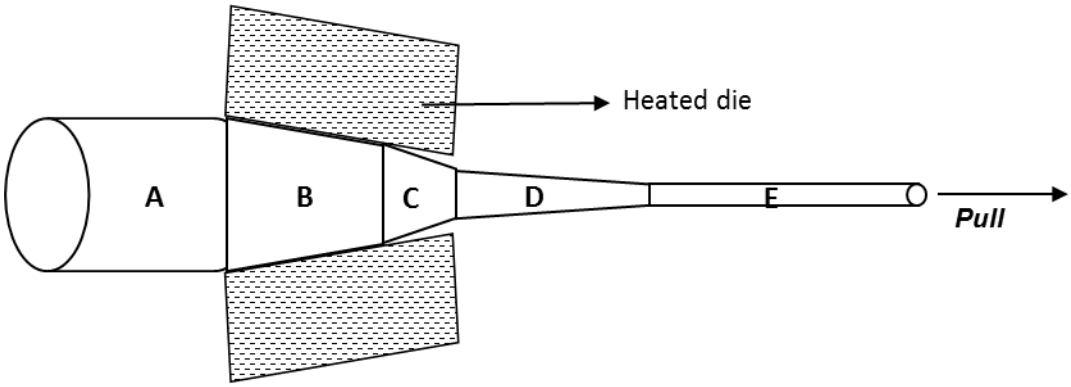

Figure 3.11: *Die-drawing of a polymer billet*

A sample undergoing die drawing can be divided into 5 different zones, as represented in figure 3.11. Region A represents an un-deformed billet, which follows the die walls as shown by region B. Depending on the strain rate and the drawing behaviour of the polymer, it may leave the die wall earlier than the exit, due to necking (region C). A change from compression to tensile extension takes place while moving from region B to C, followed by a free draw in region

D. A significant difference between the drawing within region C and region D is that the former takes place under isothermal conditions, whereas the latter takes place while the sample is cooling down. Finally, the polymer cools down below the glass transition temperature and exhibits no change in the geometry (region E). The degree of deformation imparted by the die drawing process is characterised by a 'nominal draw ratio, R_N' and an 'actual draw ratio, R_A'; Where, R_N is the ratio of the initial cross-sectional area to that at the die exit, and R_A is the ratio of the initial and final cross sectional areas of the product (Vgenopoulos, 2012).

The morphological features developed during the process of drawing depend on draw speed, draw ratio, molecular weight of the polymer, and the drawing temperature (Bigg, 1976). The drawing transforms the lamellae into microfibrils. Microfibrils from the same spherulite or the lamellar stack are bundled together into larger fibrils as the draw ratio increases (Tormala, 1992).

Die drawing of PLA has been utilised to produce biomedical devices such as pins, screws (Nordstrom *et al.*, 2001; Saikku-Backstrom *et al.*, 2000) and spiral or knitted stents (Petas *et al.*) with enhanced mechanical properties. Compounding a drug with such biomedical devices combines the advantages of higher mechanical strength with bioresorbability and controlled drug release (Tormala *et al.*, 2003).

3.8.1.3. Miscellaneous solid-state methods

A great deal of work has been done using hydrostatic extrusion as a method of polymer orientation (Mead *et al.*, 1979; Nakamura *et al.*, 2001; Nakayama and Kanetsuna, 1977; Pan *et al.*, 1987). In contrast to die drawing, extrusion involves pushing a sample through a suitable die and hence offers a better control over the final dimensions of the sample. Moreover, since hydrostatic extrusion uses compressive forces (as opposed to the tensile forces in die drawing), cavitation is avoided even at higher draw ratios. Therefore materials oriented to a higher draw ratio by hydrostatic extrusion have higher

mechanical strength than those oriented by die drawing (Mohanraj *et al.*, 2006). The properties of the extruded material depend on the extrusion rate, the extrusion temperature and the molecular weight of the polymer.

In die drawing, a visible macro neck is formed which gives rise to anisotropic transformation of the structure. Conversely, extrusion involves gradual transformation of nearly isotropic matrix into a highly anisotropic one, through formation of several invisible micro-necks throughout the matrix. In hydrostatic extrusion a fluid filled inside a pressure vessel transmits the extrusion force. Alternatively, the force can be generated directly by a piston; referred to as 'the ram extrusion'. Owing to the lubricant action of the fluid in the hydrostatic extrusion, homogenously oriented product can be produced at a lesser haul-off load as opposed to the ram extrusion (Coates and Ward, 1978).

Biaxial orientation can be achieved by extrusion of the molten polymer matrix through an annular die (Choi *et al.*, 1982; Kwack *et al.*, 1988) or alternatively by passing a softened polymer mass through rollers having separation lesser than the polymer mass thickness (Wilchinsky, 1963). The prior process is called film blowing and has been widely used in making plastic bags. The tubular mass extruded out of annular die is blown by air to form a bubble, which is then taken up by rollers in the form of double-layered film.

3.8.2. Fluid-state processes

Fluid-state processes are predominantly used for preparation of fibres. The polymer can exist in a fluid-state either as a melt or as a solution. When the molten polymer passes through a die or a spinneret onto a chilled roller, the process is called as 'the melt spinning'. The extensional flow of the melt is the principal route for orientation of the polymer chains in the spinning direction. Thermolabile polymers, which degrade at high temperature, cannot be processed using melt spinning; instead, they are spun in the solution form. A concentrated, viscous solution of a polymer is similarly passed through the

spinnerets into a heated column or an anti-solvent. Such a process is referred to as solution spinning.

3.9. Morphological developments associated with orientation of PLA

The deformation behaviour and growth of crystalline morphology in PLA matrices, during the process of orientation depends on the strain rate, draw ratio, processing temperature, molecular weight and percentage racemisation. Tensile deformation of PLA is postulated to happen in a triphasic manner (Kokturk *et al.*, 2002). At low draw ratios only the disentanglement and orientation of amorphous chains takes place in the drawing direction. This is followed by formation of a mesophase with architectural framework for further organisation. The last stage involves development of three dimensional crystalline structures. No orientation is observed if the draw rate is lower than the inverse of chain relaxation time. Nevertheless, the strain rate higher than plastic deformation limit of the crystalline region results into fragmentation of crystallites and consequent cavitation. Takagi *et al.* (2004) highlighted the correlation between strain induced crystallisation and draw ratio. Films stretched to a draw ratio 2 showed higher elongation at failure, primarily due to amorphous orientation. From draw ratio 3 onwards, strain induced crystallisation restricts further drawability of the matrix, evidenced as a fall in the elongation at failure. However this is valid only for lower drawing temperatures. At higher temperatures, thermal crystallisation predominates and even films drawn to a draw ratio of 2 show crystallisation (Wong *et al.*, 2008). Zhang *et al.* (2011) suggested that, for up to 100% deformations, orientation of amorphous phase and strain induced crystallisation occurs. During 100 - 160% deformation, critical stress is exceeded and leads to the destruction of formed crystals and cavitation. This is accompanied by the formation of new crystals from already ordered amorphous chains. This phenomenon continues until cavitation dominates the crystal growth, where the sample starts to fail.

At lower deformation temperature preferential orientation of amorphous chains is followed by strain induced crystallisation of already oriented amorphous chains. Therefore a highly oriented matrix is generated, whose crystallinity rises with the draw ratio. At higher drawing temperatures, greater chain mobility results in copious chain relaxation coupled with enhanced thermal crystallisation. Consequently, matrices with higher crystallinity and poor orientation are generated (Mulligan and Cakmak, 2005)

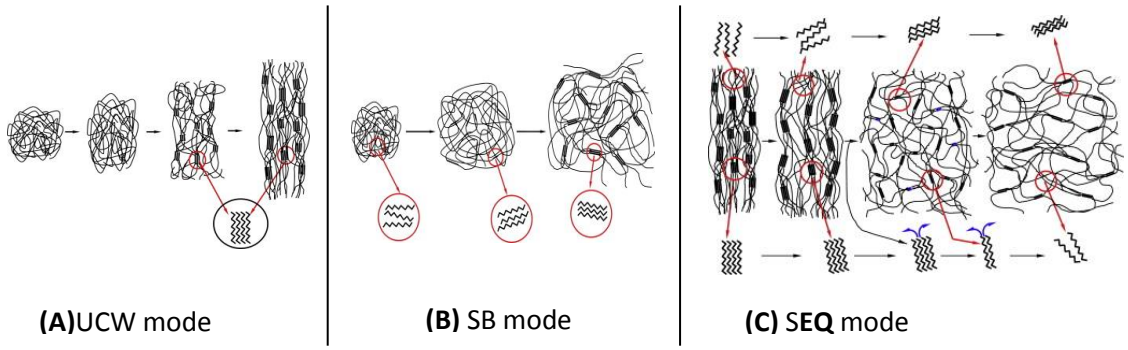

Figure 3.12: *Deformation mechanism in the uniaxial constant width and the biaxial drawing modes. (Adapted from: (Ou and Cakmak, 2008))*

The resultant morphology varies with tensile stretching modes, namely uniaxial constant width (UCW), simultaneous biaxial (SB) and sequential biaxial (SEQ) stretching (Ou and Cakmak, 2008). UCW stretching leads to orientation of polymer chains in the stretching direction (figure 3.12 - A), which is accompanied by strain induced crystallisation above a certain strain. Increase in degree of orientation and crystallinity accompanies further extension. When such a film is sequentially drawn in the transverse direction, the preliminary draw ratio plays a key role in deciding the new morphology developed. If the first drawing has achieved higher-level crystalline order due to a high draw ratio, transverse stretching leads to destruction of the existing lamellae and their restructuring into the new drawing direction (figure 3.12 - C). Whereas, if the crystalline phase in not well developed in initial drawing direction due to a lower draw ratio, simple rotation of the crystallites may occur with little damage to the

existing structure. In the SB mode, randomly distributed chains are simultaneously extended along two perpendicular axes (figure 3.12 - B). This reduces the statistical probability of the like chain interactions; consequently, a lower crystallinity is developed in the SB mode than the SEQ mode.

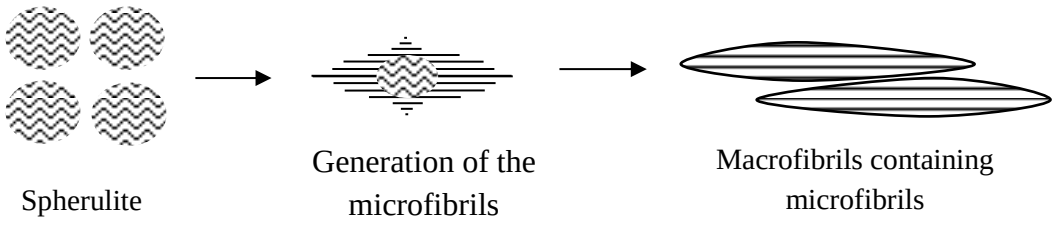

Figure 3.13: *Spherulite deformation leading to formation of macrofibrils.*

The morphological changes associated with die drawing of PLA are not comprehensively reported. However, an understanding can be developed by studying the corresponding changes associated with related polymers. Die-drawing of an amorphous polymer matrix can generate varied crystalline morphologies depending upon the draw ratio and the processing conditions. Contrarily, a crystalline matrix is gradually transformed from an isotropic structure to an anisotropic structure with respect to the draw ratio (figure 3.13). A detailed microscopic analysis of high molecular weight polyethylene (HMWPE) rods, drawn to different draw ratios, revealed the changes in crystalline structure during die-drawing (Li and Lee, 1993). Undrawn material showed the presence of spherulites. These were aligned along the drawing direction at smaller draw ratios. With a further increment in the draw ratio, the spherulitic structure disappeared and oriented sheaf-like lamellae were formed. Ultimately, at a draw ratio of about 12, plastic deformation of the lamellae led to formation of microfibrils (Ajji *et al.*, 1997; Li and Lee, 1993). Further extension would generate spindle like macro-fibrils bundled together from the individual micro-fibrils (Peterlin, 1975). The correlation between the draw ratio and oriented structure may follow a different scale for PLA. Nevertheless, formation

of the fibrillar structure, from a spherulitic initial morphology has been confirmed by several reports (Pohjonen *et al.*, 1997; Tormala, 1992; Tormala, 1993).

3.10. Methods for deliberate manipulation of PLA crystallinity

It has been extensively reported in the literature that the level of crystallinity and organisation of the crystalline phase plays a significant role in affecting drug release from PLA matrices (section 3.12). Strain induced crystallisation is an event that invariably accompanies solid state orientation of PLA and may have influence on the drug release profile of the oriented matrices. Nevertheless, crystallinity of PLA can also be manipulated deliberately by various approaches, as described below.

Crystallization of optically pure PLLA is extremely sluggish. Consequently, an amorphous polymer can be obtained by cooling from the melt, at rates as low as 5 °C/min (Salmeron Sanchez *et al*., 2007). Although no crystal growth occurs during such cooling, it generates several dormant nuclei (Yasuniwa *et al*., 2006). These subsequently lead to “cold” crystallisation of PLA if the temperature is raised above the glass transition. Pyda *et al*. (2004) confirmed that the extent of cold crystallisation can be controlled by varying the heating rate; where faster heating rates result in lower degree of crystallinity.

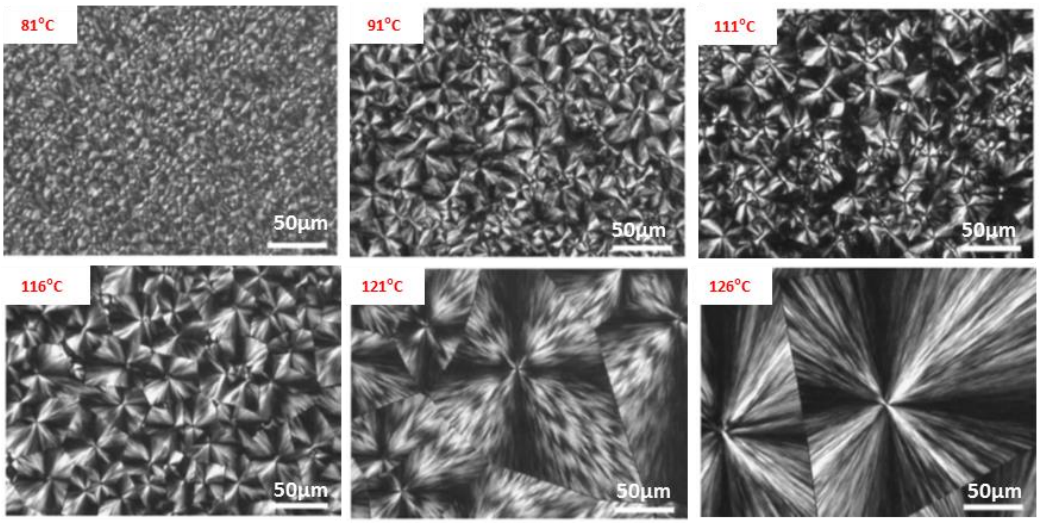

Figure 3.14: *Optical micrographs between crossed polars for samples isothermally crystallized at various temperatures (adapted from (Yasuniwa et al., 2006))*

Crystallisation of PLA from solution, melt state or isothermal crystallisation at temperatures exceeding 120 °C results in formation of the α crystalline form (Kawai *et al*., 2007). Contrarily, when isothermally crystallised at temperatures below 120 °C, generation of the α' Form has been reported (Zhang *et al*., 2006). Both the α Form and the α' Form contain -10/3 helical PLA chains that are packed into a pseudo-orthorhombic unit cell. However, the α' Form lacks secondary structural order, which makes such packing, slightly disordered (Wasanasuk and Tashiro, 2011). Isothermal crystallisation or annealing represents the easiest method to raise crystallinity of previously amorphous PLA. Due to the absence of a thermal gradient, spherulitic morphology is generated in such a crystallisation process. Here, the nucleation density decreases with temperature, while the crystal size increases (figure 3.14) (Yasuniwa *et al*., 2006).

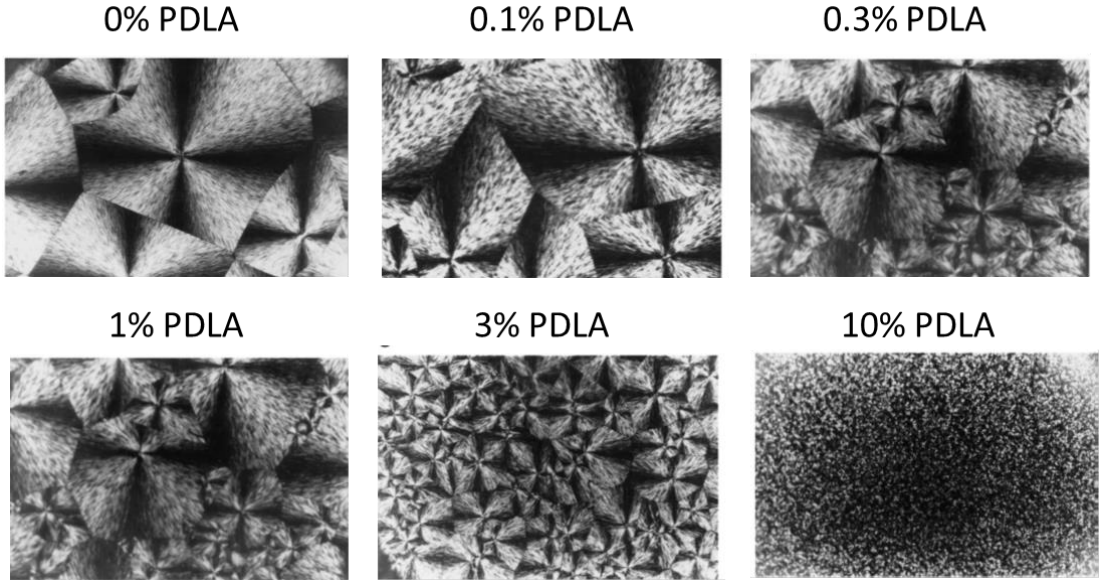

Figure 3.15: *Polarized optical photomicrographs of PLLA films containing different contents of PDLA crystallized at 135 °C (adapted from (Tsuji et al., 2006)).*

The rate of isothermal crystallisation of poly (L-lactic acid) (PLLA) and the size of spherulite can be controlled by addition of a small percentage of poly (D-lactic acid) (PDLA) (Tsuji *et al*., 2006). The PDLA forms a stereo-complex with PLLA which substantially changes the crystallisation kinetics of the latter, due to

short induction period, extremely high growth rate and greater nucleation density of stereocomplex spherulites (Tsuji and Ikada, 1996). Here the stereocomplex acts as a nucleating agent (figure 3.15).

Organic and inorganic nucleating agents have been extensively used in controlling crystallisation of PLA. Nucleating agents reduce the energy barrier for nucleation, by acting as epitaxial templates for polymer crystallization. Therefore, efficiency of nucleation depends on the epitaxial match of the polymer's crystalline unit cell with that of the nucleating agent. The organic nucleating agents for PLA include chemical nucleating agents such as sodium salts of organic acids; e.g. sodium stearate (Li and Huneault, 2007). Such nucleating agents induce scission of the ester linkages and transfer sodium cations to newly generated carboxyl end groups. This leads to formation of polymeric ionomers, which subsequently aggregate and act as nucleation templates. Nam *et al*. (2006) evidenced stronger nucleation of PLA by N-N-ethylenebis (12-hydroxystearamide) (EBHSA). Addition of 1% EBHSA enhanced nucleation density, crystallisation rate and crystallinity; contrarily, the spherulite size reduced.

Among the inorganic nucleating agents, talc is often used as a reference to compare the nucleation ability of the physical additives. Use of talc as a nucleating agent has shown almost seven fold faster crystallisation in PLA, due to 500 times higher nucleation density (Kolstad, 1996). In another study, addition of corn-starch exhibited a marked increase in crystallinity as well as crystallisation rate of PLA (Park *et al*., 1999). It was evidenced that the size of the starch granule critically influenced the level of crystallinity and crystal size in the nucleated polymer.

Crystallisation of PLA melt in the presence of a temperature gradient leads to generation of lamellar stacks instead of spherulites. Similarly, application of shear to the molten polymer can result in formation of shish-kebab crystals (section 3.7) (Xu *et al*., 2012; Yamazaki *et al*., 2010). In the presence of an

extensional flow (e.g. injection moulding) the polymer chains stretched along the flow direction nucleate into the shish strands, while the relaxed chains crystallise as lateral outgrowths (kebabs).

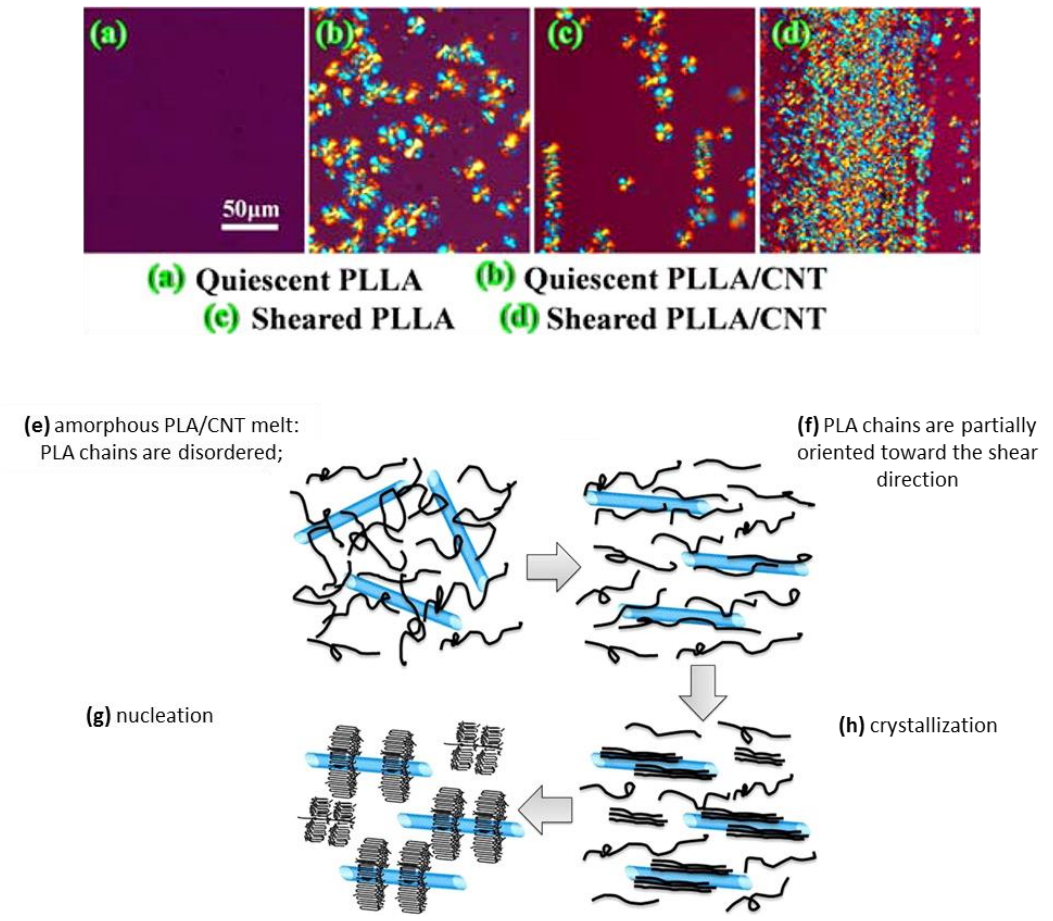

Figure 3.16: *Enhanced shear-induced crystallization caused by CNTs in PLA melt (adapted from (Tang et al., 2012))*

Generation of the shish-kebab morphology is challenging in the case of PLA due to its semi-rigid backbone and short chain length. This results in breakdown of the shear induced nuclei into random coils once the application of shear ceases. Xu *et al*. (2012) successfully generated shish-kebab crystals in injection moulded PLA by utilisation of the oscillation shear injection moulding (OSIM) machine. This machine imposes very high shear flow on molten PLLA in the mould cavity by reciprocal movement of two pistons during the packing stage. The authors confirmed the diameter of shish-kebab PLA crystals to be

around 0.7 μm, with a long period of ~20 nm. Such arrangement further contained the α crystalline form of PLA. Tang *et al*. (2012) generated shish-kebab PLA crystals by adding carbon nanotubes (CNTs) to the sheared PLA melt during injection moulding. The CNTs were thought to provide an anchoring surface for the extended set of PLA nuclei and prevent their relaxation (figure 3.16).

3.11. Effect of orientation on physical properties of polymers

The process of orientation leads to restructuring of a polymer such that anisotropic properties are developed. The most prominent effect of polymer orientation is improvement of mechanical strength (Baji *et al*., 2010; Bigg, 1976). Mechanical properties of films can be augmented in a single or two directions, by uniaxial or biaxial drawing respectively (Yu *et al.*, 2008). Another orientation induced dynamic change that has tremendous industrial significance is improved barrier properties. Decreased gas/ water vapour permeability due to orientation can be attributed to densification of the barrier phase of the polymer matrix (Liu *et al.*, 2002). For example, chain orientation in PET is accompanied by a transformation from the 'Gauche' to the 'Trans' conformation. When in 'Trans' conformation, polymer chains are densely packed; hence have reduced permeability. Additionally, strain induced crystallisation, that accompanies the orientation process can also enhance the barrier properties, owing to the reduced gas/vapour solubility of the crystalline phase. For similar reasons, solid-state orientation also reduces the biodegradability of a polymer (Lee *et al.*, 1997). Cia *et al.* (1996) evidenced diminished susceptibility of PLA to enzymatic degradation, when subjected to orientation. To sum up, there are several prominent changes in the properties oriented polymers. This suggests a possibility of engineering drug release by polymer orientation.

3.12. Correlation between the polymer crystallinity and drug release

Solid-state orientation of PLA is usually associated with a rise in the crystallinity of the polymer matrix. Therefore, the effect of crystallinity on drug

release must be known, for better comprehension of the effect of orientation on drug release from the PLA matrices. Release of a bioactive agent from a semicrystalline polymer depends on the volume fraction of the amorphous and the crystalline phases, their organisation, cross-linking density and size of the solute (Barrer, 1957). Here, the crystalline phase act as physical cross-links, thereby altering the space distribution of the amorphous phase. Since water permeation and drug diffusion occurs through the amorphous phase, a change in its distribution further changes the transport properties of the matrix (Barrer, 1957). In such cases, diffusion of a drug may still be treated as Fickian with the effective diffusion coefficient $\mathbf{D_{im}}$ defined as $\mathbf{D_{im} = AD/B.}$ Where D is the diffusion coefficient in a completely amorphous polymer, A is the “detour ratio” which accounts for reduction in solute mobility due to the tortuosity of diffusion paths between crystallites, and B relates to the density of the crystalline cross-links (Peterlin, 1979).

Since drug release from PLA/PLGA significantly varies with the polymer molecular weight, pH of the bathing fluid and physico-chemical properties of the incorporated drug; there are varied opinions in the literature, regarding the overall effect of crystallinity on drug release from such matrices.

While studying release of progesterone from PLA microspheres, Izumikawa *et al.* (1991) observed that the amorphous spheres released the drug less rapidly than the crystalline spheres. Authors correlated this to the bulk interactions between the drug and the polymer matrix. Lower polymer crystallinity suggests better drug dispersion and increased drug–polymer interactions, consequently resulting into slower drug release. Withstanding the above explanation, Hurrel *et al. (2002)* observed higher burst release from annealed and slow crystallised PGA films than that from quenched films. They attributed it to exclusion of the drug from the crystalline phase, which creates a supersaturated amorphous phase, resulting in partitioning of the drug towards the surface. However, drug release in the later stages was independent of the

initial crystallinity. Upon permeation of water, the hydrolysed polymer chains undergo insertion crystallisation. Owing to this, all the matrices reached nearly the same crystallinity by the end of 10 days. Therefore, the mass loss profile was same for all the matrices, irrespective of the initial crystallinity, which further resulted into the same drug release profile.

In another study, Miyajima *et al.* (1997) observed faster initial drug release from crystalline PLA films than amorphous films. For PLA of molecular weight 4000 g/mol, drug release from the crystallised films was monophasic and followed the Higuchi diffusion model. On the contrary, quenched films showed extremely slow initial release superimposed with a rise in the crystallinity. This was subsequently followed by a faster release phase (Miyajima *et al.*, 1997).

Tsuji *et al.* published a series of papers discussing the effect of initial crystallinity, crystalline thickness and spherulite size on hydrolytic degradation of higher molecular weight (13,00,000 g/mol) PLLA (Tsuji and Ikada, 1998; Tsuji and Ikada, 2000b; Tsuji *et al.*, 2000). For the first time they observed PLLA degradation by surface erosion, when the *in vitro* pH was 10. Under such conditions, the rate of weight loss per unit surface area decreased linearly with the rise in the initial crystallinity of PLLA film (Tsuji and Ikada, 1998). When the *in vitro* pH was changed to a near neutral pH (7.4), the degradation occurred by the bulk erosion mechanism. For matrices undergoing homogenous bulk erosion, Tsuji *et al.* (2000b) observed a lag until the weight loss began. The length of the lag phase increased as the crystallinity decreased. The overall rate of weight loss was higher for the matrices having higher initial crystallinity. The size of spherulites had no influence on the hydrolysis rate of PLLA in either types of release mechanisms (Tsuji and Ikada, 1998). The characteristics of PLA degradation were also reflected in the drug release profiles obtained by several other authors (Frank *et al.*, 2005; Hurrell and Cameron, 2001a; Hurrell and Cameron, 2002; Zilberman, 2005).

3.13. The effect of solid-state polymer orientation on drug release

The exact effect of polymer orientation on the release of a bioactive agent can vary between reservoir and matrix systems. It is well understood that the oriented films have enhanced barrier properties (Lee *et al.*, 2000; Liu *et al.*, 2002). Therefore, a highly oriented membrane can retard drug release from a reservoir type of system. The only reported example of this is the use of a biaxially oriented, heat shrinkable, rate controlling membrane by Higuchi *et al.* (1973b) for making slower release reservoir systems.

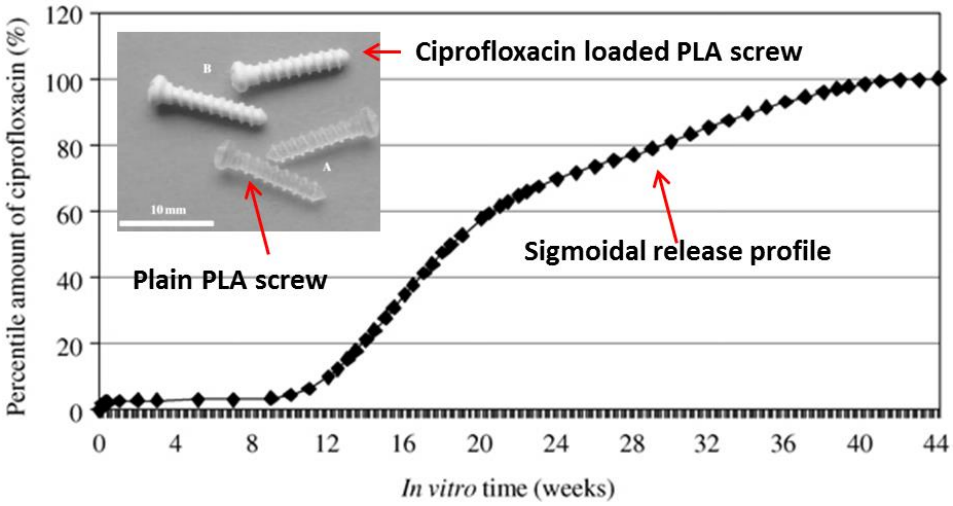

Figure 3.17: *Cumulative release profile of ciprofloxacin from the reinforced PLA screws (adapted from (Veiranto et al., 2002))*

The situation is poorly understood in the case of matrix type systems, since both diffusion and erosion mechanisms shape drug release. Tormala *et al.* (2009; 2008; 2002) have done the pioneering work in examining drug release from the solid-state oriented matrix type systems. The only three reports available in the literature are from the same research group. Amongst them, Veiranto *et al.* (2002) explored delivery of ciprofloxacin to an infected bone through a fixation screw. The screw was manufactured by co-extrusion of ciprofloxacin and PLA into a rod, which was then reinforced by die drawing. The rod was finally machined into the screw geometry. The screw showed complete

drug release within 44 weeks, *in vitro*. The release profile was sigmoidal (figure 3.17) with initial sluggish drug release until the 8th week. Thereafter, drug release was accelerated for a few weeks, finally reaching a plateau. Tormala *et al*. (2008) described use of polymer orientation as a method of enhancing drug release from a bioresorbable polymer matrix like PLA. Any process where a drug is compounded with the polymer and the composite matrix is then drawn at temperatures above Tg was believed to accelerate the drug release (figure 3.18). Nikkola *et al*. (2009) suggested a novel approach of controlling drug release by hot-compressing a melt-extruded, a die-drawn and a radiation sterilised billet to form a composite billet. The drug release profile of the composite matrix was a combination of drug release from the individual components.

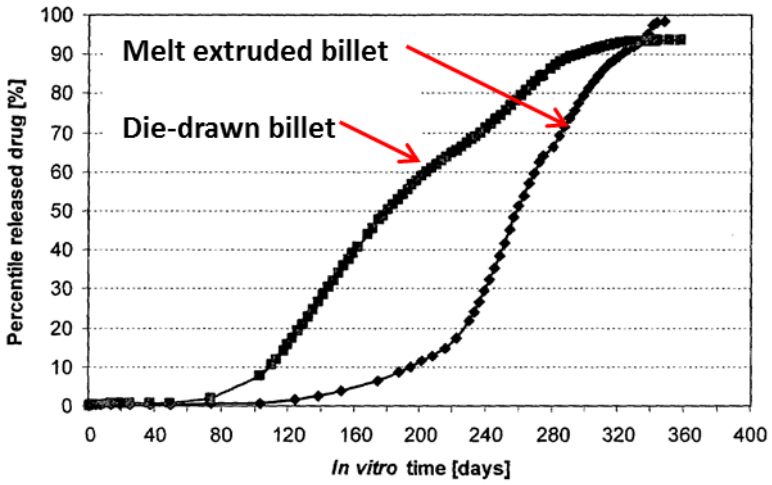

Figure 3.18: *Acceleration of drug release after solid-state orientation (Tormala et al., 2008)*

Available literature mentioning the effect of polymer orientation on drug release is inadequate, since no attempts have been made to understand the mechanism by which polymer orientation may affect drug release. Moreover, the effect of different degrees of orientation has not been studied. Orientation of polymer leads to development of anisotropic or directionally dependent

properties. Consequently, drug release in the direction parallel to polymer chain orientation can be different from that in the perpendicular direction. Previous reports have failed to characterise this phenomenon and have considered drug release as a bulk property. Importantly, a role played by the physical and the polymorphic state of a drug in affecting polymer orientation and resultant drug release profile has not been considered. The aim of this study is to address these limitations and construct a fuller picture about drug release from oriented matrices.

4. Materials and methods

4.1. Materials

Natureworks PLA, grade 4043D was procured through Resinex, UK. The weight-average molecular weight determined by GPC was 133 000 g/mol. The D-isomer content was approximately 2% w/w of the polymer (Mulligan and Cakmak, 2005). The resin has a melting temperature of 155 °C, crystallisation temperature between 100 – 120 °C and glass transition around 58 °C. This was also confirmed through DSC. Theophylline (Molecular weight (mol. wt.) = 180.17 $g.mol^{-1}$, batch no. - TAM-V/110316, Purity ≥ 99%) was supplied by KORES (India) Ltd. Mumbai, India. It has melting point (MP) of 273 °C, however starts degrading above 230 °C. Curcumin (Mol. wt. = 368.38 $g.mol^{-1}$, Batch no. ASB-00003927-101) was purchased from ChromaDex, USA (supplied through LGC stands, UK). The certificate of analysis stated the purity and melting point to be 99.7% and 183 °C respectively.

Other model compounds namely, paracetamol (Mol. wt. = 151.16 $g.mol^{-1}$, MP = 169 °C, Purity ≥ 99%); aspirin (Mol. wt. = 180.16 $g.mol^{-1}$, MP = 136 °C, Purity ≥ 99.5%); caffeine (Mol. wt. = 194.19 $g.mol^{-1}$, MP = 235 °C, Purity ≥ 98.5%), nicotinamide (Mol. wt. =122.12 $g.mol^{-1}$, MP = 128 °C, Purity ≥ 98.5%), citric acid (Mol. wt. = 192.12 $g.mol^{-1}$, MP = 153 °C, Purity ≥ 99.5%), and ascorbic acid (Mol. wt. =176.12 $g.mol^{-1}$, MP = 190 °C, Purity ≥ 98%) were purchased from Sigma-Aldrich, UK; whereas, sodium salicylate (Mol. wt. =160.10 $g.mol^{-1}$, MP > 300 °C , Purity ≥ 99.5%) was purchased from Alfa Aesar.

- **SECTION A: PROCESSING TECHNIQUES**

4.2. Extrusion compounding of PLA with model drugs

Twin screw extrusion was used as a scalable blending method in the current study (Manas-Zloczower, 2012). The polymer and the model drugs (shortlisted after thermo-gravimetric screening) were dried using a vacuum oven

set at 80 °C for 4 hours, immediately before processing. Since PLA was available as pellets and the model drugs were powders, dry blending prior to extrusion was not feasible. Therefore, 5% w/w mixtures of the model drugs with PLA were prepared by the following method.

The Drug and the polymer were fed to the extruder using two different feeders, set to operate at different feeding rates. A Movacolor MC Micro12 feeder was used for the model drugs; whereas, A Brabender DDW-MD0-RT-1.5 gravimetric feeder was used for the PLA pellets. The Movacolor MC Micro12 was set to operate at 5% gravimetric output of the Brabender DDW-MD0-RT-1.5. Both feeders were calibrated before every compounding operation. Melt extrusion was carried out using a 'Thermo Scientific Pharmalab 16' twin-screw extruder having 16 mm barrel bore diameter, 40:1 barrel length to diameter ratio and 15.6 mm screw diameter. The screw configuration and the temperature profile were set as listed in table 4.1 (Kulkarni, 2013). The extruder was operated at a screw speed of 80 rpm.

Table 4.1: *The screw configuration and the temperature profile used in the twin screw extruder, during melt compounding*

Approximate zones	**Feeding**	**2**	**3**	**4**	**5**	**6**	**7**	**8**			**9**		**10**		**Die**
Temperature (°C)	25	45	77	100	125	150	170	180			180		180		180
Screw element type	C	C	C	C	C	C	C	M30	M60	M90	M90	C	C	D	-
L/D (total = 40)	4	4	4	4	4	4	4	2.25	1.25	0.5	0.5	3.5	2.5	1.5	-

*(C = conveying element, D = discharge element, M30 = mixing element arranged at 30° to the previous element, M60 = mixing element arranged at 60° to the previous element, M90 = mixing element arranged at 90° to the previous element)

Neat PLA was extruded in a similar fashion in order to evaluate the effect of melt compounding on the virgin polymer itself. Moreover, to verify the efficiency of the melt compounding operation, samples were withdrawn at

regular intervals during the extrusion process (n = 6 /hour). The withdrawn samples were dissolved separately in 2:1 - acetone: chloroform, followed by drug assay using High Performance Liquid Chromatography (HPLC) *(The HPLC methods are separately reported in the drug release studies section).

4.3. Extrusion of the neat and the drug loaded PLA films

The neat and the drug loaded PLA films were prepared by the sheet extrusion technique, utilising a single screw extruder. The details of the extrusion process are displayed in the table 4.2.

Table 4.2: *Details of the film extrusion process*

Instrument details		Dr. Collins Teach-Line E20T	**Temperature profile**	45 °C, 110 °C, 160 °C, 170 °C and 170 °C for the feed throat, the compression zone, the metering zone, the adapter and the die respectively
1	**Screw diameter (mm)**	20	**Screw speed**	50 rpm
2	**Screw length (L/D)**	25	**Take up roll temperature**	50 °C
3	**Width of the slot die (mm)**	100	**Take up roll speed**	0.5 metres/minute
4	**Die gap (mm)**	*variable - 0.2/0.4/0.6/0.8	**Distance between the die exist and the take up roll**	150 mm

In brief, the polymeric material (virgin polymer or drug loaded extrudates) was dried in a vacuum oven (80 °C for 4 hours), immediately prior to extrusion and transferred directly to the extruder hopper. The extruder hopper was continuously purged with dry nitrogen during the extrusion process, in order to minimise moisture absorption. A cast sheet was extruded through the single screw extruder, equipped with a slit die. The die gap was adjusted to produce drug loaded PLA films with different thicknesses (0.2 mm, 0.4 mm, 0.6 mm, and 0.8 mm). The initial thicknesses of the films were selected such that the final thickness after tensile stretching remained constant (0.2 mm). The temperature

profile and the screw speed were set as listed in table 4.2. The temperature of the uptake roller and its distance from the die exit were decided based on preliminary trials to produce uniform films. The speed of the uptake roll was kept equivalent to the exit velocity of the polymer sheet from the slit die. This was necessary to minimise orientation in the extruded films (Sreenivas *et al.*, 2011a).

4.4. Solid-state orientation of PLA films

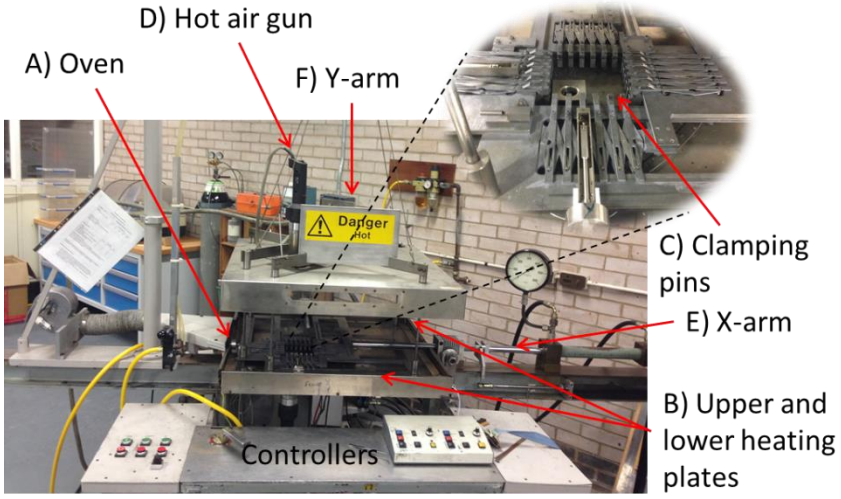

Figure 4.1: *The long stretcher used for orientation of PLA films.*
A) Oven, **B)** Upper and lower oven plates, **C)** Clamping pins, **D)** Heat gun, **E)** X-arm of the stretcher and **F)** Y-arm of the stretcher.

Neat and drug loaded PLA films were oriented using a T.M. Long biaxial film stretcher (figure 4.1). A square sample (60 mm X 60 mm) was cut from the extruded sheets. The sample was gripped from all sides by means of the clamping pins within the stretcher. Temperature of the oven (the upper and the lower plate) was set to a desired value (table 4.3). Hot air, having the same temperature as that of the oven plates was blown at the sample for 120 seconds from the heat guns positioned above and below the sample. The softened sample was extended at a previously decided strain rate (table 4.3), to a desired draw ratio (eqn. 4.1) by pneumatic movement of the X and Y arms of the stretcher. Details of the oven temperatures, strain rates and the draw ratio

are discussed below. On complete extension, the oven was opened and the sample was allowed to cool before it was removed from the clamps.

$$\text{Draw ratio} = \lambda = \frac{\text{Final length along a fixed axis (X or Y)}}{\text{Original length along the same axis}} \qquad \textbf{(Equation 4.1)}$$

The experiments focussed on orientation of the PLA films were divided in two stages. In the first stage, 30 different samples of the oriented films were prepared each from neat extruded PLA films as well as from those containing 5% w/w theophylline or 5% w/w curcumin. This was achieved by varying the oven temperature, strain rate, stretching direction and the draw ratio, as summarised in table 4.3. These samples were utilised for studying the effect of orientation process variables on organisation of the amorphous-crystalline domains (structure) within the resultant films. For simplification of this study, films with single initial thickness (0.6 mm) were used.

Table 4.3: *Summary of different variables used in orientation of the PLA films*

Batch no.	Mode of orientation	Variable 1 Oven temperature	Variable 2 Strain rate	Variable 3 draw ratio (λ)	Total samples	Parameter studied
1	UCW	70 °C, 80 °C, 90 °C	0.12 sec^{-1}, 0.57 sec^{-1}, 1.2 sec^{-1}	3X1Y **(constant)**	3 x 3 = 9	Effect of temperature and strain rate - 3^2factorial
2	SB	70 °C, 80 °C, 90 °C	0.12 sec^{-1}, 0.57 sec^{-1}, 1.2 sec^{-1}	2X2Y **(constant)**	3 x 3 = 9	
3	SEQ	80 °C **(constant)**	0.57 sec^{-1} **(constant)**	2X2Y, 3X3Y, 2X3Y, 3X2Y, 2X4Y, 4X2Y	6	Effect of sequential stretching
4	UCW	80 °C **(constant)**	0.57 sec^{-1} **(constant)**	2X1Y, 3X1Y, 4X1Y, 5X1Y	4	Effect of uniaxial and biaxial draw ratio
5	SB	80 °C **(constant)**	0.57 sec^{-1} **(constant)**	2X2Y, 3X3Y	2	
6	Un-oriented	80 °C	-	1X1Y	1	-
Total					30 + 1	

*(X and Y indicates primary and secondary drawing axis respectively, therefore associated numbers indicates the strain along that axis. E.g. 3X1Y means stretched to thrice of the original length along X-axis, keeping the width constant).

The correlation between the oriented structure and the draw ratio was studied in uniaxial and biaxial stretching mode. The uniaxial mode was restricted to constant width drawing (UCW), where the samples were stretched lengthwise, without allowing any change in their width (figure 4.2 - A). Biaxial drawing involved stretching the films either simultaneously along the length and the width (simultaneous biaxial -SB) (figure 4.2 - B) or stretching them in a single direction at first, followed by stretching in the second direction (sequential biaxial - SEQ) (figure 4.2 - C). Samples up to a draw ratio of 5X were prepared in the UCW mode; while for the SB and the SEQ mode, samples stretched along both the axes to twice and thrice the original dimensions were prepared. Moreover, samples with a varied degree of extension along the X and Y axis were produced using the SEQ mode (table 4.3, figure 4.2). These included 2X3Y, 3X2Y, 2X4Y and 4X2Y; where X-axis represents the first drawing direction, while Y-axis represents the second drawing direction. All of these samples were oriented at 80 °C, using 0.57 sec^{-1} strain rate.

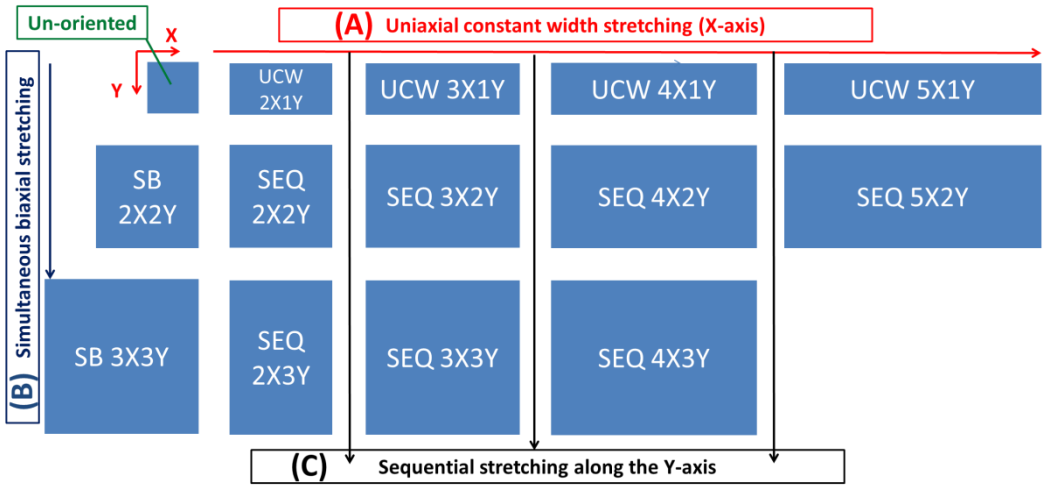

Figure 4.2: *Orientation of PLA films using different stretching modes*

The effect of drawing temperature and strain rate on the resultant oriented structure was studied in UCW and the SB modes (table 4.3). For each of these modes, three temperatures (70 °C, 80 °C and 90 °C), and three strain rates

(0.12 sec^{-1}, 0.57 sec^{-1} and 1.2 sec^{-1}) were studied. The UCW samples were stretched to a constant draw ratio of 3X; while, the SB samples were extended along two perpendicular axes to twice its original length and width (λ = 2X2Y).

The second stage of the film orientation experiments was focussed on drug release testing. Based on the stage 1 results, UCW films with uniaxial draw ratios between 1X – 4X, and SB and SEQ films with the biaxial draw ratio of 2X2Y were selected for the drug release studies. Variable thickness of the oriented films may present a challenge in quantification of the effect of orientation on polymer degradation and drug release. Moreover, such films have different drug content per unit surface area, which will in turn affect the concentration gradient. In order to minimise an influence of these variables, films utilised in drug release and related characterisations were prepared from the extruded films with different initial thickness, such that the oriented films will have a constant thickness (0.2 mm).

4.5. Extrusion moulding of rods

PLA rods containing 5% w/w paracetamol were prepared by single screw extrusion using a Dr. Collin Teachline E20T extruder, equipped with a billet mould containing four cylindrical cavities (figure 4.3 - C). The diameter and the length to diameter ratio of the extruder screw were 20 mm and 25 L/D respectively; whereas the length and the diameter of the mould cavities were 160 mm and 14 mm respectively. Each cavity contained a plunger (figure 4.3 - D) which moves towards the rear end, as the polymer melt is filled in the mould cavities. The mould was attached to the extruder in a vertical position by means of an adapter (figure 4.3 - B). The adapter served to change the flow direction of polymer melt from horizontal in the extruder to vertical in the mould. Both adapter and the mould were heated by external band heaters, controlled by Eurotherm® temperature controllers.

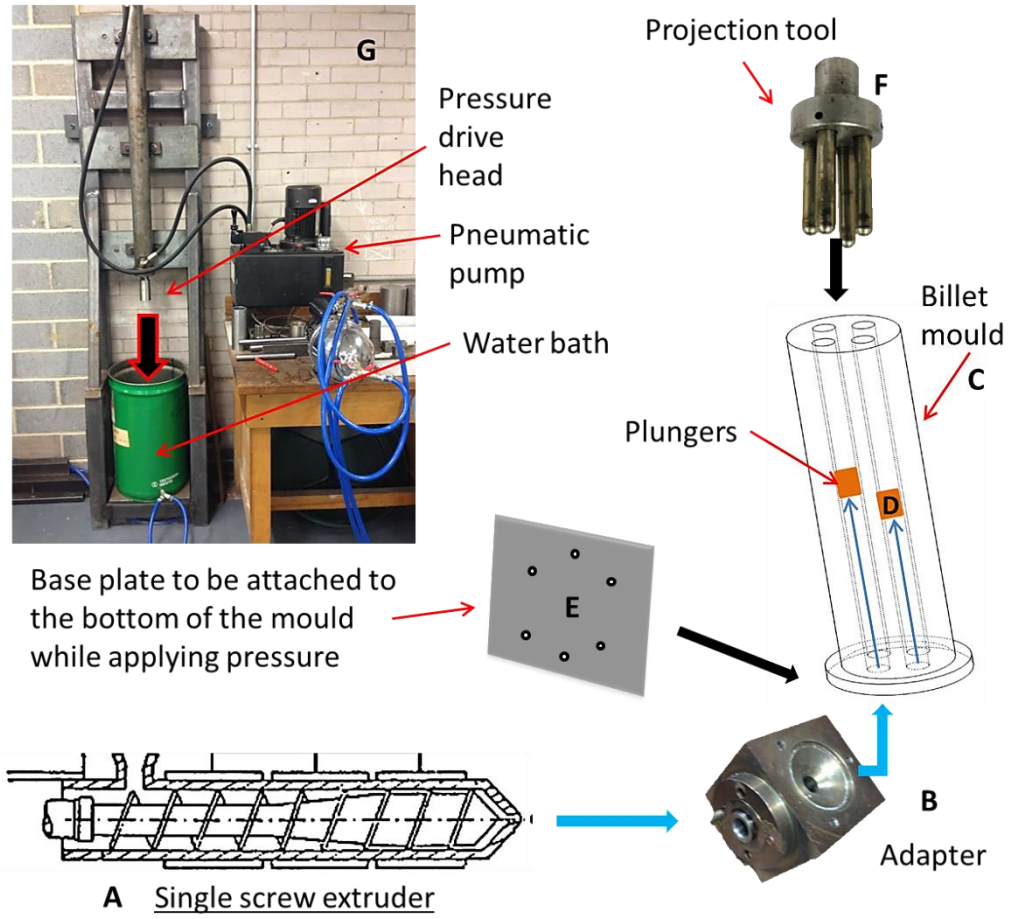

Figure 4.3: *Billet manufacturing assembly.*

A) Single-screw extruder, **B)** Adapter, **C)** Billet mould, **D)** Plungers, **E)** Base plate, **F)** Projection tool, **G)** Pneumatic device used for applying pressure. *(blue arrows indicate polymer flow).

The PLA extrudates previously compounded with 5% w/w paracetamol were dried in a vacuum oven at 45 °C for 24 hours, immediately prior to extrusion and filled into the extruder hopper covered with dry nitrogen blanket. The temperature profile of the extruder was set to 45 °C, 110 °C, 160 °C, 170 °C and 170 °C for feed throat, compression zone, metering zone, adapter and the mould respectively. The screw speed was 50 rpm. All four cylindrical cavities of the mould were allowed to fill completely with the polymer melt containing paracetamol. This was indicated by the movement of all four plungers to the top end of the mould. Following this, the mould was removed from the extruder and the base plate (figure 4.3 - E) was rapidly screwed to the bottom end that was previously connected to the adapter. A tool shown in figure

4.3 - F was placed on the top end of the die, such that each projection lay on the plunger in each of the cylindrical cavity. The assembly was placed in an empty water bath and a pneumatic pressure of about 13.79 MPa was applied from the top end using the instrument (figure 4.3 - G) built in house. This step prevents formation of voids if the polymer undergoes shrinkage while cooling. The water bath was slowly filled with cold water and the die assembly was allowed to cool. Finally, the water bath was emptied, the pressure was released, and the billets were removed.

4.6. Orientation of rods by die drawing

4.6.1. The apparatus

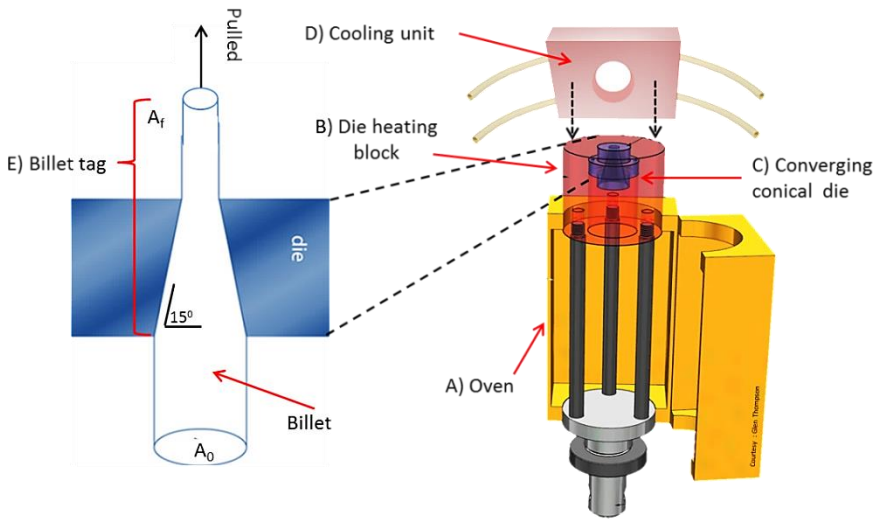

Figure 4.4: *Die drawing rig used for orientation of PLA rods*

The die-drawing rig (figure 4.4) designed and manufactured at the University of Bradford was utilised for unidirectional orientation of paracetamol loaded rods. The apparatus comprised of an aluminium oven (figure 4.4 - A), a die heating block (figure 4.4 - B) and a converging conical die (figure 4.4 - C) with a wall angle of 15°. The diameter of the broader end of the die cavity was 15 mm, while that of the narrower end was 6.25 mm. The die had additional 2 mm long section with the fixed diameter of 6.25 mm (parallel walls) at the narrower end. The aluminium oven was heated by blowing hot air (30 litres per

minute) through a heating element placed at the back of the oven. The temperature of the die heating block was elevated by band heaters. The air temperature within the oven was monitored by two independent thermocouples placed at the top and the bottom of the oven. The entire assembly was mounted on a Messphysik BETA 20-7, 5/8 x 18 universal (tensile) testing machine.

4.6.2. The method

From a drug release studies perspective, it was important to have oriented rods with different draw ratios, but the same diameter. This was achieved by machining the extruded billets to different initial diameters, such that drawing them through the 6.25 mm conical die will produce rods with varied draw ratios but having a constant final diameter. The draw ratio in the case of rods is given by equation 4.2. Preliminary trials revealed that the necking behaviour (sec 3.8.1.2) resulted in the final rod diameter of 6 mm, when the mentioned billets were die-drawn at 40 mm/min crosshead speed. Therefore the initial diameters calculated using equation 4.2 were 6 mm, 8.48 mm, 10.4 mm, 12 mm and 13.4 mm for the draw ratios in an order from 1 to 5 respectively.

$$\lambda_r = \frac{A_0}{A_f} \qquad \textbf{(Equation 4.2)}$$

Where, $\boldsymbol{\lambda_r}$ is the draw ratio of a drawn billet, $\mathbf{A_0}$ is the initial cross sectional area of the undrawn billet and $\mathbf{A_f}$ is the final cross sectional area of the drawn billet.

A tag (diameter = 6 mm, parallel length = 18 mm, inclined length = 10 mm, inclination = 15°) (figure 4.4 - E) was machined onto every billet. A hole was drilled at the centre of the rear end of the billet for inserting a thermocouple. The billet was placed in the oven such that the tag will protrude through the die exit and can be held between the grips attached to the cross-head of Messphysik. The oven controller temperature was set to 85 °C which resulted in the oven air temperature and the billet temperature of 70 °C, when incubated for appropriate time as per the thickness of the billet. The incubation times were 3 minutes, 5

minutes, 8 minutes and 10 minutes for the billets oriented to draw ratio 2, 3, 4 and 5 respectively (thicknesses 6 mm, 8.48 mm, 10.4 mm, 12 mm and 13.4 mm respectively). The die temperature was adjusted to 75 °C.

When the billet temperature reached 70 °C, it was pulled through the die by moving the crosshead of the tensometer. The pulling regime was divided into two stages. In the first stage the tag was pulled out slowly. The crosshead speed was increased from 1.25 mm/min to 10 mm/min in 4 steps. Each step was executed when the load achieved a plateau in the load vs extension curve. The rod exiting from the die was constantly sprayed with FRE 400 refrigerant spray in order to prevent excessive necking. Once the entire tag was pulled out of the die, the process was halted and the section pulled out was re-clamped. In the second stage, the speed was increased from 1.25 mm/min to 40 mm/min in 6 steps, in a manner similar to tag pulling. No freeze spray was used in the second stage; instead, cooling was provided 10 mm above the die exit by circulating cold water through the assembly shown in figure 4.4 - D.

- **SECTION B: CHARACTERISATION TECHNIQUES**

4.7. Thermal characterisation of the pure model drugs and the polymer

4.7.1. Thermo-gravimetric analysis

Thermal stability of virgin PLA and the model drugs listed in the materials section was assessed through thermo-gravimetric analysis (Barbooti and Al-Sammerrai, 1986; Ribeiro *et al.*, 1996), using a TA instruments TGA Q5000 (V3.13 Build 261). Approximately 5 mg of each sample was loaded onto the aluminium pans. Two different experiments were performed; namely, temperature ramp TGA and isothermal TGA. In the prior, a ramp rate of 10 °C/min was used for heating the sample from 25 °C to 250 °C; whereas, in the latter, the samples were heated at the rate of 30 °C/min to 180 °C and held isothermal for 30 minutes. The sample was maintained under dry nitrogen

blanket during the experiment. TA Universal analysis 2000® and Microsoft Excel® 2010 were used for data analysis.

4.7.2. Differential scanning calorimetry (DSC)

Melting points and the glass transition behaviour of the individual model drugs and their melt extruded mixtures with PLA were measured using a TA Instruments Q2000 differential scanning calorimeter (with RSC90 cooling unit). Approximately 5 mg of the sample was loaded on standard aluminium pans and the aluminium lid was crimped over it. A ramp rate of 10 °C/min was selected for heating from 0 °C to 300 °C in the case of theophylline and sodium salicylate and 30 °C to 250 °C for the rest of the model drugs. TA Universal analysis 2000® along with Microsoft Excel® 2010 was used for data analysis.

4.8. Assessment of polymorphic changes in the model drugs after thermal treatment.

In order to evaluate polymorphic changes during melt extrusion, the pure model drugs (further utilised for drug release studies) were subjected to a temperature regime similar to melt extrusion. The powdered forms of the model drugs (as supplied by the manufacturer) were placed in a crucible and equilibrated at 180 °C for 15 minutes in a vacuum oven. The crucibles were cooled rapidly by quenching in dry ice. The resultant material along with unprocessed pure drugs and melt compounded drug - PLA extrudates were further characterised by infra-red spectroscopy (Salari and Young, 1998), x-ray diffractometry (Seton *et al.*, 2010) and hot stage microscopy (Sanphui, 2012).

4.8.1. Fourier Transform Infrared spectroscopy (FTIR)

The IR spectra of the pure, heat treated and the melt compounded forms of the model drugs were collected by a Perkin-Elmer Spectrum 100 spectrophotometer, equipped with a standard deuterium triglycinesulfate (DTGS) detector and a single reflection diamond/ ZnSe universal ATR (attenuated total reflectance) accessory. The samples were directly placed on

the ATR crystal and pressure was applied using the applicator accessory, to ensure intimate contact between the crystal and the sample. Five scans were performed in the wavenumber range 4000 cm^{-1} to 650 cm^{-1},for each sample (Qi *et al.*, 2008; Seton *et al.*, 2010). All measurements were performed in triplicate. The raw spectra were further processed using Thermo-scientific Grams® AI software. (The same method was used for obtaining the FTIR spectra of the oriented films).

4.8.2. Powder X-ray diffractometry

X-ray diffractograms of the pure model drugs and their heat treated forms were acquired using a Bruker D8 X-ray powder diffractometer. The instrument used a Cu Kα radiation source (40 kV voltage and a filament emission of 40 mA) producing an X-ray wavelength of 1.54 Å. The receiving and the scatter slits were 1° and 0.2° respectively. Samples were placed on low background silicon holders and were scanned between 2 - 30° (2θ), in 0.01° increments, with a scanning speed equivalent to the step width per second. The melt compounded material was hot - compressed into thin films and analysed by the Wide Angle X-ray Diffraction (WAXD) technique described in the section 4.13.

4.8.3. Hot stage microscopy

The solubility status of the shortlisted model drugs in the PLA matrix was visualised using a Zeiss Axioplan-2 microscope equipped with an AxioCam MRc5 CCD camera and a Linkam 44 hot stage (THMS600) (Tadworth, UK). The drug loaded PLA extrudates obtained from melt compounding were sectioned (approximately 50 µm thick), using a Leica RM2265 rotary microtome. The sections were heated from 25 °C to 180 °C, with an underlying heating rate of 30 °C/min and held isothermally for 15 minutes. This was followed by cooling back to 25 °C at a rate of 30 °C/min. The images of all three stages; namely, pre-heating (50 °C), isothermal stage (180 °C) and post cooling stage (50 °C) were captured by the CCD camera, using Axiovision (4.5) software.

4.9. Rheological testing

Rheological behaviour of virgin PLA, neat extruded PLA and the extruded mixtures with curcumin, paracetamol, theophylline and sodium salicylate was investigated on an Anton Paar Physica MCR 501 rheometer. All the systems were studied in oscillation mode, using a strain amplitude sweep, frequency sweep and time sweep experiments. A parallel plate geometry with plate diameter 25 mm was used. The distance between the plates was adjusted to 1 mm. Polymer sample was added on the bottom plate and the separation between plates was reduced to experimental distance, once the set temperature was achieved in the furnace.

4.9.1. Amplitude sweep

A dynamic strain amplitude sweep was performed in order to determine the linear viscoelastic region (LVER) for PLA between 160 °C to 210 °C, in gradations of 10 °C. The sample was subjected to differential strain amplitudes ranging between 0.01 to 100% at a constant angular frequency of 1 rad. sec^{-1}. Changes in the storage modulus (G') and the loss modulus (G'') were monitored.

4.9.2. Frequency sweep

Samples were subjected to varied angular frequency (ω), between 0.1 to 100 rad. sec^{-1}, at a constant strain value of 1% that lies within the LVER of studied PLA systems. Temperatures ranging from 160 °C to 210 °C were used in steps of 10 °C. Storage modulus (G'), loss modulus (G'') and complex viscosity (η*) were monitored against angular frequency.

4.9.3. Time sweep

Time dependent stability of the polymer melt at each of the above mentioned temperatures was measured by subjecting the melt to a constant angular frequency of 1 rad.sec^{-1}, and a constant strain amplitude of 1%, for 30

minutes at the desired temperature. Complex viscosity was measured against time, with each measurement taken 5 seconds apart.

4.10. Assessment of PLA molecular weight degradation after thermal processing

Molecular weight degradation of PLA after melt compounding, film extrusion and billet extrusion was assessed using a Waters ACQUITY advanced polymer chromatography (APC™) system, coupled with an RI detector. Separation was achieved by a column bank consisting of Waters Aquity XT 125 (Effective molecular weight range 1000 - 30,000 g/mol) and XT 450 columns (Effective molecular weight range 20000 - 400,000 g/mol), each having 4.6 mm internal diameter and 150 mm length. The chromatographic conditions were as follows. The isocratic mobile phase was chloroform, injection volume was 30 µl, the flow rate was 0.3 ml/min and the temperature of the column bank and detector was 30 °C. The calibration curve was obtained by using 3 different polystyrene standards (Waters ReadyCal Kit), each containing a mixture of four narrow molecular weight fractions (table 4.4). 0.5% w/v solution of each of the processed samples was prepared and measured on the APC system using the abovementioned parameters. The APC method for PLA was developed based on preliminary trials and previous GPC reports (Gerlach, 1993). The results were processed by Empower 3® software. The calibration curve and the equation for the same were obtained using a 5th order polynomial fit. This was used for calculation of the molecular weight of the processed PLA samples

Table 4.4: *Molecular weight fractions in the ReadyCal calibration kit*

Vial	Vial 1	Vial 2	Vial 3
Mol. Weight (Da)	2460000	1170000	552000
	271000	125000	62500
	34000	17300	8900
	3460	1250	570

4.11. Identification of oligomeric degradation products by gas-chromatography/ mass-spectrometry (GC/MS)

The viscosity as well as the molecular weight of PLA significantly dropped when processed with sodium salicylate at elevated temperatures. The oligomeric degradation products generated during melt extrusion of PLA, with and without sodium salicylate were separated and individually identified using an Agilent Technologies (USA) 7890A gas chromatographic separation unit (GC), coupled with a triple quadrupole 5975 EI/CI mass spectrometric detector (MSD). Samples were prepared by dissolving 150 mg of the extrudates in 5 ml of 2:1- acetone: chloroform. 1 µl of the sample was injected at 250 °C into a capillary column with the following specifications; HP-5-MS, 25 m x 0.25 mm, 0.25 µm film thickness. Helium was used as a carrier gas with a flow rate of 0.66 ml/min. At the beginning of the experiment, the column oven was equilibrated at 40 °C for 5 minutes, followed by heating to 350 °C at a rate of 10 °C /min. Finally it was held isothermally at 350 °C for 10 minutes. The MSD source temperature was set to 230 °C while the quadrupoles were held at 150 °C. The fragmentation patterns were obtained in the scanning mode set to scan mode between m/z 50 - 800 amu. Agilent MSD Chem-station® software was used for data acquisition and processing. The fragmentation patterns obtained for individual species were compared with the NIST database and previous reports on thermal degradation of PLA (Kopinke *et al.*, 1996; McNeill and Leiper, 1985).

4.12. Modulated DSC (MDSC) for determination of percentage crystallinity

A conventional MDSC experiment was performed between the temperatures of 35 °C – 220 °C, using a TA instruments Q2000 differential scanning calorimeter. Approximately 5mg of the sample was loaded into a standard aluminium pan with a crimped aluminium lid. Modulation amplitude was set to 0.5 °C with heating rate 5 °C/minute and modulation time of 100 seconds. Curves for reversible and irreversible heat flow were obtained by TA

universal analysis software. Normalised enthalpies of cold crystallisation and re-crystallisation were calculated from the exotherms visible on the irreversible heat flow curve. The normalised enthalpy of melting was obtained from integration of the endotherm on the reversible heat flow curve. Percentage crystallinity was calculated from the equation 4.3 (Solarski *et al.*, 2005).

$$\%\ \text{Crystallinity} = \frac{\Delta H\ \text{melting} - (\Delta H\ \text{cold crystallisation} + \Delta H\ \text{recrystallisation})}{\Delta H\ \text{fusion for}\ 100\%\ \text{crystalline PLA}}$$

…(Equation 4.3)

4.13. Characterisation of PLA films using 'Wide Angle X-ray Diffraction' (WAXD)

The WAXD patterns were obtained in a flat plane geometry using a Rigaku, MicroMax-007hf high intensity microfocus rotating anode x-ray imaging system. The diffractomer was operated with monochromatised Cu Kα (1.54 Å) radiation, at 40 kV voltage, 30 mA filament current. The sample to detector distance was 100 mm. The raw data was obtained as 2 dimensional WAXD patterns as well as single dimensional diffractograms, i.e. Intensity Vs 2θ (diffraction angle) curves. Crystallinity index was calculated from the diffractograms using equation 4.4, without background subtraction (Kawakami *et al.*, 2008). *(Refer appendix for 2D WAXD data analysis method)

$$\%\ \text{Crystallinity(WAXD)} = \frac{\text{Area under crystalline peaks}}{\text{Total area under amorphous halo and crystalline peaks}} \text{X}100$$

…(Equation 4.4)

$$F_h = \frac{3(\cos^2\phi) - 1}{2} \qquad \textbf{(Equation 4.5)}$$

$$\text{Where,} \langle \cos^2\phi \rangle_{hkl} = \frac{\int_0^{\pi/2} I(\phi)\cos^2\phi \sin\phi d\phi}{\int_0^{\pi/2} I(\phi)\sin\phi d\phi} \qquad \textbf{(Equation 4.6)}$$

ϕ = azimuthal angle and **I(ϕ)** = scattered intensity along the azimuthal angle ϕ.

The molecular orientation of the crystalline phase was quantified through Herman's orientation function. The 2D WAXD patterns were converted into the intensity Vs azimuthal angle (ϕ) graphs by integrating the intensity of the crystalline reflection in the (200/110) hkl lattice plane over an azimuthal semicircle (Kawakami *et al.*, 2008). Herman's orientation function was calculated using the equation 4.5 and 4.6 (Zhang *et al.*, 2011).

4.14. Mechanical testing of oriented films

Simple tensile tests (ASTM D638) were performed on dumbbell shaped samples (ASTM type V; gauge length = 9.5 mm, width = 3.15 mm, variable thickness) cut from oriented films. An Instron® 5900 series mechanical testing system was used along with Bluehill2® software for data analysis. The experiment was performed at 30 °C, with 1 KN load cell and extension rate of 100 mm/ minute. Engineering stress (load/ original cross sectional area) vs. engineering strain (change in length/ original length) curves were used for calculation of the ultimate tensile strength and Young's modulus.

4.15. Surface energy determination by static contact angle measurement

4.15.1. Mathematics

The change in surface free energy following orientation of blank and drug loaded PLA films was calculated by the Owens/Wendt theory (Owens and Wendt, 1969).

$$(y = m . x + c)$$

$$\frac{(\cos\theta+1)\gamma_L}{2\,(\gamma_L^D)^{\frac{1}{2}}} = (\gamma_f^P)^{\frac{1}{2}}\frac{(\gamma_L^P)^{\frac{1}{2}}}{(\gamma_L^D)^{\frac{1}{2}}} + (\gamma_f^D)^{\frac{1}{2}} \qquad \textbf{(Equation 4.7)}$$

Where, γ_L= overall surface tension of the probe liquid, γ_L^D = dispersive component of the surface tension of the probe liquid, γ_L^P = polar component of the surface tension of the probe liquid. γ_f^D= dispersive component of the surface energy of the film, γ_f^P= polar component of the surface energy of the film and θ = the contact angle between the probe liquid and the film.

The overall surface energy for each sample, divided into the contributions from the Van-der-Waals dispersive interactions and the dipole or hydrogen bonding type polar interactions was obtained using equation 4.7. This equation is arranged in 'y = mx + c' format. Therefore, plotting x, and y values for a series of probe liquids, as per equation 4.7 yields a straight line, the slope of which is square root of the polar component of surface free energy and the y-intercept is the square root of the dispersive component of the surface energy. The overall surface energy (γ_f) is a sum the polar (γ_f^P) and the dispersive component (γ_f^D) (Riluson, 1999). In order to calculate the surface energy using equation 4.7, surface tensions of the probe liquids (γ_L, γ_L^D, γ_L^P) and their contact angle (θ) with the investigated surface must be known. These parameters were determined using the following method.

4.15.2. Instrumentation

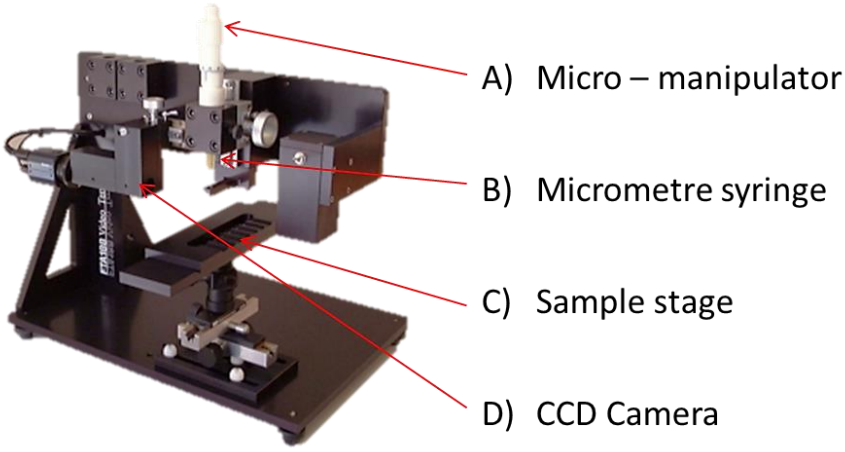

Figure 4.5: *Tensiometer used for measurement of probe liquid surface tension and their contact angle with the oriented film surfaces.*

The surface tensions of the probe liquids and their contact angle with the reference and the test materials were measured by an FTA188 tensiometer. The images were captured by an integrated CCD firewire camera (figure 4.5- D) and analysed by FTA32 software. The instrumental setup further consisted of a

tensiometer sample stage (figure 4.5 - C) enclosed within an environment control chamber and a stainless steel flat-tipped needle (0.47 mm diameter, Hamilton, UK) attached to a micrometer syringe (2.5 ml, Hamilton, UK) (figure 4.5 - B). The syringe was attached to a micromanipulator (figure 4.5 - A), which allowed precise movement of the syringe plunger, for accurate formation of a pendent drop (figure 4.6 - A) or a sessile drop (figure 4.6 - B).

4.15.3. Estimation of surface tension of the probe liquids (γ_L, γ_L^P, γ_L^D)

Ten probe liquids were selected with varied polar and dispersive nature. These included Di-iodomethane, n-hexane, n-octane, n-heptane, cyclohexane, toluene, benzyl alcohol, ethylene glycol, glycerol and triple distilled water. All probe liquids were procured from Acros chemicals and were >99% pure. The overall surface tension of the probe liquids was determined by the pendent drop method (Hansen and Rodsrud, 1991). The video camera was focused on the needle tip and a pendant drop (figure 4.6 - A) having maximum possible volume was formed with the help of the micromanipulator. An image of each drop was captured by the camera and the surface tension was calculated by the integrated image analysis software with the help of a Young-Laplace fit to the contour of a pendant drop. The measurement was performed three times.

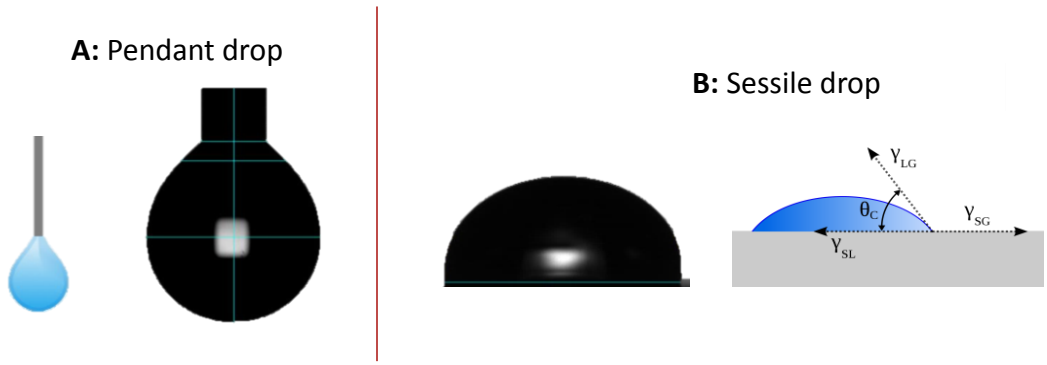

Figure 4.6: *Pictorial representation of **A)** a pendant drop and **B)** a sessile drop*

The overall surface tension of the probe liquids was divided into their polar and dispersive components by the following method reported by Riluson C. (1999). The contact angle made by the probe liquids with polytetrafluoroethylene (PTFE) were determined by the technique described in section 4.15.4. PTFE has a standard surface energy of 18 mJ/m^2. Since this is entirely contributed by the dispersive component, the 'mx' parameter in the equation 4.7 becomes zero. Therefore, the only unknown remaining in the equation, i.e. the dispersive component of the surface tension (γ_L^D) was obtained and the polar component (γ_L^P) was calculated by subtracting γ_L^D from the overall surface tension.

4.15.4. Estimation of the contact angle (θ)

The static contact angle of the probe liquids with the surface of oriented PLA films (or PTFE) was measured at room temperature (25 °C), by the sessile drop method. The blank as well as the drug loaded films oriented in the UCW mode (λ = 1X to 4X), and those oriented biaxially in the SB and the SEQ mode to the draw ratio of 2X2Y were selected as the model systems for this study. Each separate film was cleaned with distilled water, dried, grounded to remove any static charge and placed on the tensiometer sample stage. A drop of the probe liquid was deposited on the film surface through the flat-tipped needle – syringe assembly with the help of the micromanipulator. The distance between the needle and the sample surface was adjusted for every probe liquid such that the drop landed smoothly on the film surface. The images were captured at 20 fps speed for 90 seconds as soon as the drop touched the film surface. The earliest image from which there is no change in the drop shape was considered for further analysis. The contact angle from both sides of the drop was determined by integrated image analysis software. 6 replicate measurements were performed on new surfaces of the same sample (the sample was rotated by 90°after every measurement) and the average value was considered for calculation of the surface energy.

4.16. Drug release studies on oriented PLA films

Drug loaded films oriented in the UCW mode to draw ratios of 1X to 4X and those oriented in the SB and SEQ mode to a draw ratio of 2X2Y were selected as model systems for drug release studies. Film samples belonging to each model system were cut into several circular sections (5 mm diameter) using a hole punch. All circular sections were weighed and an average weight was determined. 25 circular sections from each model system (in triplicate) were submerged in 5 ml of drug release media, contained in separate glass vials. The vials were stored in an incubator-shaker set to operate at 100 rpm and 37 °C. The drug release media was composed of 0.5 M sodium phosphate buffer (2.29% w/v di-sodium hydrogen phosphate and 3.6% w/v sodium di-hydrogen phosphate), 0.5% w/v sodium dodecyl sulphate (SDS) and 5% acetone. The pH was adjusted to 6.8 using phosphoric acid. Since curcumin has poor water solubility, acetone and SDS were added to aid its dissolution (Pan *et al.*, 2006; Rahman *et al.*, 2009).

Different sampling protocols were followed for the curcumin loaded and the theophylline loaded films. In the case of theophylline loaded films, the entire (5 ml) release media was withdrawn at weekly intervals and replaced with a fresh media. The amount of released theophylline was directly quantified from the media by the HPLC method reported below.

The attempts to quantify the release of curcumin using the abovementioned method failed due to poor solution stability of curcumin (Wang *et al.*, 1997). No release could be detected for up to 4 months; probably because the curcumin released in a trace amount was below the detection limit of HPLC, when measured at daily intervals; or it degraded before reaching the detectable quantity when measured at weekly intervals. Therefore, release of curcumin was determined by the residual quantification method; i.e. by determination of the amount of curcumin remaining in the films than the amount released. A circular section was withdrawn from each model system (in

triplicate). The sample was dried, weighed and dissolved in 5 ml chloroform. The resulting solution was diluted 10 fold with acetonitrile and analysed by HPLC using the method reported below.

4.16.1. HPLC method for quantification of curcumin

The amount of curcumin remaining in the films was assayed by reversed-phase high-performance liquid chromatography (RP-HPLC) method using a Waters e-2695 separation unit coupled with a photodiode array detector (PDA-2998). A Waters Symmetry C18 column with 5 µm particle size and 4.6 mm x 150 mm column dimensions was used. The mobile phase composed of 60:40 acetonitrile: water containing 0.1% TFA (pH = 3). The mobile phase flow rate was set to 1 ml/min, the detection wavelength was 425 nm and the injection volume was 20 µl.

Standard solutions containing 10 ppm, 20 ppm, 30 ppm, 40 ppm and 50 ppm curcumin were prepared and a calibration curve was obtained by the abovementioned HPLC method. The amount of curcumin in the test solution (diluted solution of the circular film section) was determined by comparison to the calibration curve. The curcumin standards were measured during every HPLC analysis in order to account for the possible sources of error. The calibration curve was additionally utilised for calculation of the method linearity, the limit of detection (LOD) and the limit of quantification (LOQ). These values were R^2 = 0.9998, 0.36 µg/ml, and 1.09 µg/ml respectively.

4.16.2. HPLC method for quantification of theophylline

The amount of theophylline released was assayed using the same instrument, column and the chromatographic conditions as that for curcumin. However, the mobile phase, detection wavelength and injection volume were varied. The mobile phase for theophylline was composed of 25: 70 methanol : 0.05M acetate buffer pH 4 (4.1% w/v sodium acetate + 9.8 ml glacial acetic acid), while the detection wavelength and injection volume were 273 nm and

50.0 µl respectively (Butrimovitz and Raisys, 1979). Calibration curves were obtained for theophylline in a manner similar to the curcumin analysis explained above. The linear regression coefficient for this method, in the range of 10ppm – 50 ppm was 0.99, while LOD and LOQ were 1.14 µg/ml, and 3.46 µg/ml respectively.

4.17. Characterisation of the changes in the polymer properties during drug release studies

Several circular sections belonging to each model system (curcumin and theophylline loaded films with UCW draw ratio 1X-4X and SB and SEQ samples with biaxial draw ratio 2X2Y) were submerged in 5 ml of drug release medium and stored in the incubator-shaker (37 °C, 100 rpm) in parallel with the drug release studies. Nine circular sections were withdrawn from each model system at the weekly intervals and the release medium was replaced with a fresh medium. All the samples were dried and weighed. Three samples were used for the crystallinity determination (the same method as section 4.12), three were used for estimation of the molecular weight change by gel permeation chromatography (GPC) (the same method as section 4.10), while 3 samples were used for visualisation of the change in the surface morphology by scanning electron microscopy (SEM) (Hurrell and Cameron, 2001a; Hurrell and Cameron, 2001b; Hurrell and Cameron, 2002; Jackson *et al.*, 2004).

4.17.1. Assessment of the change in surface morphology after submersion into drug release media

The circular film samples withdrawn from each model system (in triplicate) were dried in a vacuum oven and visualised by a Hitachi TM3030 table-top scanning electron microscope (SEM). The microscope was operated in topology mode with a working distance of approximately 8.5 mm. An accelerating voltage of 5 kV was used for primary focusing and the voltage was increased to 15 kV when the final image was captured.

4.18. Characterisation of shrinkage in the oriented films

Curcumin loaded films oriented to a draw ratio of 2X in the UCW mode or 2X2Y in the SB or the SEQ mode, exhibited shrinkage after submersion in the drug release media. In order to rationalise this observation, the following experiment was carried out. Several tensile bars (ASTM type V; gauge length = 9.5 mm, width = 3.15 mm, thickness = 0.2 mm) were obtained from the theophylline and curcumin loaded films oriented in the UCW mode to a draw ratio of 2X. These were submerged in the release media and stored in an incubator shaker at 37 °C, with an agitation speed of 100 rpm. Three samples were withdrawn from each type of submerged films at daily intervals for up to 10 days. The dried samples were tested for changes in dimensions, crystallinity (sec. 4.12) and crystalline orientation (by WAXD – sec. 4.13).

4.19. Characterisation of anisotropic structure in the rods by WAXD

The rods oriented to different draw ratios were machined into 1 mm thick sections along the drawing direction and the perpendicular direction (figure 4.7). These sections were analysed by a Rigaku, MicroMax-007hf high intensity microfocus rotating anode x-ray imaging system in transmission mode. The experimental setup and the data analysis method were similar to that described in section 4.13.

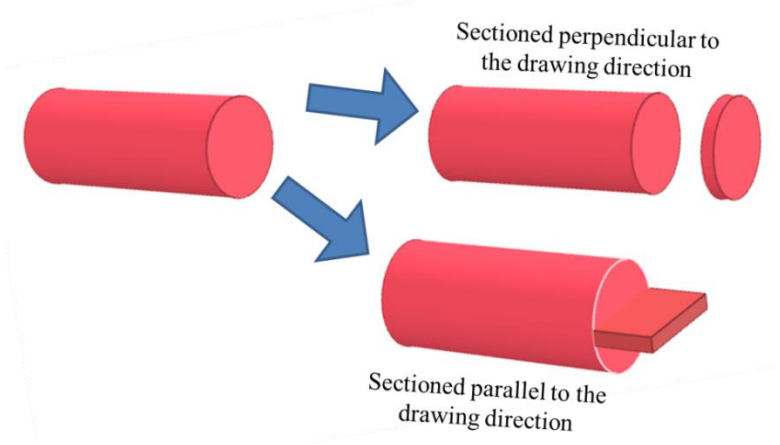

Figure 4.7: *Sectioning of the rods for WAXD studies*

4.20. Evaluation of directional drug release from oriented PLA rods

4.20.1. Sample preparation

The paracetamol loaded oriented rods representing draw ratios from 1X to 5X were cut lengthwise into 6 mm long sections. Six such samples representing each draw ratio were used for the drug release studies. Out of these, 3 samples were coated with a waterproof epoxy resin on the (lateral) curved surface, while the remaining 3 were coated on the (transverse) flat surfaces. Buehler EpoThin™ resin and hardener were used for this purpose. The resin and the hardener were mixed in the ratio 10:3.9 and the mixture was applied onto the desired surface of the rod with a brush, followed by curing at room temperature for 12 hours. Altogether 3 epoxy coats were applied.

4.20.2. Drug release studies

A total of 10 batches of the oriented rods (5 draw ratios curved surface coated + 5 draw ratios flat surface coated) were evaluated for drug release, in triplicate. The experimental protocol was same as that for the oriented drug loaded films. In brief, all samples were stored in separate glass vials containing 5 ml of the drug release media. The vials were equilibrated at 37 °C in an incubator-shaker with an agitation speed of 100 rpm. The entire (5 ml) release media was withdrawn at weekly intervals and replaced with a fresh media. The amount of released paracetamol was directly quantified from the release media by the HPLC method reported below.

4.20.3. HPLC method for quantification of paracetamol

The assay of released paracetamol was performed using a Waters e-2695 HPLC system equipped with a photodiode array detector (PDA-2998). Waters µBondapak C18 column (125Å, 10 µm, 3.9 mm X 150 mm) was used as a stationary phase; while the isocratic mobile phase composed of 15:85 acetonitrile: water containing 0.1% TFA (pH = 3). The mobile phase flow rate was 1 ml/min, the detection wavelength was 243 nm and the injection volume

was 50 µl (Gotelli *et al.*, 1977). The calibration curve for paracetamol was obtained in a manner similar to curcumin analysis (section 4.16.1). The linear regression coefficient for this method in the range of 10 ppm – 50 ppm was 0.99; whereas, the LOD and the LOQ were 0.6 µg/ml and 1 µg/ml respectively.

4.21. Measurement of molecular weight, crystallinity and morphological changes in the submerged rods

The paracetamol loaded oriented PLA rods were assessed for the changes in molecular weight, crystallinity and morphology, after being submerged in the release media for 16 weeks.

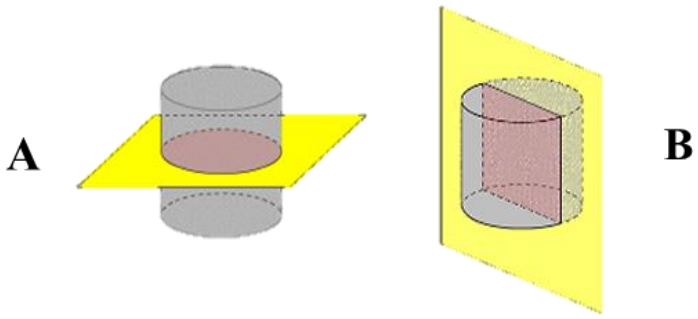

Figure 4.8: *Schematic representation of* ***(A)*** *the transverse section and* ***(B)*** *the lateral section of the PLA rods*

For studying the morphological changes, two distinct sections were obtained from the rods remaining at the end of the drug release study. A transverse section was obtained by cryo-fracturing a rod parallel to the flat surfaces (cross section) (figure 4.8 - A), while a lateral section was obtained by cryo-fracturing a rod parallel to the curved surface (figure 4.8 - B). The exposed surfaces were visualised by a scanning electron microscope using the experimental protocol explained in section 4.17.1. A part of the abovementioned rods was utilised for determination of the percentage crystallinity by MDSC (section 4.12) and the molecular weight by GPC (section 4.10).

4.22. Statistical analysis

The quantitative data in this thesis is represented as mean ± standard deviation of 'n' replications. Moreover, such data and associated claims were validated by using various statistical analysis techniques as follows.

To establish a difference between the rheological profile of various drug loaded PLA systems, the storage modulus (G') and loss modulus (G'') obtained from amplitude sweep test, at 1% amplitude were statistically compared paired t-tests. A similar comparison was made between the viscosities of the investigated model systems (obtained by frequency sweep test) as well as between the percentage drop in the viscosity observed during time sweep test. Nevertheless, the effect of various concentrations of sodium salicylate on the rheological profile and the molecular weight of PLA was validated by the paired t-test analysis. This statistical data is discussed at relevant places in chapter 5.

In chapter 6, the effect of two independent orientation process variables (namely draw rate and drawing temperature) on a dependant property variable (crystallinity, Tg, Mechanical strength) was studied by multiple regression analysis. Moreover, variation in these properties with respect to uniaxial and biaxial draw ratios was studied by paired t-test comparison between successive draw ratios (except for mechanical properties comparison, where two-way ANOVA with replication was used). Likewise, a difference between the surface free energy of the oriented films was statistically evaluated by two-way ANOVA with replication. The changes in the crystallinity, molecular weight and polydispersity of the model PLA films after aqueous submersion were validated by one-way ANOVA - Tukey's test comparison between the draw ratios at varied intervals and between the intervals. Wherever a comparison was made only between two sets of data, a paired t-test was used. A similar statistical analysis was used for establishing the differences in the drug release profiles of the investigated PLA films. Moreover, the drug release profiles were fitted to an appropriate kinetic model by linear regression analysis.

In chapter 7, a rise in the PLA rod crystallinity with respect to uniaxial draw ratios was validated by paired t-test comparisons between the successive draw ratios. Nevertheless, crystallinity and molecular weights of the investigated rods were statistically compared between the draw ratios at the beginning and at the end of the drug release study by one-way ANOVA – Tukey's test. A similar comparison was made between the crystallinity and molecular weight values of the rods at the beginning and at the end of the study, and between the curved surface coated and the cross section coated rods, at a constant draw ratio. The anisotropy in the drug release rate between the cross section and the curved surface was statistically validated by paired t-test analysis. Nevertheless variation in the release rate with respect to the uniaxial draw ratio was confirmed by one-way ANOVA followed by Tukey's test.

The regression analysis was performed using Microsoft Excel®, while the rest of the statistical analysis was performed using GraphPad Instat 3® software package.

5. Understanding the materials and the processes: results & discussion

The following chapter describes the theoretical analysis and the experimental work that formed a basis for the selection of the model drugs and the model polymer. It includes characterisation of the experimental materials by techniques such as rheology, thermal analysis and gel permeation chromatography, etc. for establishing efficacy of the melt processing operations utilised in this work. The chapter further discusses the assessment of changes in the polymorphic state of the experimental materials and their degradation during melt processing. Additionally, degradation products generated during such processing and degradation mechanism are identified. Knowledge of this will ensure that the characteristics of drug release from the oriented films/ rods are correctly attributed to the morphological changes imposed solely by solid-state orientation.

5.1. Selection of the model polymer

The primary aim of this work was to evaluate the effect of solid-state polymer orientation on drug release from the polymeric matrices. Various polymer orientation methods have been widely used for manufacturing high-strength, bioresorbable medical devices from synthetic poly-esters of lactic and glycolic acid (Pohjonen *et al.*, 1997; Trieu, 2006). A stable oriented morphology can be developed in these polymers, by virtue of their semicrystalline nature and higher glass transition temperature. Moreover, their biodegradability and toxicological safety has enabled their use in controlled drug delivery to an internal organ. (Veiranto *et al.*, 2002; Witt and Kissel, 2001). Considering these aspects and material availability, poly (L-lactic acid) (PLA) was selected as the model polymer.

5.2. Screening of model compounds based on the solubility parameter

As discussed previously in the literature survey, release of a drug from a polymer matrix depends on its solubility status in that matrix. Moreover, a soluble drug and a suspended drug may influence the solid-state orientation process differently. This will in turn affect the drug release profile. In order to study such an effect, two separate model drugs were needed; the one that can remain in the crystalline suspension form, while the other, which will be soluble in the PLA matrix at 5% w/w loading. Nine model small molecules were shortlisted on this basis and after thorough consideration to the literature and laboratory safety constraints. These molecules included curcumin, theophylline, caffeine, paracetamol, aspirin, sodium salicylate, nicotinamide, ascorbic acid and citric acid.

The compatibility between the shortlisted model drugs and PLA was theoretically predicted from the reported values of Hansen's solubility parameter (HSP) (Hansen, 1969). HSP takes into consideration the cohesive energy of a molecule as a net effect of all inter-atomic and inter-molecular interactions. Therefore, when the solubility parameters of two molecules match, they are expected to be mutually compatible. Equation 5.1 was utilised for calculation of the total solubility parameter (δ_t). δ_t is composed of three partial solubility parameters, namely δ_d, δ_p and δ_h, which represent the contributions from Van der Waals dispersive forces, polar interactions between the induced and the existing dipoles and hydrogen bonding respectively. Values of the individual solubility parameters for each model drug and PLA are reported in table 5.1

$$\delta_t = \sqrt{(\delta_d{}^2 + \delta_p{}^2 + \delta_h{}^2)} \qquad \textbf{(Equation 5.1)}$$

Cohesive energy contribution from the dispersive forces relates to the hydrophobic part of a molecule, whereas polar interactions and hydrogen bonding are associated with hydrophillicity. It is clear from table 5.1 that PLA is

significantly hydrophobic and therefore will accommodate a hydrophobic drug very easily. Since all model molecules listed in table 5.1 have a hydrophobic (δ_d) component comparable to PLA, they are expected to be compatible with PLA to a greater or lesser extent. Whether they will remain as a solid solution or a crystalline suspension (at 5% w/w concentration in PLA), depends on the contribution from the remaining solubility parameters.

Table 5.1: *Partial solubility parameters for the shortlisted model compounds*

Material	Solubility parameter ($J^{1/2}$ $m^{-2/3}$)				Reference
	δ_d	δ_p	δ_h	δ_t	
Poly lactic acid	17.6	9.7	11.8	23.3	(Liu *et al.*, 2004)
Curcumin	17.4	6	10.9	21.39	(Fabien and Isabelle, 2009)
Paracetamol	17.8	10.5	13.9	24.91	(Hansen, 2004)
Aspirin	20.61	7.56	10.81	24.47	(Roberts *et al.*, 1991)
Theophylline	19.4	14.2	13.2	27.43	(Huu-Phuoc *et al.*, 1987)
Caffeine	20.65	7.16	18.61	28.71	(Huu-Phuoc *et al.*, 1987)
Sodium salicylate	16.55	21.01	16.58	31.47	(Barra *et al.*, 2000)
Nicotinamide	19.96	13.11	13.08	27.23	(Cutrignelli *et al.*, 2008)
Ascorbic acid	18	9.8	21.6	29.78	(Hansen, 2004)
Citric acid	20.9	8.2	21.9	31.36	(Jarvas *et al.*, 2011)

The total solubility parameters of theophylline, caffeine, sodium salicylate, nicotinamide, ascorbic acid and citric acid are significantly higher than PLA, owing to a higher energy contribution from the hydrophilic interactions. Theoretically, these molecules will have low solubility in the PLA matrix and are expected to remain as a separate crystalline phase even at low concentrations. Therefore, these molecules can represent the class of PLA insoluble model drugs. On the contrary, curcumin, paracetamol and aspirin have poor cohesive energy contribution from the polar and the hydrogen bonding interaction, which makes them predominantly hydrophobic. A close match between the partial as well as the total solubility parameters of PLA and the aforementioned three molecules suggests higher compatibility. Since all three of them have melting

points lower than or within the melt processing window of PLA (figure 5.1) (Lim *et al*., 2008), co-melting in a twin screw extruder followed by instantaneous solidification can lead to formation of an glassy solution, where the drug is present in a solution state or a molecularly dispersed amorphous state in PLA (Greenhalgh *et al*., 1999; Lakshman *et al*., 2008).

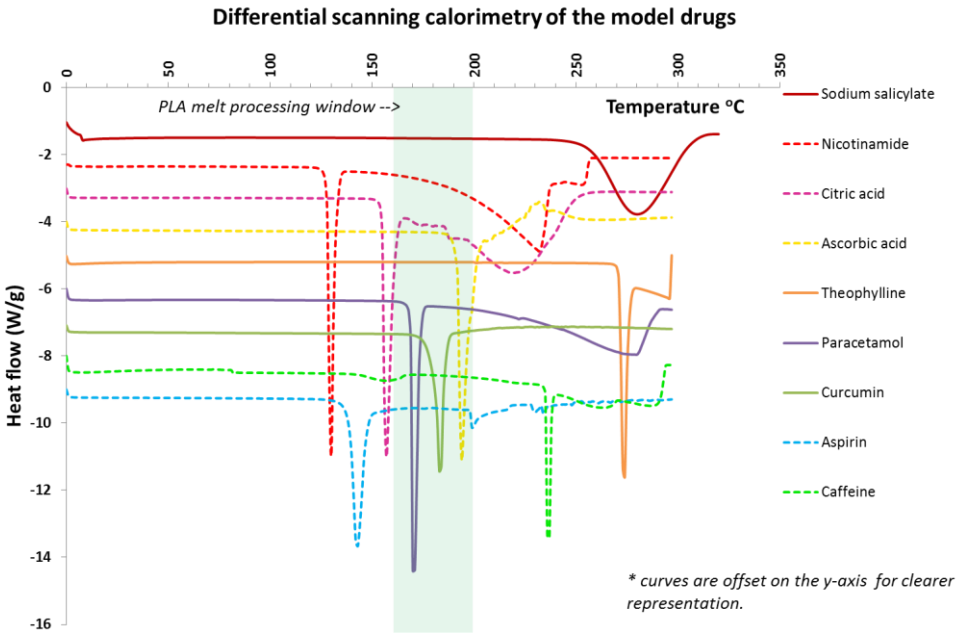

Figure 5.1: *Melting endotherms of the model compounds obtained by DSC.*

Among the PLA insoluble model molecules, theophylline, sodium salicylate, ascorbic acid and caffeine have higher melting points than the melt processing window for PLA (figure 5.1). Therefore, if present as a suspension in the PLA matrix, the size of the suspended particles will be same as that before melt compounding. Contrarily, citric acid and nicotinamide melts at 153 °C and 128 °C respectively. Therefore their particle size will be dictated by the rate at which the composite material is cooled from the molten state to the ambient conditions.

5.3. Thermal stability of the model compounds

The drug loaded PLA matrices further studied in this work were prepared by melt extrusion. Therefore, the suitability of the shortlisted drugs was

established by studying their thermal stability, through thermo-gravimetric analysis. A decomposition temperature was initially determined for the shortlisted model drugs, by monitoring the weight loss, as they were heated at the rate of 10 °C/min. figure 5.2 presents a comparison of the percent weight remaining as a function of temperature. It is clear that sodium salicylate, curcumin and theophylline underwent negligible weight loss until 250 °C. A slight weight loss was observed for paracetamol starting at 200 °C. The remaining model drugs, namely ascorbic acid, aspirin, citric acid, caffeine, and nicotinamide underwent significant thermal degradation with decomposition temperatures 180 °C, 140 °C, 150 °C, 170 °C and 155 °C respectively. Nicotinamide and caffeine showed complete weight loss by 250 °C; whereas citric acid lost almost 80% of its original weight due to thermal decarboxylation between 150 °C – 212 °C (Barbooti and Al-Sammerrai, 1986). A smaller weight loss was exhibited by ascorbic acid and aspirin due to their stepwise decomposition (Ribeiro *et al*., 1996).

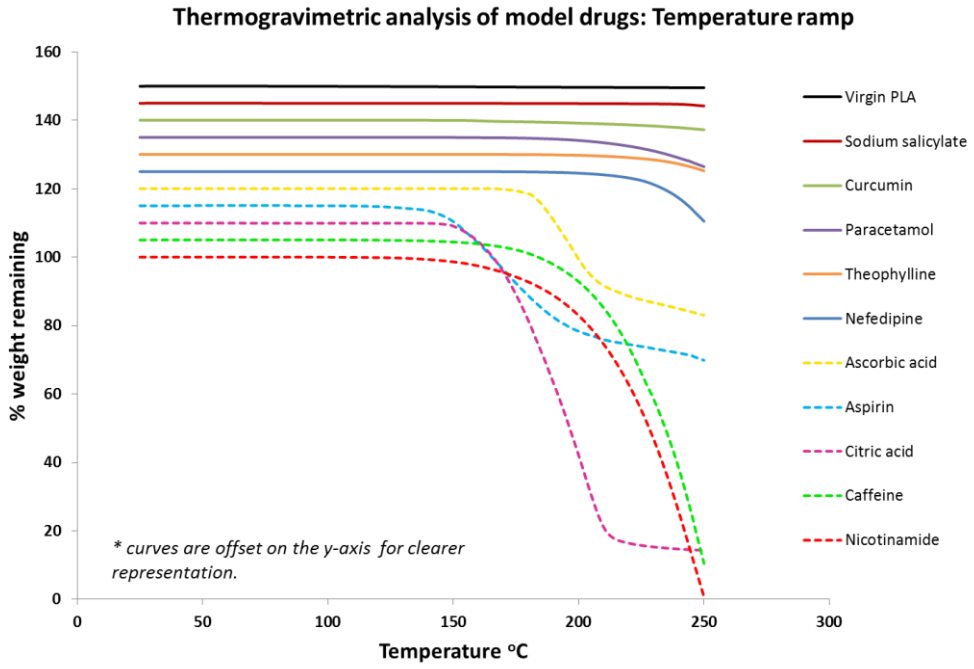

Figure 5.2: *Thermo-gravimetric analysis of the pure model compounds (temperature ramp method)*

The decomposition temperature determined by temperature ramp TGA may not be very precise, as the underlying heating rate decides the time for which the material is exposed to a particular temperature. A more accurate idea can be obtained by exposing the material to a constant temperature for prolonged duration. Based on the rheological studies (sec 5.6) 180 °C was decided as a suitable melt extrusion temperature. Therefore, thermal stability of the model drugs at this temperature was evaluated by rapidly (30 °C/min) heating them to 180 °C and holding isothermally for 30 minutes. Figure 5.3 represents the percentage weight remaining as a function of time for all of the shortlisted model drugs. It is evident that sodium salicylate, curcumin, paracetamol, and theophylline were stable for extended durations at 180 °C, whereas ascorbic acid, citric acid, caffeine, aspirin and nicotinamide exhibited pyrolysis. Although the weight loss shown by ascorbic acid was only about 25%, the material was completely charred at the end of the test.

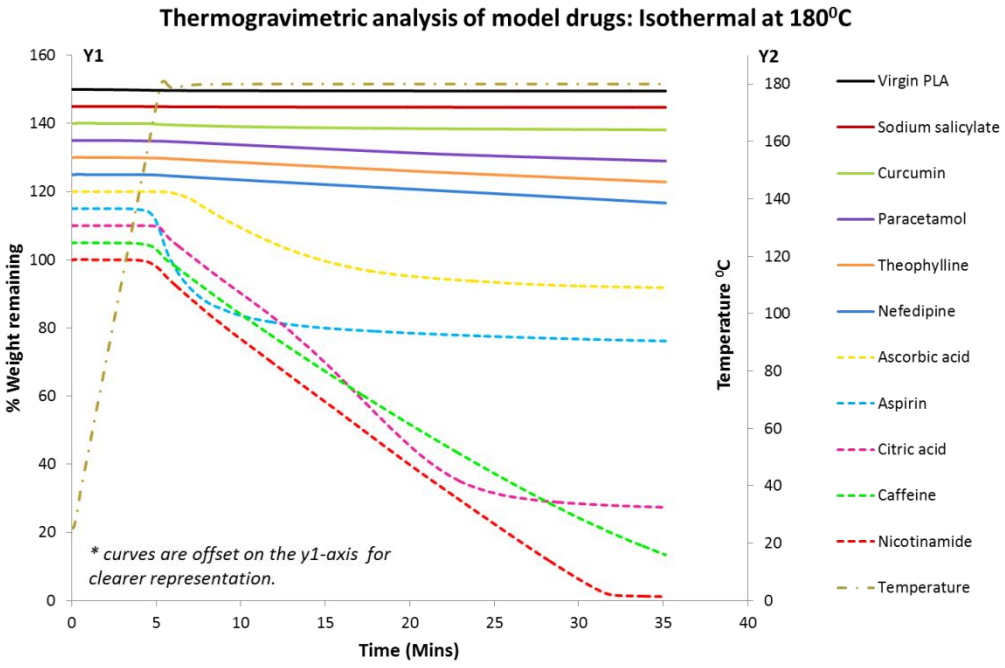

Figure 5.3: *Thermo-gravimetric analysis of the pure model compounds (isothermal 180 °C)*

5.4. Selection of the model drugs

The thermogravimetric analysis results clearly suggested that only sodium salicylate, curcumin, paracetamol, and theophylline were suitable for melt processing. Considering the thermal stability and the solubility parameters, theophylline and sodium salicylate were shortlisted as the thermostable model drugs which may remain suspended in PLA at 5% w/w concentration; while, curcumin and paracetamol were shortlisted as the thermostable drugs that can potentially form a glassy solution in PLA at 5% w/w loading.

Assessment of the melt compounded model systems by rheology and gel permeation chromatography further revealed that sodium salicylate led to degradation of PLA, evidenced as a significant fall in viscosity and molecular weight (discussed separately in sections 5.7). On the contrary, theophylline formed a well dispersed, stable suspension at 5%w/w loading. Therefore, only theophylline was utilised as a PLA insoluble model drug that can remain in the suspension state within PLA matrices.

Glass transition temperatures (Tg) of the amorphous forms of curcumin, and paracetamol are 69.49 °C (Pawar *et al.*, 2012), and 22.85 °C (Sibik *et al.*, 2014) respectively. Owing to the similarity between the glass transition temperature of curcumin and PLA, curcumin may produce minimal changes in the thermal properties of the compounded system. Moreover, the amorphous solid solution of curcumin with PLA will have greater stability owing to a higher combined Tg than the paracetamol loaded PLA. Therefore, curcumin was initially selected as a model drug that can form a glassy solution in PLA. It was later realised during the drug release studies that quantification of a minuscule amount of curcumin released from the oriented PLA matrices was challenging, due to its poor solution stability (irrespective of the pH). This limitation was overcome in the case of oriented films by measuring the amount of curcumin remaining in the films, rather than the amount released. However, this approach

was unsuitable for the rod geometry. Therefore paracetamol was used as a model drug for studying the directional drug release from the oriented rods.

5.5. The effect of melt processing on the physical and polymorphic state of the model drugs

It is important to know the physical and the polymorphic state of an active pharmaceutical ingredient (API) in the melt extruded matrix, as this may profoundly affect the drug release profile. A drug can be present in the polymer matrix as a separate crystalline or amorphous phase. Alternatively, it can form a solid solution depending upon its concentration in the polymer phase and the degree of interaction between them (Qi *et al.*, 2008). Thermal treatment during melt extrusion can potentially alter the polymorphic state as well as the solubility of a drug in the polymer phase. Therefore, temperature induced changes in the *(pure)* model drugs were studied by subjecting them to a thermal regime, similar to the melt processing conditions utilised in this study (referred as heat treatment – isothermal at 180 °C followed by quenching - sec 4.8). The resultant material along with the melt extruded 'drug + PLA' mixtures were analysed by FTIR spectroscopy, X-ray diffractometry and hot-stage microscopy.

When heated to 180 °C curcumin and paracetamol were molten, while theophylline remained in the solid-state (referred as C_{ht}, $P_{ht,}$ T_{ht} respectively henceforth). Curcumin turned orange - red on melting and maintained the same colour when quench cooled, while paracetamol formed a clear glass following quenching. An obvious consequence of quenching from the melt is conversion to the amorphous state. Since the melt extruded material is cooled rapidly as soon as it leaves the die, it may show a similar change in the polymorphic state of the aforementioned drugs. Withstanding this rationale, the melt compounded PLA containing 5% w/w curcumin was dark orange in colour; while, the paracetamol (5% w/w) containing PLA extrudates were transparent (referred as C_{ext} and P_{ext} respectively). Since theophylline was un-molten at the compounding temperature, the extrudates (T_{ext}) were opaque and white in

colour. The change in the polymorphic state of the model drugs, speculated above is experimentally confirmed in the following sections.

5.5.1. Assessment by Fourier Transform Infra-red (FTIR) spectroscopy

Figure 5.4 displays the FTIR spectra of the unprocessed/ raw paracetamol, and the heat treated paracetamol (P_{ht}). Distinct peaks in the spectrum of raw paracetamol at the wavenumber 3168 cm^{-1}, a triplet of peaks between 1256 -1225 cm^{-1} and 807.07 cm^{-1} peak with a shoulder confirmed the presence of the polymorphic Form I. Following heat treatment, 3168 cm^{-1} peak corresponding to H-bonded O-H stretching was shifted to 3203 cm^{-1} and the triplet of the peaks corresponding to Aryl-N, C-N and C-O stretching was converted to a single broad peak at 1226.83 cm^{-1} (Moynihan and O'Hare, 2002). Moreover, the shoulder to the peak at 807 cm^{-1} representing out of plane bending of C-H, disappeared. These changes confirmed that equilibration at 180 °C followed by quenching, converted the Form I paracetamol to the amorphous state (Zimmermann and Baranovic, 2011).

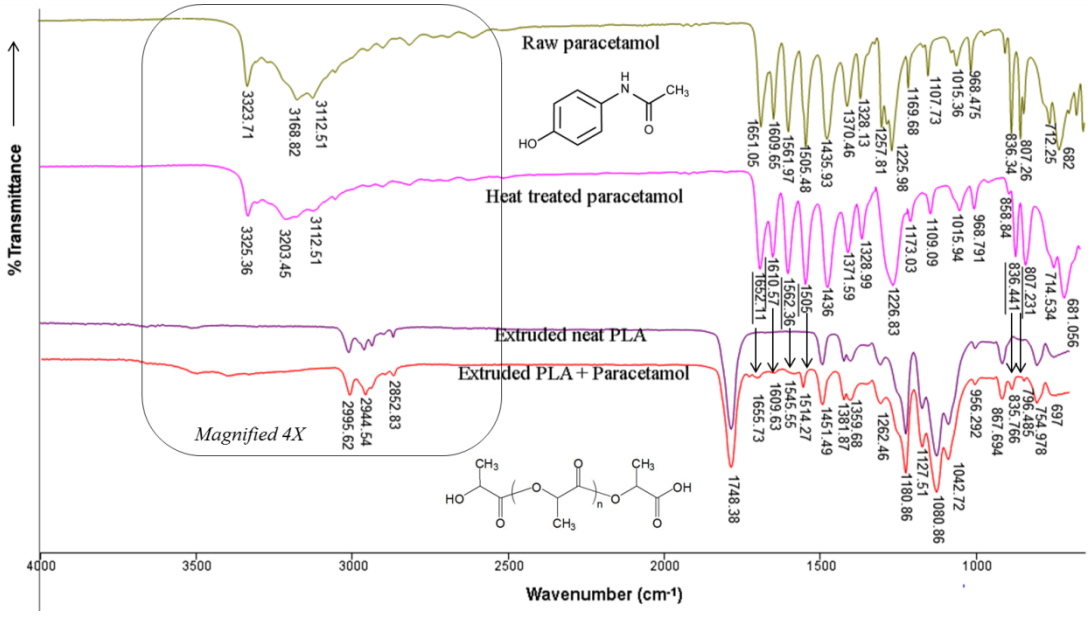

Figure 5.4: *Comparison of ATR-FTIR spectra of raw paracetamol (olive green), heat treated paracetamol (pink), neat extruded PLA (purple) and PLA melt compounded with paracetamol (red).*

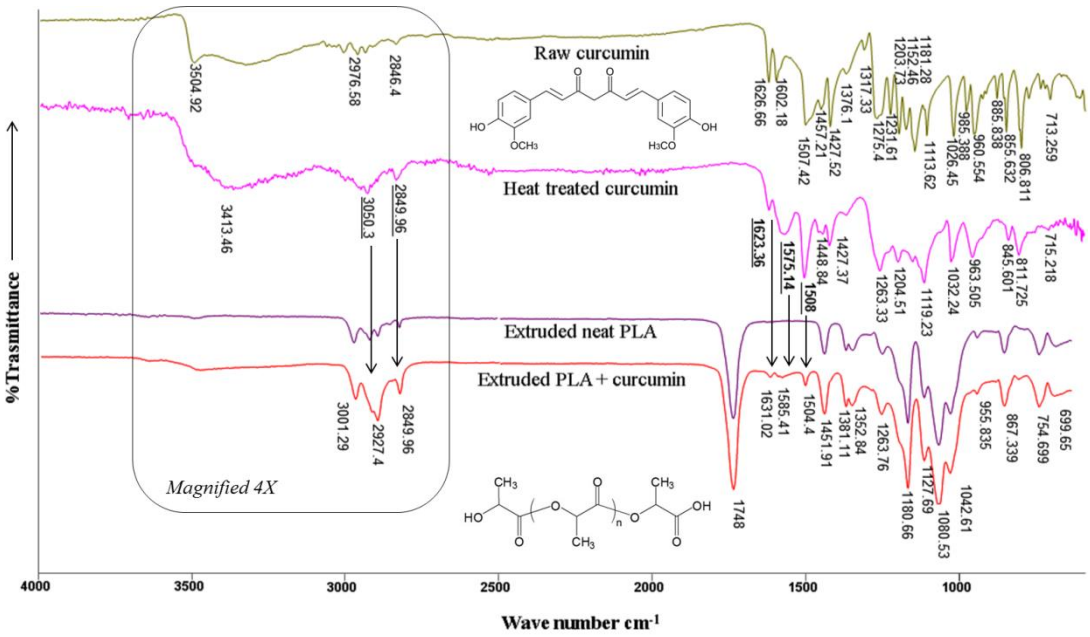

Figure 5.5: *Comparison of ATR-FTIR spectra of raw curcumin (olive green), heat treated curcumin (pink), neat extruded PLA (purple) and PLA melt compounded with curcumin (red).*

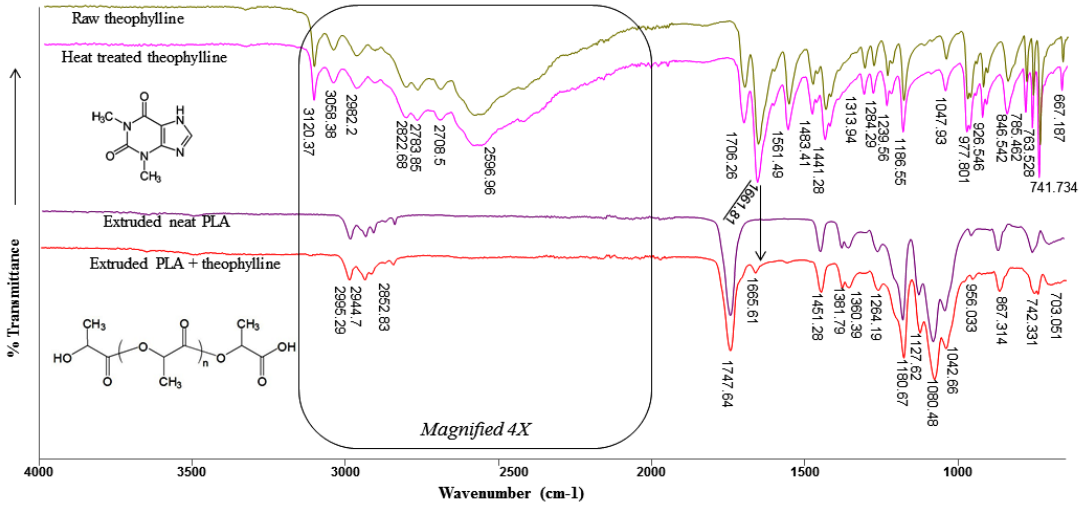

Figure 5.6: *Comparison of ATR-FTIR spectra of raw theophylline (olive green), heat treated theophylline (pink), neat extruded PLA (purple) and PLA melt compounded with theophylline (red).*

Examination of the IR spectra belonging to the unprocessed and the heat treated curcumin (C_{ht}) (figure 5.5) led to a similar set of observations. The phenolic O-H stretching peak at 3500.92 cm^{-1} and the aromatic C=C peak at 1602 cm^{-1} in the IR spectrum of raw curcumin became broader and were shifted

to 3413.06 cm^{-1} and 1575.14 cm^{-1} respectively in the IR spectrum of C_{ht}. Moreover the peak corresponding to C-O stretching (1231 cm^{-1}) disappeared after heat treatment. The characteristic differences in the IR spectrum of the unprocessed curcumin and the C_{ht} suggested that the red-orange material generated after heat treatment was the amorphous form of curcumin, while the unprocessed yellow coloured curcumin was present in the polymorphic Form I. (Sanphui, 2012; Wegiel *et al*., 2014), Contrarily, the IR spectrum of theophylline exhibited no change after heat treatment (figure 5.6). Since the reported (Seton *et al*., 2010) IR spectra for the Form I and the Form II of theophylline match, the polymorphic form of theophylline could not be identified from the FTIR studies.

The IR spectra of the melt compounded matrices were mainly contributed to by PLA. The distinguishing PLA peaks were evident at wavenumbers of 1748 cm^{-1}, 1180.66 cm^{-1} and 1080.53 cm^{-1}, corresponding to the stretching vibrations of aliphatic C=O, asymmetrical stretching of C-O-C and symmetrical stretching of C-O-C respectively (figure 5.4 - figure 5.6) (Nikolic *et al*., 2010). The IR spectrum of curcumin loaded PLA (5% w/w) (figure 5.5) showed extra peaks at 1504.4 cm^{-1}, 1585.41 cm^{-1} and 1631.2 cm^{-1}, which correspond to the amorphous curcumin. Moreover, the peaks at 2849.96 and 2927.4 cm^{-1} belonging to PLA were enlarged due to an additive effect of the related peaks in the amorphous curcumin spectrum (Thi Thu Trang *et al*., 2012). Similarly, several new peaks appeared in the IR spectrum of paracetamol loaded PLA (5% w/w) (figure 5.4), which matched with the IR spectrum of amorphous paracetamol. These included peaks at 1655.73 cm^{-1}, 1609.63 cm^{-1}, 1545.55 cm^{-1}, 1514.24 cm^{-1}, 836.76 cm^{-1} and 796.48 cm^{-1}. The above mentioned observations confirmed that curcumin and paracetamol were present in the amorphous state after melt extrusion with PLA. Nevertheless the appearance of specific new peaks indicates a possibility of a binding interaction between the amorphous drug phase and PLA. Whether the amorphous drug phase was molecularly mixed with the polymer phase (solid solution) or it existed as a separate phase must be further confirmed by microscopy. The IR spectrum of

PLA remained largely unaltered after melt extrusion with 5% w/w theophylline. This suggests a poor interaction between PLA and theophylline, the latter being present as a separate crystalline phase.

5.5.2. Assessment by X-ray diffraction techniques

The polymorphic state of the model drugs was further verified by X-ray diffraction studies. The characteristic crystalline reflections observed in the PXRD (Powder X-Ray Diffraction) pattern of the unprocessed curcumin, paracetamol and theophylline are labelled on the respective diffractograms (figure 5.7 - A, B, C respectively). These included the peaks observed at 2θ: 8.89, 17.24, 18.16, 24.68, 21.20, 25.74, 27.34 ±0.2° for curcumin (figure 5.7 - A), at 2θ:12.096, 15.51, 18.17, 23.39, 24.32 and 26.51 ± 0.2° for paracetamol (figure 5.7 - B) and those observed at 2θ: 7.08, 12.5, 14.27, 23.96, 25.47 and 27.28 ± 0.3° for theophylline (figure 5.7 - C).

Cross referencing with the available literature confirmed that the unprocessed curcumin (Sanphui *et al.*, 2011) and the unprocessed paracetamol (Wang *et al.*, 2011; Zaki, 2011) were present in their polymorphic Form I, while theophylline was present in the Form II (Seton *et al.*, 2010). The diffraction pattern of C_{ht} and P_{ht} exhibited a hump, coupled with absence of all crystalline diffraction peaks. This observation further established that C_{ht} and P_{ht} were present in the amorphous form. On the contrary, the PXRD pattern of T_{ht} was unchanged, signifying no polymorphic change in theophylline after heat treatment. Among the compounded systems, only the theophylline containing PLA matrix showed the presence of a few crystalline peaks matching with the diffractogram of theophylline Form II. Therefore it is safe to state that theophylline was present as a crystalline suspension in PLA; while, curcumin and paracetamol formed a glassy (amorphous) phase.

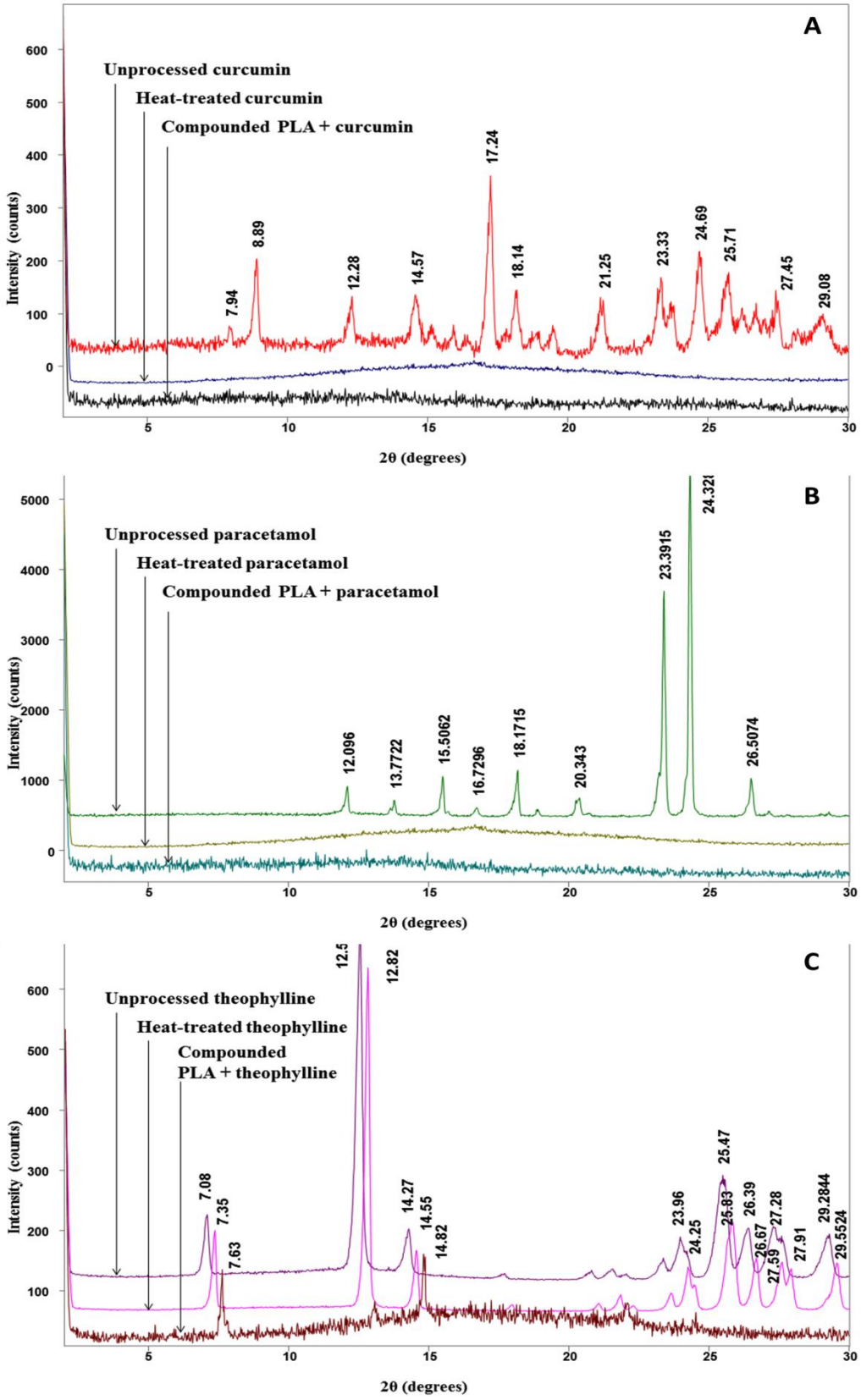

Figure 5.7: *X-ray diffractograms for the pure model drugs, heat treated model drugs and that melt compounded with PLA.*

A) Curcumin, **B)** Paracetamol and **C)** Theophylline

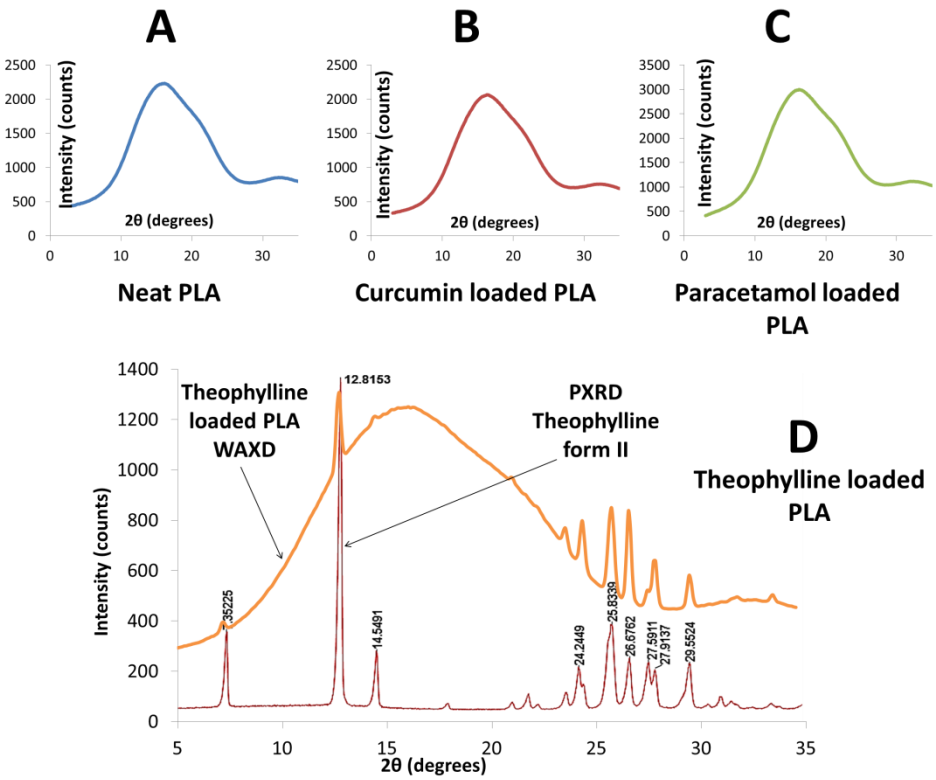

Figure 5.8: *WAXD- diffractograms of the PLA films with and without model drugs.* **A)** Neat PLA film, **B)** Curcumin loaded PLA film, **C)** Paracetamol loaded PLA rods and **D)** Theophylline loaded PLA films.

Drug loaded matrices (films & rods) were prepared by a single-screw extruder, which involved re-melting the compounded material followed by extrusion into the suitable geometry. Therefore, the drug loaded matrices were assessed by Wide Angle X-ray Diffraction (WAXD), in order to confirm the polymorphic state of the drug as well as the polymer. The diffraction intensity V/s diffraction angle (2θ) curves representing each model system are summarised in the figure 5.8. Both paracetamol and curcumin loaded PLA matrices showed a single hump similar to neat PLA films. On the contrary, the theophylline loaded films showed a large hump along with a few smaller peaks at 2θ: 7.08, 12.5, 23.96, 25.47 and 27.28 ± 0.3° corresponding to the Form II of theophylline. Therefore it is clear that the theophylline loaded films contained a suspension of the crystalline theophylline (Form II) in amorphous PLA. Contrarily, curcumin and paracetamol remained in an amorphous state, either molecularly mixed with the amorphous PLA or as a separate phase.

5.5.3. Visualisation of the physical state of the model drugs in PLA

The solubility status of the model drugs in PLA was validated by visualisation of the solid and melt phases of the compounded systems by hot-stage microscopy. Table 5.2 presents three sets of images for each system; the first column denotes the solid-state of the compounded matrices at room temperature, the second column represents the molten state (t = 180 °C) and the third displays the post cooling state.

Table 5.2: *Comparison of the microscopic images of the model drug loaded systems in the pre-melting, the molten and the post cooling stage*

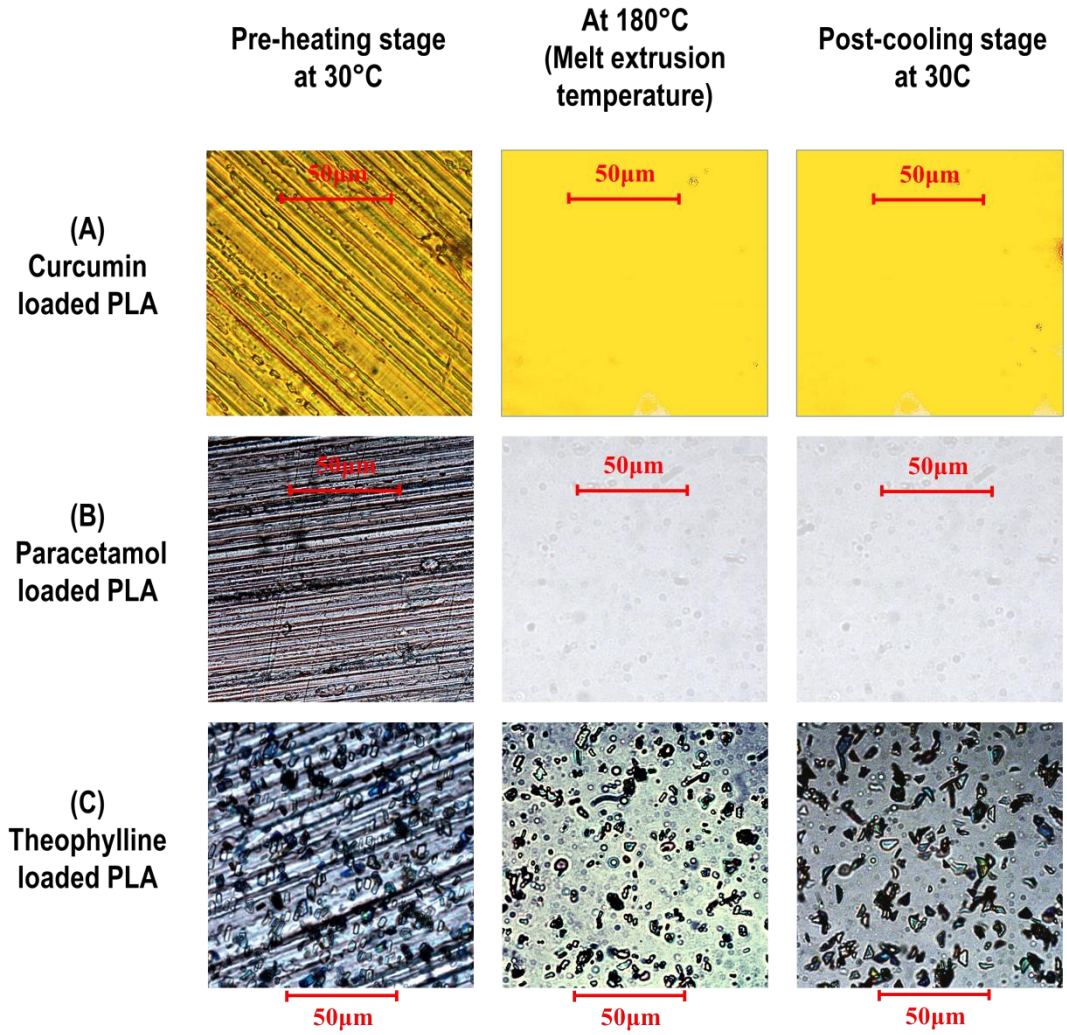

The microscopic images of curcumin (table 5.2 - A) and paracetamol (table 5.2 - B) loaded systems revealed a complete absence of the crystalline form of

these model drugs in the pre-melting stage, as well as while cooling from the melt. Moreover, no phase separation was observed in the molten state, suggesting that both of these drugs formed a solution with PLA at 5% w/w loading. When analysed by DSC, both paracetamol and curcumin loaded PLA matrices showed a single glass transition. Moreover, no melting endotherm was observed at temperatures corresponding to the melting points of pure paracetamol and curcumin. Therefore, the results confirmed formation of a glassy solution of paracetamol or curcumin in PLA (Qi *et al*., 2008). In contrast to this, theophylline was present as a crystalline suspension in the un-molten composite matrix as well as in the PLA melt (table 5.2 - C). Interestingly, growth of theophylline crystals was observed during the cooling stage. This observation signifies that a part of the added theophylline was soluble in the PLA melt, which crystallised out on cooling, due to the seeding action provided by already existing crystals.

5.6. Rheological testing

Rheology relates to measurement of flow-induced deformation in the material. It is often used as a tool for establishing suitable melt processing conditions for various polymers. Nevertheless, degradation of a polymer after being subjected to a thermo-mechanical treatment can be traced using rheology. It further helps in understanding the interaction between fillers and their interaction with the polymer matrix. Therefore, virgin PLA as well as the melt compounded (drug + PLA) material was evaluated by rheology.

5.6.1. Amplitude sweep analysis

In amplitude sweep tests, the storage modulus - G’ and the loss modulus - G’’ are measured as a function of strain amplitude, at a constant strain rate. For viscoelastic materials such as polymer melts, G’ correlates to the amount of energy stored in the form of elastic links, which can be spent in order to regain the original structure. Contrarily, G’’ is a measure of the energy barrier for initiating a deformation.

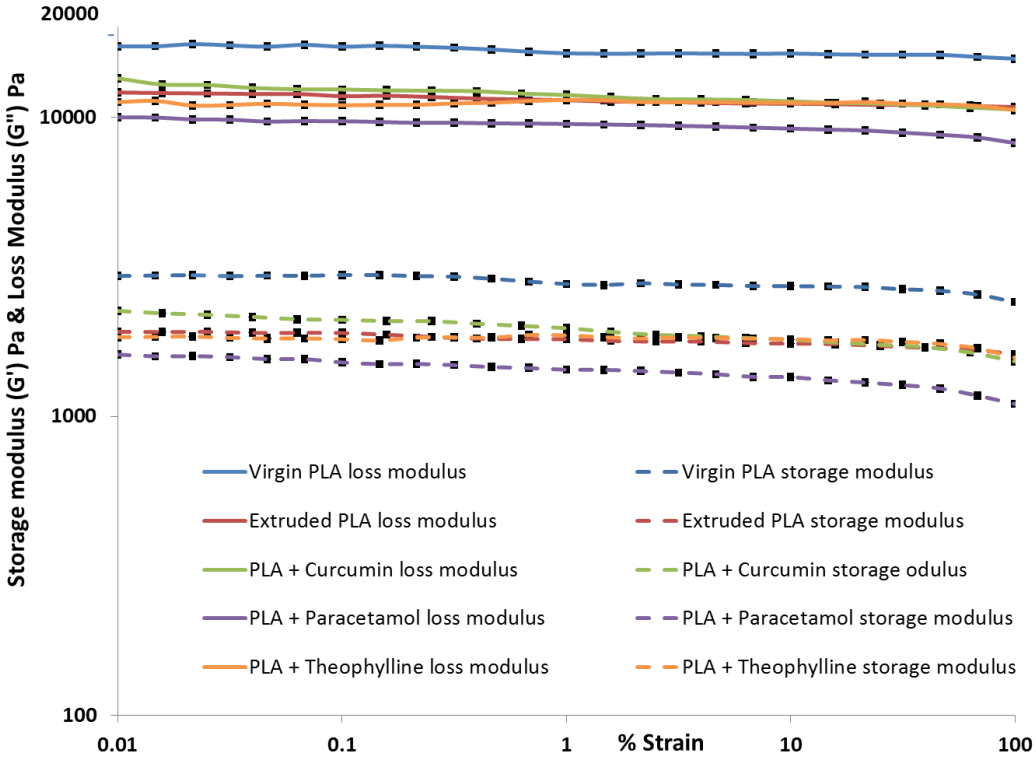

Figure 5.9: *Amplitude sweep analysis of the model PLA systems at 160 °C*

Notes - G' (dashed) and G" (solid line) against % strain for virgin PLA (blue), neat extruded PLA (red) and PLA compounded with 5% curcumin (green), 5% paracetamol (purple), 5% theophylline (orange). The average of 3 replicate measurements is plotted. The error bars (black dots) represent the standard deviation.

Melt extruded PLA (filled and unfilled) exhibited lower G' and G'' profiles than virgin PLA, at all test temperatures (figure 5.9, figure 5.10). A statistical comparison of G' was made by paired t-tests at 1% strain amplitude. This data for 160 °C and 210 °C test temperatures is reviewed in table 5.3. It is clear that G' of the extruded systems was significantly lower than that of virgin PLA. This can be attributed to the minor, un-avoidable molecular weight degradation incidental to the melt extrusion technique. The statistical difference between G' of the neat extruded PLA and the melt compounded systems was significant at all test temperatures, except for that between extruded PLA and theophylline loaded PLA at 210 °C (table 5.3). Nevertheless, this difference was unsubstantial for the curcumin and theophylline loaded systems. Among the extruded systems the paracetamol loaded PLA exhibited the lowest G' at all

studied temperatures (figure 5.9, figure 5.10). The amorphous paracetamol has significantly lower glass transition temperature (22 – 23 °C) than PLA (55 – 60 °C). Moreover, it formed a solid solution with PLA. Therefore, the G' and G" of the paracetamol loaded PLA were reduced by virtue of the plasticisation by paracetamol (Pillin *et al*., 2006). A similar effect was not observed for curcumin and theophylline, since curcumin has a glass transition temperature equivalent to that of PLA, while theophylline was present as a separate crystalline phase.

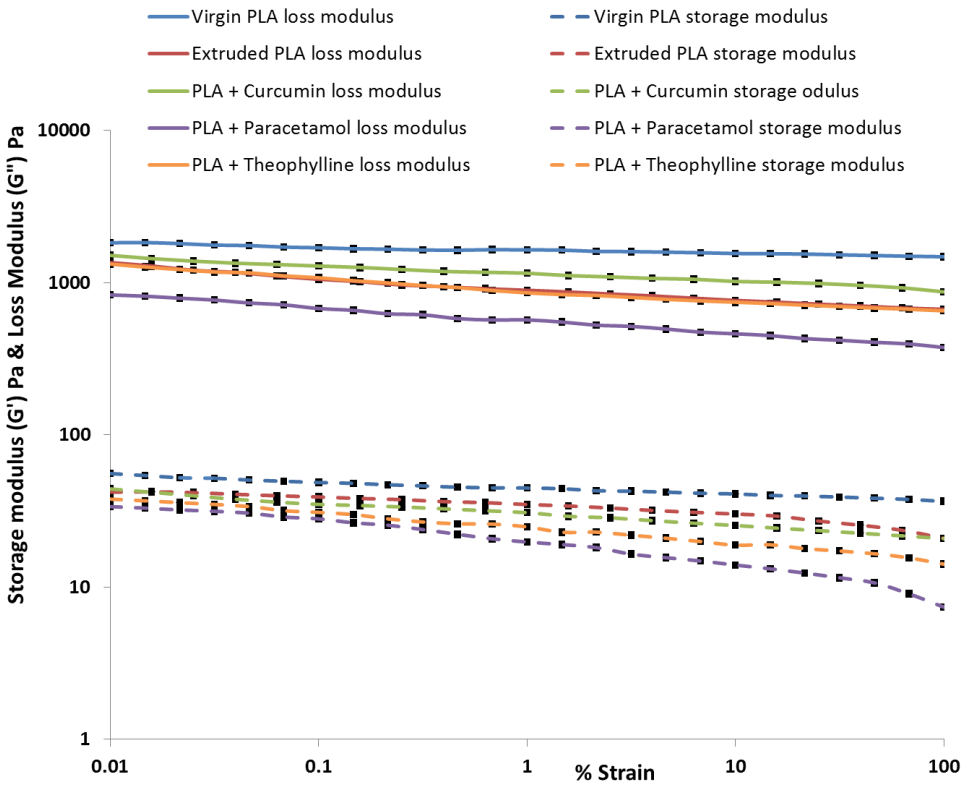

Figure 5.10: *Amplitude sweep analysis of the model PLA systems at 210 °C.*

Notes - Comparison of G' (dashed) and G" (solid line) against % strain for virgin PLA (blue), neat extruded PLA (red) and PLA melt compounded with 5% curcumin (green), 5% paracetamol (purple), 5% theophylline (orange).

The average of 3 replicate measurements is plotted. The error bars (black dots) represent the standard deviation.

Table 5.3: *Statistical analysis of the amplitude sweep test results: comparison of G' at 1% strain amplitude*

G' at 1% strain amplitude (and 1 Rad. Sec^{-1} angular frequency) (Mean ± SD, n = 3)					
	Virgin PLA	Extruded Neat PLA	Curcumin loaded PLA (CPLA)	Theophylline loaded PLA (PPLA)	Paracetamol loaded PLA (TPLA)
160 °C	2770.885 ± 2.9610	1809.664 ± 3.0029	1972.074 ± 5.2949	1864.727 ± 4.0590	1432.558 ± 3.2141
210 °C	16371.23 ± 36.1910	11410.36 ± 13.2064	11873.71 ± 38.3322	11428.21 ± 12.4320	9503.858 ± 7.5086
Statistical comparison by paired t-test					
Significance at 160 °C	Virgin Vs Extruded	P < 0.0001, t = 394.78	**Significance at 210 °C**	Virgin Vs Extruded	P < 0.0001, t = 223.04
	Extruded Vs CPLA	P < 0.0001, t = 46.21		Extruded Vs CPLA	P = 0.0025, t = 19.795
	Extruded Vs TPLA	P = 0.0003, t = 18.89		Extruded Vs TPLA	P = 0.1869, t = 1.704
	Extruded Vs PPLA	P < 0.0001, t = 148.49		Extruded Vs PPLA	P < 0.0001, t = 217.37

Notes: The null hypothesis was that the compared samples were statistically the same

P > 0.05 = The difference between the compared samples is **not statistically significant**
0.05 > P > 0.01 = The difference between the compared samples is **statistically significant**
0.01 > P = The difference between the compared samples is **highly significant**

One important implication of the amplitude sweep is to determine the linear viscoelastic region (LVER). In this region, the storage modulus remains constant, irrespective of the applied stress. Since the LVER is correlated to the structural integrity of the material under study, it is recommended that the viscosity measurement by frequency sweep tests should be carried out within the LVER. This ensures a non-destructive testing of the material. A strain amplitude of 1% was selected for further studies, as it lies within the LVER for all PLA systems under investigation.

5.6.2. Frequency sweep test: analysis of the complex viscosity

Viscosity of PLA melt depends on its molecular weight, percentage racemisation, crystallinity and the presence/ absence of branching (Lim *et al.*, 2008). The filled as well as the unfilled PLA under investigation exhibited a constant 'zero shear viscosity' which was followed by shear thinning at higher angular frequencies (figure 5.11). Shear thinning was diminished at elevated temperatures, owing to a drop in the zero shear viscosity itself. A 10 °C rise in the temperature produced 40 ± 3% fall in the value of the complex viscosity. This observation was comparable to the previous reports on different grades of PLA (Cooper-White and Mackay, 1999). A temperature induced drop in the zero shear viscosity coupled with shear thinning, can significantly enhance the flow of the molten materials and their mixing, during melt extrusion.

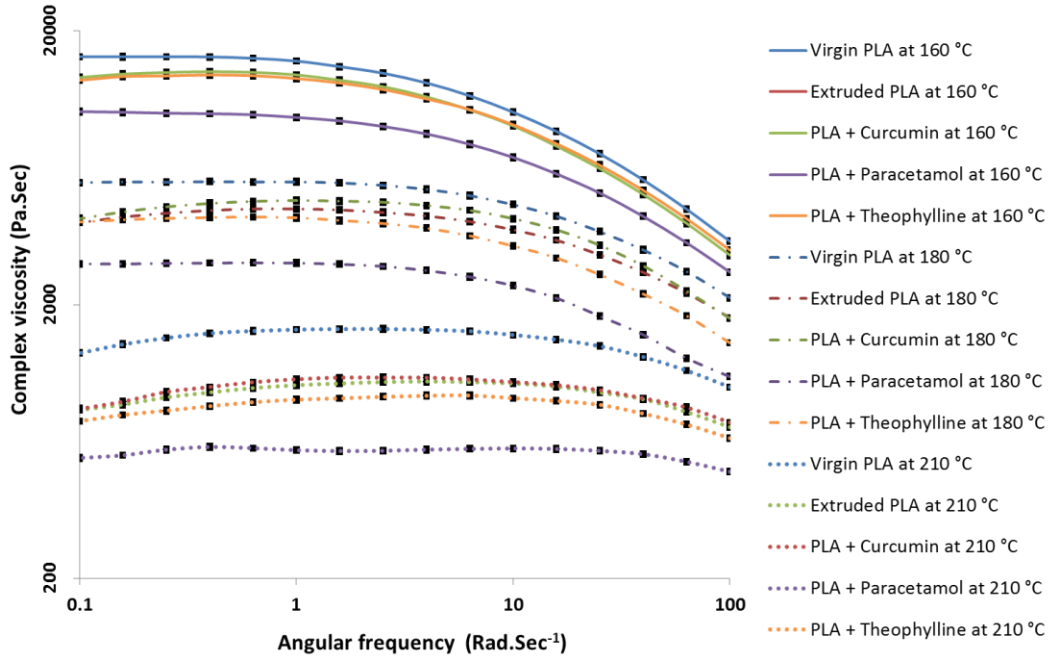

Figure 5.11: *Comparison of complex viscosity against angular frequency curves for the model drug loaded PLA systems at various test temperatures*

Notes: 160 °C (solid line), 180 °C (dashed line) and 210 °C (dotted line) for virgin PLA (blue), neat extruded PLA (red) and PLA melt compounded with 5% curcumin (green), 5% paracetamol (purple), 5% theophylline (orange).

The average of 3 replicate measurements is plotted. The error bars (black dots) represent the standard deviation.

Figure 5.11 displays a comparison of the 'complex viscosity Vs angular frequency' curves, for the investigated systems at 160 °C, 180 °C, and 210 °C test temperatures. (Only three test temperatures are included here for a clearer representation). Figure 5.11 confirms that melt extrusion led to a drop in the viscosity of the extruded systems (both filled and un-filled). The viscosities of the investigated systems at 1 Rad.sec^{-1} and 100 Rad.Sec^{-1} were statistically compared by paired t-tests (table 5.4). The statistical treatment confirmed that there was a significant difference between the zero shear viscosities (1 Rad.sec^{-1}) of the investigated systems. Albeit, such a difference between the neat extruded PLA and the curcumin loaded PLA was unsubstantial (figure 5.11).

As discussed previously in the amplitude sweep section, the lower viscosity of the melt-extruded systems can be attributed to the molecular weight degradation that could not be avoided, although PLA was pre-dried and processed at temperatures not exceeding 180 °C. Extreme susceptibility of PLA to thermolysis and hydrolysis during melt extrusion has been previously documented (Carrasco *et al*., 2010; Taubner and Shishoo, 2001; Wang *et al*., 2008). In addition to temperature and residual moisture, screw configuration and screw speed also influence the molecular weight degradation during melt extrusion. Higher screw speed or a configuration that produces a greater shear, leads to molecular weight degradation due mechanical impact and localised generation of the frictional heat. On the contrary, lower screw speeds enhance molecular weight degradation by prolonging the residence time. Wang *et al*. (2008) observed minimal process induced degradation of PLA at 180 °C and 50 rpm screw speed, using a twin screw extruder with 16 mm diameter and 25 L/D ratio. The twin-screw extruder used in the current study was equipped with 16 mm diameter and 40 L/D ratio screws; therefore a proportionately higher (80 rpm) screw speed was used.

Table 5.4: *Statistical analysis of the frequency sweep test results: comparison of the zero shear viscosity and the viscosity at 100 Rad.sec^{-1} angular frequency, between the studied model systems.*

Statistical comparison of the viscosity by paired t-test							
Zero shear viscosity (Pa.s)	160 °C	Virgin Vs Extruded Neat	P < 0.0001, t = 198.52	Viscosity at 100 Rad.Sec^{-1} (Pa.s)	160 °C	Virgin Vs Extruded Neat	P = 0.0003, t = 53.97
		Extruded Neat Vs CPLA	P < 0.0001, t = 81.44			Extruded Neat Vs CPLA	P = 0.0609, t = 3.86
		Extruded Neat Vs PPLA	P < 0.0001, t = 99.31			Extruded Neat Vs PPLA	P < 0.0001, t = 116.70
		Extruded Neat Vs TPLA	P = 0.0022, t = 21.14			Extruded Neat Vs TPLA	P = 0.0071, t = 11.78
	180 °C	Virgin Vs Extruded Neat	P < 0.0001, t = 116.93		180 °C	Virgin Vs Extruded Neat	P = 0.0001, t = 85.20
		Extruded Neat Vs CPLA	P = 0.0002, t = 21.32			Extruded Neat Vs CPLA	P = 0.1091, t = 2.77
		Extruded Neat Vs PPLA	P = 0.0006, t = 39.72			Extruded Neat Vs PPLA	P < 0.0001, t = 278.10
		Extruded Neat Vs TPLA	P < 0.0001, t = 198.52			Extruded Neat Vs TPLA	P < 0.0001, t = 188.59
	200 °C	Virgin Vs Extruded Neat	P < 0.0001, t = 135.01		200 °C	Virgin Vs Extruded Neat	P < 0.0001, t = 132.81
		Extruded Neat Vs CPLA	P = 0.0012, t = 29.10			Extruded Neat Vs CPLA	P = 0052, t = 13.86
		Extruded Neat Vs PPLA	P < 0.0001, t = 242.49			Extruded Neat Vs PPLA	P < 0.0001, t = 102.43
		Extruded Neat Vs TPLA	P < 0.0001, t = 38.97			Extruded Neat Vs TPLA	P = 0.0011, t = 29.70

Notes: Actual data is represented in figure 5.11

The null hypothesis was that the compared samples were statistically the same

P > 0.05 = The difference between the compared samples is **not statistically significant**

0.05 > P > 0.01 = The difference between the compared samples is **statistically significant**

0.01 > P = The difference between the compared samples is **highly significant**

The theophylline loaded PLA showed a slightly greater viscosity drop than the neat extruded PLA; whereas, the paracetamol loaded PLA showed a significantly greater drop in the viscosity, at all test temperatures (figure 5.11, table 5.4). Since the molecular weight degradation (sec. 5.8) in the abovementioned systems did not exceed that shown by the neat extruded PLA, a greater drop in the viscosity relates to a factor other than thermal degradation. In the case of paracetamol loaded PLA, this can be attributed to the plasticisation action of the molecularly dispersed amorphous paracetamol.

Owing to the presence of theophylline as a crystalline suspension in PLA, the composite system should ideally show a greater viscosity than the neat extruded PLA (Pluta *et al*., 2007). However, the viscosity of the theophylline loaded PLA was lower than that of the neat extruded PLA ($P < 0.01$). Similar results were obtained by Gu *et al*. (2009) when PLA was filled with less than 10% w/w of calcium carbonate ($CaCO_3$) (the particle size was comparable to the theophylline particle size used in this study). The peculiar behaviour of the PLA composites was attributed to weakening of the inter-chain interactions by the filler particles. At lower loadings, the inter-particulate interactions between the filler particles are insufficient to raise the viscosity of the composite material (by network formation). Nevertheless, presence of poorly compatible filler weakens the particle-matrix interactions as well as the interactions between the polymer chains. Theophylline similar to $CaCO_3$ shows poor cohesive interactions with PLA (sec. 5.2), which can explain the drop in the G', G" and viscosity of the theophylline loaded PLA.

5.6.3. Time sweep at a constant temperature

Thermal stability of a polymer melt with respect to time can be studied by subjecting it to a constant strain amplitude, angular frequency and temperature, over an extended duration (Sodergard and Nasman, 1994). Figure 5.12 displays a comparison of the viscosity changes with time, for virgin PLA and the drug loaded PLA, at 160 °C, 180 °C and 210 °C test temperatures.

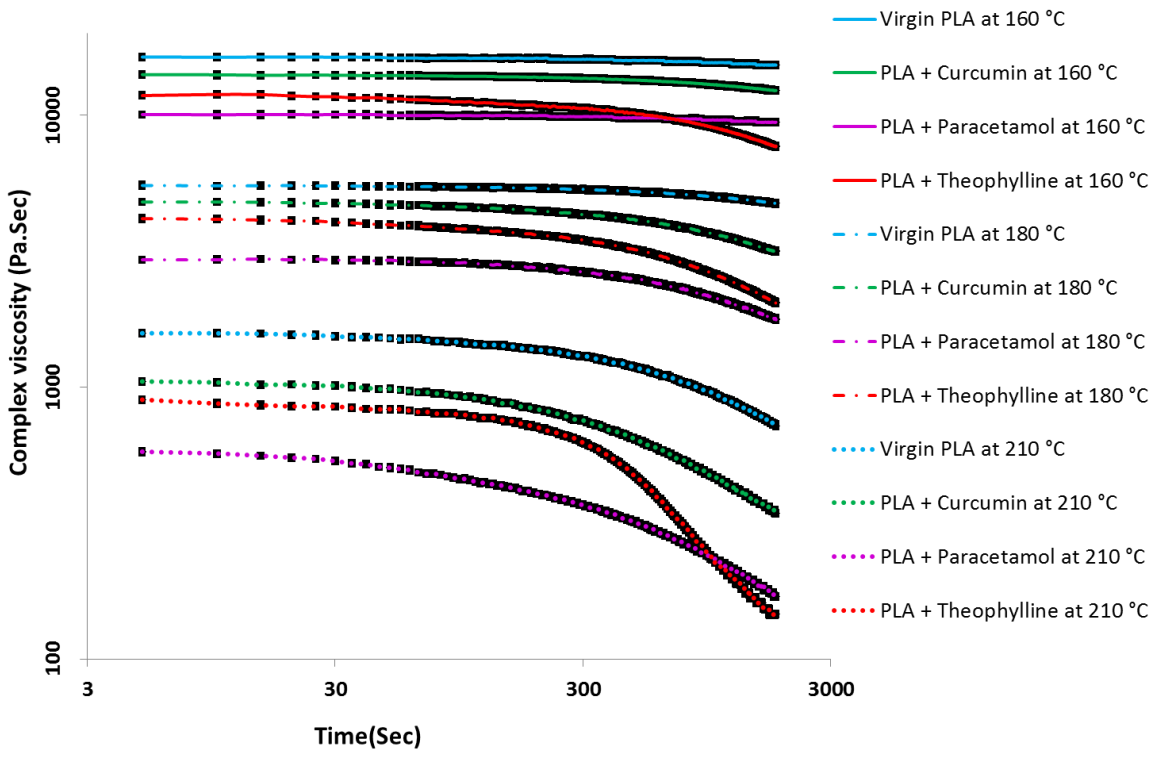

Figure 5.12: *Time sweep test for evaluation of the thermal stability of the model drug loaded PLA systems.*

Note: The figure shows a comparison of the complex viscosity against time, at 160 °C (solid line), 180 °C (dashed line) and 210 °C (dotted line) for virgin PLA (blue) and the PLA melt compounded with 5% curcumin (green), 5% paracetamol (pink), 5% theophylline (red).

*The average of 3 replicate measurements is plotted. The error bars (black dots) represent the standard deviation.

It is evident that the viscosity of virgin PLA (blue curves in figure 5.12) remained reasonably constant over the 30 minutes duration, when tested between 160 °C and 180 °C. At these temperatures the total viscosity drop at the end of the test was restricted to less than 15% of the initial value (table 5.5). However, the drop in the viscosity was more prominent with a further rise in the test temperature, above 180 °C. Thermal degradation of PLA can be minimised by removing the trace amount of water and restricting the processing temperature and residence time to the minimum possible value (Taubner and Shishoo, 2001). Therefore, 180 °C was considered as an appropriate temperature for the melt compounding operation, since it can produce a suitable viscosity drop without causing significant polymer degradation. As explained

previously (sec 5.6.2), the screw speed was fixed to 80 rpm in order to balance the adverse effects of the prolonged residence time and shear induced degradation. This decision was entirely based on the literature reports (Taubner and Shishoo, 2001; Wang *et al*., 2008). Nevertheless, PLA was dried carefully before any melt processing.

Table 5.5: *Statistical comparison of the time sweep results represented in figure 5.12*

Percentage drop in the viscosity in 30 minutes (Mean ± SD, n = 3)			
Sample	**160 °C**	**180 °C**	**200 °C**
Virgin PLA	6.62 ± 0.5855	14.02 ± 0.3846	54.39 ± 0.3154
Curcumin loaded PLA (CPLA)	12.55 ± 0.1842	39.52 ± 0.1047	70.27 ± 0.0487
Paracetamol loaded PLA (PPLA)	6.37 ± 0.0277	34.51 ± 0.2076	67.66 ± 0.2009
Theophylline Loaded PLA (TPLA)	35.16 ± 0.0642	50.86 ± 0.3331	83.77 ± 0.0194
Statistical comparison by paired t-test			
Virgin Vs CPLA	160 °C	P = 0.0036, t = 16.727	
	180 °C	P = 0.0001, t = 89.075	
	200 °C	P = 0.0002, t = 69.928	
Virgin Vs PPLA	160 °C	P = 0.5361, t = 0.7405	
	180 °C	P < 0.0001, t = 100.99	
	200 °C	P < 0.0001, t = 75.340	
Virgin Vs TPLA	160 °C	P = 0.0004, t = 48.639	
	180 °C	P < 0.0001, t = 125.36	
	200 °C	P < 0.0001, t = 161.04	

Note: The null hypothesis was that the compared samples were statistically the same

P > 0.05 = The difference between the compared samples is **not statistically significant**
0.05 > P > 0.01 = The difference between the compared samples is **statistically significant**
0.01 > P = The difference between the compared samples is **highly significant**

Time sweep studies were performed on the melt compounded systems, in order to assess their thermal stability when subjected to further processing; i.e. extrusion of sheets and billets. Repeated thermal processing significantly reduces thermal stability of PLA. The oligomers generated in the previous thermal cycle catalyse the molecular weight reduction by the trans-esterification reaction (Jamshidi *et al*., 1988). Among the compounded systems studied here, the paracetamol loaded PLA (purple curves in figure 5.12) displayed the highest

thermal stability, whereas the theophylline loaded PLA (orange curves in figure 5.12) was least stable. The curcumin loaded PLA exhibited an intermediate behaviour (orange curves in figure 5.12). This was confirmed statistically by comparison of the total viscosity drop over the 30 minutes of the test duration, using paired t-tests (table 5.6). At 160 °C test temperature the drop in viscosity of the paracetamol loaded PLA was equivalent to that exhibited by virgin PLA ($P = 0.53$). However, at higher test temperature the paracetamol loaded systems underwent a greater viscosity reduction ($P < 0.001$). Similarly, the remaining systems showed significantly higher ($P < 0.01$) viscosity drop than virgin PLA, during the time sweep test. The viscosity reduction exhibited by curcumin loaded PLA was comparable to the paracetamol loaded PLA; nevertheless that in the case of theophylline loaded PLA was substantially higher (table 5.6, figure 5.12).

A higher stability in the case of PPLA can be attributed to the plasticisation action provided by paracetamol. This may lower the thermal degradation of PLA by reducing the mechanical impact and generation of the frictional heat. In the case of curcumin, the same can be attributed to the potent antioxidant and free radicle scavenging activity (Ak and Gulcin, 2008), which may prevent the oxidative thermolysis of PLA. A detailed study focused on understanding these mechanisms was beyond the scope of this project. Overall, the results suggest that the compounded systems must be processed at lower temperatures than the virgin polymer and the residence time should be kept minimal. Therefore, the film and billet extrusion was carried out with a temperature profile as follows; feeding zone = 45 °C, compression zone = 110 °C, metering zone = 160 °C, and the die set to 170 °C, with the screw speed of 50 rpm.

5.6.4. Summary

From the above discussion is it clear that PLA melt exhibit a temperature dependent, predominantly viscous behaviour at lower shear rates. The glass transition of the drug and its solubility in the PLA matrix, significantly affects the

rheological behaviour as well as the thermal stability of the PLA melt. A safe processing window for PLA lies between 160 °C and 180 °C, with 180 °C being the most favourable temperature for compounding operation and 170 °C for further extrusion into billets and sheets. Moreover, the screw speed must be adjusted such a way to balance the adverse effects of the prolonged residence time and the shear induced degradation. This was fixed to 80 rpm for extrusion compounding and to 40 rpm for further extrusion into different geometries, based on the reviewed literature.

5.7. Assessment of PLA degradation in the presence of sodium salicylate

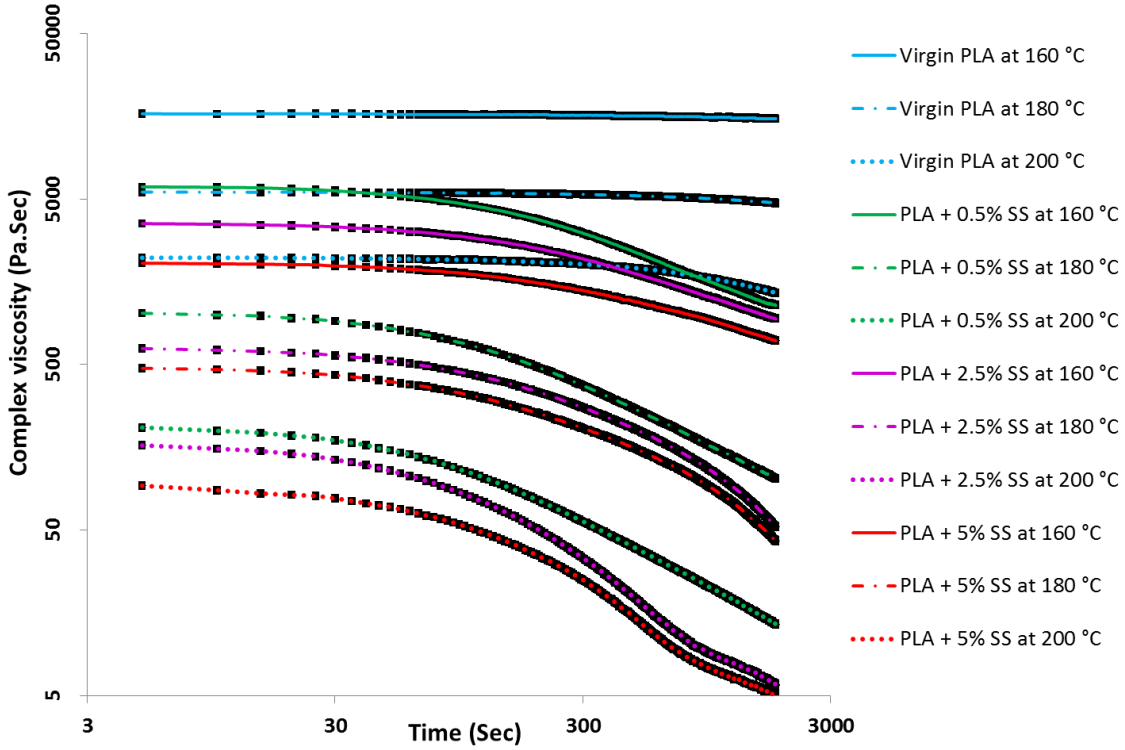

Figure 5.13: *Time sweep test for analysis of thermal stability of PLA in presence of sodium salicylate*

Note: The above figure shows a comparison of the complex viscosity against time, at 160 °C (solid line), 180 °C (dashed line) and 200 °C (dotted line) for virgin PLA (blue) and PLA melt compounded with 0.5% (green), 2.5% (pink) and 5% SS (red) sodium salicylate.

*The average of 3 replicate measurements is plotted. The error bars (black dots) represent the standard deviation.

Sodium salicylate (SS) was initially selected as a model drug that can remain in a crystalline suspension state in PLA. However, rheological studies revealed that the storage and the loss moduli of the composite material were extremely unstable. Moreover, the zero shear viscosity of the composite PLA containing 5% w/w sodium salicylate was only 1/6th of the virgin PLA viscosity at 160 °C. Since the viscosity of the neat extruded PLA was almost 80% of the virgin PLA viscosity (at 160 °C), the effect of SS addition was notably large. To evaluate this effect, the following experiments were carried out on the melt extruded composite material, containing three different loadings of sodium salicylate; i.e. 0.5%, 2.5% and 5%w/w.

Table 5.6: *Statistical comparison of the time sweep results represented in figure 5.13*

Percentage drop in the viscosity in 30 minutes (Mean ± SD, n = 3)			
Sample	**160 °C**	**180 °C**	**200 °C**
Virgin PLA	6.62 ± 0.5855	14.02 ± 0.3846	38.94 ± 0.1367
PLA + 0.5% Sodium salicylate (SS)	80.76 ± 0.649	90.02 ± 0.635	93.52 ± 0.245
PLA + 2.5% Sodium salicylate (SS)	73.48 ± 0.829	91.67 ± 0.493	96.44 ± 0.206
PLA + 5% Sodium salicylate (SS)	66.05 ± 0.1078	91.01 ± 0.695	94.61 ± 0.516
Statistical comparison by paired t-test			
Virgin Vs 0.5% SS	160 °C	P < 0.0001, t = 141.91	
	180 °C	P < 0.0001, t =177.31	
	200 °C	P < 0.0001, t = 336.96	
0.5% Vs 2.5% SS	160 °C	P = 0.0013, t = 11.977	
	180 °C	P = 0.0380, t = 3.56	
	200 °C	P = 0.0006, t = 15.80	
2.5% Vs 5% SS	160 °C	P = 0.0042, t = 15.39	
	180 °C	P = 0.2722, t = 1.342	
	200 °C	P = 0.0294, t = 5.71	

Note: The null hypothesis was that the compared samples were statistically the same

P > 0.05 = The difference between the compared samples is **not statistically significant**
0.05 > P > 0.01 = The difference between the compared samples is **statistically significant**
0.01 > P = The difference between the compared samples is **highly significant**

Figure 5.13 summarises the results obtained in the time sweep rheology experiments, performed on the composite PLA containing different loadings of sodium salicylate. It is clear that the viscosity of the composite material was significantly lower than that of virgin PLA at all test temperatures. Moreover, the viscosity at a fixed test temperature reduced as the concentration of sodium salicylate increased. Figure 5.13 further reveals that the stability of the PLA melt was significantly reduced after compounding with sodium salicylate. The viscosity of virgin PLA remained stable for 30 minutes at 160 °C test temperature; while it started reducing approximately after 14 minutes at 200 °C. On the contrary, the viscosity of the composite PLA containing sodium salicylate started reducing only after a minute at 160 °C; while at 200 °C it reduced almost instantaneously. A plasticiser decreases melt viscosity of a polymer but it rarely reduces thermal stability (Ljungberg and Wesslen, 2002). Therefore, the results suggest that sodium salicylate might have enhanced thermal degradation of PLA.

Statistical comparison of the total viscosity drop during 30 minutes of the test duration (table 5.6), revealed the following. At 160 ℃, there was a significant ($P < 0.001$) difference between the viscosity drops produced by various loadings of SS. However, the total viscosity drop exhibited an inverse relation with the amount of SS at this temperature. This peculiarity could not be investigated further. At 180 ℃ and 200 ℃, merely 0.5% of SS produced 90.02 ± 0.635 % drop in the viscosity. The viscosity drop produced by the higher loadings was not substantially different as it ranged between 90 – 96%. The results of time sweep rheological experiments on the SS composite PLA were coherent with the molecular weights of these systems.

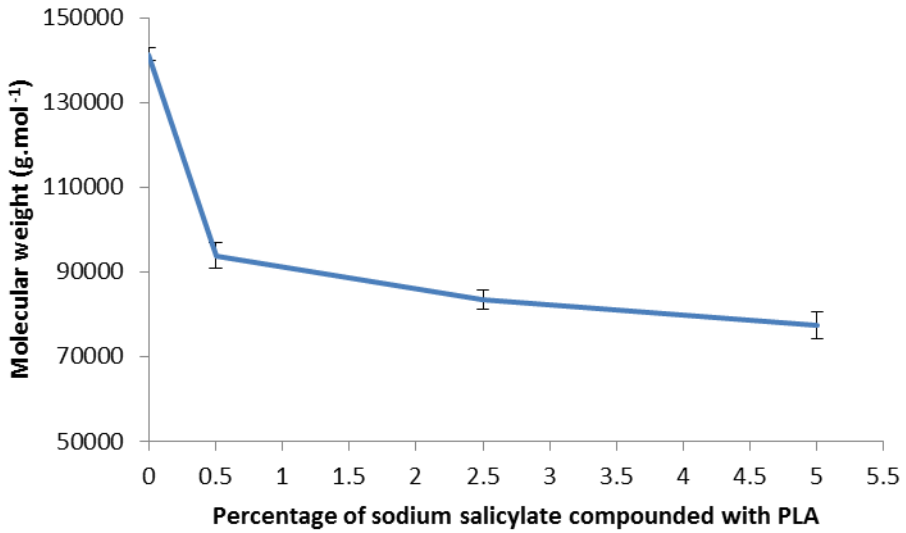

Figure 5.14: *Molecular weight degradation of PLA after melt compounding with various loading of sodium salicylate.*

*The graph represents the mean ± standard deviation, where n = 3.

The 0% sodium salicylate loading signifies neat extruded PLA

Table 5.7: *Statistical comparison of the molecular weight of the PLA melt compounded with various amounts of sodium salicylate.*

Statistical comparison by paired t-test	
Extruded PLA Vs **0.5%** SS	P = 0.0018, t = 23.496
0.5% SS Vs **2.5%** SS	P = 0197, t = 4.568
2.5% SS Vs **5%** SS	P = 0.0785, t = 2.627

Note: The null hypothesis was that the compared samples were statistically the same

P > 0.05 = The difference between the compared samples is **not statistically significant**

0.05 > P > 0.01 = The difference between the compared samples is **statistically significant**

0.01 > P = The difference between the compared samples is **highly significant**

The molecular weight degradation of PLA during melt compounding with SS was confirmed by GPC (figure 5.14). A substantial ($p < 0.01$; table 5.7) molecular weight reduction was observed at 0.5% SS loading. Statistical analysis revealed that the difference between molecular weights of the neat extruded PLA and the PLA containing 0.5% SS was highly significant. The statistical significance reduced as the SS loading increased (table 5.7).

Accordingly, the difference between molecular weights of 2.5% SS loaded PLA and 2.5% SS loaded PLA was statistically insignificant (or may be referred to as possibly significant based on the P-value) (table 5.7). The results clearly suggest that sodium salicylate caused thermal degradation of PLA; however, increasing the concentration of sodium salicylate did not substantially enhance the degradation.

Li *et al.* (2007) reported a 2.5 fold drop in the zero shear viscosity of PLA (tested at 180 °C), when it was melt compounded with 0.5% sodium stearate. They attributed it to the chain scission induced by sodium stearate. Previous reports on the utilisation of organic salts as nucleating agents for polyesters such as PET have confirmed that the nucleation mechanism involves a prior chemical reaction between the molten polyester and the organic salt (Legras *et al.*, 1983; Zhang, 2004). Precisely, organic salts such as sodium stearate transfer the sodium ion to random carboxyl oxygen of the polyester, leading to extensive scission of the polyester backbone (Legras *et al.*, 1983; Zhang, 2004). The same mechanism can explain the elevated thermal degradation of PLA in the presence of sodium salicylate.

5.8. Thermal degradation of PLA during melt processing

A significant limitation associated with melt processing of PLA is its tendency to undergo thermal degradation. The extent of degradation depends on the processing temperature, presence of moisture, the residence time and the mechanical impact resulting from the screw geometry and rotation speed (Wang *et al.*, 2008). Taubner *et al.* (2001) observed 15% reduction in the number average molecular weight (Mn) when pre-dried PLA was processed in a twin-screw extruder at 210 °C. Lowering the screw speed from 120 rpm to 20 rpm or increasing the processing temperature to 240 °C, augmented the molecular weight loss by 25% and 34% respectively. Moreover, when the resin was pre-equilibrated at 20 °C/ 65% RH, merely 0.3%, w/w moisture caused a dramatic molecular weight reduction to almost 35% of the original Mn.

Table 5.8: *Summary of the molecular weight changes in PLA after melt compounding with the model drugs and sheet / billet extrusion.*

Compounded system	Mw (g.mol^{-1})	Polydispersity
Virgin PLA	149634 ± 1785	1.66 ± 0.0261
Neat extruded PLA	141356 ± 1520	1.59 ± 0.0323
Melt compounded PLA + 5% curcumin (twin-screw)	143758 ± 2607	1.55 ± 0.0659
PLA + 5% curcumin sheets (single-screw)	142573 ± 2831	1.55 ± 0.0863
Melt compounded PLA + 5% paracetamol (twin-screw)	141287 ± 2414	1.58 ± 0.0604
PLA + 5% paracetamol billets (single-screw)	138134 ± 2141	1.54 ± 0.0778
Melt compounded PLA + 5% theophylline (twin-screw)	139352 ± 2079	1.55 ± 0.0716
PLA + 5% theophylline sheets (single-screw)	135732 ± 2804	1.55 ± 0.0508
PLA + 0.5% sodium salicylate	93897 ± 3151	1.52 ± 0.1098
PLA + 2.5% sodium salicylate	83531 ± 2350	1.46 ± 0.0589
PLA + 5% sodium salicylate	77485 ± 3219	1.4 ± 0.084

*The molecular weight and polydispersity values are expressed as mean ± standard deviation, where n=3.

Knowledge of molecular weight degradation is necessary, since it adversely affects the melt strength and the properties of the resulting matrices. The oligomers generated as a by-product of the degradation process, catalyse further breakdown during another melt processing cycle or even hydrolytic degradation during clinical application. Importantly, the effect of degradation can be reflected on the tensile deformation behaviour of the drug loaded PLA matrices and consequently on the drug release profile.

Table 5.8 summarises the changes in the molecular weight after each processing stage, determined using GPC. It is evident that extrusion of virgin PLA through a twin screw extruder at 180 °C led to a drop in the molecular weight by approximately 6%. Except sodium salicylate, all other model drugs remained inert and therefore a drop in the molecular weight after the compounding stage was approximately 4%, 6% and 7% for the curcumin, paracetamol and theophylline loaded PLA respectively. A smaller drop in the molecular weight of the curcumin loaded PLA might be attributed to the potent antioxidant and the radical scavenging activity of curcumin (Ak and Gulcin,

2008). This might have lowered the thermal degradation of PLA by the oxidative and the radical induced mechanisms. On the contrary, higher degradation induced by sodium salicylate correlates to the attack on the carboxyl oxygen of PLA by the cationic sodium (Legras *et al.*, 1983). Importantly, the change in the molecular weight was negligible ($P > 0.05$, by paired t-test), when the drug loaded PLA was further melt extruded into different geometries (rods/films) using a single screw extruder. This can be attributed to lower extrusion temperature and lesser shear stress produced by the single screw extruder. The reduction in the molecular weight observed in the current study, during both single- and twin-screw extrusion was significantly lower than the literature reports (Gogolewski *et al.*, 1993; Taubner and Shishoo, 2001; Wang *et al.*, 2008); which validates the efficiency of the extrusion processes utilised here (Lim *et al.*, 2008).

5.9. Mechanism behind thermal and sodium salicylate induced degradation of PLA

Low molecular weight degradation products generated during thermal degradation of PLA may potentially affect its tensile deformation behaviour and its hydrolytic degradation in the drug release media (Tsuji and Ikada, 1998). Consequently, the drug release profile from oriented matrices can be altered. The oligomeric degradation products generated during melt extrusion of PLA were identified by gas chromatography/mass spectrometry (GC/MS). This study was supplemented by identification of the degradation products generated during melt compounding of PLA with sodium salicylate, in order to confirm the mechanism of degradation in the presence of such a drug. GC/MS allows separation of the individual degradants by gas chromatography. Each separated species is subsequently detected by the mass spectrometer. The mass spectra obtained in the current study were compared with the NIST reference database and with previous reports on pyrolysis of PLA (Kopinke *et al.*, 1996; Luderwald, 1979; McNeill and Leiper, 1985).

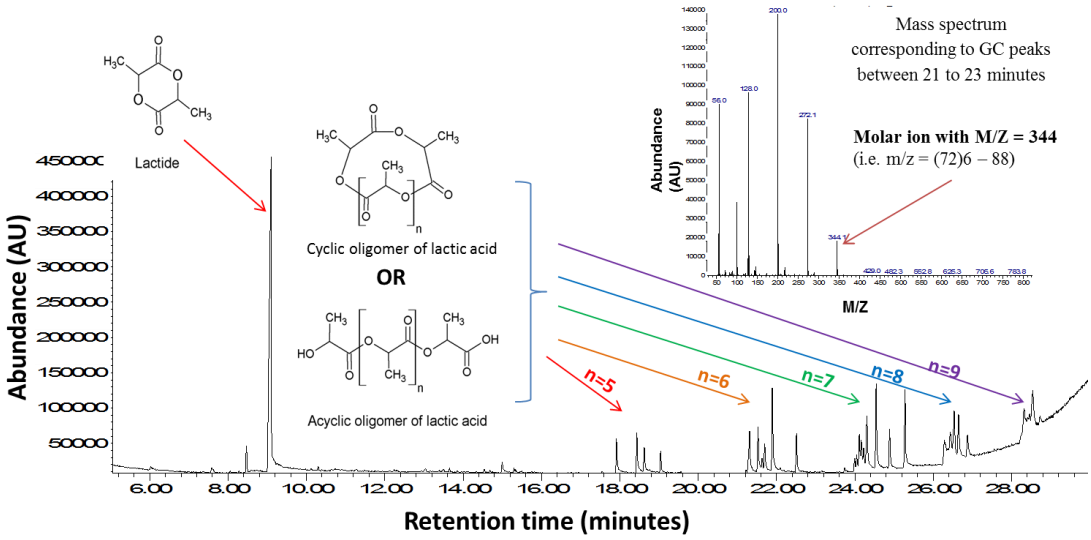

Figure 5.15: *GC/MS chromatogram of neat extruded PLA with the individual components identified from the corresponding mass spectra.*

*(inset mass spectrum corresponding to the GC peaks observed between 21 to 23 minutes).

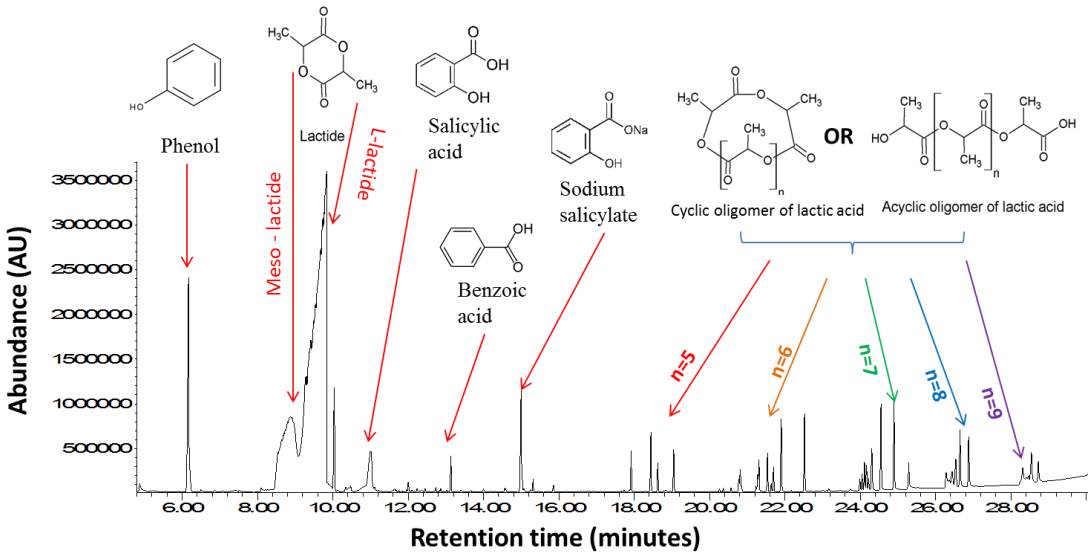

Figure 5.16: *GC/MS chromatogram of PLA melt compounded with 5% w/w sodium salicylate*

*(The individual components were identified from the mass spectra).

The identified species are displayed on the respective gas-chromatograms for the neat extruded PLA (figure 5.15) and the composite system containing 5% sodium salicylate (figure 5.16). The gas chromatogram of neat extruded PLA and composite PLA showed a characteristic series of peaks between the retention time (R_t) window of 18 to 28 minutes. The mass spectra corresponding

to these peaks contained distinctive bands at m/z (mass to charge ratio) 72.n – 88, representing the cyclic oligomers of lactic acid (McNeill and Leiper, 1985). Here, the m/z = 72 corresponds to the lactic acid monomer unit; whereas, 'n' signifies the number of monomer units present in an oligomer. Ionisation of the lactic acid oligomers in the mass spectrometer leads to rapid elimination of CO_2 (m/z 44) and acetaldehyde (m/z 44). Therefore the fragmentation pattern for the lactic acid oligomers is observed at m/z values 72.n - 88 (Kopinke *et al.*, 1996; Luderwald, 1979). Oligomers with monomer units between n = 5 to n = 12 were identified in the gas chromatogram of the neat extruded and the filled PLA. The R_t of the oligomers increased with their molar mass (figure 5.15 & figure 5.16). (The same oligomers were also identified by liquid chromatography/mass spectrometry, which validates that the oligomers were not generated as a result of the GC/MS thermal regime). Interestingly, the oligomers exhibited a cluster of peaks in the gas-chromatogram, which corresponded to the same mass spectrum. For the pentamer (n = 5), 4 clear peaks were observed between R_t = 18 -19 minutes; while the hexamer showed existence of 5 peaks. Kopinke *et al.* (1996) obtained a similar gas-chromatogram, when PLA (mol wt. = 99400 g/mol) was flash pyrolysed between 400 – 600 °C. The cluster of peaks in the gas-chromatogram was attributed to generation of optical isomers of lactic acid oligomers during degradation.

Mcneill *et al.* (1985) proposed that the thermal degradation of PLA occurs primarily by intra- and inter- molecular ester exchange reactions (figure 5.17). If the free hydroxyl end of PLA reacts with a carboxyl group of the same lactic acid unit, acetaldehyde and carbon monoxide are generated (figure 5.17 - A). Nevertheless, depending upon the location of the carboxyl group that faces the attack by the hydroxyl oxygen, the resulting product can be a lactide dimer (figure 5.17 - B) or a cyclic oligomer with more than two repeat units (figure 5.17 - C).

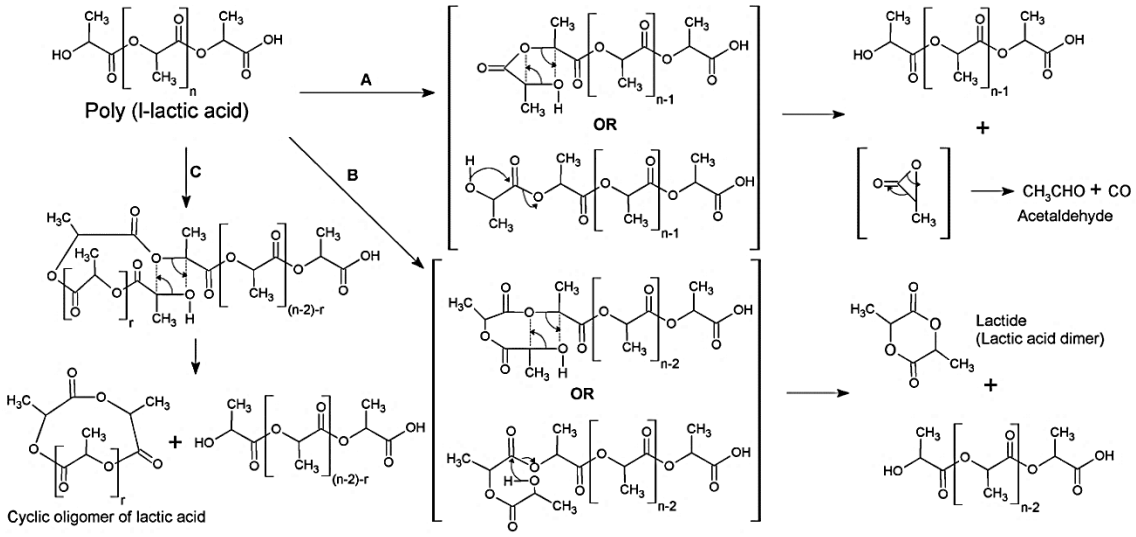

Figure 5.17: *Thermal degradation of PLA by trans-esterification pathway.*

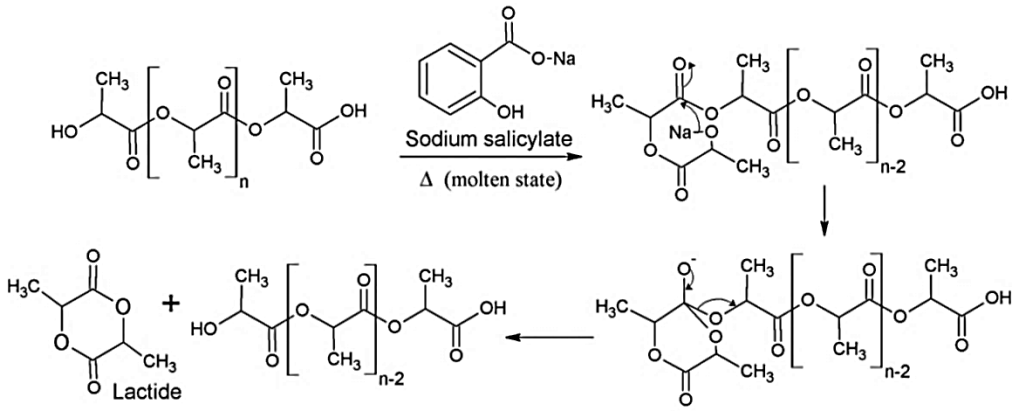

Figure 5.18: *Mechanism for thermal degradation of PLA in presence of sodium salicylate.*

The gas chromatogram of neat extruded PLA showed an intense peak at R_t = 9 minutes (figure 5.15). The mass spectrum corresponding to this peak revealed the presence of a lactide dimer. Since the intensity of this peak was at least 2.5 times higher than any other peak, lactide dimer was perhaps the largest individual degradation product obtained in the current study. Generation of lactide in the neat extruded PLA can be attributed to traces of Sn- catalyst. The PLA utilised in the current study was synthesised (by Natureworks LLC) by Sn-catalyzed polymerisation of L,L-lactide (Gruber and O'Brien, 2005). It being a reversible equilibrium reaction also causes depolymerisation of PLA by the

traces catalyst left in the polymer (Fan *et al*., 2004a; Fan *et al*., 2004b). When PLA is present in the molten state, 'Sn' can react with the free hydroxyl ends, forming Sn-alkoxide anions (figure 5.18). The alkoxide anions further attack the carbonyl carbon in the adjacent lactate unit, resulting in the formation of an optically pure lactide dimer (Fan *et al*., 2004b; Gruber and O'Brien, 2005).

A large lactide peak was also observed in the chromatogram of the composite PLA containing 5% sodium salicylate. However, it was split into a smaller and a larger peak with R_t = 8.5 minutes and 9.5 minutes respectively (figure 5.16). Since both of these peaks correspond to the same mass spectrum, they essentially represent optical isomers of lactide. The earlier eluting peak represents the meso-lactide, while the latter represents L,L-lactide (Fan *et al*., 2004b) As mentioned above, the Sn catalysed depolymerisation leads to formation of optically pure lactide dimers. Therefore, a mechanism other than Sn catalysed depolymerisation must be contributing in degradation of the sodium salicylate loaded PLA. A possible mechanism may involve transfer of Na^+ (sodium cations) to the alkoxy end group of PLA chains. The sodium alkoxide may subsequently cause unzipping depolymerisation of PLA in a manner similar to Sn^{+2} (tin) ions (figure 5.18). Traces of sodium cations if present during polymerisation of isotropically pure lactic acid, are known to promote formation of the meso-lactide by the same polymerisation reaction as Sn^{+2} ions (Gruber *et al*., 1992). Therefore, splitting of the lactide GC peak confirms involvement of the sodium cations, generated from sodium salicylate, in augmenting the thermal depolymerisation of PLA. In addition to the depolymerisation mechanism, literature confirms that the sodium salts of organic acids cause scission of the polyester backbone by transferring sodium ions to random carboxyl groups. However, this reaction pathway has been only observed for PET and not for PLA (Legras *et al*., 1983). Nevertheless, the current GC-MS analysis could not identify the by-products which would validate the existence of the random scission reaction.

In summary, it can be concluded that the thermal degradation of PLA during melt extrusion simultaneously follows several mechanisms (Kopinke *et al.*, 1996). These include depolymerisation into the lactide dimer, inter and intramolecular trans-esterification leading to generation of lactide oligomers, etc. Sodium salicylate augments thermal degradation of PLA by providing sodium cations that react with the carboxyl oxygen and cause depolymerisation (Legras *et al.*, 1983; Zhang, 2004).

5.10. Summary of the materials understanding studies

This chapter described selection of the model polymer and the model drugs. Curcumin, theophylline and paracetamol were selected as thermostable and inert model drugs, based on extensive screening of the shortlisted molecules. Curcumin and paracetamol at 5% w/w loading represent polymer (PLA) soluble model drugs; while theophylline at 5% w/w loading represents an insoluble drug that can remain in a suspension state within the polymer matrix. In this research, melt extrusion was used a scalable method for compounding model drugs with PLA and for preparation of drug loaded films or billets. Changes in the polymorphic state of the experimental materials (model drugs & PLA) and their degradation during melt extrusion can potential affect solid-state deformation behaviour of the composite matrices, their hydrolytic degradation and the resultant drug release profile. In order to understand these changes, the experimental materials were studied by thermal analysis, X-ray diffraction, IR spectroscopy and gel permeation chromatography. This information along with rheological characterisation was used for development of an efficient melt extrusion process, which will cause minimal degradation of the investigated materials. Nevertheless, degradation products generated during melt extrusion were identified by gas chromatography - mass spectroscopy (GC-MS). Such a comprehensive understanding of the experimental materials will ensure that the characteristic features of drug release from oriented materials are correctly attributed to polymer orientation.

6. Drug release from the oriented PLA films: results & discussion

This chapter relates to solid-state orientation of drug loaded PLA films and characterisation of the resultant films for drug release. The initial section is dedicated to investigation of the effect of strain rate, drawing temperature, draw ratio and the nature of drug on the morphology of oriented films. Development of oriented morphology in these films is discussed with respect to WAXD, MDSC and mechanical testing results. Based on these results, selected samples were further evaluated for changes in the surface polarity and the morphological changes underwent by the films after aqueous submersion. Finally, the results of drug release testing are discussed with an attempt to identify a correlation between the oriented structure of the films and drug release.

6.1. Effect of drawing conditions on the thermal properties of oriented PLA films

Three important thermal events, namely glass transition (Tg), cold-crystallisation (Tcc) and enthalpy of melting are closely related to the physical structure of a polymer. Since Tg corresponds to the energy required for bestowing mobility to the amorphous polymer chains, it is shifted towards higher temperatures upon orientation of the amorphous section. On the contrary, Tcc shares an inverse relation with the degree of polymer orientation. Finally, the normalised enthalpy of melting allows calculation of the percentage crystallinity of the oriented matrices.

6.1.1. Effect of drawing temperature and strain rate on crystallinity

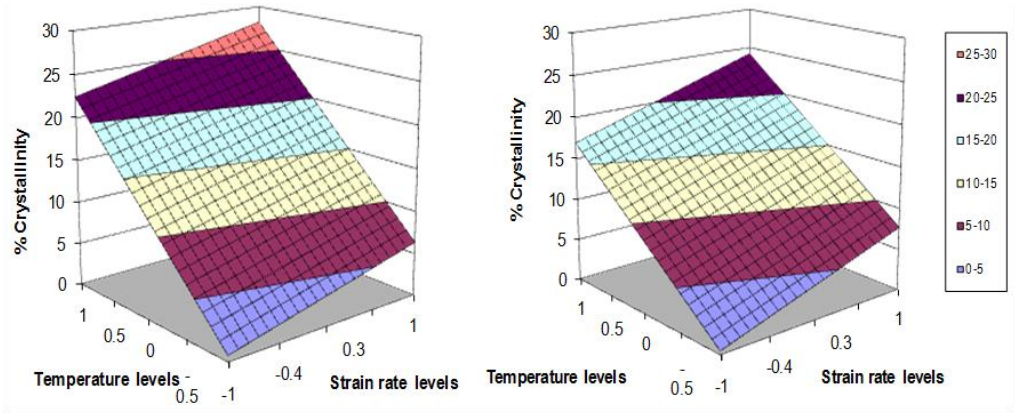

CPLA films – Multiple regression

$\hat{y} = 14.61 + 10.85X_1 + 2.81X_2$

$R^2 = 0.9952$, F - value = 123.20

$P < 0.05$ (For the above polynomial constants)

TPLA films – Multiple regression

$\hat{y} = 12.84 + 8.24X_1 + 3.63X_2$

$R^2 = 0.9964$, F - value = 167.68

$P < 0.05$ (For the above polynomial constants)

Figure 6.1: *Effect of strain rate (X_1-axis) and drawing temperature (X_2-axis) on crystallinity (Z-axis) of* ***(A)*** *curcumin and* ***(B)*** *theophylline loaded films (5% w/w drug loading), oriented uniaxially with a constant width (UCW) to a draw ratio 3X.*

* The surface response plots were obtained by multiple regression analysis, details of which are represented below the respective plots. The drawing temperatures; namely 70 °C, 80 °C and 90 °C, and the strain rates 0.12 sec^{-1}, 0.57 sec^{-1}, 1.2 sec^{-1} are expressed as -1, 0 and +1 factorial levels respectively.

Figure 6.1 displays the effect of strain rate and drawing temperature on the crystallinity of the uniaxially (uniaxial constant width - UCW – λ = 3X) oriented drug loaded films. For simplification the PLA films containing 5% w/w of curcumin and 5% w/w theophylline are referred to as CPLA films and TPLA films respectively. The Neat PLA films exhibited exactly the same response as shown by the CPLA films and therefore it is not separately reported here. It is clear that a rise in both strain rate and drawing temperature elevated the percent crystallinity of the films. The effect of temperature was significantly larger than that of the strain rate. Higher crystallinity at elevated temperatures can be attributed to thermally enhanced chain mobility, which increases the

probability of them registering into favourable positions (Mahendrasingam *et al.*, 2005; Mulligan and Cakmak, 2005).

The lowest values of crystallinity observed for the UCW oriented (λ = 3X) neat PLA, CPLA and TPLA films were 0.77 ± 0.69%, 0.43 ± 0.23% and 0.79 ± 0.82% respectively, when oriented at 70 °C and 0.12 sec^{-1}. Contrastingly, 90 °C and 1.2 sec^{-1} drawing conditions led to significantly higher crystallinity, i.e. 28.91 ± 1.04%, 28.30 ± 1.61% and 25.04 ± 1.67% for the neat PLA, CPLA and the TPLA films respectively. The effect of drawing temperature on crystallinity of the UCW oriented (λ = 3X) TPLA (figure 6.1 - B) was less prominent than that observed with the corresponding neat and the CPLA films. This potentially indicates a reduction in the thermally stimulated chain movement and resultant inter-chain interactions due to interference by the suspended theophylline particles.

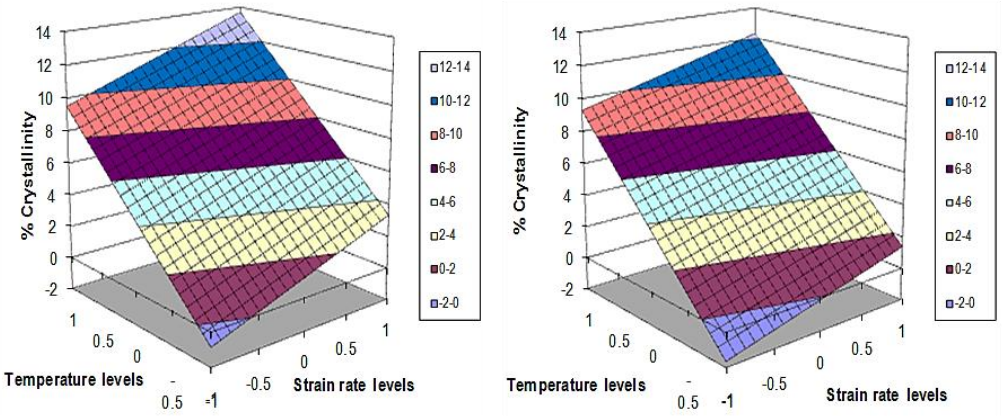

Figure 6.2: *Effect of strain rate (X_1-axis) and drawing temperature (X_2-axis) on crystallinity (Z-axis) of* ***(A)*** *curcumin and* ***(B)*** *theophylline loaded films, oriented in simultaneous biaxial mode to a biaxial draw ratio 2X2Y.*

* The surface response plots were obtained by multiple regression analysis, details of which are represented below the respective plots. The drawing temperatures; namely 70 °C, 80 °C and 90 °C, and the strain rates 0.12 sec^{-1}, 0.57 sec^{-1}, 1.2 sec^{-1} are expressed as -1, 0 and +1 factorial levels respectively.

The crystallinity surface maps for the biaxially oriented films (λ = 2X2Y) (figure 6.2) revealed that the effect of drawing temperature and strain rates on the crystallinity of such films followed the same correlation observed with the UCW oriented films. Albeit, the overall crystallinity was substantially ($P< 0.001$) lower in the biaxially oriented films. A lower crystallinity is developed in simultaneous biaxial (SB) mode (figure 6.2), on account of the fact that simultaneous stretching in two perpendicular direction makes like-chain interactions difficult (Ou and Cakmak, 2008). Similar to the UCW oriented films, the effect of drawing temperature on the crystallinity of the SB oriented films was substantially greater than that of the strain rate. Nevertheless, the SB oriented TPLA films exhibited lower crystallinity than the SB oriented neat and the CPLA films at studied drawing conditions (figure 6.2).

Altogether, it can be said that the drawing temperature is a major influencing factor on the crystallinity of the uniaxially (UCW) and biaxially (SB) drawn films. The rise in the crystallinity with higher strain rates is due to the early onset of strain induced crystallisation (Zhang *et al.*, 2011); whereas in the case of temperature it can be attributed to augmented chain mobility (Mahendrasingam *et al.*, 2005). Results suggest that the rise in the crystallinity is a dynamic phenomenon, which is co-dependent on the underlying temperature and strain rate. The results further highlighted the role of the model drugs in affecting the drawing behaviour of PLA. The differential effect of the model drugs is perhaps attached to their physical form and interaction with the polymer chains.

6.1.2. Effect of drawing temperature and strain rate on glass transition temperature

The glass transition temperature is closly related to the degree of orientation. Therefore, mapping the changes in glass transition temperature (Tg) with respect to tensile stretching variables allowed better understanding of the effect of these variable on the resultant oriented structure of the films. This

data is summerised in figure 6.3. For all the films a rise in the strain rate shifted the glass transition towards higher temperatures (figure 6.3), indicating improvement in the amorphous orientation. A faster stretching leaves less scope for the oriented polymer chains to undergo relaxation during the tensile stretching process. Therefore the degree of orientation is augmented with a rise in the strain rate (Mahendrasingam *et al*., 2005).

In contrast to the effect of strain rate, glass transition temperature of the oriented films followed an inverse relationship with drawing temperature (except for the UCW oriented TPLA films). At '-1' temperature level, i.e. 70 °C, the glass tansition temperature of the oriented films was highest followed by the '0 level (80 °C)' and finally the '+1 level (90 °C)'. Distinguishingly, the glass transition of the films oriented at 70 °C was recognised as a deep endothermic relaxation event, suggesting ordering of the amorphous chains (Kokturk *et al*., 2002; Wong *et al*., 2008). With a rise in drawing temperature, Tg of the oriented films reduced. This correlation was also confirmed by the negative value of the polynomial constant (X_1) representing the effect of drawing temperature (figure 6.3). At elevated temperatures, the polymer chains can undergo rapid relaxation, resulting in a matrix with poor overall orientation (Mahendrasingam *et al*., 2005).

The regression analysis represented in figure 6.3 further suggested that Tg of the UCW and SB oriented CPLA films was also influenced by an interaction between the temperature and the strain rate. This was evidenced as statistically significant ($P < 0.05$) coefficient of the interaction term X_1X_2. Moreover, it signifies that one of the independent variables influences the other independent variable, consequently affecting the dependent variable (i.e. crystallinity) in an indirect manner. An interaction between draw temperature and strain can therefore be associated with generation of a frictional heat at higher strain rates or faster chain slippage at greater drawing temperature.

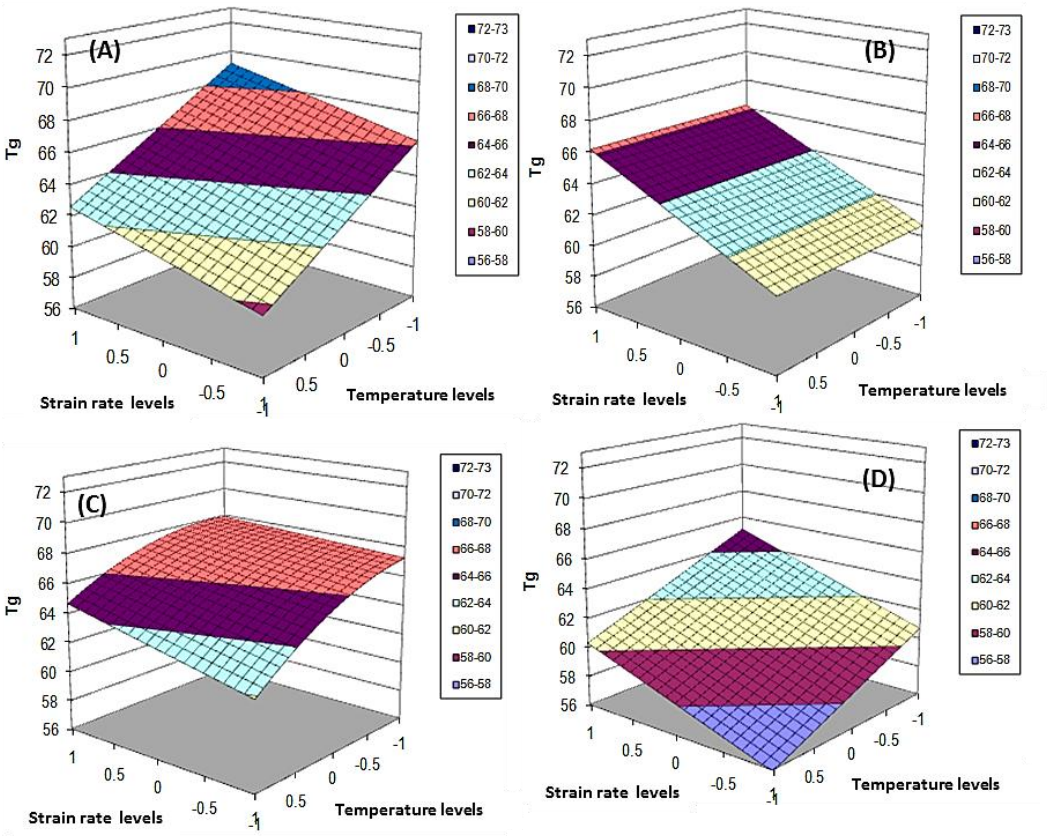

(A) UCW CPLA films

$\hat{y} = 64.13 - 3.29X_1 + 1.47X_2 - 0.58X_1X_2$

$R^2 = 0.994801$, F - value = 114.81

$P < 0.05$ (For the above polynomial constants)

(B) UCW TPLA films

$\hat{y} = 63.45 + 2.75X_2$

$R^2 = 0.990605$, F - value = 63.27

$P < 0.05$ (For the above polynomial constants)

(C) SB CPLA Films

$\hat{y} = 66.64 - 2.06X_1 + 0.86X_2 - 0.90X_1^2 + 0.54X_1X_2$

$R^2 = 0.992328$, F - value = 77.61

$P < 0.05$ (For the above polynomial constants)

(D) SB TPLA films

$\hat{y} = 61.001 - 2.38X_1 + 2.20X_2$

$R^2 = 0.983458$, F - value = 35.67

$P < 0.05$ (For the above polynomial constants)

Figure 6.3: *Effect of strain rate (X_1-axis) and drawing temperature (X_2-axis) on glass transition temperature (Z-axis) of oriented films.*

(A) Curcumin loaded films UCW draw ratio 3X, **(B)** Theophylline loaded films UCW draw ratio 3X, **(C)** Curcumin loaded films SB draw ratio 2X2Y and **(D)** Theophylline loaded films SB draw ratio 2X2Y.

* The surface response plots were obtained by multiple regression analysis, details of which are represented below the respective plots. The drawing temperatures; namely 70 °C, 80 °C and 90 °C, and the strain rates 0.12 sec^{-1}, 0.57 sec^{-1}, 1.2 sec^{-1} are expressed as -1, 0 and +1 factorial levels respectively.

The effect of drawing temperature on the crystallinity of the oriented films was opposite to its effect on the glass transition temperature. A combined analysis of the changes in glass transition and crystallinity of the oriented films suggests that a drawing temperature of 70 °C promoted generation of an oriented amorphous matrix with minimal crystallinity. The films processed at 80 °C contained highly oriented amorphous and crystalline regions; whereas at 90 °C, highly crystalline matrices with inferior overall orientation were produced. The effect of strain rate and drawing temperature was more prominent for UCW orientation (figure 6.3 – A, B) compared to the SB mode (figure 6.3 – C, D); withstanding the fact that UCW stretching generates highly anisotropic structure, while an orthotropic structure is developed in the SB mode.

The coloured surface map (figure 6.3) clearly established that there was a significant difference in the glass transition of the oriented films with respect to the added model drug. At all studied strain rate – temperature combinations, oriented neat PLA films exhibited the highest Tg, followed by oriented CPLA films and finally oriented TPLA films. Tg of the oriented neat and the oriented CPLA films showed an inverse relation to drawing temperature (figure 6.3 - A, C). Contrarily, the drawing temperature did not produce any significant change in the glass transition of the oriented TPLA films (figure 6.3 - C & F). Here the coefficient representing the effect of drawing temperature was statistically insignificant ($P > 0.05$) and was excluded from the regression equation. Since the Tg of the un-oriented TPLA films was same as that of un-oriented neat PLA films, the above observation clearly relates to the effect of suspended theophylline on the tensile deformation of PLA. It may alternatively mean that the presence of a crystalline drug may interfere with the polymer chain mobility (Pukanszky, 1990).

6.2. Effect of drawing conditions on the oriented structure of PLA films

Changes in the crystallinity and glass transition temperature of the oriented PLA films confirmed that tensile deformation of PLA films is highly sensitive to temperature and strain rate. This correlation was further evaluated through WAXD studies.

2D WAXD patterns representing UCW oriented CPLA and TPLA films are displayed in figure 6.4. The oriented structure generated during UCW stretching (λ = 3X) of PLA films at 70 °C, was predominantly amorphous in nature. This was observed in the WAXD patterns, as the equatorial amorphous halo (figure 6.4 - C1, T1). When processed at 0.12 sec^{-1} strain rate, no crystalline bands were observed. However, at 0.57 sec^{-1} /70 °C, faint crystalline reflections appeared in the (203) and the mirror crystallographic planes (figure 6.4 - C2, T2). These reflections further intensified at 1.2 sec^{-1} strain rate, indicating a rise in crystallinity (figure 6.4 - C3, T3).*(refer to appendix for 2D- WAXD data analysis method details)

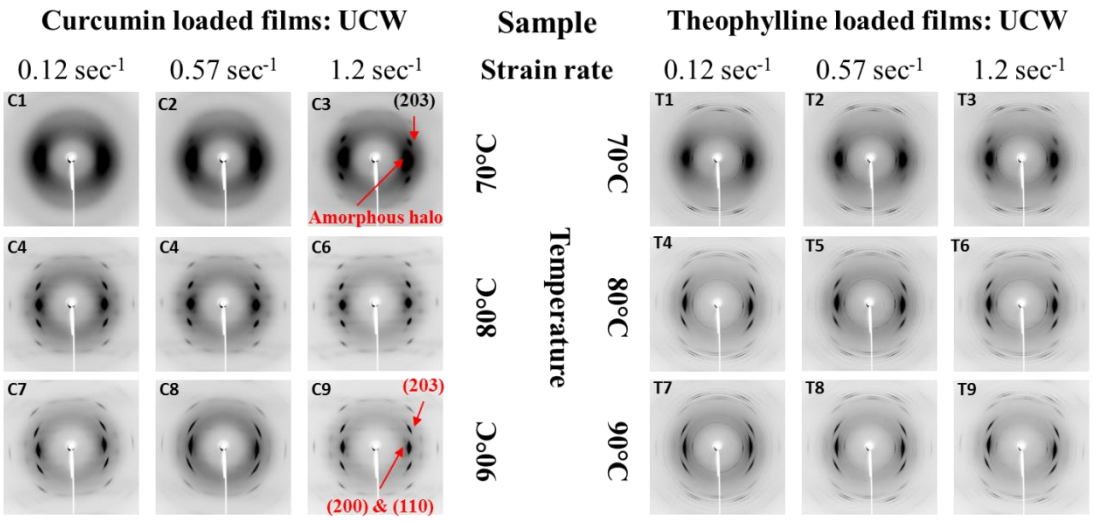

Figure 6.4: *Effect of strain rate and drawing temperature on WAXD pattern of drug loaded PLA films, oriented uniaxially with a constant width to a draw ratio of 3X.*

PLA films oriented at 80 °C and 90 °C showed well defined crystalline reflections in the (200, 110) and (203) crystallographic planes (figure 6.4 - C4-C9 & T4-T9). The azimuthal spread of these reflections reduced at higher strain rates, signifying improvement in the degree of orientation. Contrary to the effect of strain rate, a rise in the drawing temperature from 80 °C to 90 °C increased the azimuthal spread of the crystalline reflections. Higher chain mobility at elevated temperatures causes relaxation of several oriented chains (Zhang *et al*., 2011). Consequently, when the thermally stimulated chain relaxation becomes substantial, an inferior degree of orientation is produced.

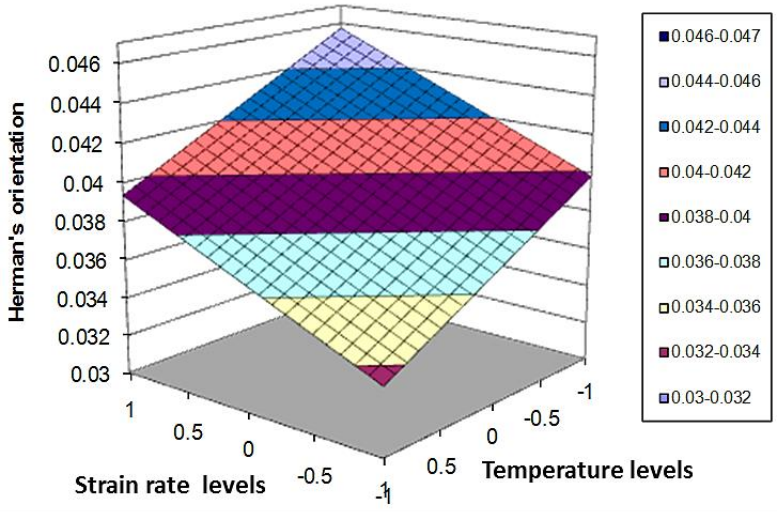

CPLA films – Multiple regression

$\hat{y} = 0.038 - 0.003X_1 + 2.002X_2 + 0.001X_1^2 + 0.001X_1X_2$

$R^2 = 0.994769$, F - value = 114.11

$P < 0.05$ (For the above polynomial constants)

Figure 6.5: *Effect of strain rate and drawing temperature on Herman's orientation function of curcumin loaded PLA films, oriented uniaxially with a constant width to a draw ratio 3X.*

* The surface response plot was obtained by multiple regression analysis, details of which are represented below the plot. The drawing temperatures; namely 70 °C, 80 °C and 90 °C, and the strain rates 0.12 sec^{-1}, 0.57 sec^{-1}, 1.2 sec^{-1} are expressed as -1, 0 and +1 factorial levels respectively.

The degree of uniaxial orientation can be quantified by Herman's orientation function (sec 4.13 – eqn. 4.5). A surface map representing changes in the orientation function with respect to drawing temperature and strain rate is displayed in figure 6.5. It is evident that the orientation function increased almost linearly with strain rate. Contrarily, it shared an inverse relationship with drawing temperature.

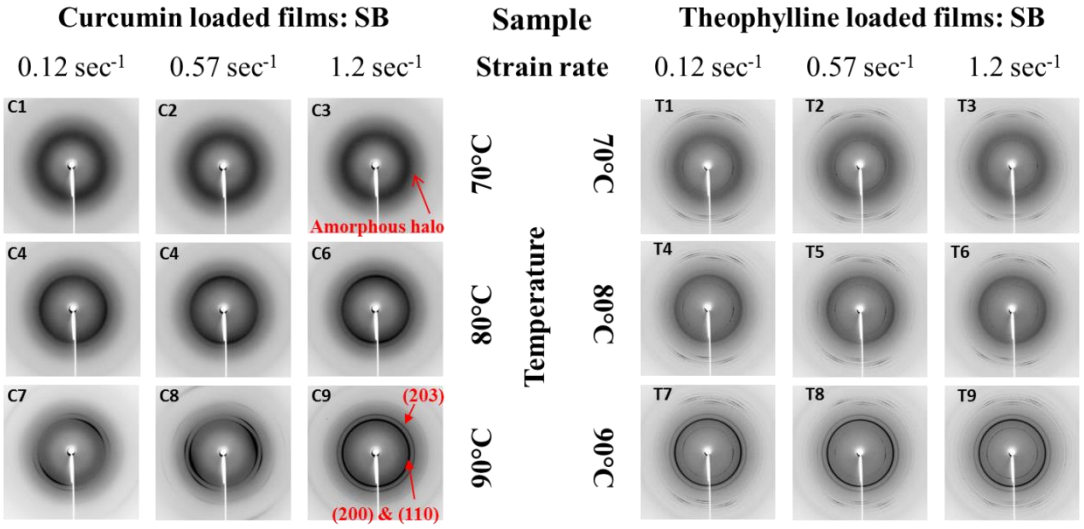

Figure 6.6: *Effect of strain rate and drawing temperature on WAXD diffraction pattern of drug loaded PLA films, oriented in simultaneous biaxial mode to a biaxial draw ratio 2X2Y.*

Films oriented in SB mode (λ = 2X2Y) showed peculiar WAXD patterns (figure 6.6). When subjected to SB stretching at 70 °C, a diffuse ring representing an isotropic amorphous phase was observed (figure 6.6 - C1-C3 & T1-T3). Films processed at 80 °C showed faint (110, 200) and (203) crystalline reflections overlapping on the sharp amorphous halo. However, they appeared as a complete azimuthal ring, suggesting a lack of anisotropy (figure 6.6 - C4-C6 & T4-T6). Curcumin loaded PLA films exhibited a slightly different behaviour at 90 °C drawing temperature. When oriented at 1.2 sec^{-1} strain rate (at 90 °C), the WAXD pattern of the mentioned films displayed a complete crystalline ring (figure 6.6. - C7). At 0.57 sec^{-1} strain rate, the crystalline reflections appeared at

approximately 23° angle to the equator (figure 6.6 - C8); while they shifted to 45°at 0.12 sec^{-1} strain rate (figure 6.11 - C9). Surprisingly, such a trend was not observed in the WAXD patterns belonging to theophylline loaded PLA films (figure 6.6 - T7–T9). The peculiarities of the WAXD data for SB oriented films could not be explained at this stage. However the WAXD patterns confirmed the role of drawing temperature in enhancing thermal crystallisation of SB oriented films.

Altogether, WAXD data confirmed that the oriented structure of the PLA films resulting from the process of solid-state orientation significantly depends upon the underlying temperature and strain rate. The PLA films studied here developed a predominantly amorphous structure at 70 °C drawing temperature. Such structure showed orientation of the amorphous chains in the drawing direction, with negligible crystallinity. At 80 °C a crystalline matrix was produced which contained highly oriented amorphous PLA chains anchored by oriented crystalline links. Raising the temperature augmented the chain mobility excessively. Therefore, a highly crystalline matrix with poor orientation was generated at 90 °C. It was also evidenced that faster strain rates improved the degree of orientation. Nevertheless, they also accelerated the onset of strain induced crystallisation. Considering these factors, 80 °C drawing temperature and 0.57 sec^{-1} strain rate were considered as the optimum parameters for onward studies.

6.3. Correlation between draw ratio and thermal properties of oriented PLA films

6.3.1. Effect of draw ratio (λ) on crystallinity

PLA undergoes complex changes in structure upon tensile drawing. At a constant drawing temperature and strain rate, evolution of the crystalline structure with respect to draw ratio can be understood by mapping crystallinity of the oriented PLA films. Figure 6.7 displays the changes in the crystallinity of

drug loaded films following uniaxial constant width (UCW) and sequential biaxial (SEQ) stretching to different draw ratios.

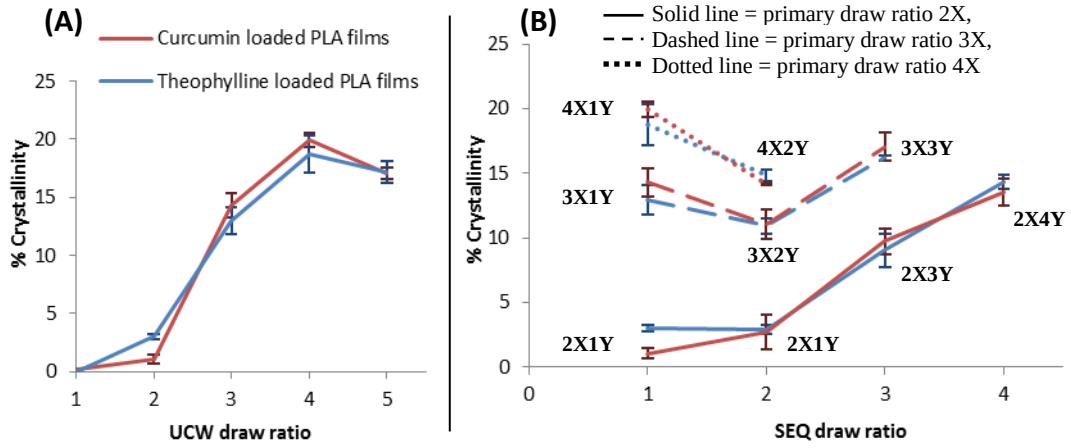

Figure 6.7: *Effect of draw ratio on crystallinity of drug loaded PLA films oriented at 80 °C, using 0.57 sec^{-1} strain rate.*

Note: A) UCW oriented films, **B)** Sequentially oriented films (draw ratios are individually labelled.)

*The red curve represents CPLA films, while the blue curve represents TPLA films.

**The graph represents the mean ± standard deviation, where n = 3.

Table 6.1: *Statistical comparison of the crystallinity of UCW oriented PLA films*

Paired t-test - Uniaxial draw ratio comparison					
CPLA	1X Vs 2X	P = 0.0702, t = 3.50	**TPLA**	1X Vs 2X	P = 0.0024, t = 20.26
	2X Vs 3X	P = 0.0007, t = 19.79		2X Vs 3X	P = 0.0032, t = 14.43
	3X Vs 4X	P = 0.0037, t = 7.88		3X Vs 4X	P = 0.0089, t = 5.08
	4X Vs 5X	P = 0.0036, t = 6.24		4X Vs 5X	P = 0.2296, t = 1.48
Paired t-test - model drug comparison					
1X	CPLA Vs TPLA	P = 0.0152, t = 8.02			
2X (2X1Y)	CPLA Vs TPLA	P = 0.0046, t = 6.82			
3X (3X1Y)	CPLA Vs TPLA	P = 0.2157, t = 1.41			
4X (4X1Y)	CPLA Vs TPLA	P = 0.3375, t = 1.17			
5X (5X1Y)	CPLA Vs TPLA	P = 0.8683, 0.17			

Table 6.2: *Statistical comparison of the crystallinity of SEQ oriented PLA films*

Paired t-test - Sequential biaxial draw ratiocomparison					
CPLA	2X1Y Vs 2X2Y	P = 0.1664, t = 1.97	**TPLA**	2X1Y Vs 2X2Y	P = 0.8804, t = 0.16
	2X2Y Vs 2X3Y	P = 0.0027, t = 7.242		2X2Y Vs 2X3Y	P = 0.0106, t = 7.871
	2X3Y Vs 2X4Y	P = 0.0109, t = 4.51		2X3Y Vs 2X4Y	P = 0.0097, t = 6.46
	3X1Y Vs 3X2Y	P = 0.023, t = 3.590		3X1Y Vs 3X2Y	P = 0.0749, t = 2.65
	3X2Y Vs 3X3Y	P = 0.0026, t = 6.71		3X2Y Vs 3X3Y	P = 0.0021, t = 13.63
	4X1Y Vs 4X2Y	P = 0.0029, t = 16.35		4X1Y Vs 4X2Y	P = 0.0426, t = 4.08
Paired t-test - model drug comparison					
2X2Y	CPLA Vs TPLA	P = 0.7671, t = 0.33			
2X3Y	CPLA Vs TPLA	P = 0.5069, t = 0.73			
2X4Y	CPLA Vs TPLA	P = 0.346, t = 1.11			
3X2Y	CPLA Vs TPLA	P = 0.8629, t = 0.18			
3X3Y	CPLA Vs TPLA	P = 0.2831, t = 1.41			
4X2Y	CPLA Vs TPLA	P = 0.1209, t = 2.46			

Note: The null hypothesis was that the compared samples were statistically the same

P > 0.05 = The difference between the compared samples is **not statistically significant**
0.05 > P > 0.01 = The difference between the compared samples is **statistically significant**
0.01 > P = The difference between the compared samples is **highly significant**

During UCW stretching, there was only a minor change in crystallinity of the TPLA films drawn to twice their original length (λ = 2X) (figure 6.7 - A). This change was statistically insignificant in the case of CPLA films (table 6.1). A lack of crystallinity change can be attributed to plastic deformation of the amorphous chains without an onset of strain induced crystallisation (Ou and Cakmak, 2008; Zhang *et al*., 2011).

Crystallinity rapidly increased to 14.3 ± 1.13 % at λ = 3X (figure 6.7 - A), followed by a moderate rise to 19.92 ± 0.6% at λ = 4X. On further drawing, there was a fall in crystallinity of the CPLA films, while the crystallinity of the TPLA films remained statistically the same. An apparent fall in the crystallinity at λ = 5X can be attributed to fragmentation of the existing crystals (Zhang *et al*., 2011). The difference in crystallinity of the PLA films with respect to draw ratio was validated by statistical comparison using paired t-tests. This information is

summarised in table 6.1. Moreover, a comparison between the oriented CPLA and the TPLA films revealed that there was statistically insignificant ($P > 0.05$) difference between the mentioned films when oriented to UCW $\lambda \geq 5X$.

Sequential biaxial orientation of the films involves primary stretching along the main axis (X-axis) followed by secondary stretching along the perpendicular axis (Y-axis). Therefore, the oriented structure developed in the primary stretching direction shapes the structure evolution in the secondary direction. When the draw ratio along the primary stretching axis was low ($\lambda = 2X$), no crystallinity was developed (figure 6.7 - A). In such a case, extension in the perpendicular direction, initially leads to rotation of the existing structure (Hinrichsen *et al*., 1981a). Consequently, crystallinity of the films did not change significantly ($P > 0.05$, table 6.2) up to a draw ratio of 2Y along the secondary axis (i.e. biaxial $\lambda = 2X2Y$- figure 6.7 - B). Following this, there was a rapid growth in the crystallinity with respect to the secondary draw ratio ($P < 0.05$, table 6.2). Films drawn to higher draw ratios along the primary axis already have a well-developed crystalline order along that axis (figure 6.7 - A). Therefore, secondary drawing along the perpendicular axis disrupts the existing structure, perceived as a fall ($P < 0.05$, table 6.2) in the crystallinity (figure 6.7 – B) (Ou and Cakmak, 2008). Further drawing along the secondary axis generates newer crystals oriented in the secondary drawing direction. Therefore, the films oriented to the biaxial draw ratio of 3X3Y exhibited higher crystallinity than the films oriented to the draw ratio of 3X2Y. All the changes in the crystallinity of the sequentially oriented films were statistically validated by paired t-tests. This information is summarised in table 6.2.

6.3.2. Effect of draw ratio on glass transition

Glass transition temperature is closely related to the degree of orientation of the polymeric matrix (Mulligan and Cakmak, 2005). For UCW stretching, Tg increased moderately up to a draw ratio 2X (figure 6.8 - A). This difference was statistically siginificant for the CPLA films; while it was insignificant for the TPLA films (table 6.3). Overall, it suggests that a nematic structure is developed at λ ≥ 2X. On further drawing to λ ≥ 3X, a rise in the degree of orientation was accompanied by generation of crystals that can stabilise the oriented chains. Therefore, at UCW draw ratios of 3X and above, a sharp rise in the Tg of the oriented PLA films was observed (figure 6.8 - A). The rise in the Tg with respect to UCW draw ratio was statistically validated by paired t-tests. This information is summarised in table 6.3. Statistical comparison further revealed that there was no significant difference between the Tg of the CPLA and the TPLA films oriented to a same draw ratio (table 6.3) (except for UCW λ = 4X).

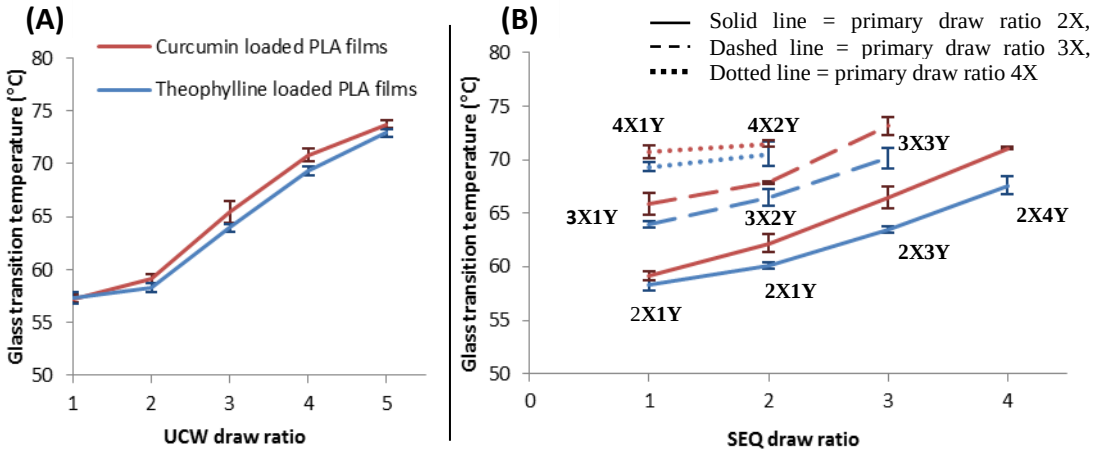

Figure 6.8: *Effect of draw ratio on the glass transition temperature of drug loaded PLA films oriented at 80 °C, using 0.57 sec^{-1} strain rate.*

Note: **A)** UCW oriented films, **B)** Sequentially oriented films (draw ratios are individually labelled).

*The red curve represents CPLA films, while the blue curve represents TPLA films.

**The graph represents the mean ± standard deviation, where n = 3.

Table 6.3: *Statistical comparison of the glass transition temperature of UCW oriented PLA films*

Paired t-test – UCW draw ratio comparison					
CPLA	1X Vs 2X	P = 0.0052, t = 5.89	TPLA	1X Vs 2X	P = 0.0852, t = 2.30
	2X Vs 3X	P = 0.0034, t = 9.72		2X Vs 3X	P = 0.0001, t = 17.26
	3X Vs 4X	P = 0.0033, t = 7.69		3X Vs 4X	P < 0.0001, t = 17.65
	4X Vs 5X	P = 0.0041, t = 6.94		4X Vs 5X	P = 0.0004, t = 11.38
Paired t-test - model drug comparison.					
1X	CPLA Vs TPLA	P = 0.8692, t = 0.18			
2X (2X1Y)	CPLA Vs TPLA	P = 0.0755, t = 2.38			
3X (3X1Y)	CPLA Vs TPLA	P = 0.1161, t = 2.40			
4X (4X1Y)	CPLA Vs TPLA	P = 0.0347, t = 3.38			
5X (5X1Y)	CPLA Vs TPLA	P = 0.0559, t = 2.67			

Table 6.4: *Statistical comparison of the glass transition temperature of SEQ oriented PLA films*

Paired t-test - Sequential biaxial draw ratio comparison					
CPLA	2X1Y Vs 2X2Y	P = 0.0092, t = 5.76	**TPLA**	2X1Y Vs 2X2Y	P = 0.0064, t = 5.64
	2X2Y Vs 2X3Y	P = 0.006, t = 5.62		2X2Y Vs 2X3Y	P = 0.0002, t = 13.26
	2X3Y Vs 2X4Y	P = 0.016, t = 7.52		2X3Y Vs 2X4Y	P = 0.008, t = 7.87
	3X1Y Vs 3X2Y	P = 0.0724, t = 3.41		3X1Y Vs 3X2Y	P = 0.016, t = 5.31
	3X2Y Vs 3X3Y	P = 0.007, t = 10.75		3X2Y Vs 3X3Y	P = 0.0068, t = 5.29
	4X1Y Vs 4X2Y	P = 0.1635, t = 1.82		4X1Y Vs 4X2Y	P = 0.1838, t = 1.81
Paired t-test - model drug comparison					
2X2Y	CPLA Vs TPLA	P = 0.0313, t = 4.18			
2X3Y	CPLA Vs TPLA	P = 0.0315, t = 4.69			
2X4Y	CPLA Vs TPLA	P = 0.0174, t = 7.06			
3X2Y	CPLA Vs TPLA	P = 0.0823, t = 3.11			
3X3Y	CPLA Vs TPLA	P = 0.0141, t = 4.18			
4X2Y	CPLA Vs TPLA	P = 0.2637, t = 1.45			

Note: The null hypothesis was that the compared samples were statistically the same

P > 0.05 = The difference between the compared samples is **not statistically significant**
0.05 > P > 0.01 = The difference between the compared samples is **statistically significant**
0.01 > P = The difference between the compared samples is **highly significant**

For films sequentially oriented in the perpendicular direction, Tg increased with draw ratio along the secondary axis (figure 6.8 - B). A statistical comparison of the Tg change with secondary draw ratio is reported in table 6.4. A significant change in Tg was observed when the strain along the primary axis was low; alternatively meaning that lower orientation in the primary direction leaves a larger scope for structure development in the second stretching direction. The glass transition of the films with higher primary draw ratios (λ = 3X & 4X- fig. 6.8 - A) remained statistically the same with subsequent stretching in the perpendicular direction, at a lower secondary draw ratio (3X2Y, 4X2Y). Further stretching in the secondary direction lead to a rise in Tg (figure 6.7 - B). Surprisingly, the difference between Tg of the sequentially oriented CPLA and TPLA films was statistically significant (table 6.4) when the primary draw ratio was lower. Overall, the results suggest that secondary stretching in the perpendicular direction initially disturbs the order in the first stretching direction. However, the resultant chains and the previously un-oriented chains are organised in the second direction on subsequent drawing.

6.4. Evolution of oriented structure during uniaxial constant width and sequential biaxial stretching of PLA films

Oriented structure of the films was predicted from WAXD data based on the 2D WAXD patterns, the crystallinity index, and the degree of orientation. The crystallinity values obtained by WAXD were within the standard error window of those obtained by MDSC and therefore are not separately discussed.

Development of the oriented structure during UCW and sequential drawing of the drug loaded PLA films is summarised in figure 6.9, through WAXD patterns. WAXD patterns revealed that PLA films oriented to a UCW draw ratio of 2X mainly contained oriented amorphous chains, visible as a concentration of the amorphous halo in the equatorial direction (figure 6.9 - 2X1Y). On further drawing in the UCW mode (figure 6.9 - 3X1Y), there was a rapid growth of the crystalline bands characteristic of the α crystalline form of PLA (Kokturk *et al*.,

2002). This observation is in agreement with the findings of Hoogsteen *et al*. (1990) and Wong *et al*. (2008), who reported that tensile drawing of PLA at temperatures significantly below the melting point generates the lamellar α crystalline form; whereas at near melting temperatures, complete rearrangement into the fibrillar β Form occurs. The α Form has a pseudo-orthorhombic unit cell, with crystallographic dimensions: a = 10.7 Å, b = 6.45 Å, c = 27.8 Å. Here, the PLA chains are organised into a -10/3 helical conformation; which is reflected in the scattering pattern, as the bands on (211) crystallographic plane having a repeat distance of 3 nm (Mahendrasingam *et al*., 2005). At a UCW draw ratio of 4X (figure 6.9 - 4X1Y), the azimuthal spread of crystalline reflections was reduced, indicating further improvement in the crystalline order. In the single dimensional diffractogram, this was reflected as intensification of peaks at 2θ = 16.7° and 19.1° representing crystalline reflections in the (200, 110) and (203) crystallographic planes respectively. A slight broadening of the same crystalline bands in the 2D WAXD pattern along with a small drop in their corresponding 1D diffractogram intensities was observed at an UCW draw ratio of 5X (figure 6.9 - 5X1Y). This signifies fragmentation of the existing crystals due to applied deformation stress; however, the structural order remains intact (Kokturk *et al*., 2002).

WAXD patterns for films sequentially stretched in the second direction, matched with the structure evolution predicted on the basis of crystallinity and Tg changes. When a film with a uniaxial draw ratio of 2X was subsequently drawn along the perpendicular axis, the existing scattering bands were rotated towards the secondary drawing direction (figure 6.9 - 2X2Y). At this stage no significant crystallinity was developed, rather the amorphous halo became slightly more diffuse, suggesting that the existing structure was lost during the rotation process. On further extension along the secondary axis (λ = 2X3Y) (figure 6.9 - 2X3Y), newer population of the oriented crystals developed, giving rise to (200), (110) and (203) reflections along the meridian. A diffuse nature of these reflections signifies poorer orientation of the crystalline phase in the

second direction. Increasing the sequential (Y-axis) draw ratio to 2X4Y resulted in the films with higher crystallinity but little improvement in the orientation was observed (figure 6.9 - 2X4Y).

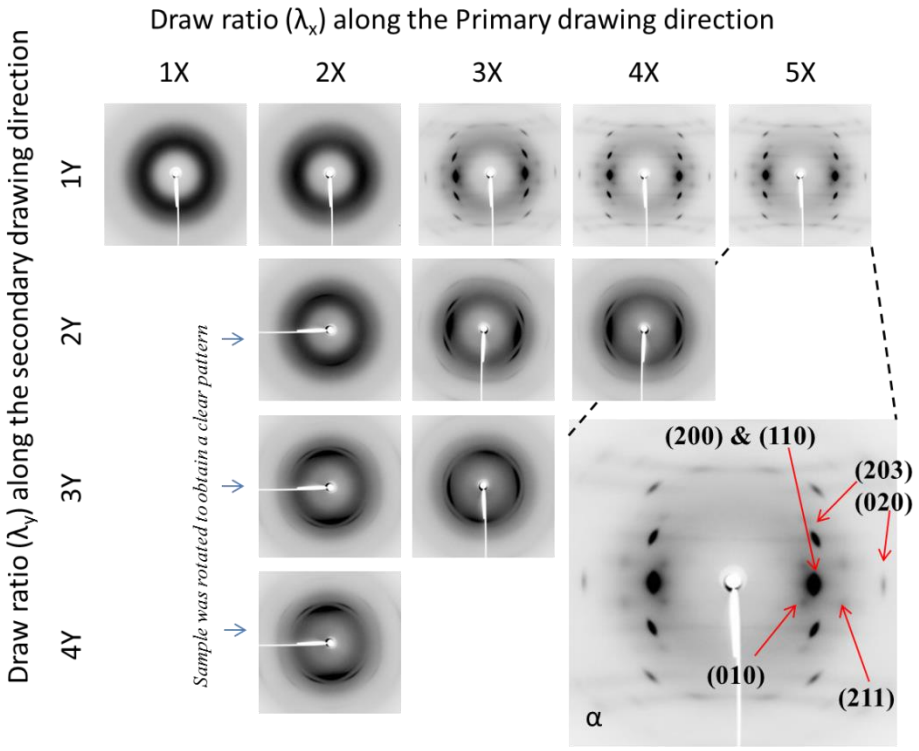

Figure 6.9: *Effect of uniaxial and sequential biaxial draw ratio on WAXD diffraction patterns of oriented curcumin loaded films.*

*(**α** – Characteristic reflections of the α crystal form of PLA (Kokturk *et al*., 2002))

Transverse drawing of the samples with UCW/ primary draw ratios of 3X and 4X clearly displays splaying of the existing three dimensional order (figure 6.9 - 3X2Y, 4X2Y). For a lower draw ratio along the secondary axis, the azimuthal spread of the characteristic crystalline reflections increased. When subjected to additional transverse drawing, a second population of the oriented crystals were generated, yielding a cross hatched pattern as displayed in figure 6.9 - 3X3Y (Ou and Cakmak, 2008).

Films oriented in simultaneous biaxial mode to a biaxial draw ratio of 2X2Y showed development of a diffuse isotropic scatter, resembling an un-oriented

amorphous film. At λ = 3X3Y, the (200, 110) and (203) bands appeared in the equatorial as well as the meridional planes, generating a cross-hatched pattern (similar to figure 6.9 - 3X3Y). The results signified that simultaneous stretching in two perpendicular directions in the SB mode leads to the generation of a bi-directionally equivalent structure (Ou and Cakmak, 2008).

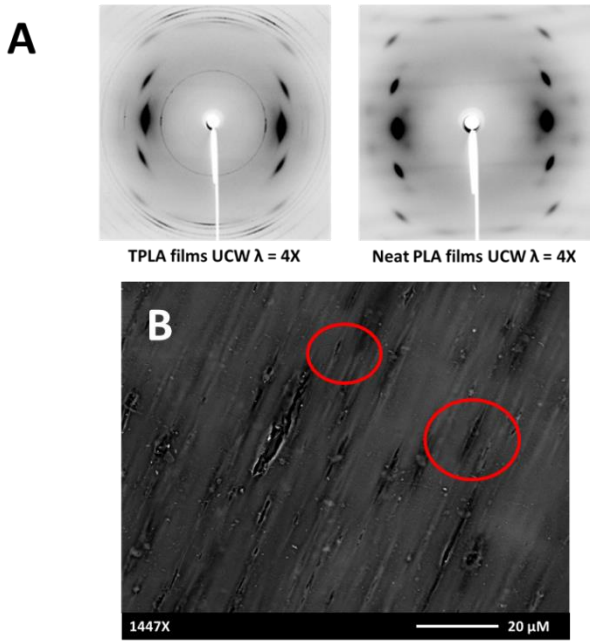

Figure 6.10: *Distinctive features of oriented TPLA films*

A) Comparison of the 2D WAXD patterns of the neat PLA and the TPLA films oriented in the UCW mode to a draw ratio of 4X1Y, **B)** SEM image of the cryo-fractured surface of the abovementioned TPLA film.

A distinctive feature was observed in the WAXD patterns of oriented TPLA films (figure 6.10 - A). The azimuthal spread of crystalline reflections corresponding to PLA was larger in the case of oriented TPLA films than the corresponding neat PLA films. A diffuse WAXD pattern may result from either poor orientation of the matrix and/or cavitation (Wang *et al*., 2014). It was previously reported that the presence of poorly cohesive particles in the suspension state may restrict the freedom of polymer chain movement during tensile drawing (Pukanszky, 1990). This phenomenon may explain the inferior orientation in the TPLA films, also evidenced as a lower Tg and a lower Herman's orientation parameter (sec 6.5), compared to neat PLA films having

the same draw ratio. Moreover, the SEM images of surfaces of oriented TPLA films (figure 6.10 - B) confirmed the presence of voids. Tensile extension of PLA may generate voids at the location of suspended theophylline particles, owing to a poor cohesive interaction between them (sec. 5.2, 5.6) (Kim *et al*., 2008). Therefore, the diffuse WAXD pattern shown by the oriented TPLA films can be attibuted to the combined effect of void formation and inferior orientation.

6.5. Quantification of the degree of orientation

The degree of unidirectional orientation can be quantified by Herman's orientation function (sec 4.13 – eqn. 4.5). The orientation function was found to increase with the UCW draw ratio for neat as well as drug loaded PLA films (figure 6.11). The slope of the curve was highest between the draw ratio of 2X and 3X, followed by a less steep rise. A combined analysis of the orientation function and the 2D-WAXD patterns suggested that the investigated films showed development of an oriented structure in 3 distinguished steps (at 80 °C drawing temperature and 0.57 sec^{-1} strain rate). A nematic phase with orientation of the amorphous chains was generated at λ = 2X. The major structural changes occurred between λ = 2X and λ = 3X, due to generation of an oriented crystalline order. Further drawing merely improved the structural order existing at λ = 3, by aligning of the previously un-oriented chains (Mulligan and Cakmak, 2005; Wong *et al*., 2008). In SEQ mode, the orientation function in the primary drawing direction (X-axis) reduced sharply, when the films were sequentially stretched in the perpendicular direction (Y-axis). Contrarily, the orientation function in the secondary direction increased gradually, with respect to the secondary (Y-axis) draw ratio.

Curcumin loaded PLA films showed a higher degree of orientation than neat PLA films and theophylline loaded PLA films, at individual draw ratios. The degree of orientation was lowest for the theophylline loaded PLA films. This can perhaps be attributed to the presence of theophylline in the crystalline suspension state, which supposedly hampered the PLA chain movement during

tensile deformation (sec. 6.4). No explanation was found for the higher degree of orientation in the curcumin loaded films.

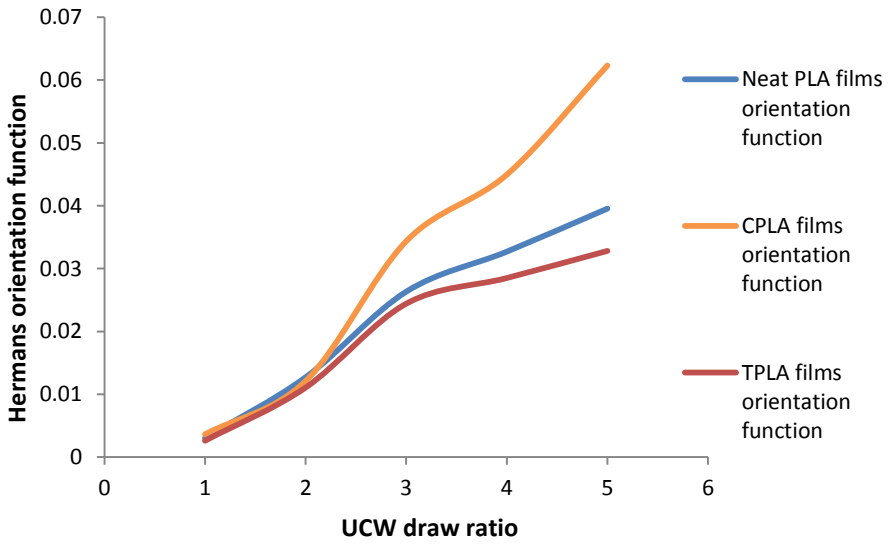

Figure 6.11: *Changes in Herman's orientation function with respect to the UCW draw ratio.*

In summary, drug loaded films showed a systematic evolution of oriented structure with respect to the draw ratio. An anisotropic structure was developed in UCW stretching, while biaxial stretching generated various morphologies depending up on the draw ratio along two perpendicular axes. Since, UCW stretching showed the most prominent changes in oriented structure, drug loaded films having UCW draw ratio between 1X - 4X, were shortlisted for drug release studies. At the current stage, considering the experimental feasibility, the drug release study on the biaxially oriented films was restricted to films having a biaxial draw ratio of 2X2Y (both SB & SEQ).

6.6. Mechanical properties of the oriented films

Mechanical properties of a material are critically associated with its physical structure. These include, Young's modulus - which is a measure of the elastic nature of the material; yield strength - representing the inherent strength

of the material without any plastic deformation; ultimate tensile strength and lastly, the strain or total extension at failure.

Changes in ultimate tensile strength and Young's modulus against the draw ratio of neat PLA and drug loaded PLA films is summarised in table 6.5. The tensile strength of neat and drug loaded PLA films was improved when subjected to uniaxial as well as biaxial orientation. For UCW stretching, the tensile properties were enhanced only in the drawing direction; while for the SB orientation, they were statistically the same ($P > 0.05$, paired t-test), in both the medional and the transverse directions. The improvement in mechanical strength and modulus after UCW orientation was significantly greater than that after SB orientation ($P < 0.05$, paired t-test). Interestingly, the tensile strength and the modulus of the films with UCW draw ratio of 2X, even exceeded that of the SB oriented films having a biaxial draw ratio of 3X3Y. This can be attributed to the preferential unidirectional orientation of the polymer chains in UCW mode (sec. 6.4).

The ultimate tensile strength and Young's modulus data was statistically compared by 2-way ANOVA with replication. The oriented films were analysed separately depending upon the mode of orientation (e.g. UCW, SB, SEQ). In each mode, the columns represent different model drugs, while the row represents increasing draw ratios. The statistical comparison of the tensile strength is summerised in table 6.6, while that of Young's modulus is represented in table 6.7.

Table 6.5 and the ANOVA summary tables (table 6.6, table 6.7) confirmed that a continuous enhancement in mechanical strength and Young's modulus was observed with increasing draw ratios, regardless of the drawing mode. For the UCW oriented films the change was more prominent between draw ratios of 2X and 3X, perhaps due to generation of an oriented crystalline structure at λ = 3X (sec. 6.4). The yield strength of the oriented films followed the same trend as

that displayed by their ultimate tensile strength. Contrarily, the strain at failure exhibited an inverse relationship with draw ratio.

Table 6.5: *Tensile properties of oriented neat PLA and drug loaded films with respect to the uniaxial and biaxial draw ratio.*

Stretching mode	Draw ratio	Ultimate tensile strength (MPa) (Mean ± SD; n = 3)			Young's modulus (MPa) (Mean ± SD; n = 3)		
		Neat PLA films	CPLA films	TPLA films	Neat PLA films	CPLA films	TPLA films
UCW *(drawing direction)*	1X1Y	51.87 ± 2.12	50.88 ± 2.36	52.03 ± 4.45	1502.05 ± 9.57	1493.03 ± 23.33	1763.42 ± 35.1
	2X1Y	91.55 ± 2.95	96.02 ± 2.76	82.9 ± 0.94	2070.66 ± 17.91	2009.42 ± 23.49	2257.17 ± 60.98
	3X1Y	141.94 ± 4.54	146 ± 4.28	130 ± 2.86	2950.74 ± 42.27	3159.16 ± 46.68	2865.24 ± 45.88
	4X1Y	171.63 ± 2.24	179.74 ± 6.26	162.1 ± 2.25	3384.6 ± 15.84	3527.78 ± 26.46	3234.48 ± 19.58
	5X1Y	200.46 ± 2.28	211.1 ± 3.08	191.93 ± 1.9	4065 ± 12.39	4027.05 ± 22.74	3923.48 ± 18.8
Sequential *(second direction)*	2X2Y	80.65 ± 1.27	81.04 ± 0.93	75.31 ± 3.37	1615.5 ± 12.27	1598.6 ± 54.22	1896.18 ± 0.88
	2X3Y	102.82 ± 6.42	103.2 ± 2.32	99.36 ±1.92	1894.31 ± 15.44	1804.44 ± 85.97	2136.05 ± 36.16
	2X4Y	117.96 ± 3.48	120 ± 2.59	114 ± 1.97	2702.9 ± 7.9	2731.5 ± 29.31	2563.62 ± 17.87
	3X2Y	91.24 ± 2.56	97.7 ± 1.93	94.71 ± 4.35	1933.86 ± 32.4	1979.48 ± 24.06	1833.54 ± 26.87
	3X3Y	104.49 ± 2.45	112.59 ± 3.18	106.1 ± 1.75	2511.18 ± 17.52	2677.52 ± 40.85	2323.02 ± 5.32
	4X2Y	121.53 ± 1.85	121.99 ± 2.99	119.53 ± 1.3	2925.96 ± 28.91	2928.66 ± 53.35	2946.44 ± 44.96
SB	2X2Y	72.76 ± 3.11	74.59 ± 1.53	74.78 ± 1.14	1726.4 ± 42.77	1740.13 ± 28.92	1926.18 ± 30.67
	3X3Y	89.18 ± 2.97	92.04 ± 6.62	86.47 ± 2.54	1915.2 ± 31.91	1907.22 ± 36.35	2062.99 ± 33.3

* The mechanical properties of the SEQ oriented films reported here, were measured in the second stretching direction.

Table 6.6: *Two-way ANOVA (with replication) summary tables for tensile strength comparison*

1. UCW drawing ultimate tensile strength						
Source of Variation	*SS*	*df*	*MS*	*F*	*P-value*	*F crit*
Rows	131203	4	32800	3041.95	1.16×10^{-38}	2.6896
Columns	1272.99	2	636.4963	59.02	3.98×10^{-11}	3.3156
Interaction	431.45	8	53.9320	5.00	0.00053	2.2661
Within	323.48	30	10.7826			
Total	133231	44				

2. SEQ drawing ultimate tensile strength						
Source of Variation	*SS*	*df*	*MS*	*F*	*P-value*	*F crit*
Rows	10791.86	5	2158.37	260.30	3.36×10^{-27}	2.4771
Columns	193.9926	2	96.9963	11.69	0.000122	3.2594
Interaction	132.9324	10	13.2932	1.60	0.145293	2.1060
Within	298.5006	36	8.2916			
Total	11417.28	53				

3. SB drawing ultimate tensile strength						
Source of Variation	*SS*	*df*	*MS*	*F*	*P-value*	*F crit*
Rows	1037.85	1	1037.857	85.99	8.04×10^{-7}	4.7472
Columns	25.7083	2	12.8541	1.06	0.375137	3.8852
Interaction	28.3057	2	14.1528	1.17	0.342609	3.8852
Within	144.8190	12	12.0680			
Total	1236.69	17				

* The relevant data is displayed in the table 6.5

Note: The null hypothesis was that the compared samples were statistically the same

P > 0.05 = The difference between the compared samples is **not statistically significant**
0.05 > P > 0.01 = The difference between the compared samples is **statistically significant**
0.01 > P = The difference between the compared samples is **highly significant**

Table 6.7: *Two-way ANOVA (with replication) summary tables for Young's modulus comparison*

1. UCW drawing Young's modulus						
Source of Variation	*SS*	*df*	*MS*	*F*	*P-value*	*F crit*
Rows	33958939	4	8489735	8553.478	2.2×10^{-45}	2.689628
Columns	18810.17	2	9405.086	9.475702	0.000646	3.31583
Interaction	521007	8	65125.87	65.61486	6.88×10^{-17}	2.266163
Within	29776.43	30	992.5477			
Total	34528533	44				

2. SEQ drawing Young's modulus						
Source of Variation	SS	df	MS	F	P-value	F crit
Rows	10835013	5	2167003	1672.158	1.51×10^{-41}	2.477169
Columns	5390.427	2	2695.214	2.07975	0.139719	3.259446
Interaction	610041	10	61004.1	47.07355	1.18×10^{-17}	2.106054
Within	46653.53	36	1295.931			
Total	11497098	53				

3. SB drawing Young's modulus						
Source of Variation	*SS*	*df*	*MS*	*F*	*P-value*	*F crit*
Rows	121376.6	1	121376.6	103.2297	3.02×10^{-7}	4.747225
Columns	118839.4	2	59419.72	50.53593	1.43×10^{-6}	3.885294
Interaction	2045.581	2	1022.791	0.869874	0.443828	3.885294
Within	14109.5	12	1175.791			
Total	256371.2	17				

* The relevant data is displayed in the table 6.5

Note: The null hypothesis was that the compared samples were statistically the same

P > 0.05 = The difference between the compared samples is **not statistically significant**
0.05 > P > 0.01 = The difference between the compared samples is **statistically significant**
0.01 > P = The difference between the compared samples is **highly significant**

Sequential orientation of the films in the transverse direction showed similar improvent in the mechanical properties along the second stretching axis. However, the rise in mechanical strength with respect to the transverse draw

ratio was smaller than that observed with an increament in the UCW draw ratio ($P < 0.05$, paired t-test). This can be supported by the WAXD findings (sec. 6.4), which confirmed that previous stretching along the primary axis (X-axis) limits the structure development along the perpendicular axis (Y-axis) on subsequent stretching.

The model drugs produced negligible change in the mechanical properties of un-oriented PLA films. However, their effect was evident when such films were subjected to solid-state orientation (table 6.6 and table 6.7 column comparison). The un-oriented TPLA films and the neat PLA films had equivalent tensile strength. However, the oriented TPLA films exhibited lower tensile strength than the corresponding neat PLA and CPLA films at all UCW draw ratios. A similar change was also observed in the SEQ oriented TPLA films. As explained in the previous section (sec. 6.4), poor affinity between the suspended theophylline particles and the PLA matrix leads to generation of voids during tensile extension of the TPLA films (Kim *et al*., 2008). Nevertheless, the overall structural order within oriented TPLA films was inferior to the corresponding neat PLA and CPLA films. Therefore, poor mechanical properties of the theophylline loaded films at higher draw ratios can be clearly correlated with the abovementioned factors. Mechanical strength of the CPLA films was higher than both neat PLA films and TPLA films. This observation is aligned with the trend in Herman's orientation factor (figure 6.11), which suggested that CPLA films had a higher degree of orientation at a particular draw ratio than the corresponding neat and TPLA films. Despite of the difference in the mechanical strength, the Young's moduli of these films did not statistically vary with respect to the added drug (table 6.7). A peculiarity was observed in the case of SB oriented films. At a constant draw ratio, the difference between the mechanical strength of the neat PLA, CPLA and TPLA films was statistically insignificant (table 6.6). Nevertheless, the mentioned films showed statistically significant difference between their Young's moduli (table 6.7).

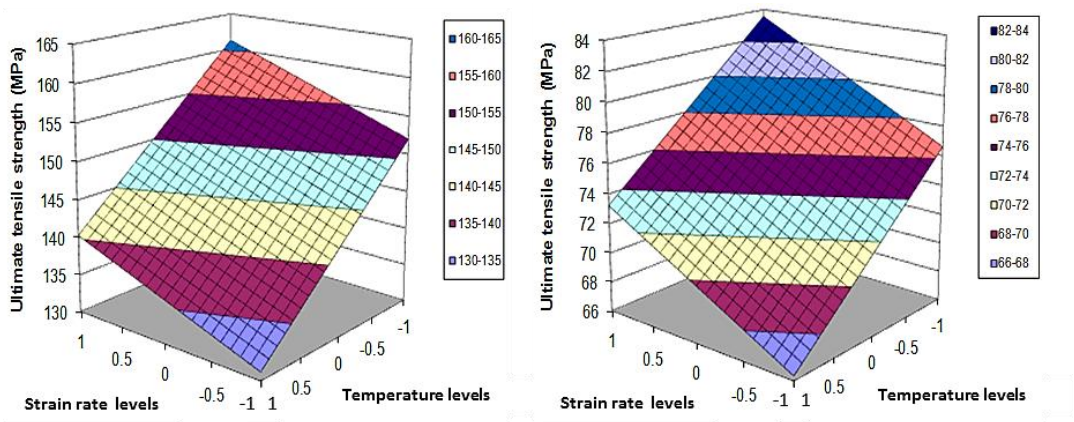

UCW CPLA films – Multiple regression

$\hat{y} = 117.32 - 8.35X_1 + 3.69X_2$

$R^2 = 0.996603$, F - value = 176.04

$P < 0.05$ (For the above polynomial constants)

SB CPLA films – Multiple regression

$\hat{y} = 91.19 - 6.17X_1 + 4.14X_2 - 1.98X_1^2 - 1.46X_1X_2$

$R^2 = 0.99471$, F - value = 112.84

$P < 0.05$ (For the above polynomial constants)

Figure 6.12: *Effect of strain rate and drawing temperature on the ultimate tensile strength of* ***A)*** *curcumin loaded films uniaxially oriented with a constant width (UCW) to λ = 3X and* ***B)*** *curcumin loaded films simultaneous biaxially (SB) oriented to λ = 2X2Y*

* The surface response plots were obtained by multiple regression analysis, details of which are represented below the respective plots. The drawing temperatures; namely 70 °C, 80 °C and 90 °C, and the strain rates 0.12 sec^{-1}, 0.57 sec^{-1}, 1.2 sec^{-1} are expressed as -1, 0 and +1 factorial levels respectively.

The mechanical properties closely reflected the changes in the oriented structure of the drug loaded PLA films, with respect to the underlying drawing conditions. The effect of temperature and strain rate on the tensile strength of oriented PLA films is represented in figure 6.12 through an example of the oriented CPLA films. Evidently, the films oriented at 70 °C (-1 temperature level) had highest mechanical strength, followed by films oriented at 80 °C (0 level) and lastly those oriented at 90 °C (+1 level). Moreover, the drawing temperature exhibited an inverse relationship with the strain at failure. Higher mechanical strength and extensibility of the films stretched at 70 °C can be attributed to their strong amorphous orientation. Contrarily, a rise in the crystallinity at higher temperatures may have lowered the mechanical strength and extensibility, by increasing the brittleness of the matrix. The effect of strain rate was less

pronounced than that of the drawing temperature. Nevertheless, higher strain rates generated films with higher mechanical strength. The overall effect of drawing conditions on the tensile strength was more closely aligned with the corresponding degree of orientation. In summary, the mechanical properties of oriented films showed a significant correlation to their physical structure. Therefore, a similar change may also be expected in the drug release properties of the oriented films.

6.7. Correlation between surface free energy and the oriented structure of the films

The hydrophobic or the hydrophilic nature of the bulk of an untreated polymeric film can be inferred from its surface free energy (Stachewicz *et al.*, 2012). The surface free energy of PLA films, further utilised in the drug release studies was determined here. These included, CPLA and TPLA films oriented in UCW mode to $1X \leq \lambda \leq 4X$, in SB mode to $\lambda = 2X2Y$ and in SEQ mode to $\lambda = 2X2Y$. Neat PLA films with corresponding draw ratios were used as a control to study the effect of added drug. The surface energy was derived from contact angles made by ten diverse probe liquids with the film surface (Owens and Wendt, 1969). The mathematical description of the method is detailed in the section 4.15.1.

The alkane series probe liquids (n-octane, n-heptane, n-hexane, and cyclohexane) which are non-polar in nature, completely wetted the PLA film surface, exhibiting a zero contact angle. The contact angle did not change after orientation of the films; neither was there a difference with respect to the added drug. This clearly highlights the hydrophobic nature of PLA. Since, the abovementioned probe liquids made a same contact angle with PLA films, only one amongst them, i.e. cyclohexane was used further.

The surface energy of un-oriented neat PLA films, derived from the contact angle values for cyclohexane, di-iodomethane and the remaining non-alkane probe liquids (toluene, benzyl alcohol, ethylene glycol, glycerol and

water – **'7-probe liquids approach'**) was 38.37 mJ/m^{-2}. Gruber *et al.* (1998) and Auras *et al.* (2004) separately reported the total surface energy of PLA films (Natureworks, 98% L-isomer) to range between 42 - 44 mJ/m^{-2}. It has been previously confirmed that the surface energy measured by any method, involving an interaction between the probe liquids and a solid surface is sensitive to the liquids used (Cava *et al.*, 2007). Therefore, the lower values of the surface energy obtained in this study can be attributed to the selection of the probe liquids. The sensitivity of the Owens-Wendt method increases when probe liquids with higher surface tension and those making a larger contact angle are used. Considering the above fact, a second approach for calculation of surface energy was adopted. In this approach, only 3 probe liquids, namely water ($\boldsymbol{\gamma}_L^{Dispersive}$=20.70 mJ/m^{-2}, $\boldsymbol{\gamma}_L^{Polar}$=52.10 mJ/m^{-2}), Glycerol ($\boldsymbol{\gamma}_L^{Dispersive}$= 38.10mJ/m^{-2}, $\boldsymbol{\gamma}_L^{Polar}$= 25.30mJ/m^{-2}) and di-iodomethane ($\boldsymbol{\gamma}_L^{Dispersive}$= 50.07mJ/m^{-2}, $\boldsymbol{\gamma}_L^{Polar}$=0 mJ/m^{-2}) were used. The surface energy values obtained by the **'3-probe liquids approach**' more closely matched with previously reported values.

Table 6.8 and table 6.9 list the surface energy of neat and drug loaded PLA films obtained by the '7-liquids' and the '3-liquids' approach respectively. The overall surface energy was divided into a polar and a dispersive component. Either of the components for the studied systems were separately compared by 2-way ANOVA statistical test. In such comparison, the columns represented films containing different model drugs, while the rows represented different draw ratios. The summary of the statistical analysis is given in table 6.10 and table 6.11.

The results confirmed that compounding with curcumin did not produce any significant change in the surface energy of both un-oriented and oriented PLA films (table 6.8, table 6.9) The difference between the surface energies (both polar and dispersive) of the neat and CPLA films was statistically insignificant when measured by the '7-liquids' approach (table 6.10 – A, C).

Contrarily, such a difference between the surface energies of neat PLA and TPLA films was highly significant (table 6.10 – B, D). Surface roughness in the theophylline loaded films resulted in a higher contact angle values for the most of the probe liquids. The greatest difference was observed in the water contact angle, which was approximately 10° higher than that for the corresponding neat PLA films. This led to a reduction in the polar component and a small rise in the dispersive component of the surface energy of the TPLA films. When measured by the '3-liquids' approach, dispersive energies of both CPLA and TPLA were statistically similar to the neat PLA films. Nevertheless, a significant difference was observed in their polar energies (table 6.11).

Table 6.8: *Surface energy of the model PLA films estimated by the Owens-Wendt method, using 'the 7-probe liquids approach' (cyclohexane, di-iodomethane, toluene, benzyl alcohol, ethylene glycol, glycerol and water).*

Sample	Surface energy using 7 probe liquids ($mJ.m^{-2}$)					
	Neat PLA		Curcumin loaded PLA		Theophylline loaded PLA	
	γ_f^D	γ_f^P	γ_f^D	γ_f^P	γ_f^D	γ_f^P
Un-oriented	25.5	10.96	25.41	10.77	27.63	5.11
UCW 2X	25.83	12.54	25.88	11.68	27.86	6.54
UCW 3X	25.56	16.27	25.72	14.66	27.31	10.1
UCW 4X	25.28	18.94	25.59	16.7	26.89	13.19
SB 2X2Y	25.56	10.72	25.39	10.41	27.47	5.09
SEQ 2X2Y	25.92	10.06	25.98	10.22	27.88	5.42

Table 6.9: *Surface energy of model PLA films estimated by the Owens-Wendt method, using 'the 3-probe liquids approach' (di-iodomethane, glycerol and water).*

Sample	Surface energy using 3 probe liquids ($mJ.m^{-2}$)					
	Neat PLA		Curcumin loaded PLA		Theophylline loaded PLA	
	γ_f^D	γ_f^P	γ_f^D	γ_f^P	γ_f^D	γ_f^P
Un-oriented	31.84	8.97	31.83	8.97	31.94	3.77
UCW 2X	33.28	9.94	33.53	9.44	33.66	4.7
UCW 3X	34.7	12.96	34.44	11.84	35.02	7.35
UCW 4X	35.43	15.12	35.25	13.39	36.08	9.80
SB 2X2Y	31.67	9.02	31.88	8.63	31.5	3.24
SEQ 2X2Y	31.29	8.98	31.53	8.51	31.84	3.78

Notes: The surface energy was calculated from linear regression of the following equation, using the contact angle (average from 6 replicates) and the surface tension values (average from 6 replicates) obtained for the individual probe liquids (sec. 4.15). R^2 for all samples was ≥ 0.99 when measured by 3-liquid approach, while that was $0.96 \geq R^2 \geq 0.94$ when measured by 7-liquid approach.

$$\frac{(\cos\theta+1)\gamma_L}{2\,(\gamma_L^D)^{\frac{1}{2}}} = (\gamma_f^P)^{\frac{1}{2}}\frac{(\gamma_L^P)^{\frac{1}{2}}}{(\gamma_L^D)^{\frac{1}{2}}} + (\gamma_f^D)^{\frac{1}{2}} \qquad \textbf{(Equation. 4.7)}$$

Where, γ_L= overall surface tension of the probe liquid,

γ_L^D = dispersive component of the surface tension of the probe liquid,

γ_L^P = polar component of the surface tension of the probe liquid.

γ_f^D = dispersive component of the surface energy of the film,

γ_f^P = polar component of the surface energy of the film and

θ = the contact angle between the probe liquid and the film.

* The contact angle replicate measurements were performed by rotating the film surface, in order ensure that it was same in all directions. All contact angle values showed less than 5% deviation from the mean.

Table 6.10: *Two-way ANOVA summary table for statistical comparison of the surface energy calculated by the '7 – probe liquids' approach.*

A) γ_f^D Comparison Neat PLA Vs CPLA						
Source of Variation	**SS**	**df**	**MS**	**F**	**P-value**	**F crit**
Rows	0.4913	5	0.0982	6.65	0.028973	5.0503
Columns	0.0085	1	0.0085	0.57	0.481526	6.6078
Error	0.0738	5	0.0147			
Total	0.5737	11				

B) γ_f^D Comparison Neat PLA Vs TPLA						
Source of Variation	**SS**	**df**	**MS**	**F**	**P-value**	**F crit**
Rows	0.8801	5	0.1760	9.77	0.012863	5.0503
Columns	10.8111	1	10.8110	600.33	2.11×10^{-6}	6.6078
Error	0.0900	5	0.0180			
Total	11.7812	11				

C) γ_f^P Comparison Neat PLA Vs CPLA						
Source of Variation	**SS**	**df**	**MS**	**F**	**P-value**	**F crit**
Rows	97.1784	5	19.4357	45.65	0.000357	5.0503
Columns	2.1252	1	2.1252	4.99	0.075743	6.6078
Error	2.1283	5	0.4256			
Total	101.4320	11				

D) γ_f^P Comparison Neat PLA Vs TPLA						
Source of Variation	**SS**	**df**	**MS**	**F**	**P-value**	**F crit**
Rows	118.9622	5	23.7924	162.94	1.57×10^{-5}	5.0503
Columns	96.5601	1	96.5601	661.31	1.66×10^{-6}	6.6078
Error	0.7300	5	0.1460			
Total	216.2524	11				

* The relevant data is displayed in the table 6.8

Note: The null hypothesis was that the compared samples were statistically the same

P > 0.05 = The difference between the compared samples is **not statistically significant**
0.05 > P > 0.01 = The difference between the compared samples is **statistically significant**
0.01 > P = The difference between the compared samples is **highly significant**

Table 6.11: *Two-way ANOVA summary table for statistical comparison of the surface energy calculated by the '3 – probe liquids' approach.*

A) γ_f^D Comparison Neat PLA Vs CPLA						
Source of Variation	**SS**	**df**	**MS**	**F**	**P-value**	**F crit**
Rows	26.9435	5	5.3887	212.25	8.14×10^{-6}	5.0503
Columns	0.0052	1	0.0052	0.21	0.669575	6.6078
Error	0.1269	5	0.0253			
Total	27.0757	11				

B) γ_f^D Comparison Neat PLA Vs TPLA						
Source of Variation	**SS**	**df**	**MS**	**F**	**P-value**	**F crit**
Rows	32.7062	5	6.5412	144.54	2.11×10^{-5}	5.0503
Columns	0.2790	1	0.2790	6.16	0.055616	6.6078
Error	0.2262	5	0.0452			
Total	33.2116	11				

C) γ_f^P Comparison Neat PLA Vs CPLA						
Source of Variation	**SS**	**df**	**MS**	**F**	**P-value**	**F crit**
Rows	53.1809	5	10.6361	55.50426	0.000222	5.0503
Columns	1.4770	1	1.4770	7.707672	0.039074	6.6078
Error	0.9581	5	0.1916			
Total	55.6161	11				

D) γ_f^P Comparison Neat PLA Vs TPLA						
Source of Variation	**SS**	**df**	**MS**	**F**	**P-value**	**F crit**
Rows	67.3310	5	13.4662	448.74	1.26×10^{-6}	5.0503
Columns	87.2102	1	87.2102	2906.20	4.15×10^{-8}	6.6078
Error	0.1500	5	0.0300			
Total	154.6913	11				

* The relevant data is displayed in the table 6.9

Note: The null hypothesis was that the compared samples were statistically the same

P > 0.05 = The difference between the compared samples is **not statistically significant**
0.05 > P > 0.01 = The difference between the compared samples is **statistically significant**
0.01 > P = The difference between the compared samples is **highly significant**

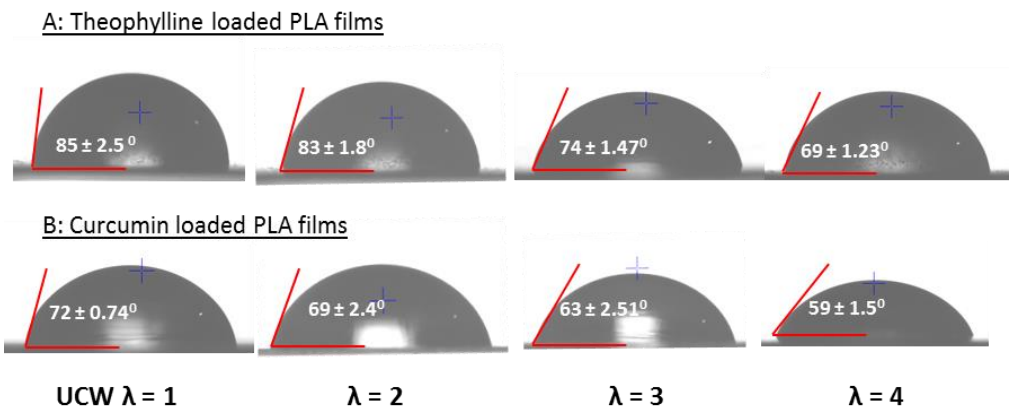

Figure 6.13: *Changes in the water contact angle of* ***A)*** *curcumin loaded PLA films and* ***B)*** *theophylline loaded PLA films after subjecting them to UCW stretching.*

*The contact angle values are represented as 'mean ± SD' of six replicate measurements

UCW extension of the films caused a reduction in the contact angle of all probe liquids, consequently leading to a rise in the total surface energy (table 6.8 & table 6.9). Since water exhibited the highest contact angle, a change in its value after uniaxial orientation was most prominently visible (figure 6.13). The surface energy values obtained by the '7-probe liquids' method (table 6.8) showed no variation in the dispersive component after UCW stretching; whereas, the polar component increased with respect to UCW draw ratio. Results of the '3-probe liquids' method (table 6.9) displayed a greater rise in the dispersive component at UCW draw ratio 2X. At λ ≥ 3X, the polar component increased by a higher margin than the dispersive component. Overall, both of the methods confirmed a rise in the polar surface energy after UCW stretching. Such a rise was statistically significant for all studied films regardless of the measurement method (table 6.10 and table 6.11)

Stachewicz *et al*. (2012) reported similar findings, when polycarbonate films were subjected to uniaxial stretching. However, the authors detected no change in the surface chemistry of the oriented polycarbonate films. When the surface of the oriented PLA films utilised in the current study was analysed by ATR-FTIR, a clear indication of the elevated dipole-dipole interaction was obtained. The FTIR spectra of the UCW oriented PLA films (λ ≥ 3X) showed the

appearance of a small peak at a wavenumber of 923 cm^{-1} and splitting of 1167 cm^{-1} peak (figure 6.14 - B). The prior represents the bending vibrations of the lactic acid 'O-H group' (figure 6.14 - B), while the latter represents 'C-O' stretching vibrations of the lactic acid/ ester group. Moreover, the peak at 712 cm^{-1} associated with the stretching vibration of the 'C=O' group was shifted to 691 cm^{-1}. All of these events became apparent at the UCW draw ratio 3X and intensified at the UCW draw ratio of 4X. The mentioned changes in the FTIR spectrum of the PLA films have been previously correlated to higher dipole interactions in the α crystalline Form of PLA, due to its -10/3 helical conformation (figure 6.14 - A) (Aou and Hsu, 2006; Wasanasuk *et al*., 2011).

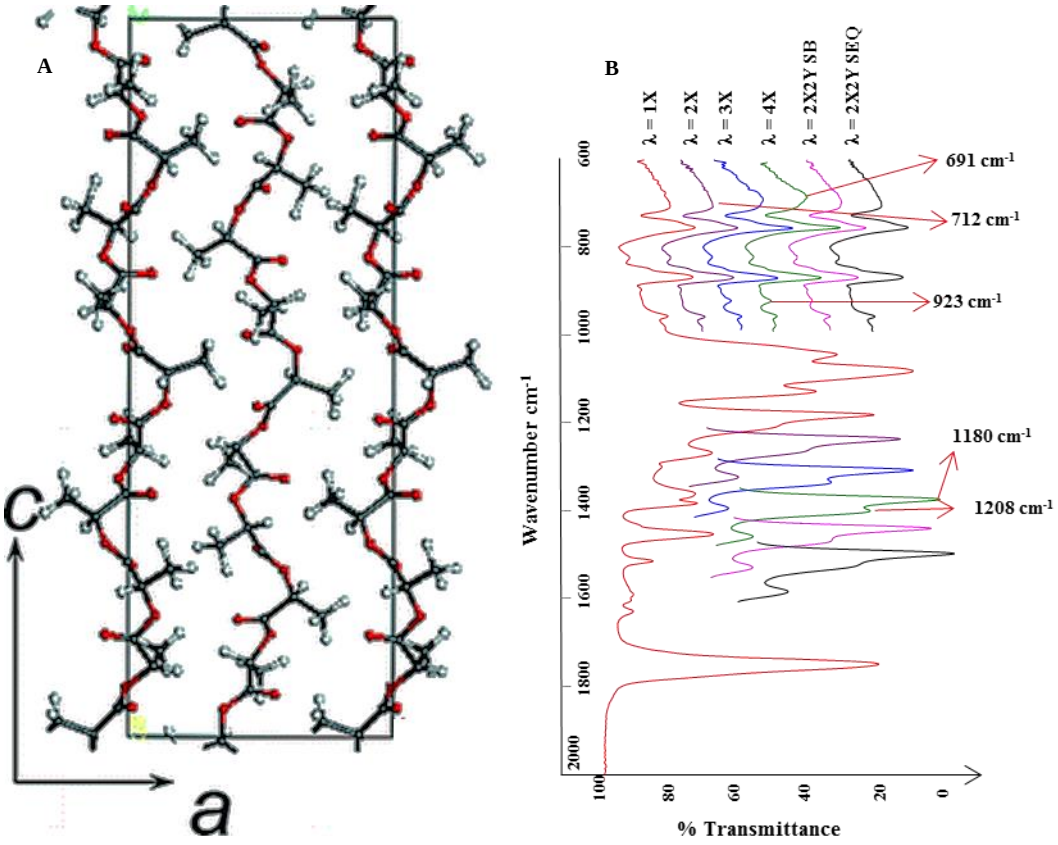

Figure 6.14: A) *Crystal structure of the α Form of PLA with its c-axis oriented in the stretching direction. (Black = carbon, White = Hydrogen, Red = Oxygen) (adapted from Wasanasuk et al. (2011)),* ***B)*** *ATR-FTIR spectra of the surfaces of oriented curcumin loaded PLA films.*

WAXD patterns of the oriented PLA films utilised in this study were discussed in the section 6.4. They confirmed that both neat and drug loaded PLA films, when subjected to UCW stretching, generated an oriented amorphous structure at a draw ratio of 2X. On further stretching, the α crystalline form was generated with its c-axis parallel to the stretching direction. Nevertheless, the number of chains organised in such a manner increased with UCW draw ratio. The crystal structure of the α Form of PLA with its c-axis oriented in the stretching direction was reported by Wasanasuk *et al*. (2011) (figure 6.14 - A). In a homogenous PLA matrix the functional groups are organised in a random manner. Contrarily, when the PLA chains are oriented in the α crystalline form (figure 6.14), the relative number of functional groups facing the surface increases. A rise in the concentration of free hydroxyl groups (red dots) augments the polar surface energy, while the dispersive energy is enhanced due to higher Van der Waals interaction, between the concentrated methyl moieties (3 white dots). At a uniaxial draw ratio of 2X, exclusive amorphous orientation might have enhanced the dispersive surface energy. However, the polarity did not increase substantially, owing to the absence of the α crystalline form.

Apparently, no change in the surface energy was observed when the films were oriented biaxially to a draw ratio of 2X2Y. Moreover, the characteristic changes in the FTIR spectra of UCW oriented films (λ ≥ 3X) were not observed in the FTIR spectra of biaxially oriented films (λ ≥ 2X2Y) (figure 6.14 - B). This can perhaps be attributed to the amorphous nature of the mentioned films, combined with a bi-directionally symmetric chain organisation. However, further studies with multiple biaxial draw ratios must be completed before drawing a safe conclusion.

Importantly, the chain organisation depicted in figure 6.14 is also repeated in the bulk of the PLA films. Therefore, augmentation of the polar surface energy due to formation of the α crystal form at the UCW λ ≥ 3X, can be viewed

as, enhancement of the overall hydrophilicity of the oriented PLA films. This may accelerate water penetration, formation of the micro-pores and subsequent drug release from these films.

6.8. Dynamic changes in the properties of drug loaded PLA films submerged in the release medium

PLA undergoes rapid hydrolytic degradation in an aqueous environment (Cam *et al.*, 1995; Li *et al.*, 1990; Vert *et al.*, 1991). The onset and the kinetics of degradation are simultaneously governed by several factors (Codari *et al.*, 2012) such as crystallinity (Tsuji and Ikada, 1997; Tsuji and Ikada, 2000b; Tsuji and Ikarashi, 2004), molecular weight (Belbella *et al.*, 1996), size and shape of the matrix (Grizzi *et al.*, 1995), pH and temperature of the aqueous environment (Belbella *et al.*, 1996; Cam *et al.*, 1995) and presence of additives (Li *et al.*, 1996). It is believed that the lower molecular weight PLA undergoes surface erosion; whereas at higher molecular weight (> 50KDa), bulk erosion becomes a dominant mechanism (Alexis, 2005). When a polyester matrix is undergoing bulk degradation, oligomers generated in the degradation process remain entrapped within the matrix, unless they are small enough to be soluble in the permeated medium. Such oligomers further catalyse the degradation process (Li *et al.*, 1990). Nevertheless, it is known that the newly generated oligomers undergo crystallisation, being plasticised by the percolated water. This further changes the morphology of the polyester matrix and the rate of hydrolytic degradation. These changes can critically influence drug release from a PLA matrix. Therefore, their prior knowledge is essential. The current study included investigation of the changes in the molecular weight, crystallinity and morphology of the drug releasing PLA films at regular intervals, after submersion into the release medium.

6.8.1. Shrinkage of oriented amorphous films

Among the two model drugs utilised in this study, curcumin formed a glassy solution in the melt quenched amorphous PLA films. On the contrary,

theophylline was present as a suspension of crystalline particles (5-25 μm) in the amorphous polymer phase. Orientation of the drug loaded PLA films to a UCW draw ratio of 2X or to a biaxial (both SB & SEQ) draw ratio of 2X2Y, led to generation of a nematic structure (sec. 6.4). Here the amorphous chains were oriented in the drawing direction; however, no strain crystallisation occurred. When such films were submerged into the drug release medium (at 37 °C), curcumin loaded PLA films (CPLA) underwent shrinkage, while theophylline loaded films (TPLA) remained stable. The shrinkage of biaxially oriented films occurred in two perpendicular directions. This led to curling of the film samples and a non-uniform change in their dimensions. Therefore, only the UCW oriented films were selected as a model system for the current study. Shrinkage in the mentioned films was characterised by measurement of the dimensional changes (in a tensile bar specimen), percentage crystallinity and 2D WAXD patterns, for 14 days after submersion in the release medium. This information is summarised in figure 6.15.

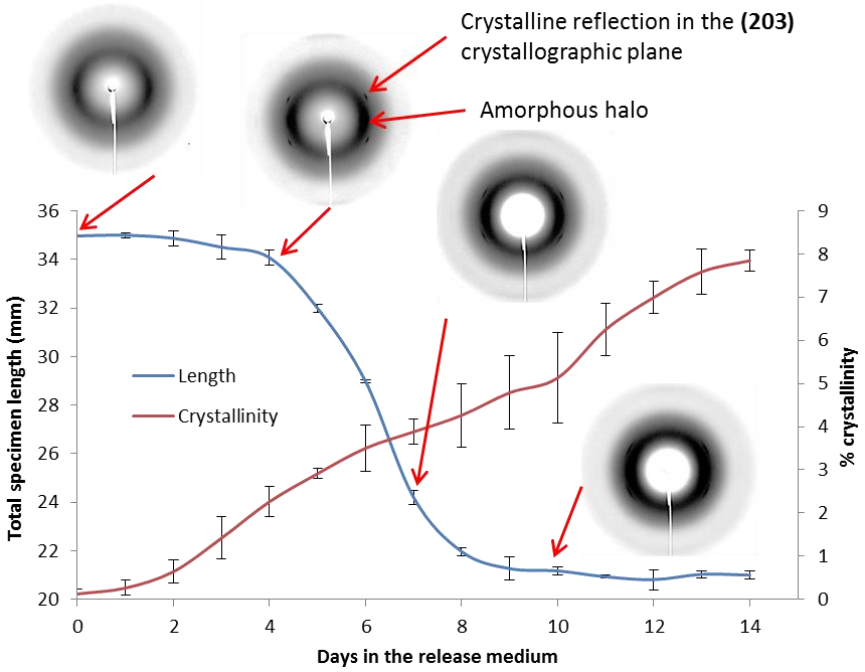

Figure 6.15: *Changes in the length, percentage crystallinity and 2D WAXD patterns of UCW 2X oriented curcumin loaded films after submersion into the release medium.*

*The crystallinity and the specimen length values are expressed as mean ± SD, where n = 6.

For convenience the TPLA and CPLA films oriented to a UCW draw ratio of 2X are referred to here as TPLA-2X and CPLA-2X respectively. Both the TPLA-2X and the CPLA-2X films showed a steady rise in crystallinity, when submerged in the release medium. Owing to the presence of crystalline theophylline particles, the dimensions and the 2D WAXD patterns of the TPLA-2X films remained unchanged for the current study duration (14 days). Conversely, the CPLA-2X films underwent rapid shrinkage between the 4^{th} and the 8^{th} day after submersion (figure 6.15). This phase was preceded by an induction period, which correlated to the time taken by the release medium to percolate into the films and cause plasticisation. The shrinkage plateaued at approximately 60% of the original specimen (tensile bar) length, by the 10^{th} day (figure 6.15). Perhaps the dimensional change was halted once the film crystallinity rose above a critical level. WAXD patterns of the submerged CPLA-2X films showed intensification of the equatorial amorphous halo and appearance of the (203) crystalline reflection, after ageing for 3 days (figure 6.15). The azimuthal spread of the equatorial halo and the (203) crystalline reflection significantly increased between the 4^{th} and the 8^{th} day. CPLA-2X films aged for 10 days showed an extremely diffuse halo, nearly forming a complete circle. The changes in the 2D WAXD patterns of the submerged CPLA-2X films confirmed that the mentioned films lost the majority of their oriented structure as they underwent shrinkage.

These results suggest that the oriented CPLA films having ≤ 5% crystallinity (due to lower draw ratios), lost the oriented structure after submersion in the release medium (at 37 °C). However, such a nematic structure was stabilised in the case of TPLA films, due to the presence of theophylline in a crystalline suspension state. Therefore, the effect of amorphous orientation on drug release might only be observed in the TPLA films. Contrarily, CPLA films which underwent shrinkage will possibly behave similar to the un-oriented films.

6.8.2. Crystallinity changes

Figure 6.16 & figure 6.17 illustrate changes in the crystallinity of drug loaded PLA matrices with respect to submersion duration. The crystallinity change was statistically validated by comparison between different draw ratios at certain time-points, and at different time-points. Such comparison was made by one-way ANOVA, followed by Tukey's test. The results of the statistical analysis are represented in the following tables: table 6.12, table 6.13, table 6.14 and table 6.15.

The crystallinity of drug loaded PLA matrices increased over the first 6 - 8 weeks and reached a constant value ranging between 35% - 40% by the end of the 8^{th} week. As confirmed in the table 6.13 and table 6.15, the difference between crystallinity at the beginning and after 8 weeks was highly significant for all studied draw ratios, regardless of the model drug. Nevertheless, these films displayed statistically equivalent crystallinity (table 6.12, table 6.14) between the 8^{th} and 10^{th} weeks. From the 12^{th} week onwards CPLA films with λ = 3X and 4X, showed comparable crystallinity levels (in general the statistical difference between them remained insignificant). Similarly, the crystallinity of the un-oriented, UCW-2X, SB-2X2Y and SEQ-2X2Y CPLA films remained equivalent (table 6.12). In the case of the TPLA films (table 6.14), 1X-2X pair, 3X-4X pair and SB-2X2Y-SEQ-2X2Y pair showed a statistically equivalent change in the crystallinity from the 12^{th} week onwards.

There was a transient reduction in the crystallinity of the inherently amorphous films from the 11^{th} week onwards (i.e. Un-oriented, UCW λ = 2X, SB λ = 2X2Y and SEQ λ = 2X2Y. These films are considered practically amorphous in the further discussion). Contrarily, films oriented to UCW draw ratios of 3X and 4X exhibited a statistically constant crystallinity until the 16^{th} week (table 6.13, table 6.15). The transient fall in crystallinity can be potentially correlated with hydrolytic degradation of the crystalline phase. (Tsuji and Ikada, 1998).

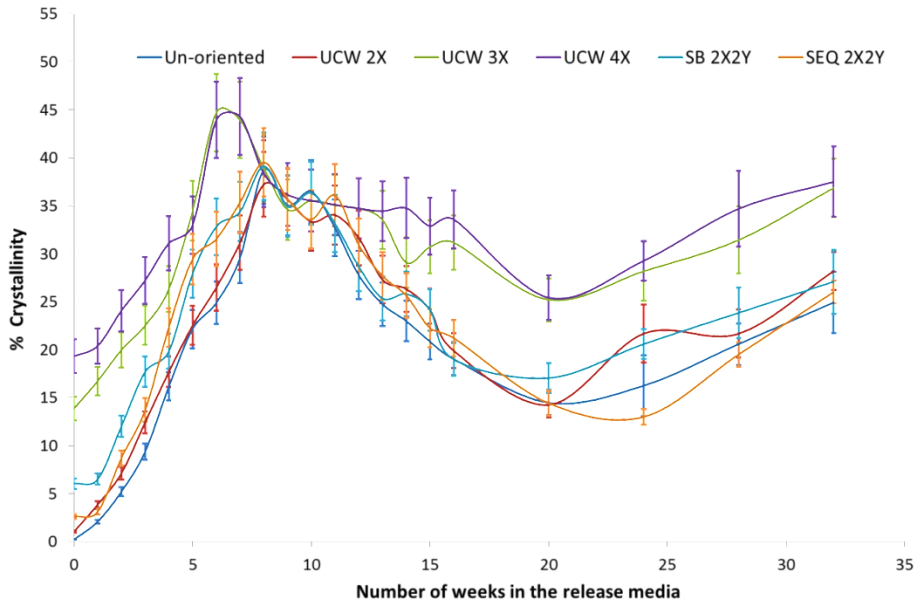

Figure 6.16: *Changes in the crystallinity of curcumin loaded PLA (CPLA) films after submersion in the release medium.*

**The graph represents % crystallinity as the mean ± standard deviation, where n = 6.

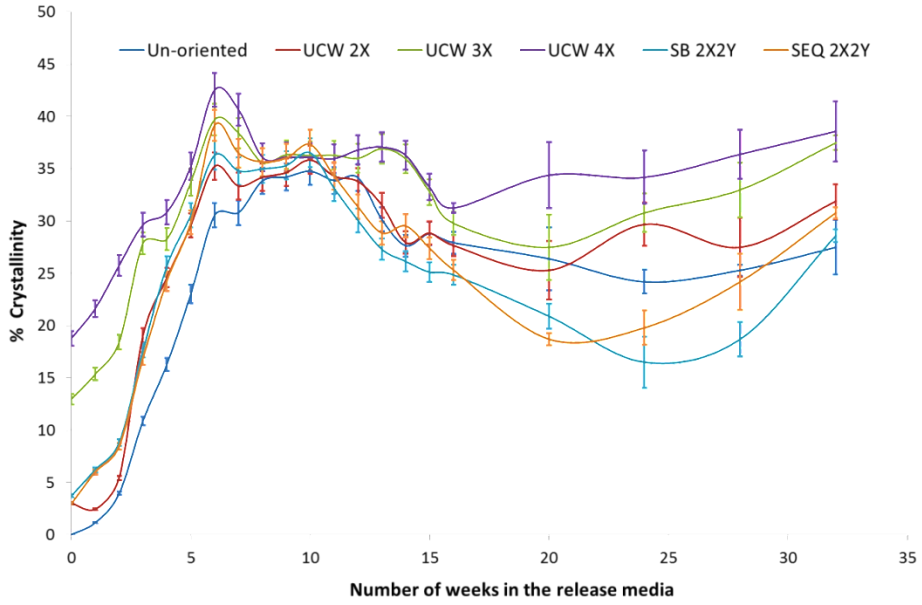

Figure 6.17: *Changes in the crystallinity of theophylline loaded PLA (TPLA) films after submersion in the release medium.*

**The graph represents % crystallinity as the mean ± standard deviation, where n = 6.

Table 6.12: *Statistical comparison of the weekly changes in the crystallinity of CPLA films after aqueous submersion – draw ration comparison*

One way ANOVA followed by Tukey's test - Draw ratio comparison								
	Week 0	Week 6	Week 8	Week 10	Week 12	Week 16	Week 24	Week 32
1X Vs 2X	P > 0.05, q = 2.21	P > 0.05, q = 1.21	P > 0.05, q = 1.04	P > 0.05, q = 2.42	P < 0.001, q = 11.46	P > 0.05, q = 0.46	P < 0.01, q = 5.39	P > 0.05, q = 2.77
1X Vs 3X	P < 0.0001, q = 36.70	P < 0.001, q = 15.38	P > 0.05, q = 0.15	P > 0.05, q = 0.72	P < 0.001, q = 13.92	P < 0.001, q = 13.31	P < 0.001, q = 11.87	P < 0.001, q = 10.18
1X Vs 4X	P < 0.0001, q = 51.35	P < 0.001, q = 14.76	P > 0.05, q = 0.25	P > 0.05, q = 0.72	P > 0.05, q = 0.92	P < 0.001, q = 15.96	P < 0.001, q = 12.95	P < 0.001, q = 10.73
1X Vs SB 2X2Y	P < 0.001, q = 15.72	P < 0.01, q = 6.14	P > 0.05, q = 0.28	P > 0.05, q = 0.12	P > 0.05, q = 1.34	P > 0.05, q = 0.04	P < 0.05, q = 4.31	P > 0.05, q = 1.85
1X Vs SEQ 2X2Y	P < 0.01, q = 6.44	P < 0.05, q = 5.15	P > 0.05, q = 0.55	P > 0.05, q = 2.23	P < 0.001, q = 11.20	P > 0.05, q = 2.40	P > 0.05, q = 3.23	P > 0.05, q = 0.92
2X Vs 3X	P < 0.001, q = 34.48	P < 0.001, q = 14.15	P > 0.05, q = 1.19	P > 0.05, q = 1.69	P > 0.05, q = 2.46	P < 0.001, q = 12.35	P < 0.001, q = 6.47	P < 0.001, q = 7.41
2X Vs 4X	P < 0.001, q = 49.13	P < 0.001, q = 13.53	P > 0.05, q = 0.79	P > 0.05, q = 1.69	P < 0.001, q = 12.38	P < 0.001, q = 15.01	P < 0.001, q = 7.55	P < 0.001, q = 7.96
2X Vs SB 2X2Y	P < 0.001, q = 13.50	P < 0.05, q = 4.91	P > 0.05, q = 1.33	P > 0.05, q = 2.29	P < 0.001, q = 10.11	P > 0.05, q = 0.99	P > 0.05, q = 1.07	P > 0.05, q = 0.92
2X Vs SEQ 2X2Y	P > 0.05, q = 4.22	P > 0.05, q = 3.92	P > 0.05, q = 1.60	P > 0.05, q = 0.18	P > 0.05, q = 0.26	P > 0.05, q = 1.45	P > 0.05, q = 1.63	P > 0.05, q = 1.85
3X Vs 4X	P < 0.001, q = 14.65	P > 0.05, q = 0.61	P > 0.05, q = 0.41	P > 0.05, q = 0.69	P < 0.001, q = 14.84	P > 0.05, q = 2.65	P > 0.05, q = 1.07	P > 0.05, q = 0.55
3X Vs SB 2X2Y	P < 0.001, q = 20.98	P < 0.001, q = 9.23	P > 0.05, q = 0.13	P > 0.05, q = 0.60	P < 0.001, q = 12.57	P < 0.001, q = 13.34	P < 0.001, q = 7.55	P < 0.001, q = 8.33
3X Vs SEQ 2X2Y	P < 0.001, q = 30.26	P < 0.001, q = 10.22	P > 0.05, q = 0.41	P > 0.05, q = 1.51	P > 0.05, q = 2.72	P < 0.001, q = 10.90	P < 0.001, q = 15.10	P < 0.001, q = 9.25
4X Vs SB 2X2Y	P < 0.001, q = 35.63	P < 0.001, q = 8.61	P > 0.05, q = 0.54	P > 0.05, q = 0.60	P > 0.05, q = 2.26	P < 0.001, q = 16.00	P < 0.001, q = 8.63	P < 0.001, q = 8.88
4X Vs SEQ 2X2Y	P < 0.001, q = 44.91	P < 0.001, q = 9.61	P > 0.05, q = 0.81	P > 0.05, q = 1.51	P < 0.001, q = 12.12	P < 0.001, q = 13.55	P < 0.001, q = 16.18	P < 0.001, q = 9.81
SB 2X2Y Vs SEQ 2X2Y	P < 0.001, q = 9.27	P > 0.05, q = 0.99	P > 0.05, q = 0.27	P > 0.05, q = 2.11	P < 0.001, q = 9.85	P > 0.05, q = 2.44	P > 0.05, q = 0.75	P > 0.05, q = 0.92

Table 6.13: *Statistical comparison of the weekly changes in the crystallinity of CPLA films after aqueous submersion – duration comparison*

One way ANOVA followed by Tukey's test - Weeks comparison						
	1X	2X	3X	4X	SB-2X2Y	SEQ-2X2Y
Week 0 Vs Week 8	P < 0.001, q = 37.44	P < 0.001, q = 41.24	P < 0.001, q = 21.96	P < 0.001, q = 15.19	P < 0.001, q = 31.28	P < 0.001, q = 42.73
Week 0 Vs Week 16	P < 0.001, q = 18.29	P < 0.001, q = 21.49	P < 0.001, q = 15.15	P < 0.001, q = 11.38	P < 0.001, q = 12.23	P < 0.001, q = 21.54
Week 0 Vs Week 32	P < 0.001, q = 24.04	P < 0.001, q = 30.94	P < 0.001, q = 20.14	P < 0.001, q = 14.51	P < 0.001, q = 19.90	P < 0.001, q = 27.10
Week 8 Vs Week 16	P < 0.001, q = 19.15	P < 0.001, q = 19.75	P > 0.05, q = 1.82	P > 0.05, q = 3.80	P < 0.001, q = 19.05	P < 0.001, q = 21.18
Week 8 Vs Week 32	P < 0.001, q = 13.40	P < 0.001, q = 10.30	P < 0.05, q = 4.98	P > 0.05, q = 0.67	P < 0.001, q = 11.37	P < 0.001, q = 15.63
Week 16 Vs Week 32	P < 0.01, q = 5.74	P < 0.001, q = 9.44	P < 0.001, q = 6.80	P > 0.05, q = 3.13	P < 0.001, q = 7.67	P < 0.01, q = 5.55

* Actual data displayed in figure 6.16

Table 6.14: *Statistical comparison of the weekly changes in the crystallinity of TPLA films after aqueous submersion – draw ration comparison*

One way ANOVA followed by Tukey's test - Draw ratio comparison								
	Week 0	Week 6	Week 8	Week 10	Week 12	Week 16	Week 24	Week 32
1X Vs 2X	P < 0.001, q = 20.31	P < 0.001, q = 8.11	P > 0.05, q = 0.64	P > 0.05, q = 1.94	P > 0.05, q = 0.70	P > 0.05, q = 0.74	P < 0.001, q = 6.70	P < 0.01, q = 6.03
1X Vs 3X	P < 0.001, q = 87.68	P < 0.001, q = 15.80	P > 0.05, q = 3.28	P > 0.05, q = 2.66	P > 0.05, q = 3.55	P < 0.05, q = 4.73	P < 0.001, q = 8.04	P < 0.001, q = 13.71
1X Vs 4X	P < 0.001, q = 127.02	P < 0.001, q = 20.77	P > 0.05, q = 4.17	P > 0.05, q = 2.37	P < 0.05, q = 5.07	P < 0.001, q = 8.47	P < 0.001, q = 12.18	P < 0.001, q = 15.21
1X Vs SB 2X2Y	P < 0.001, q = 25.05	P < 0.001, q = 9.95	P > 0.05, q = 2.13	P > 0.05, q = 3.16	P < 0.001, q = 7.86	P < 0.001, q = 7.91	P < 0.001, q = 9.37	P > 0.05, q = 1.50
1X Vs SEQ 2X2Y	P < 0.001, q = 20.04	P < 0.001, q = 14.89	P > 0.05, q = 3.35	P < 0.05, q = 4.57	P < 0.01, q = 5.36	P < 0.001, q = 6.74	P < 0.01, q = 5.36	P < 0.05, q = 4.52
2X Vs 3X	P < 0.001, q = 67.36	P < 0.001, q = 7.74	P > 0.05, q = 2.63	P > 0.05, q = 0.72	P > 0.05, q = 4.26	P < 0.01, q = 5.47	P > 0.05, q = 1.34	P < 0.001, q = 7.67
2X Vs 4X	P < 0.001, q = 106.71	P < 0.001, q = 12.66	P > 0.05, q = 3.52	P > 0.05, q = 0.43	P < 0.01, q = 5.78	P < 0.001, q = 9.21	P < 0.01, q = 5.48	P < 0.001, q = 9.18
2X Vs SB 2X2Y	P < 0.05, q = 4.73	P > 0.05, q = 1.84	P > 0.05, q = 1.48	P > 0.05, q = 1.22	P < 0.001, q = 7.15	P < 0.001, q = 7.16	P < 0.001, q = 16.07	P < 0.05, q = 4.52
2X Vs SEQ 2X2Y	P > 0.05, q = 0.27	P < 0.001, q = 6.78	P > 0.05, q = 2.70	P > 0.05, q = 2.63	P < 0.05, q = 4.66	P < 0.01, q = 5.99	P < 0.001, q = 12.05	P > 0.05, q = 1.50
3X Vs 4X	P < 0.001, q = 39.33	P < 0.05, q = 4.92	P > 0.05, q = 0.89	P > 0.05, q = 0.28	P > 0.05, q = 1.52	P > 0.05, q = 3.74	P > 0.05, q = 4.14	P > 0.05, q = 1.50
3X Vs SB 2X2Y	P < 0.001, q = 62.62	P < 0.01, q = 5.89	P > 0.05, q = 1.15	P > 0.05, q = 0.50	P < 0.001, q = 11.42	P < 0.001, q = 12.64	P < 0.001, q = 17.41	P < 0.001, q = 12.20
3X Vs SEQ 2X2Y	P < 0.001, q = 67.63	P > 0.05, q = 0.95	P > 0.05, q = 0.07	P > 0.05, q = 1.91	P < 0.001, q = 8.92	P < 0.001, q = 11.47	P < 0.001, q = 13.39	P < 0.001, q = 9.18
4X Vs SB 2X2Y	P < 0.001, q = 101.97	P < 0.001, q = 10.82	P > 0.05, q = 2.04	P > 0.05, q = 0.79	P < 0.001, q = 12.93	P < 0.001, q = 16.38	P < 0.001, q = 21.55	P < 0.001, q = 13.71
4X Vs SEQ 2X2Y	P < 0.001, q = 106.98	P < 0.01, q = 5.87	P > 0.05, q = 0.82	P > 0.05, q = 2.19	P < 0.001, q = 10.44	P < 0.001, q = 15.21	P < 0.001, q = 17.54	P < 0.001, q = 10.69
SB 2X2Y Vs SEQ 2X2Y	P < 0.05, q = 5.01	P < 0.05, q = 4.94	P > 0.05, q = 1.22	P > 0.05, q = 1.40	P > 0.05, q = 2.49	P > 0.05, q = 1.16	P > 0.05, q = 4.02	P > 0.05, q = 3.02

Table 6.15: *Statistical comparison of the weekly changes in the crystallinity of TPLA films after aqueous submersion – duration comparison*

One way ANOVA followed by Tukey's test - Weeks comparison						
	1X	2X	3X	4X	SB-2X2Y	SEQ-2X2Y
Week 0 Vs Week 8	P < 0.001, q = 53.34	P < 0.001, q = 64.98	P < 0.001, q = 56.96	P < 0.001, q = 25.69	P < 0.001, q = 88.44	P < 0.001, q = 92.33
Week 0 Vs Week 16	P < 0.001, q = 44.04	P < 0.001, q = 51.35	P < 0.001, q = 42.31	P < 0.001, q = 18.49	P < 0.001, q = 59.79	P < 0.001, q = 63.12
Week 0 Vs Week 32	P < 0.001, q = 43.33	P < 0.001, q = 60.18	P < 0.001, q = 61.66	P < 0.001, q = 29.37	P < 0.001, q = 70.34	P < 0.001, q = 78.58
Week 8 Vs Week 16	P < 0.001, q = 9.29	P < 0.05, q = 4.79	P > 0.05, q = 3.70	P > 0.05, q = 3.68	P < 0.001, q = 28.64	P < 0.001, q = 29.20
Week 8 Vs Week 32	P < 0.001, q = 10.01	P < 0.001, q = 13.62	P < 0.001, q = 14.65	P < 0.001, q = 7.19	P < 0.001, q = 18.09	P < 0.001, q = 13.73
Week 16 Vs Week 32	P > 0.05, q = 0.71	P < 0.001, q = 8.82	P < 0.001, q = 19.35	P < 0.001, q = 10.88	P < 0.001, q = 10.55	P < 0.001, q = 15.46

* Actual data displayed in figure 6.17

Figure 6.16 and figure 6.17 further reveal that the percentage crystallinity increased again after the 20th week. There are two possibilities here. Firstly, erosion of the degraded amorphous phase may cause a relative rise in the percentage crystallinity. Secondly, degraded oligomers may undergo extensive crystallisation. Distinguishingly, the crystallinity of the films oriented to UCW $\lambda \geq$ 3X, was higher than the remaining studied films, during this phase.

When plasticised by water, PLA undergoes 'insertion crystallisation' (Hurrell and Cameron, 2002; Tsuji *et al*., 2000). Here the crystallisation occurs on templates provided by the existing crystals. Consequently, the inherent crystalline structure plays a key role in affecting the crystallisation process. The films oriented to UCW draw ratios of 3X and 4X, already have a well-developed crystalline order, in the form of lamellar α crystals (sec. 6.4). Therefore insertion crystallisation in these films will follow the same structural order. Contrarily, insertion crystallisation of the previously amorphous films (i.e. un-oriented, UCW λ = 2X, SB λ = 2X2Y and SEQ λ = 2X2Y) will be random, leading to generation of large sized, spherulitic crystals (Hurrell and Cameron, 2002; Tsuji *et al*., 2000). Therefore a difference in the length of the plateau crystallinity phase and the post-plateau crystallinity of the studied films can be associated with the differences in their crystalline structure.

6.8.3. Molecular weight degradation

The drug loaded PLA films investigated here showed a significant reduction in molecular weight upon exposure to the release medium. The changes in the weight average molecular weight (Mw) of the CPLA and the TPLA films (deduced from GPC) are summarised in figure 6.18 and figure 6.19 respectively. The molecular weight reduction was statistically compared between the draw ratios, using one-way ANOVA, followed by Tukey's test. The results of this are presented in table *6.16* and table 6.17. Nevertheless, comparison between individual time-points of a same draw ratio was made using a paired t-test, wherever suitable.

6.8.3.1. The lag in onset of molecular weight degradation

Macromolecular degradation of un-oriented PLA films started almost instantaneously after submersion into the release medium, and a monotonous Mw reduction was observed. Oriented films showed a lag before the loss of molecular weight began. The onset of degradation was delayed until the 6^{th} week, for TPLA films oriented to a UCW draw ratio of 4X and biaxially oriented TPLA films (both SB and SEQ; λ = 2X2Y). Nevertheless, such a phase was 5 weeks longer for the TPLA films with UCW draw ratios of 2X and 3X. This observation was statistically validated by comparison of the molecular weight at the beginning of the study and after 5 and 6 weeks, by paired t-tests. Secondly, when compared by one-way ANOVA – Tukey's test (table 6.17), there was a statistically insignificant difference in the molecular weight of oriented TPLA films for the first 5 weeks. Such a trend continued for another week in the case of UCW λ = 4X and biaxially oriented TPLA films. Contrarily, un-oriented TPLA films showed a highly significant difference in molecular weight (compared to the oriented films) since the beginning of the study.

Oriented CPLA films showed a slightly different trend. CPLA films oriented in UCW mode, to draw ratios of 3X and 4X showed practically no molecular weight reduction until the 7^{th} week (paired t-test, $P > 0.05$, between 0 – 7 weeks). A similar phase for the SB oriented CPLA films (λ = 2X2Y) lasted for approximately 4 weeks (paired t-test, $P > 0.05$, between 0 – 4 weeks). The lag was absent for CPLA films oriented to a UCW draw ratio of 2X and those oriented in sequential (SEQ) biaxial mode (λ = 2X2Y). However, the Mw reduction for the mentioned films was slower for the initial 6 weeks, followed by a rapid fall. Biaxially oriented (λ = 2X2Y) CPLA films and those oriented to a UCW draw ratio of 2X clearly exhibited a shorter lag than corresponding TPLA films. This can perhaps be attributed to shrinkage of the abovementioned CPLA films in the drug release medium, leading to partial loss of their orientation (sec. 6.8.1). The above observations were also validated in the one-way ANOVA

Tukey's test analysis (table 6.16), which showed a statistically insignificant difference in the molecular weights of UCW λ ≥ 3X and SB 2X2Y CPLA films for the first 4 weeks. The difference between the molecular weights of UCW λ = 3X and λ = 4X CPLA films continued to be insignificant for an additional 2 weeks. Contrarily, the remaining films exhibited a highly significant difference in the molecular weight when compared to UCW λ ≥ 3X CPLA films and among themselves. A delayed onset of molecular weight degradation for PLA matrices with higher inherent crystallinity has been reported previously (Pistner *et al.*, 1993). However, in the current study, oriented films which were practically amorphous (UCW – λ = 2X, SB & SEQ – λ = 2X2Y), also showed a lag. Therefore the lag observed here correlates more correctly with the structural organisation than the crystallinity. Orientation of polymeric matrices enhances molecular packing of the polymer chains. This perhaps reduces access of the water to the hydrolytic cleavage sites (Qureshi *et al.*, 2000). Consequently, such matrices show a delayed onset of degradation or a slower rate of degradation (Cho *et al.*, 2003). .

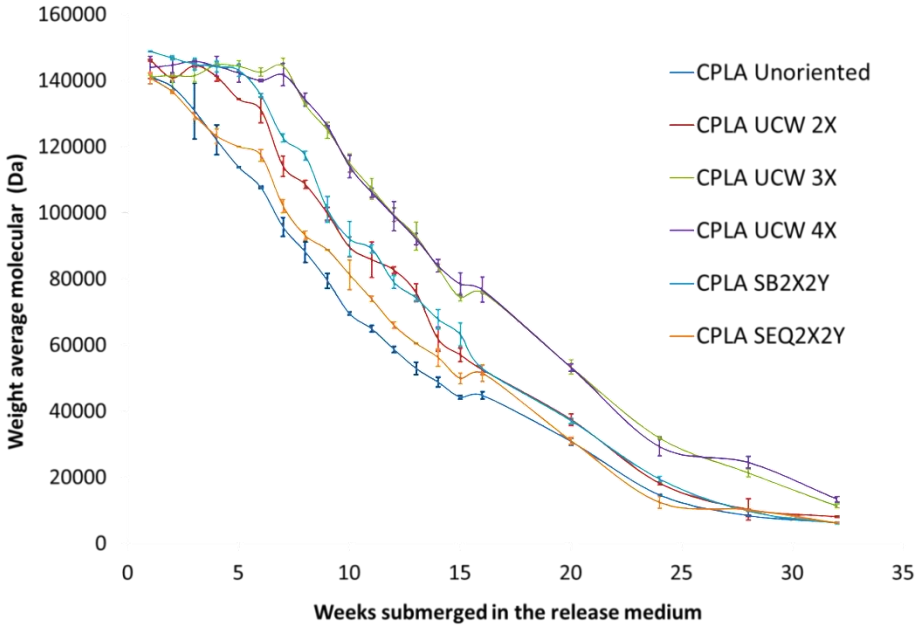

Figure 6.18: *Changes in the weight average molecular weight (Mw) of curcumin loaded PLA (CPLA) films with respect to aging in the release medium.*

**The graph represents molecular weight as the mean ± standard deviation, where n = 6.

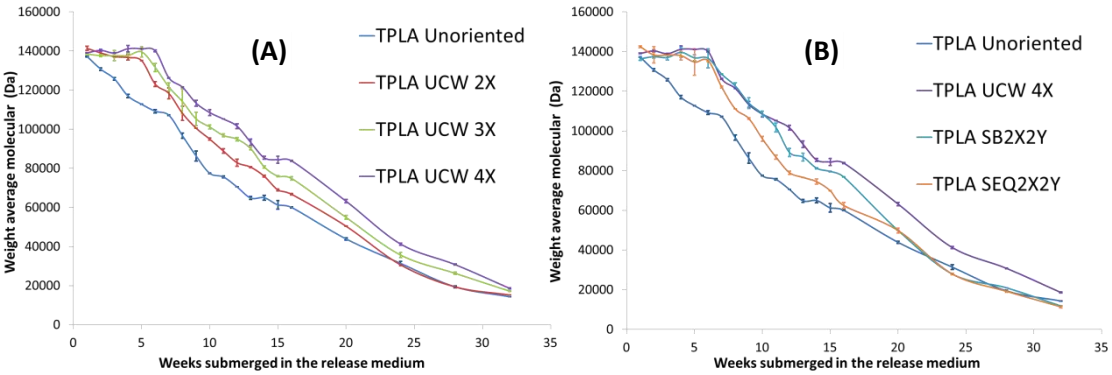

Figure 6.19: *Changes in the weight average molecular weight (Mw) of theophylline loaded PLA (TPLA) films with respect to aging in the release medium.*

A) Uniaxially (UCW) oriented films, **B)** Biaxially oriented films compared with UCW λ = 4X

**The graph represents molecular weight as the mean ± standard deviation, where n = 6.

Table 6.16: *Statistical comparison of the molecular weight changes in the CPLA films after aqueous submersion (data shown in figure 6.18).*

One way ANOVA followed by Tukey's test - Draw ratio comparison							
	Week 2	Week 3	Week 4	Week 5	Week 6	Week 16	Week 32
1X Vs 2X	P > 0.05 q = 2.93	P < 0.001 q = 9.16	P < 0.001 q = 18.32	P < 0.001 q = 33.51	P < 0.001 q = 31.12	P < 0.001 q = 9.15	P < 0.001 q = 10.53
1X Vs 3X	P > 0.05 q = 3.61	P < 0.001 q = 7.12	P < 0.001 q = 21.78	P < 0.001 q = 49.87	P < 0.001 q = 46.29	P < 0.001 q = 36.86	P < 0.001 q = 28.85
1X Vs 4X	P < 0.001 q = 6.94	P < 0.001 q = 10.02	P < 0.001 q = 21.33	P < 0.001 q = 46.49	P < 0.001 q = 42.88	P < 0.001 q = 37.81	P < 0.001 q = 41.22
1X Vs SB 2X2Y	P < 0.001 q = 9.18	P < 0.001 q = 9.44	P < 0.001 q = 21.27	P < 0.001 q = 47.84	P < 0.001 q = 37.03	P < 0.001 q = 9.68	P > 0.05 q = 0.55
1X Vs SEQ 2X2Y	P > 0.05 q = 1.55	P > 0.05 q = 0.99	P > 0.05 q = 1.2	P < 0.001 q = 10.12	P < 0.001 q = 12.86	P < 0.001 q = 7.97	P > 0.05 q = 0.09
2X Vs 3X	P < 0.01 q = 6.80	P < 0.01 q = 6.78	P < 0.01 q = 13.46	P < 0.001 q = 16.36	P < 0.001 q = 15.17	P < 0.001 q = 27.72	P < 0.001 q = 18.32
2X Vs 4X	P < 0.01 q = 9.4	P < 0.01 q = 8.86	P < 0.01 q = 7.01	P < 0.001 q = 12.98	P < 0.001 q = 11.76	P < 0.001 q = 28.66	P < 0.001 q = 30.69
2X Vs SB 2X2Y	P < 0.01 q = 6.25	P < 0.01 q = 8.27	P < 0.01 q = 12.95	P < 0.001 q = 14.33	P < 0.01 q = 5.91	P > 0.05 q = 0.53	P < 0.001 q = 11.08
2X Vs SEQ 2X2Y	P < 0.05 q = 4.48	P < 0.001 q = 10.16	P < 0.001 q = 17.12	P < 0.001 q = 23.39	P < 0.001 q = 18.26	P > 0.05 q = 1.17	P < 0.001 q = 10.44
3X Vs 4X	P > 0.05 q = 3.33	P > 0.05 q = 2.9	P > 0.05 q = 0.45	P > 0.05 q = 3.38	P > 0.05 q = 3.41	P > 0.05 q = 0.94	P < 0.001 q = 12.37
3X Vs SB 2X2Y	P < 0.01 q = 5.57	P > 0.05 q = 2.31	P > 0.05 q = 0.51	P > 0.05 q = 2.03	P < 0.001 q = 9.26	P < 0.001 q = 27.19	P < 0.001 q = 29.4
3X Vs SEQ 2X2Y	P < 0.05 q = 5.16	P < 0.001 q = 8.12	P < 0.001 q = 20.58	P < 0.001 q = 39.75	P < 0.001 q = 33.43	P < 0.001 q = 28.89	P < 0.001 q = 28.76
4X Vs SB 2X2Y	P > 0.05 q = 2.25	P > 0.05 q = 0.59	P > 0.05 q = 0.06	P > 0.05 q = 1.35	P < 0.01 q = 5.85	P < 0.001 q = 28.13	P < 0.001 q = 41.77
4X Vs SEQ 2X2Y	P < 0.001 q = 8.48	P < 0.001 q = 11.02	P < 0.001 q = 20.13	P < 0.001 q = 36.38	P < 0.001 q = 30.02	P < 0.001 q = 29.84	P < 0.001 q = 41.13
SB 2X2Y Vs SEQ 2X2Y	P < 0.001 q = 10.73	P < 0.001 q = 10.43	P < 0.001 q = 20.07	P < 0.001 q = 37.72	P < 0.001 q = 24.17	P > 0.05 q = 1.7	P > 0.05 q = 0.64

Table 6.17: *Statistical comparison of the molecular weight changes in the TPLA films after aqueous submersion (data shown in figure 6.19). .*

One way ANOVA followed by Tukey's test - Draw ratio comparison							
	Week 2	Week 3	Week 4	Week 5	Week 6	Week 16	Week 32
1X Vs 2X	P < 0.001, q = 10.62	P < 0.001, q = 22.17	P < 0.001, q = 28.41	P < 0.001, q = 18.18	P < 0.001, q = 15.16	P < 0.001, q = 21.61	P < 0.001, q = 8.14
1X Vs 3X	P < 0.001, q = 8.87	P < 0.001, q = 23.22	P < 0.001, q = 29.91	P < 0.001, q = 21.84	P < 0.001, q = 24.57	P < 0.001, q = 47.60	P < 0.001, q = 25.30
1X Vs 4X	P < 0.001, q = 12.34	P < 0.001, q = 25.66	P < 0.001, q = 34.94	P < 0.001, q = 23.14	P < 0.001, q = 33.83	P < 0.001, q = 76.46	P < 0.001, q = 37.84
1X Vs SB 2X2Y	P < 0.001, q = 8.60	P < 0.001, q = 21.91	P < 0.001, q = 32.70	P < 0.001, q = 19.64	P < 0.001, q = 30.14	P < 0.001, q = 53.92	P < 0.001, q = 22.24
1X Vs SEQ 2X2Y	P < 0.001, q = 9.77	P < 0.001, q = 24.33	P < 0.001, q = 30.30	P < 0.001, q = 17.90	P < 0.001, q = 28.79	P < 0.001, q = 7.89	P < 0.001 q = 25.94
2X Vs 3X	P > 0.05, q = 1.74	P > 0.05, q = 1.05	P > 0.05, q = 1.50	P > 0.05, q = 3.66	P < 0.001, q = 9.40	P < 0.001, q = 25.98	P < 0.001, q = 17.15
2X Vs 4X	P > 0.05, q = 1.72	P > 0.05, q = 3.48	P < 0.05, q = 4.96	P < 0.05, q = 4.96	P < 0.001, q = 18.67	P < 0.001, q = 54.85	P < 0.001, q = 29.70
2X Vs SB 2X2Y	P > 0.05, q = 2.01	P > 0.05, q = 0.26	P > 0.05, q = 4.29	P > 0.05, q = 1.46	P < 0.001, q = 14.98	P < 0.001, q = 32.31	P < 0.001, q = 30.38
2X Vs SEQ 2X2Y	P > 0.05, q = 0.84	P > 0.05, q = 2.16	P > 0.05, q = 1.88	P > 0.05, q = 0.279	P < 0.001, q = 13.63	P < 0.001, q = 13.71	P < 0.001, q = 34.08
3X Vs 4X	P > 0.05, q = 3.46	P > 0.05, q = 2.43	P < 0.05, q = 5.03	P > 0.05, q = 1.30	P < 0.001, q = 9.26	P < 0.001, q = 28.86	P < 0.001, q = 12.54
3X Vs SB 2X2Y	P > 0.05, q = 0.27	P > 0.05, q = 1.31	P > 0.05, q = 2.79	P > 0.05, q = 2.19	P < 0.01, q = 5.57	P < 0.01, q = 6.32	P < 0.001, q = 47.54
3X Vs SEQ 2X2Y	P > 0.05, q = 0.89	P > 0.05, q = 1.11	P > 0.05, q = 0.38	P > 0.05, q = 3.94	P > 0.05, q = 4.22	P < 0.001, q = 39.70	P < 0.001, q = 51.24
4X Vs SB 2X2Y	P > 0.05, q = 3.74	P > 0.05, q = 3.75	P > 0.05, q = 2.24	P > 0.05, q = 3.49	P > 0.05, q = 3.69	P < 0.001, q = 22.53	P < 0.001, q = 60.09
4X Vs SEQ 2X2Y	P > 0.05, q = 2.57	P > 0.05, q = 1.32	P < 0.05, q = 4.64	P < 0.05, q = 5.24	P < 0.05, q = 5.04	P < 0.001, q = 68.56	P < 0.001, q = 63.78
SB 2X2Y Vs SEQ 2X2Y	P > 0.05, q = 1.17	P > 0.05, q = 2.42	P > 0.05, q = 2.40	P > 0.05, q = 1.74	P > 0.05, q = 1.34	P < 0.001, q = 46.02	P > 0.05, q = 3.69

Notes: The null hypothesis was that the compared samples were statistically the same

P > 0.05 = The difference between the compared samples is **not statistically significant**
0.05 > P > 0.01 = The difference between the compared samples is **statistically significant**
0.01 > P = The difference between the compared samples is **highly significant**

6.8.3.2. The decline phase

GPC chromatograms revealed that the peaks corresponding to PLA shifted towards a higher elution volume as the submersion duration increased. However, all the peaks remained monomodal in nature, indicating uniform degradation throughout the bulk of the films. Since PLA undergoes bulk

degradation, the degraded oligomers remain entrapped within the matrix. These further catalyse the degradation of the bulk, consequently generating a surface to centre differential in the degradation rate. In the case of thin films, such a differential is generally insignificant and therefore may not be detected by GPC. The current results agree with the findings of Grizzi *et al.* (1995), who reported that thin PLA films (0.3 mm) degraded homogeneously, as opposed to thick sheets (2 mm), where surface to centre differential in the hydrolytic degradation generated bimodal GPC peaks.

The molecular weight vs submersion duration curves for UCW oriented TPLA films remained nearly parallel to that of the un-oriented films (figure 6.19-A), beyond the lag phase. Therefore, if the lag phase was ignored, the mentioned films showed practically no difference in the degradation rate. On the contrary, biaxially oriented TPLA films showed a slightly higher degradation rate (figure 6.19 - B), evidenced as a greater slope of the regression lines corresponding to their molecular weight vs submersion duration curves (between 7 – 14 weeks). The duration for 50% reduction in molecular weight ($t_{1/2}$) was approximately 12, 15, 17, 19, 17 and 15 weeks for the un-oriented, UCW 2X, UCW 3X, UCW 4X, SB 2X2Y and SEQ 2X2Y films respectively. Despite the fact that biaxially oriented TPLA films showed a longest lag phase amongst the oriented TPLA films, existence of a shorter $t_{1/2}$ further confirmed their faster degradation. Such a trend was not clearly identified in the case of biaxially oriented (λ = 2X2Y) CPLA films, perhaps due to their shrinkage. The molecular weight vs submersion duration curves (figure 6.18) remained almost parallel for all CPLA films, after the initial lag phase. $t_{1/2}$ for CPLA films with a following set of orientation profiles; namely, un-oriented, UCW 2X, UCW 3X, UCW 4X, SB 2X2Y and SEQ 2X2Y was 10, 13, 17, 17, 13 and 11 weeks respectively. Overall the statistical comparison confirmed that, at a fixed (post - lag) submersion duration, both CPLA and TPLA films with different degrees of orientation had significantly different molecular weights (table 6.16 and table 6.17). This factor can significantly impact drug release from these films.

Comparison of the molecular weight vs submersion duration curves and the $t_{1/2}$ values for the CPLA and the TPLA films further highlighted that the molecular weight degradation was higher in un-oriented and shrunk CPLA films. Contrarily films oriented to UCW draw ratios of 3X and 4X exhibited similar degradation, irrespective of the added drug. This observation was validated by statistical comparison between the percentage molecular weight degradation exhibited by CPLA films and TPLA films, following 16 weeks submersion. A highly significant ($P < 0.001$ by a paired t-test) difference was found between the molecular weight reduction shown by the un-oriented CPLA and TPLA films. Contrarily, the difference between UCW ≥ 3X CPLA and TPLA films was statistically insignificant ($P > 0.05$ by a paired t-test). Molecular weight degradation can substantially enhance the diffusivity of a drug through the polymer matrix. Nevertheless, the space created by degradation of the polymer chains can be occupied by the percolated medium, leading to formation of 'water filled channels'. The presence of water filled channels further accelerates drug release.

Overall, the results confirmed that both uniaxial and biaxial orientation of the drug loaded PLA films delayed the onset of hydrolytic degradation, in a neutral (pH 6.8) bathing medium. After the lag, un-oriented and uniaxially oriented TPLA films showed a comparable degradation rate, whereas biaxially oriented films exhibited a slightly faster degradation. Such an effect was not observed in the biaxially oriented CPLA films as they underwent shrinkage and partially lost their oriented structure. Several studies have previously reported retardation of hydrolytic degradation of PLA fibres, following uniaxial orientation by hot drawing (Cai *et al.*, 1996; Jamshidi *et al.*, 1986). However, studies on PLA films have reached largely inadequate conclusions (Burg and Shalaby, 1998; Lee *et al*., 2001b; Tsuji *et al*., 2005). Tsuji *et al.* (Tsuji *et al.*, 2005) found that enzymatic degradation of PLA, which takes place primarily by a surface erosion mechanism was hindered by biaxial orientation. On the contrary, hydrolytic bulk degradation was unaffected by orientation; it was rather

influenced by the inherent crystallinity of the matrices. Similarly, Burg *et al.* (1998) detected no difference in the weight average molecular weight reduction between uniaxially oriented PLA films and un-oriented films from which they were obtained.

6.8.4. Polydispersity changes

All drug loaded PLA films studied here showed a rise in the polydispersity since the beginning of the molecular weight degradation. In the case of TPLA films the rise in the polydispersity continued till the 16^{th} week (figure 6.21); while CPLA films showed a plateau between the 10^{th} and the 16^{th} week (figure 6.20) ($P > 0.05$, 10^{th} week Vs 12^{th} Vs 14^{th} Vs 16^{th} week by one-way ANOVA followed by Tukey's test). Figure 6.20 and figure 6.21 further suggest that un-oriented films exhibited the highest polydispersity amongst the studied films, for the entire study duration. A statistical comparison was made (at four different time points) between the polydispersity of the films with varied draw ratios, by one-way ANOVA – Tukey's test. This data is presented in table 6.18. The polydispersity Vs submersion duration curves along with statistical analysis confirmed that UCW – 2X films exhibited significantly lower polydispersity than un-oriented films for the first 16 weeks (regardless of the model drug). The polydispersity of the UCW – 3X and UCW – 4X films was statistically equivalent ($P > 0.05$, table 6.18); nevertheless it was lower than that of the UCW – 2X films.

It was further observed that the polydispersity of SB and SEQ oriented TPLA films (λ = 2X2Y) was statistically equivalent to each other and to UCW-3X/4X films (figure 6.21 – B; table 6.18 - $P > 0.05$). Conversely, the polydispersity of SB oriented CPLA films was statistically equivalent to that of the UCW-2X films; and polydispersity of SEQ oriented CPLA films was equivalent to that of the un-oriented films (figure 6.20 – B; table 6.18). Burg and Shalaby (1998) reported that the isotropic structure of un-oriented films allows hydrolytic chain cleavage to occur at random locations along the chain length.

Contrarily, a highly ordered structure (sec. 6.4) of the oriented matrices results in a more regular chain cleavage. Therefore, lower polydispersity of the oriented films can be attributed to this phenomenon.

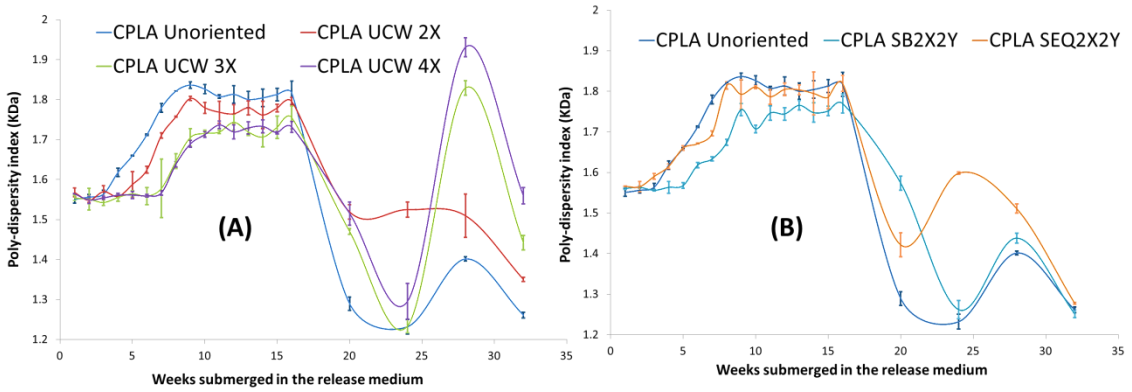

Figure 6.20: *Changes in the polydispersity (PD) of curcumin loaded PLA (CPLA) films with respect to aging in the release medium.*

A) Uniaxially (UCW) oriented films, **B)** Biaxially oriented films

**The graph represents polydispersity as the mean ± standard deviation, where n = 6.

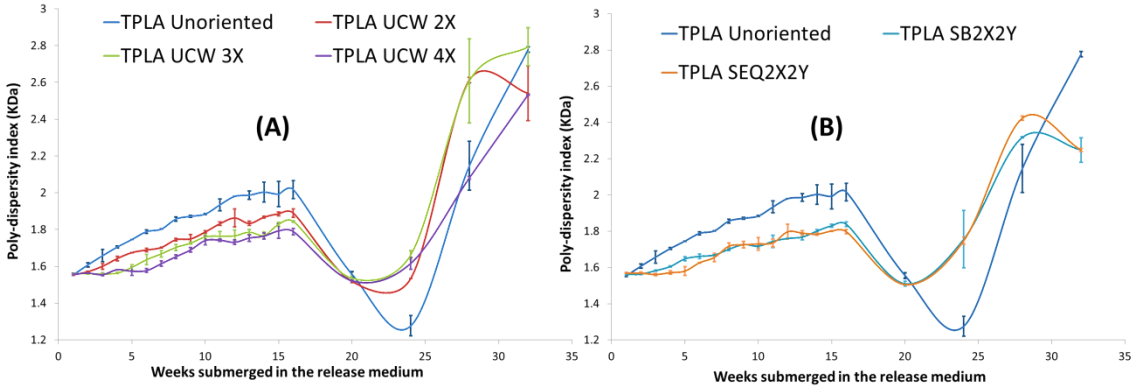

Figure 6.21: *Changes in the polydispersity (PD) of the theophylline loaded PLA (TPLA) films with respect to aging in the release medium*

A) Uniaxially (UCW) oriented films, **B)** Biaxially oriented films

**The graph represents molecular weight as the mean ± standard deviation, where n = 6.

Table 6.18: *Statistical comparison of the polydispersity changes in the PLA films after aqueous submersion*

One way ANOVA followed by Tukey's test								
	TPLA Films				CPLA Films			
	Week 1	Week 6	Week 12	Week 24	Week 1	Week 6	Week 12	Week 24
1X Vs 2X	P > 0.05, q = 0	P < 0.001, q = 16.86	P < 0.001, q = 9.7	P < 0.001, q = 8.91	P < 0.01, q = 6.42	P < 0.001, q = 21.46	P < 0.01, q = 6.23	P < 0.001, q = 26.62
1X Vs 3X	P > 0.05, q = 2.95	P < 0.001, q = 25.71	P < 0.001, q = 17.71	P < 0.001, q = 13.35	P > 0.05, q = 1.11	P < 0.001, q = 37.51	P < 0.001, q = 8.95	P < 0.001, q = 20.94
1X Vs 4X	P > 0.05, q = 1.34	P < 0.001, q = 35.74	P < 0.001, q = 20.61	P < 0.001, q = 11.74	P < 0.05, q = 5.15	P < 0.001, q = 37.39	P < 0.001, q = 12.05	P < 0.001, q = 26.18
1X Vs SB 2X2Y	P > 0.05, q = 4.03	P < 0.001, q = 21.41	P < 0.001, q = 18.13	P < 0.001, q = 16.6	P > 0.05, q = 3.68	P < 0.001, q = 22.98	P < 0.001, q = 8.84	P < 0.001, q = 32.96
1X Vs SEQ 2X2Y	P < 0.001, q = 8.32	P < 0.001, q = 27.31	P < 0.001, q = 15.07	P < 0.001, q = 16.31	P > 0.05, q =0.79	P > 0.05, q = 1.11	P > 0.05, q = 1.06	P < 0.001, q = 15.3
2X Vs 3X	P > 0.05, q = 2.95	P < 0.001, q = 8.85	P < 0.001, q = 8.01	P < 0.05, q = 4.45	P < 0.01, q = 5.31	P < 0.001, q = 16.05	P > 0.05, q = 2.72	P < 0.01, q = 5.69
2X Vs 4X	P > 0.05, q = 1.34	P < 0.001, q = 18.88	P < 0.001, q = 10.9	P > 0.05, q = 2.84	P > 0.05, q = 1.27	P < 0.001, q = 15.93	P < 0.01, q = 5.82	P > 0.05, q = 0.44
2X Vs SB 2X2Y	P > 0.05, q = 4.03	P < 0.05, q = 4.55	P < 0.001, q = 8.42	P < 0.001, q = 7.7	P > 0.05, q = 2.74	P > 0.05, q = 1.52	P > 0.05, q = 2.61	P < 0.01, q = 6.34
2X Vs SEQ 2X2Y	P < 0.001, q = 8.32	P < 0.001, q = 10.45	P < 0.01, q = 5.37	P < 0.001, q = 7.4	P > 0.05, q = 0.71	P < 0.001, q = 11.35	P < 0.05, q = 5.17	P < 0.001, q = 11.32
3X Vs 4X	P > 0.05, q = 1.61	P > 0.05, q = 1.03	P > 0.05, q = 2.89	P > 0.05, q = 1.61	P > 0.05, q = 4.05	P > 0.05, q = 0.12	P > 0.05, q = 3.1	P < 0.05, q = 5.24
3X Vs SB 2X2Y	P > 0.05, q = 1.07	P > 0.05, q = 4.3	P > 0.05, q = 0.41	P > 0.05, q = 3.25	P > 0.05, q = 2.58	P < 0.001, q = 14.52	P < 0.05, q = 5.11	P < 0.001, q = 12.02
3X Vs SEQ 2X2Y	P < 0.01, q = 5.37	P > 0.05, q = 1.6	P > 0.05, q = 2.64	P > 0.05, q = 2.96	P < 0.05, q = 4.6	P < 0.001, q = 27.4	P < 0.001, q = 7.89	P < 0.01, q = 5.64
4X Vs SB 2X2Y	P > 0.05, q = 2.68	P < 0.001, q = 14.33	P > 0.05, q = 2.48	P < 0.05, q = 4.86	P > 0.05, q = 1.47	P < 0.001, q = 14.4	P < 0.05, q = 5.22	P < 0.001, q = 6.78
4X Vs SEQ 2X2Y	P < 0.001, q = 6.98	P < 0.001, q = 8.43	P < 0.01, q = 5.53	P < 0.05, q = 4.57	P > 0.05, q = 0.55	P < 0.001, q = 27.28	P < 0.001, q = 11	P < 0.001, q = 10.88
SB 2X2Y Vs SEQ 2X2Y	P > 0.05, q = 4.29	P > 0.05, q = 3.9	P > 0.05, q = 3.06	P > 0.05, q = 0.29	P > 0.05, q = 2.02	P < 0.001, q = 12.88	P < 0.001, q = 7.78	P < 0.001, q = 17.66

Notes: For actual data refer figure 6.20 and figure 6.21

The null hypothesis was that the compared samples were statistically the same

P > 0.05 = The difference between the compared samples is **not statistically significant**
0.05 > P > 0.01 = The difference between the compared samples is **statistically significant**
0.01 > P = The difference between the compared samples is **highly significant**

A sharp decline in polydispersity was observed between the 16th and 24th week, followed by another plateau or a sharp rise. This event corresponded to dramatic changes in the film properties as listed below. (Note: - after 16 weeks, the samples were withdrawn every 4 weeks, and not weekly)

A. The weight loss shown by drug loaded PLA films was negligible until the 16th week. By the 24th week, the films lost 10 – 20% of their original weight. The weight loss was lower (12 ± 3%) for the uniaxially oriented films with $\lambda \geq 3X$. Biaxially oriented films lost more weight (17 ± 2%), which was aligned with the faster molecular weight degradation exhibited by them. By the 32nd week the weight loss for un-oriented and biaxially oriented TPLA films was 27 ± 4%, while that for UCW 2X, UCW 3X and UCW 4X TPLA films was 21 ± 2.8%, 18 ± 1.44% and 17 ± 2.1% respectively. CPLA films showed a slightly higher weight loss during the abovementioned interval. It was within the window of 32 ± 6% for the un-oriented, UCW-2X and the biaxially oriented films; while that for UCW-3X and UCW-4X films was 22 ± 5.34%.

B. By the 20th week, a significant reduction in the mechanical strength of the circular film sections made them extremely brittle. Samples withdrawn at the 28th week sampling interval were extremely fragile and easily fractured even on delicate handling.

C. Scanning electron microscopy revealed little change in the surface and the cross section of the films until the 16th week. At the 20th week, several large cracks appeared on the surface. Samples withdrawn after 28 weeks of submersion showed significant degradation of the films. Here the surface appeared as a partially degraded crust, exposing the extensively degraded inner structure. *(SEM results are summarised in the following section).

The above results suggest that hydrolytic bulk degradation of PLA reached a critical stage by the 20th sampling week, where the outer crust started cracking and released the entrapped oligomers. Following this, the matrix became highly porous, allowing more water to percolate and cause hydrolysis.

These events marked the beginning of the erosion phase, where the PLA films started breaking apart. Therefore, drug release in this phase will be tremendously accelerated.

6.8.5. Changes in the morphology of drug loaded PLA films

Drug loaded PLA films showed little change in their surface morphology for 16 weeks after submersion into the drug release medium (figure 6.22). No change in the cryo-fractured cross sections of the films (fractured perpendicular to the film surface) could be detected for the first 11 weeks. Samples withdrawn at the 12th week showed few cracks and several nano-sized pores on the cross section (figure 6.23). The number and the size of the pores increased between the 11th and the 20th week. However, their distribution appeared random. (Note: - after 16 weeks, the samples were withdrawn every 4 weeks and not weekly)

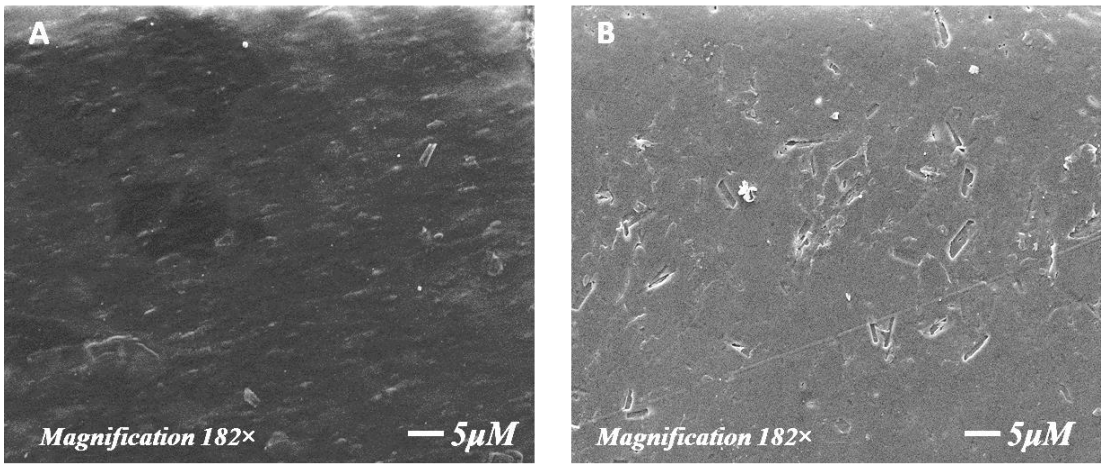

Figure 6.22: *Transverse surfaces of drug loaded PLA films after 16 weeks of submersion in the release medium.*

A) Un-oriented CPLA films representing all CPLA films, **B)** Un-oriented TPLA films representing all TPLA films

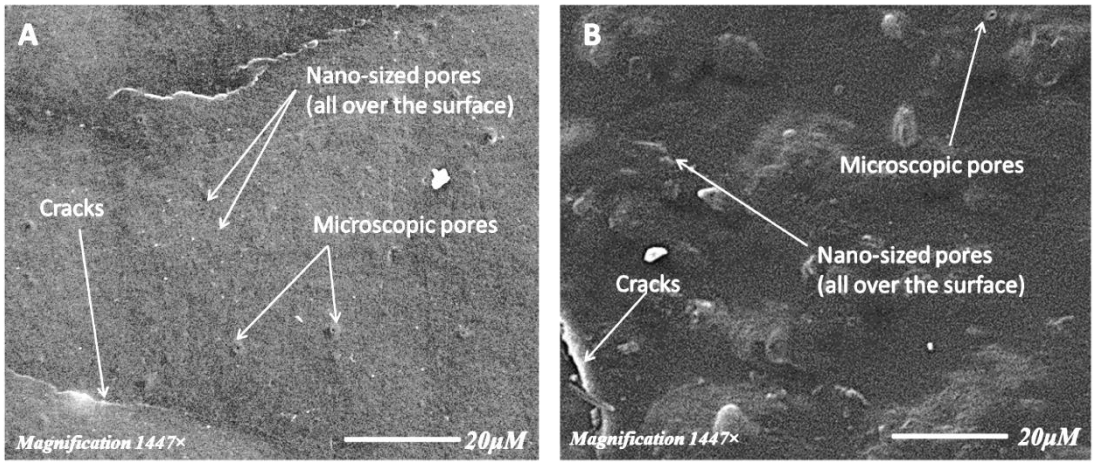

Figure 6.23: *Cryo-fractured cross sections of drug loaded PLA films aged for 12 weeks in the release medium.*

A) Un-oriented CPLA films representing all CPLA films, **B)** Un-oriented TPLA films representing all TPLA films

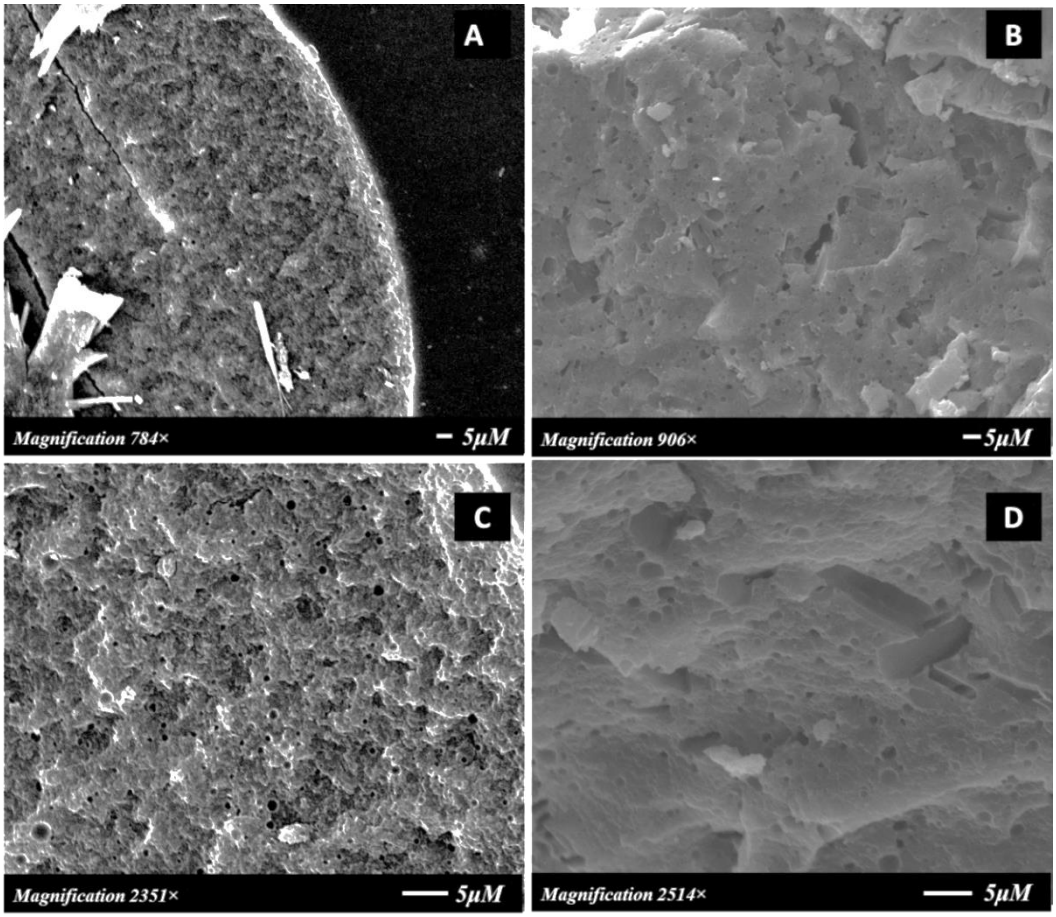

Figure 6.24: *Cryo-fractured cross sections of un-oriented drug loaded PLA films aged for 20 weeks in the release medium.*

A & C) Un-oriented CPLA films, **B & D)** Un-oriented TPLA films.

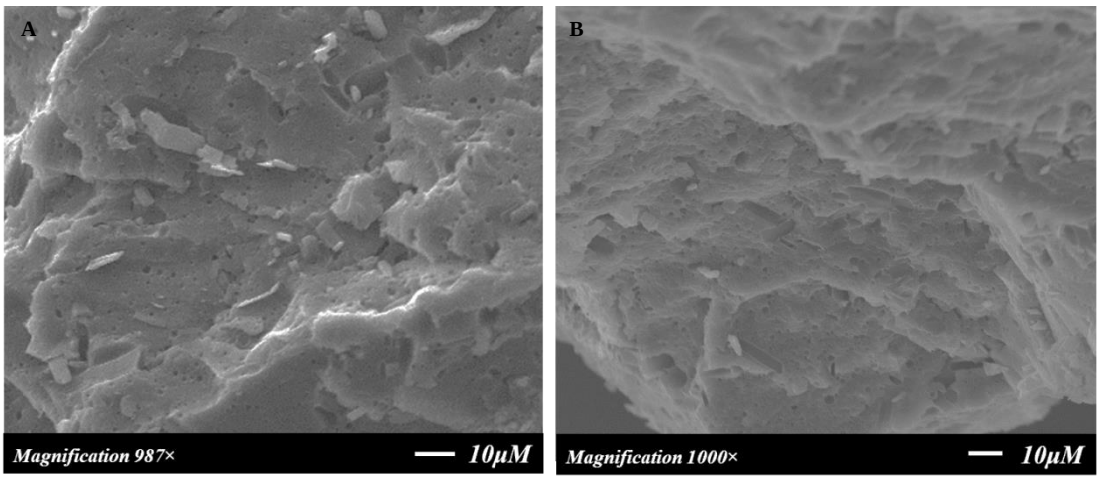

Figure 6.25: *Cryo-fractured cross sections of oriented TPLA films aged for 20 weeks in the release medium.*

A) UCW oriented TPLA films with λ = 4X, **B)** SB oriented TPLA films with λ = 2X2Y.

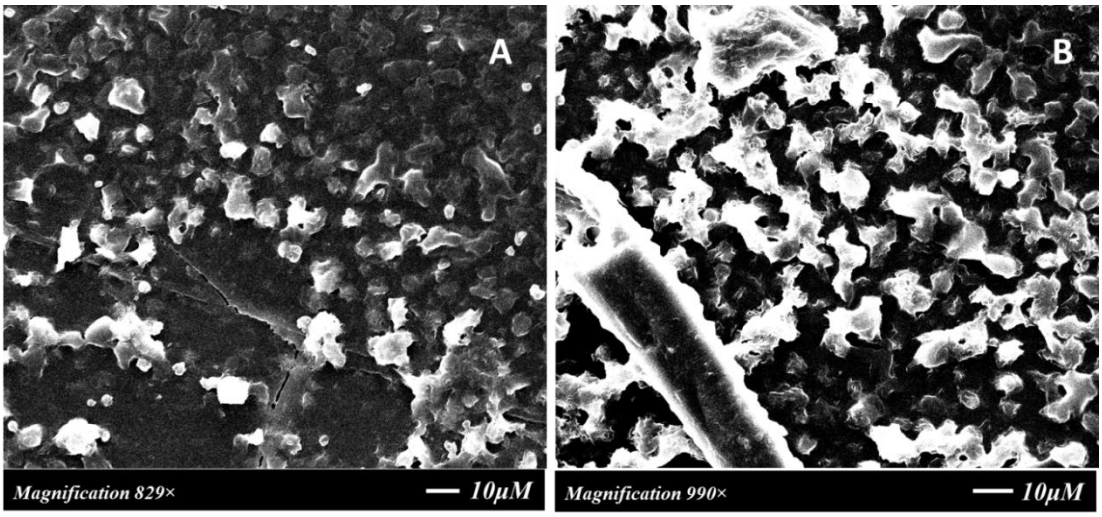

Figure 6.26: *Transverse surfaces of the un-oriented CPLA films **A)** aged for 24 weeks and **B)** aged for 28 weeks in the release medium.*

*(Represents the transverse surfaces of the following films at corresponding sampling interval; CPLA films – un-oriented, UCW-2X, SB-2X2Y, SEQ-2X2Y and TPLA films - un-oriented, UCW-2X, SEQ-2X2Y)

At the 20th week, the cross section revealed a highly porous structure of the degraded matrices. These pores correlate to the channels created by permeated water. Therefore, their number and size continuously increases as the PLA is degraded further. For films withdrawn after 20 weeks, the shape of the pores was uniform circular; while, their diameter varied from approximately 0.85 to 3.5 μm for TPLA films (figure 6.24 - A & C). CPLA films showed slightly smaller pores, ranging between approximately 0.18 – 2.1 μm (figure 6.24 - B & D). This indicates variation in the hydrolytic degradation of PLA with respect to the added drug (Li *et al*., 1996). The morphological changes observed until the 20th week were constant for un-oriented and oriented films (figure 6.25 - A & B).

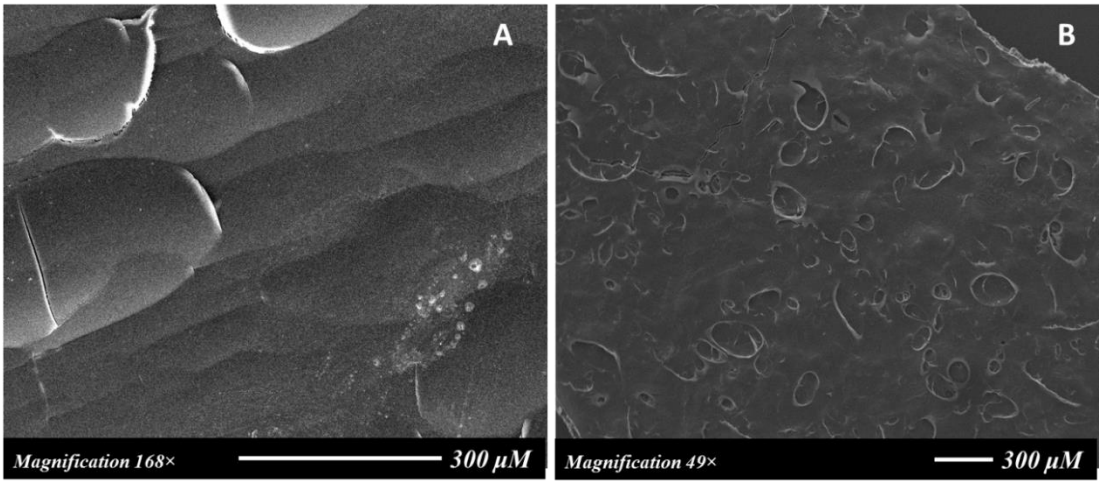

Figure 6.27: *Transverse surfaces of oriented drug loaded PLA films aged for 24 weeks in the release medium.*

A) UCW oriented TPLA films with λ = 4X, **B)** SB oriented TPLA films with λ = 2X2Y.

Few cracks appeared on the transverse surfaces of the films at the 20th week. The cracks became wider on further degradation (24th week onwards). This overlapped with appearance of white circular spots on the surface of the following films; namely, CPLA films – un-oriented, UCW-2X, SB-2X2Y, SEQ-2X2Y and TPLA films - un-oriented, UCW-2X, SEQ-2X2Y. (figure 6.26 - A). These spots were raised above the film surface by the 28th week and few

showed a hole in the centre (figure 6.26 - B). Cam *et al*. (1995) observed a similar morphology in hydrolytically degraded PLA films, which they described as partially degraded spherulitic crystals. A hole in the centre signifies that degradation of spherulites occurs from the centre. No such morphology was observed in UCW oriented films with λ ≥ 3X (figure 6.27 - A), perhaps due to the presence of α crystals (lamellar stacks). Similarly, the raised white spots were also absent in SB oriented TPLA films. Instead, the mentioned films showed large (50-150 μm) circular holes on the surface (figure 6.27 - B). Since these were not previously observed and their size was significantly larger than the size of theophylline particles, they cannot be correlated with the cavitation during biaxial stretching of the TPLA films. Tsuji *et al*. (2005) observed formation of such holes when biaxially oriented films were degraded enzymatically. They attributed this to detachment of large sized spherulites from the surface.

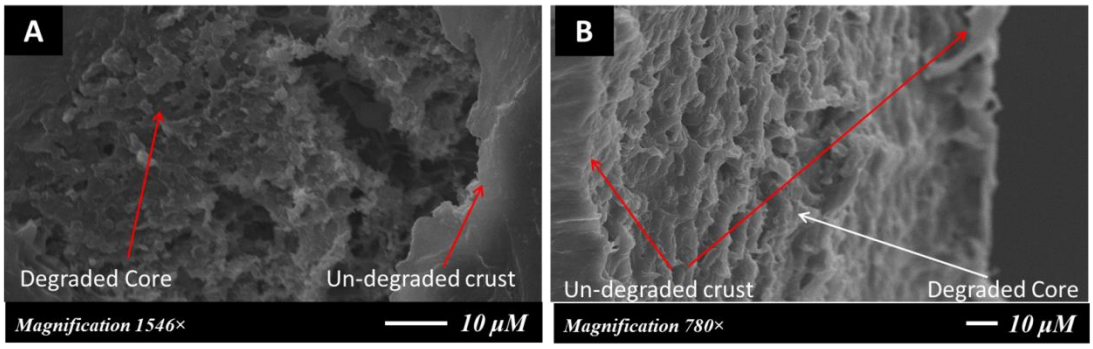

Figure 6.28: *SEM images of **A)** the transverse surface and **B)** the cross section of un-oriented TPLA films aged for 32 weeks in the release medium.*

Cross sections of the film samples withdrawn after 24 weeks showed a degraded core, sandwiched between two un-degraded thin layers (figure 6.28 - B). This distinguishing morphology was also observed on the transverse surface of the films, after 32 weeks aging in the release medium. The transverse surface of the mentioned films showed a ruptured outer crust at several locations, revealing the internal degraded core (figure 6.28 - A). It is known that

bulk degradation of PLA causes accumulation of the oligomers within the matrix. These oligomers accelerate degradation of the bulk (Burg and Shalaby, 1998; Grizzi *et al*., 1995; Tsuji and Ikarashi, 2004). Therefore, a difference between the degradation rate of the bulk and the surface generates a morphological distinction between them. The less degraded outer layer further prevents leaching of the oligomers. When the outer layer is substantially degraded, it starts falling apart. At this stage the erosion of PLA is significantly enhanced. Perhaps, such a morphological difference was not detected during molecular weight determination, owing to the lower thickness (0.2 mm) of the studied films (Grizzi *et al*., 1995).

6.8.6. Summary

The overall changes in drug loaded PLA films following aqueous submersion are summarised in figure 6.29. These were aligned with the Li *et al*. (1990) model, explaining the hydrolytic degradation of PLA. In brief, water penetrates into the films and reaches a saturation concentration within 2 - 3 weeks duration. The percolated water causes hydrolysis of the polymer chains. When the rate of water penetration is higher than the hydrolysis rate, PLA undergoes bulk degradation. In the current study, this was evidenced as a monotonous fall in the molecular weight of the films. The resultant oligomers remain entrapped in the bulk, unless they are small enough to be soluble in the permeated medium. The oligomers can either degrade further or undergo insertion crystallisation. This event was recognised as a rise in the crystallinity of the studied films.

By the end of the 8^{th} week, all studied films reached a constant crystallinity (approximately 35%). Meanwhile, the path followed by percolated water is transformed into the water filled channels. The presence of water in these channels causes degradation of the surrounding polymer. Consequently the size and number of channels increase as the PLA matrix is degraded further. Such channels were observed in the cross section of the studied PLA films, as

pores with varied diameters (0.18 – 3.5 µm). The smaller size of the channels allows transport of the soluble material, but release of the oligomers is restricted.

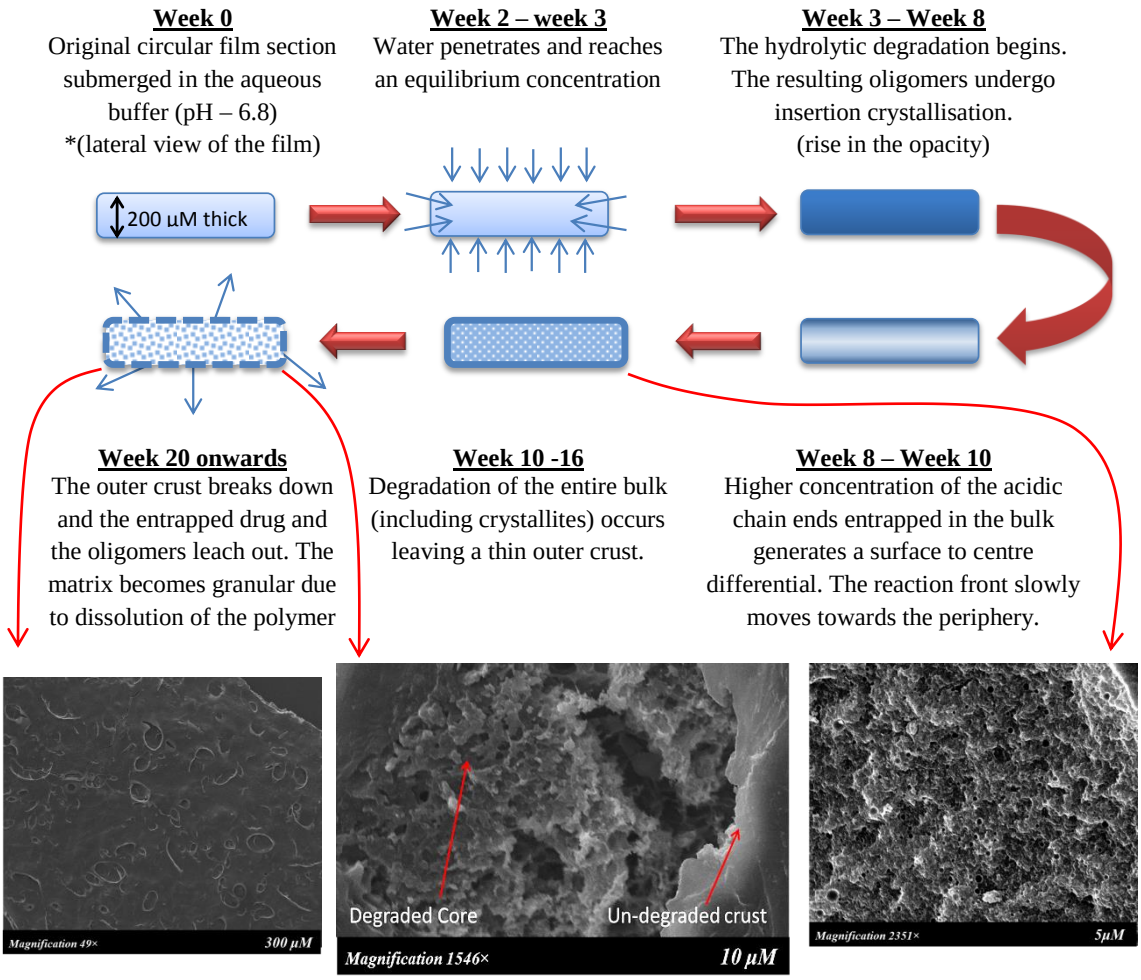

Figure 6.29: *Summary of the changes in PLA films after ageing into the release medium.*

Accumulation of the oligomers augments degradation of the bulk due to elevated concentration of the chain ends. Augmented degradation of the bulk compared to the surface creates a morphological distinction between them. In the current study this was observed as a thin crust-like layer surrounding the bulk. From the 20th week onwards, the crust developed larger cracks, which perhaps allowed erosion of the entrapped material (drug and oligomers). This phase was characterised by beginning of the weight loss. Finally, the matrix

started falling apart from the 32nd week onwards. The abovementioned mechanism suggests that drug release for the initial 3 weeks will occur predominantly by diffusion through the hydrated polymer matrix. Between 3-16 weeks, degradation of the polymer matrix coupled with formation of the water filled channels can augment drug release. Nevertheless, after 16 weeks, erosion of the films will cause substantial acceleration of drug release.

The results confirmed that the nature of the added drug and solid-state orientation of the films significantly influenced the hydrolytic degradation of PLA. The curcumin loaded films showed higher molecular weight degradation than the theophylline loaded films. Uniaxial as well as biaxial orientation delayed the onset of degradation, owing to lower hydrolytic susceptibility of the polymer chains in their oriented configuration (Lee *et al*., 2001a). Insertion crystallisation of the biaxially oriented films generates large sized, imperfect crystals, which can degrade easily, compared to the more perfect lamellar crystals in uniaxially oriented films. Consequently, the biaxially oriented films exhibited a sharper fall in molecular weight after the onset of degradation. Since the hydrolytic degradation of the films varied with respect to the method and the degree of orientation, these films can similarly show a difference in the drug release profile.

6.9. Drug release from oriented films

'Drug release' refers to the process of migration of a drug from the bulk of a polymeric device to the bulk of the release medium. There has been a growing interest to impose a control over this process. This research focuses on systematic investigation of the suitability of polymer orientation for achieving the same. The previous sections of this thesis have described the changes in drug loaded PLA films that occurred during melt-extrusion, solid-state orientation or after submersion into the release medium. This knowledge will help in justifying the drug release profile of the oriented PLA films.

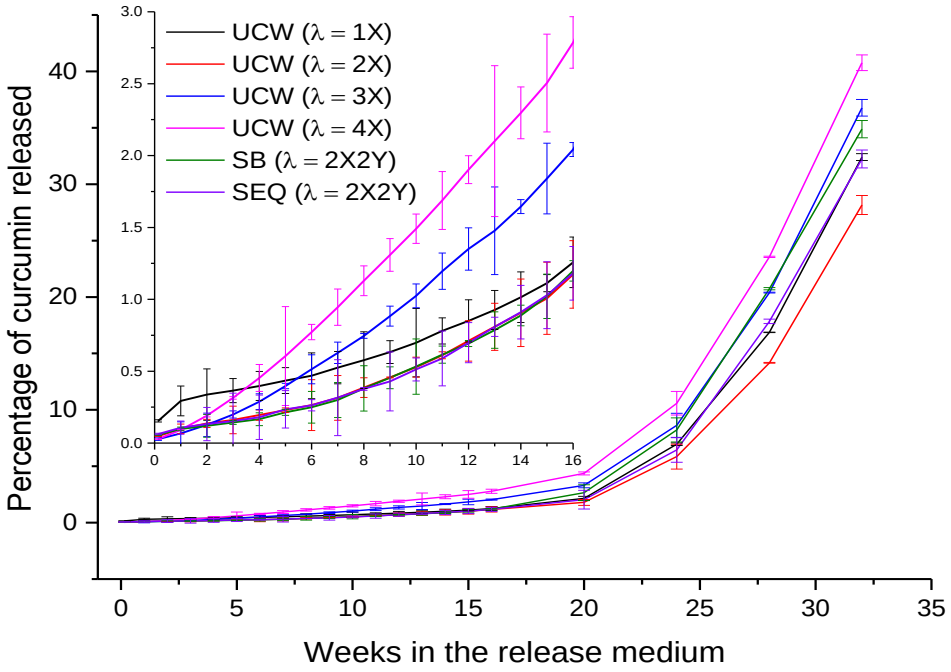

Figure 6.30: *Cumulative release of curcumin from oriented and un-oriented CPLA films over the study duration.*

*inset – magnified view between 0 – 16 weeks.

*The graph represents cumulative curcumin release as the mean ± standard deviation; for n = 6

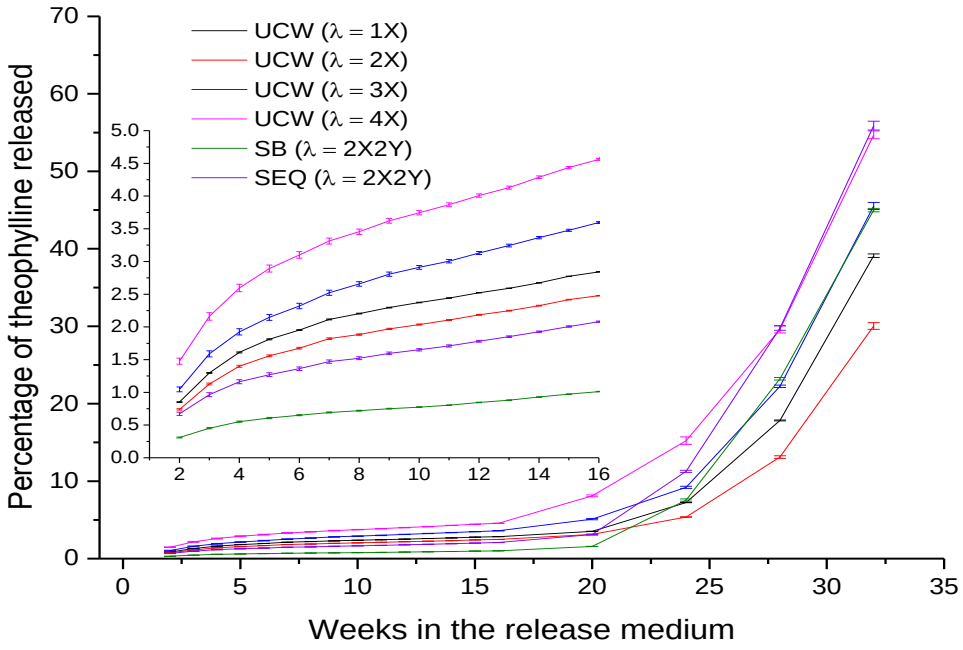

Figure 6.31: *Cumulative release of theophylline from oriented and un-oriented TPLA films over the study duration, after excluding the release during the first week.*

*inset – magnified view between 2 – 16weeks

The graph represents cumulative theophylline release as the mean ± standard deviation; n = 6.

Table 6.19: *Statistical comparison of cumulative curcumin release from CPLA films oriented to different draw ratios*

One way ANOVA followed by Tukey's test - curcumin release							
	Burst	Week 4	Week 8	Week 12	Week 16	Week 24	Week 32
1X Vs 2X	P < 0.001, q = 46.18	P > 0.05, q = 3.6	P > 0.05, q = 4.05	P > 0.05, q = 2.75	P > 0.05, q = 1.26	P > 0.05, q = 2.73	P < 0.001, q = 14.58
1X Vs 3X	P < 0.001, q = 55.23	P < 0.01, q = 6.26	P < 0.01, q = 5.49	P < 0.001, q = 9.87	P < 0.001, q = 11.76	P > 0.05, q = 4.17	P < 0.001, q = 15.01
1X Vs 4X	P < 0.001, q = 54.94	P < 0.01, q = 5.9	P < 0.001, q = 11.78	P < 0.001, q = 20.77	P < 0.001, q = 22.93	P < 0.001, q = 9.04	P < 0.001, q = 28.73
1X Vs SB 2X2Y	P < 0.001, q = 42.2	P > 0.05, q = 2.98	P > 0.05, q = 4.17	P > 0.05, q = 3.12	P > 0.05, q = 0.89	P > 0.05, q = 3.15	P < 0.001, q = 8.5
1X Vs SEQ 2X2Y	P < 0.001, q = 39.72	P > 0.05, q = 1.52	P > 0.05, q = 4.24	P > 0.05, q = 3	P > 0.05, q = 1.15	P > 0.05, q = 1.27	P > 0.05, q = 0.56
2X Vs 3X	P < 0.001, q = 9.05	P < 0.01, q = 12.51	P < 0.001, q = 7.65	P < 0.001, q = 12.62	P < 0.001, q = 13.03	P < 0.001, q = 6.9	P < 0.001, q = 29.59
2X Vs 4X	P < 0.001, q = 8.77	P < 0.001, q = 7.01	P < 0.001, q = 15.83	P < 0.001, q = 23.52	P < 0.001, q = 24.2	P < 0.001, q = 11.77	P < 0.001, q = 43.31
2X Vs SB 2X2Y	P > 0.05, q = 3.97	P > 0.05, q = 0.77	P > 0.05, q = 0.12	P > 0.05, q = 0.37	P > 0.05, q = 0.37	P < 0.01, q = 5.88	P < 0.001, q = 23.08
2X Vs SEQ 2X2Y	P > 0.05, q = 3.46	P > 0.05, q = 0.41	P > 0.05, q = 0.2	P > 0.05, q = 0.25	P > 0.05, q = 0.12	P > 0.05, q = 1.46	P < 0.001, q = 14.03
3X Vs 4X	P > 0.05, q = 0.29	P < 0.05, q = 4.49	P < 0.001, q = 8.18	P < 0.001, q = 10.9	P < 0.001, q = 11.17	P < 0.05, q = 4.87	P < 0.001, q = 13.72
3X Vs SB 2X2Y	P < 0.001, q = 13.03	P < 0.05, q = 5.29	P < 0.001, q = 7.77	P < 0.001, q = 12.99	P < 0.001, q = 12.65	P > 0.05, q = 1.01	P < 0.001, q = 6.51
3X Vs SEQ 2X2Y	P < 0.001, q = 15.51	P < 0.05, q = 4.92	P < 0.001, q = 7.85	P < 0.001, q = 12.88	P < 0.001, q = 12.91	P < 0.01, q = 5.43	P < 0.001, q = 15.56
4X Vs SB 2X2Y	P < 0.001, q = 12.74	P < 0.001, q = 7.78	P < 0.001, q = 15.95	P < 0.001, q = 23.89	P < 0.001, q = 23.82	P < 0.01, q = 5.88	P < 0.001, q = 20.23
4X Vs SEQ 2X2Y	P < 0.001, q = 15.22	P < 0.001, q = 7.42	P < 0.001, q = 16.03	P < 0.001, q = 23.78	P < 0.001, q = 24.08	P < 0.001, q = 10.3	P < 0.001, q = 29.29
SB 2X2Y Vs SEQ 2X2Y	P > 0.05, q = 2.48	P > 0.05, q = 0.36	P > 0.05, q = 0.07	P > 0.05, q = 0.12	P > 0.05, q = 0.26	P < 0.05, q = 4.42	P < 0.001, q = 9.06

Notes: For relevant data refer figure 6.30

The null hypothesis was that the compared samples were statistically the same

P > 0.05 = The difference between the compared samples is **not statistically significant**
0.05 > P > 0.01 = The difference between the compared samples is **statistically significant**
0.01 > P = The difference between the compared samples is **highly significant**

Table 6.20: *Statistical comparison of cumulative theophylline release from TPLA films oriented to different draw ratios*

One way ANOVA followed by Tukey's test - Draw ratio comparison							
	Burst	Week 4	Week 8	Week 12	Week 16	Week 24	Week 32
1X Vs 2X	P < 0.001, q = 22.93	P < 0.001, q = 15.33	P < 0.001, q = 31.89	P < 0.001, q = 52.37	P < 0.001, q = 89.66	P < 0.001, q = 20.64	P < 0.001, q = 52.41
1X Vs 3X	P < 0.001, q = 30.91	P < 0.001, q = 22.55	P < 0.001, q = 45.17	P < 0.001, q = 94.31	P < 0.001, q = 186.36	P < 0.001, q = 21.62	P < 0.001, q = 37.07
1X Vs 4X	P < 0.001, q = 41.13	P < 0.001, q = 70.93	P < 0.001, q = 124.76	P < 0.001, q = 230.27	P < 0.001, q = 424.62	P < 0.001, q = 87.88	P < 0.001, q = 90.08
1X Vs SB 2X2Y	P < 0.001, q = 53.96	P < 0.001, q = 76.4	P < 0.001, q = 147.87	P < 0.001, q = 260.06	P < 0.001, q = 451.34	P > 0.05, q = 3.49	P < 0.001, q = 34.02
1X Vs SEQ 2X2Y	P < 0.001, q = 42.58	P < 0.001, q = 32.41	P < 0.001, q = 67.99	P < 0.001, q = 115.02	P < 0.001, q = 187.78	P < 0.001, q = 44.36	P < 0.001, q = 96.97
2X Vs 3X	P < 0.001, q = 7.98	P < 0.001, q = 37.88	P < 0.001, q = 77.06	P < 0.001, q = 146.68	P < 0.001, q = 276.03	P < 0.001, q = 42.26	P < 0.001, q = 89.49
2X Vs 4X	P < 0.001, q = 18.2	P < 0.001, q = 86.26	P < 0.001, q = 156.64	P < 0.001, q = 282.63	P < 0.001, q = 514.28	P < 0.001, q = 108.51	P < 0.001, q = 142.49
2X Vs SB 2X2Y	P < 0.001, q = 31.03	P < 0.001, q = 61.07	P < 0.001, q = 115.98	P < 0.001, q = 207.69	P < 0.001, q = 361.68	P < 0.001, q = 24.13	P < 0.001, q = 86.43
2X Vs SEQ 2X2Y	P < 0.001, q = 19.66	P < 0.001, q = 17.07	P < 0.001, q = 36.1	P < 0.001, q = 62.65	P < 0.001, q = 98.12	P < 0.001, q = 65	P < 0.001, q = 149.38
3X Vs 4X	P < 0.001, q = 10.22	P < 0.001, q = 48.38	P < 0.001, q = 79.58	P < 0.001, q = 135.96	P < 0.001, q = 238.25	P < 0.001, q = 66.26	P < 0.001, q = 53
3X Vs SB 2X2Y	P < 0.001, q = 23.04	P < 0.001, q = 98.95	P < 0.001, q = 193.05	P < 0.001, q = 354.37	P < 0.001, q = 637.71	P < 0.001, q = 18.13	P > 0.05, q = 3.06
3X Vs SEQ 2X2Y	P < 0.001, q = 11.67	P < 0.001, q = 54.96	P < 0.001, q = 113.16	P < 0.001, q = 209.33	P < 0.001, q = 374.15	P < 0.001, q = 22.74	P < 0.001, q = 59.9
4X Vs SB 2X2Y	P < 0.001, q = 12.83	P < 0.001, q = 147.33	P < 0.001, q = 272.63	P < 0.001, q = 490.32	P < 0.001, q = 875.96	P < 0.001, q = 84.39	P < 0.001, q = 56.06
4X Vs SEQ 2X2Y	P > 0.05, q = 1.45	P < 0.001, q = 103.34	P < 0.001, q = 192.74	P < 0.001, q = 345.29	P < 0.001, q = 612.4	P < 0.001, q = 43.52	P < 0.001, q = 6.89
SB 2X2Y Vs SEQ 2X2Y	P < 0.001, q = 11.37	P < 0.001, q = 43.99	P < 0.001, q = 79.89	P < 0.001, q = 145.04	P < 0.001, q = 263.56	P < 0.001, q = 40.87	P < 0.001, q = 62.96

Notes: For relevant data refer figure 6.31

The null hypothesis was that the compared samples were statistically the same

P > 0.05 = The difference between the compared samples is **not statistically significant**

0.05 > P > 0.01 = The difference between the compared samples is **statistically significant**

0.01 > P = The difference between the compared samples is **highly significant**

Theophylline release from oriented and un-oriented PLA (TPLA) films followed a tri-phasic release pattern (figure 6.31). The initial phase was characterised by burst release of a large fraction of theophylline. The drug release slowed down gradually until the 16th week, following which there was a rapid surge again. Contrarily, the curcumin loaded PLA films (CPLA) exhibited negligible burst release. The amount of curcumin released between the weekly sampling intervals increased gradually until the 16th week and then continued as an exponential release phase (figure 6.30). The difference in the release profile exhibited by the mentioned model systems can be attributed to the physical state of the respective drugs within the PLA matrix.

The overall drug release profiles displayed in figure 6.30 and figure 6.31 did not show a large visual difference between the draw ratios. However a statistical comparison at different time points by one-way ANOVA – Tukey's test (table 6.19, table 6.20) revealed a significant difference between the draw ratios (except for the shrunken CPLA films). This can be attributed to the uncontrolled release of a large amount of drug after 16 weeks, which masked individual differences between the films prior to 16 weeks (in the overall drug release profile). Therefore the effect of different draw ratios on drug release from oriented PLA films was studied by dividing the total drug release in three distinct phases. These included the initial burst release phase, the second slow release phase and the final exponential release phase. Drug release in each of these phases was analysed separately.

6.9.1. Phase I: the burst release

The term 'burst release' here refers to the amount of drug released uncontrollably during the first day, after submersion into the release medium. The phenomenon is usually associated with rapid dissolution of the drug located at or near the surface. Therefore, the nature of the burst phase varies substantially with the physical state of the drug in the polymer matrix. The results of hot-stage microscopy (sec. 5.5.3) confirmed that only a small fraction

of the compounded theophylline was soluble in the molten PLA; nevertheless, it crystallised out, upon cooling the composite melt. This alternatively means that theophylline was present as a supersaturated solution in PLA, along with numerous suspended crystalline particles. Such matrices show a prominent burst release phase due to the following reasons.

A. Firstly, the drug present as a supersaturated solution can migrate towards the surface and crystallise out (Ahmed *et al*., 2008; Tzafriri, 2000).

B. The crystalline drug already located at the surface, along with the newly crystallised drug can readily dissolve instantaneously into the bathing medium (Hurrell and Cameron, 2002).

C. Dissolution of the phase separated drug creates voids, which accelerate water penetration and further dissolution of the drug particles located near the surface (Huang and Brazel, 2001).

It was previously confirmed that curcumin remained in a molecularly dispersed state within the PLA matrix (chapter 5). Moreover, the PLA extrudates containing 5% w/w curcumin showed no phase separation, when re-molten on the hot-stage microscope or while cooling from the melt state. These findings indicate that the concentration of curcumin utilised here (i.e. 5% w/w) was below its saturation solubility in PLA. Owing to a higher cohesiveness between the curcumin and PLA, its migration towards the surface can be negligible (at 5% w/w loading). Perhaps as a result of this, the burst release exhibited by the curcumin loaded PLA films was significantly lower than that observed with the theophylline loaded PLA films (figure 6.32).

Orientation of the drug loaded films diminished the amount of drug released in a burst manner (figure 6.32). For the uniaxial constant width (UCW) orientation, the burst release of theophylline decreased systematically as the uniaxial draw ratio increased. This observation was statistically validated by one-way ANOVA – Tukey's test. A highly significant ($P < 0.001$) difference was observed in the burst release from TPLA films, when individual UCW draw

ratios were compared (table 6.20). Among the biaxially oriented TPLA films, simultaneous biaxial stretching lowered the burst theophylline release to a greater extent than that observed with the sequential biaxial stretching (SEQ). The burst release from SEQ oriented (λ = 2X2Y) TPLA films was statistically equivalent to that from the UCW – 4X films (table 6.20).

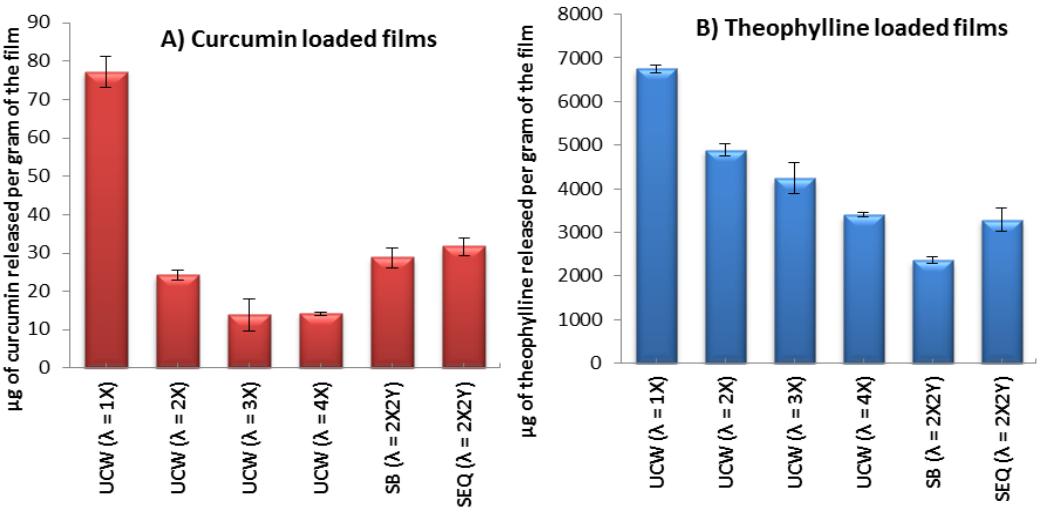

Figure 6.32: *Burst release from oriented PLA films containing* ***A)*** *curcumin and* ***B)*** *theophylline as model drugs.*

*The amount of drug released is expressed as mean ± SD, where n = 6.

Orientation of the CPLA films similarly reduced the burst release of curcumin. A substantially lower burst release was observed at the UCW draw ratio of 2X. Further extension to the UCW draw ratio of 3X progressively reduced the burst release. The statistical difference between the burst release from un-oriented, UCW-2X and UCW-3X CPLA films was highly significant ($P < 0.001$; table 6.19). The CPLA films oriented to a UCW draw ratio of 4X showed statistically equivalent burst release to that from UCW-3X films. Nevertheless, drug release from the biaxially (both SB and SEQ) oriented CPLA films was statistically equivalent to that from the UCW-2X films (table 6.19).

Burst release from the matrix type drug delivery systems (sec. 3.4) has been previously attributed to migration of the drug towards the matrix surface,

during storage (Huang and Brazel, 2001). Densification of the polymer chains after solid-state orientation of the films may hinder drug migration perpendicular to the film plane, during storage. Consequently, a lesser amount of free drug may be available on the film surface for instantaneous dissolution. Burst release can be a desired mechanism when a faster onset followed by a prolonged release of a constant drug amount is needed. However, it is unpredictable and the amount of burst can be rarely controlled. Therefore, a reduction in the burst release following orientation of the polymeric films is advantageous.

6.9.2. Phase II: diffusion driven release

6.9.2.1. Mechanism

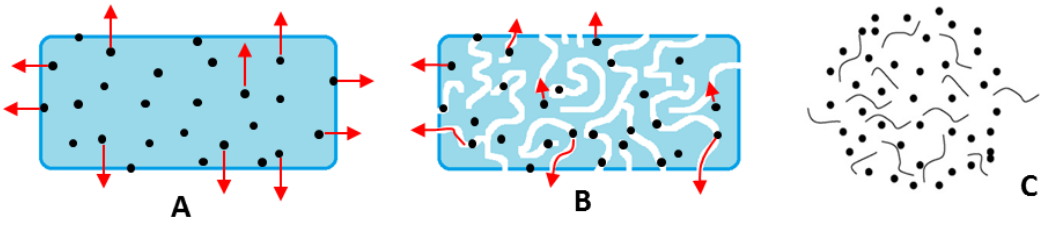

Figure 6.33: *Principle mechanisms responsible for drug release from PLA*

(A) Diffusion through the polymer, **(B)** Transport through the water-filled channels, **(C)** Erosion

Numerous mechanisms have been proposed for elucidating the release of a bioactive agent from PLA matrices. Among them, i) diffusion through the polymeric amorphous phase, ii) transport through the water filled channels, and iii) release due to polymer erosion have been evidenced as the principle mechanisms (figure 6.33) (Fredenberg *et al*., 2011). The drug loaded PLA films studied here underwent bulk hydrolytic degradation when submerged in the release medium (sec. 6.8). The oligomers generated in this process remained entrapped within the PLA matrix, without being eroded away. The path followed by the percolated medium was transformed into the fluid/water filled channels, whose number and size increased as the PLA matrix degraded further. However, weight loss due to erosion was observed only from the 20th week.

(After 16 weeks, the samples were withdrawn every 4 weeks and not weekly, therefore the 20th week was the earliest sampling time-point after the 16th week). A common trend coherent with the bulk degradation profile was evidenced in the cumulative release profile of curcumin and theophylline from CPLA and TPLA films respectively. The drug release rate was considerably slower for the first 16 weeks, compared to that from the 20th week onwards. The four weeks duration between the 16th and the 20th week perhaps represented a transition phase, following which there was an exponential rise in drug release. A similarity between the drug release profile and the degradation profile suggests that drug release up to the 16th week may have occurred by diffusion through the polymer (figure 6.33 - A) and/or transport through water filled channels (figure 6.33 - B). Nevertheless, a substantial acceleration of drug release from the 20th week onwards, correlates with erosion of the films (figure 6.33 - C).

The relative importance of the mass transport mechanisms (in phase II) may vary depending upon the physical state of a drug within the PLA matrix. Since the crystalline theophylline formed a suspension in PLA, its release in 'phase II' may predominantly occur by transport through the water filled channels. On the contrary, curcumin may equally follow both mass transport mechanisms, it being present in the solution state (sec. 5.5.3).

6.9.2.2. Kinetic expression of drug release

The primary aim of kinetic model fitting was to understand the mass transport mechanisms responsible for controlling drug release from the investigated films. Additionally, this approach allowed for the quantitative prediction of the effects of solid-state orientation on the resulting drug release kinetics (sec. 6.9.2.4).

The drug is transported from the bulk of the delivery device to the external sink by different types of mass transport processes. These include drug diffusion through the polymer phase, transport through the water filled channels,

and erosion of the polymer. Nevertheless, certain polymeric matrices exhibit osmotic movement of water into the matrix followed by diffusion of the drug through the swollen polymer or transport by dissolution in the permeated water. Drug release from a biodegradable polymer matrix simultaneously involves several of these mass transport processes. However, one of them usually plays a substantially greater role than others, and consequently acts as a principle mechanism behind drug release. In order to identify this, the drug release data is plotted as per the mathematical functions described by various empirical models (sec. 3.5). The empirical kinetic models reported in the literature describe separate mass transport mechanisms (Dash *et al*., 2010). Therefore, the model which yields the highest regression coefficient and the F – value (by ANOVA or the lowest P value) represents the most substantial mass transport process responsible for the overall drug release. Control over this process can therefore result in a control over entire drug release.

Selection of one model alternatively invalidates the other models, since each describe different mass transport process as the main drug release mechanism. However, it is not unusual that the drug release data does not agree with any of the reported models. Such situation arises due to a number of reasons as follows:

a. A mass transport mechanism, which has not been yet considered in drug release modelling, is involved. For example, pore closing – pore opening phenomena responsible for drug release from PLGA microparticles (Fredenberg *et al*., 2011).

b. There are far too many processes involved in the overall drug release. Several of these processes alter the fate/rate of the other process. For example, drug release from low molecular weight PLA/PLGA involves surface erosion as well as bulk degradation of the polymer, swelling due to osmosis and drug diffusion (Hurrell and Cameron, 2001b).

c. The principle mass transport mechanism changes from time to time. For example, depending upon the molecular weight of the drug loaded PEO matrix, the rate limiting process changes between erosion of the polymer and diffusion of the drug through swollen polymer matrix (Colo di *et al*., 2001).

d. The drug delivery device disobeys one of the fundamental assumptions made while deriving the model. For example, the Higuchi model (Higuchi, 1963), describes those systems where drug diffusion is the rate limiting step. This model assumes that the diffusivity of the drug/ polymer matrix remains constant throughout (sec. 3.4). Therefore, if a bioerodible system exhibits a change in the diffusivity due to erosion, the drug release may not conform to the Higuchi model, even if drug diffusion was the principle process.

Similar to the empirical models, drug release can be expressed by theoretical models such as the first order release and the zero order release models. The prior signifies that the drug release rate decreases progressively due to a gradual fall in the drug concentration gradient. Nevertheless, the latter indicates that irrespective of the underlying mass transport processes, the drug release rate remains constant. In the current study, the drug release data between the 2^{nd} and the 16^{th} week was fitted into the following models (sec. 3.6); namely, zero order, first order, Hixson–Crowell model, Higuchi model, and Korsmeyer–Peppas model (Dash *et al*., 2010; Higuchi, 1961; Korsmeyer *et al*., 1983; Korsmeyer and Peppas, 1981; Ritger and Peppas, 1987). Since the overall drug release from the studied PLA films was extremely low, and because multiple mass transport processes are involved in drug release from PLA, most models yielded a high R^2 value. There the most appropriate model (that can identify the principle transport mechanism) was selected based on the highest regression coefficient, highest F- value and the lowest P – value obtained from ANOVA (table 6.21).

Table 6.21: *Testing suitability of the controlled drug release models by regression analysis*

The Model	The Linearity criteria *(What was plotted)	TPLA Films λ = 4X			CPLA Films λ = 4X		
		R^2	F	P	R^2	F	P
First order kinetics	**Y-axis:** $\mathrm{Log}(Q_0 - Q_t)$, **X-axis:** time	0.9076	127	4.28 X 10^{-8}	0.9628	336	1.13 X 10^{-10}
Zero order kinetics	**Y-axis:** Q_t, **X-axis:** time	0.9058	125	4.84 X 10^{-8}	0.9971	4525	6.43 X 10^{-18}
Higuchi Model	**Y-axis:** Q_t, **X-axis:** $\sqrt{\mathrm{time}}$	0.9958	2883	1.19 X 10^{-16}	0.8994	116	7.47 X 10^{-8}
Hixson–Crowell	**Y-axis:** $Q_0^{1/3} - Q_t^{1/3}$, **X-axis:** time	0.804	53	5.98 X 10^{-6}	0.9513	254	6.52 X 10^{-10}
Korsmeyer–Peppas model	**Y-axis:** $\mathrm{Log}(Q_t/Q_0)$, **X-axis:** $\log(\mathrm{time})$	0.9881	798	2.4 X 10^{-12}	0.9881	1546	4.72 X 10^{-14}

Note: $\mathbf{Q_0}$ = Original amount of drug present in the films, $\mathbf{Q_t}$ = Cumulative drug release in time 't'. The 'p' value was calculated with α = 0.05.

In the case of TPLA films, the theophylline release data showed highest agreement with the Higuchi model. The regression coefficient for the release data when plotted according to the Higuchi model was highest. Nevertheless the F- value was substantially higher than other models. To visualise this graphically, the predicted theophylline release obtained from regression analysis, for each model was plotted along with the actual release data (figure 6.34). It can be clearly seen from figure 6.34 that theophylline release can be best explained by the Higuchi and the Korsmeyer-Peppas model (Korsmeyer *et al*., 1983). The Peppas model is the only empirical model which describes various mass transport mechanisms depending on the value of the Peppas exponent. This model is based on equation 6.1.

$$\frac{\mathbf{M_0}}{\mathbf{M_\infty}} = \mathbf{Kt^n} \qquad \textbf{(Equation 6.1)}$$

In equation 6.1, 'M_0/M_∞' signifies the fraction of the drug released; 'K' is the proportionality constant, 't' is time and 'n' is the exponent used for characterising the diffusion mechanism. For film geometry, 0.5 ≤ n corresponds to the Higuchi model, 0.5 < n < 1 to non-Fickian anomalous transport, n = 1 relates to the zero order Case II transport and n > 1 to the super case II transport. In the current study, the values of the Peppas exponent for all TPLA films were less than 0.5. This further confirmed that theophylline release occurred according to the Higuchi model. Here the plot of the percent cumulative release of theophylline between the 2nd and the 16th week, against the square root of time yielded straight lines (figure 6.35). The proportionality between the fraction of drug released and the square root of time signified that the theophylline release during this phase followed the Fickian diffusion mechanism (as explained by the Higuchi model) (Higuchi, 1963; Ritger and Peppas, 1987). Therefore, it can be safely stated that diffusion of theophylline was the rate limiting step in overall drug release.

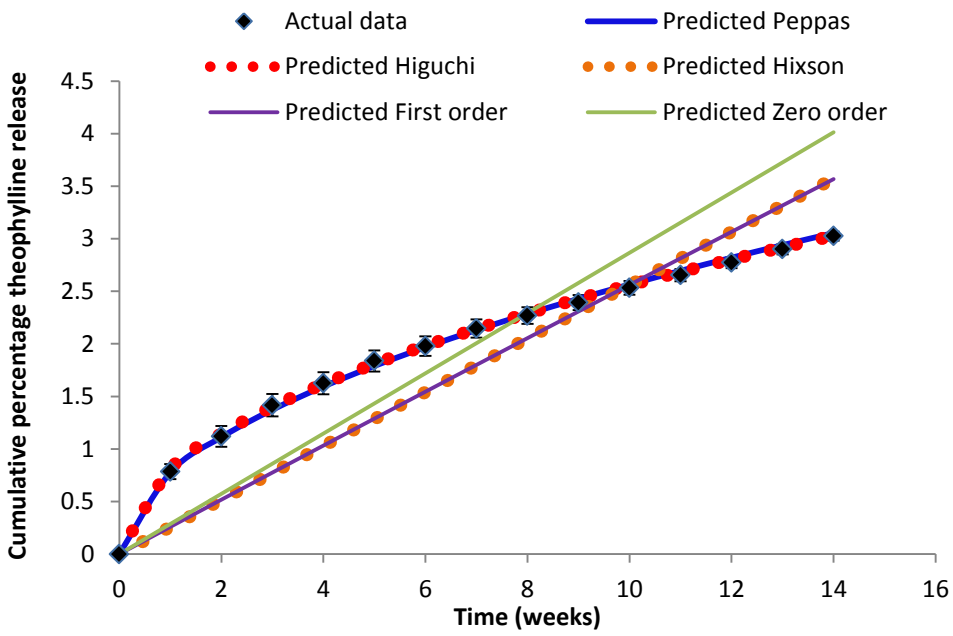

Figure 6.34: *Comparison between actual theophylline release and predicted theophylline release by various models for TPLA films oriented to λ = 4X.*

*The actual data is plotted here as mean of 6 replicates. The errors bars represent the standard deviation.

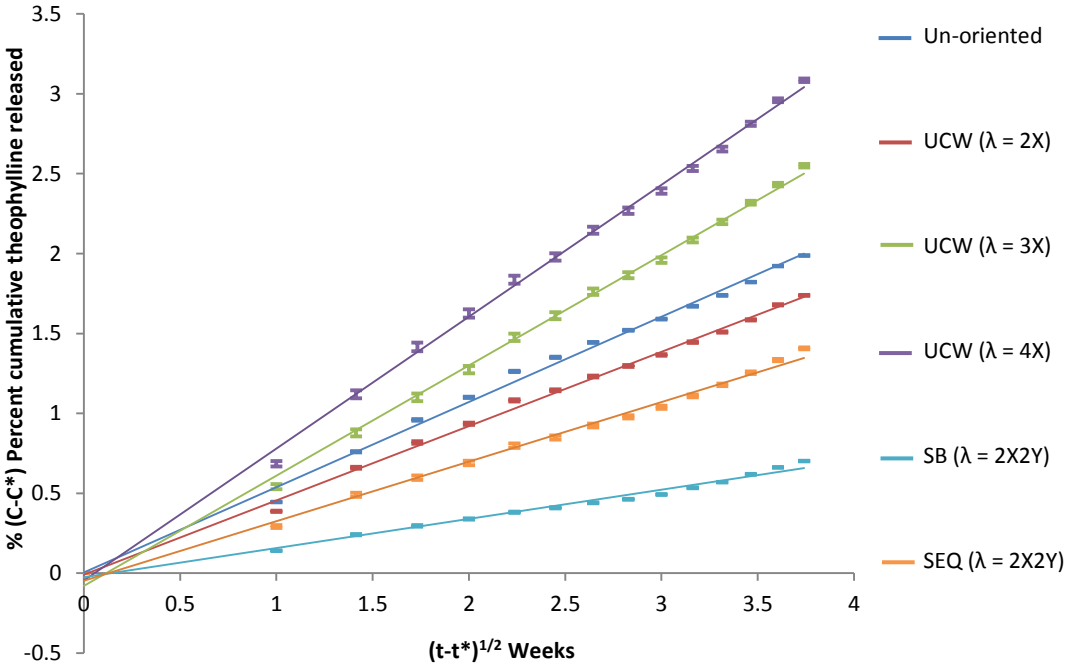

Figure 6.35: *Fraction of theophylline released against the square root of time from oriented TPLA films between 2nd and 16th week – Higuchi model.*

Note: The X-axis utilises (t-t) values signifying that the second week sampling point was considered as the starting point. Here 't' represents the individual time-point, while 't* = 2 week'. Similarly, the Y–axis utilises the cumulative (C – C*) values; where 'C' represents the cumulative drug release till the respective time-point, while 'C*' represents the cumulative drug released during the first two weeks.

*The graph represents theophylline release as the mean ± standard deviation; for n = 6

As reported in section 3.4.1, the Higuchi model was originally developed for matrix type systems made from non-erodible polymers. It was later found that the biodegradable systems, where the drug diffusion is substantially faster than polymer erosion may exhibit drug release according to the Higuchi model (Fu and Kao, 2010). The PLA films studied here underwent significant molecular weight degradation following aqueous submersion. However, due to bulk degradation, no actual erosion was observed until the 20th week. Therefore diffusion of theophylline through PLA can be considered as the principle mass transport mechanism responsible for theophylline release. According to the Higuchi model the cumulative drug release from a non-biodegradable matrix can be explained by equation 6.2, when the drug is present in the suspension

state and the total drug loading is less than 5% w/w. If the drug loading exceeds 5% w/w, the matrix becomes granular, where water percolation creates fluid filled channels. Although theophylline loading in the current study was 5% w/w, it was confirmed that similar channels were formed due to bulk degradation of the PLA films (section 6.8.5). Here theophylline can either diffuse to the external sink or towards the nearest channel (figure 6.33). Therefore theophylline release should be expressed by the modified Higuchi equation (eqn. 6.3), which takes into consideration the porosity of the matrix and the tortuosity of the fluid filled channels.

$$Q_t = \sqrt{Dt\,(2Q_0 - C_s)C_s} \qquad \textbf{(Equation 6.2)}$$

$$\mathrm{Q} = \sqrt{\left(\frac{\mathrm{D}\varepsilon}{\tau}(2\mathrm{Q}_0 - \epsilon\mathrm{C}_\mathrm{S})\mathrm{C}_\mathrm{S}\mathrm{t}\right)} \qquad \textbf{(Equation 6.3)}$$

Where, **Q =** amount of drug release per unit surface area in time 't'.

Q_0 = the total drug loading

D = combined diffusivity of theophylline through the polymer matrix and through the water filled channels.

Since, the theophylline release is expected to occur predominantly through the percolated medium, **C_s** is considered here as the saturation solubility of theophylline in the release medium. **'ε'** represents the volume fraction of the fluid filled channels and **'τ'** is the tortuosity index of such channels.

The Higuchi model considers drug release to be a layer by layer diffusion phenomenon. Upon water penetration into the system drug release initially occurs only from the outermost layers that are in direct contact with water. These include the exterior surface of the delivery device (in direct contact with the release medium) or the internal surfaces of the water filled channels (in contact with the permeated water). Firstly, the drug that is located on these surfaces in the undissolved/precipitated state solubilises in the surrounding medium. Only after the undissolved drug is completely exhausted, the drug present in the solution state within these layers is released. Once the drug

concentration in the outermost layers falls below the drug's saturation solubility, the drug in the adjacent layer starts to diffuse due to presence of a concentration gradient between these layers. Depletion of the drug in each successive layer causes solubilisation of the excess drug located in the vicinity, and its diffusion towards the depleted layers. The Higuchi model assumes that the dissolution of drug particles into the polymer phase is substantially rapid compared to the diffusion of the dissolved drug molecules through the polymer phase. Therefore, the drug diffusion acts as a rate limiting step, which depends on the concentration gradient. Since depletion of the drug from the polymer matrix causes a fall in the concentration gradient, drug release rate decreases gradually with time. The proportionality between the cumulative theophylline release and the square root of time observed in the current study explains the same phenomenon (Roseman and Higuchi, 1970).

A substantial difference between the theophylline loaded and the curcumin loaded PLA films was that the theophylline release rate reduced progressively, while the curcumin release rate remained nearly constant throughout. Therefore, the percent cumulative release of curcumin exhibited a linear relationship with time and not with the square root of it (figure 6.37). Such proportionality indicated that the release of curcumin followed zero order kinetics. This was further confirmed by comparison of R^2 and the F-values obtained for curcumin release data by various models (table 6.21). The R^2 according to the zero order model was highest for all CPLA films. Nevertheless, the F- value obtained by this model was significantly higher than any other model considered here. When the predicted curcumin release according to the selected models was plotted along with the actual data (figure 6.36), it highlighted that curcumin release more closely agreed with the zero order model and the Peppas model. The Peppas exponent for all CPLA films was 1.00 ± 0.15, which further established that curcumin released occurred according to the zero order model.

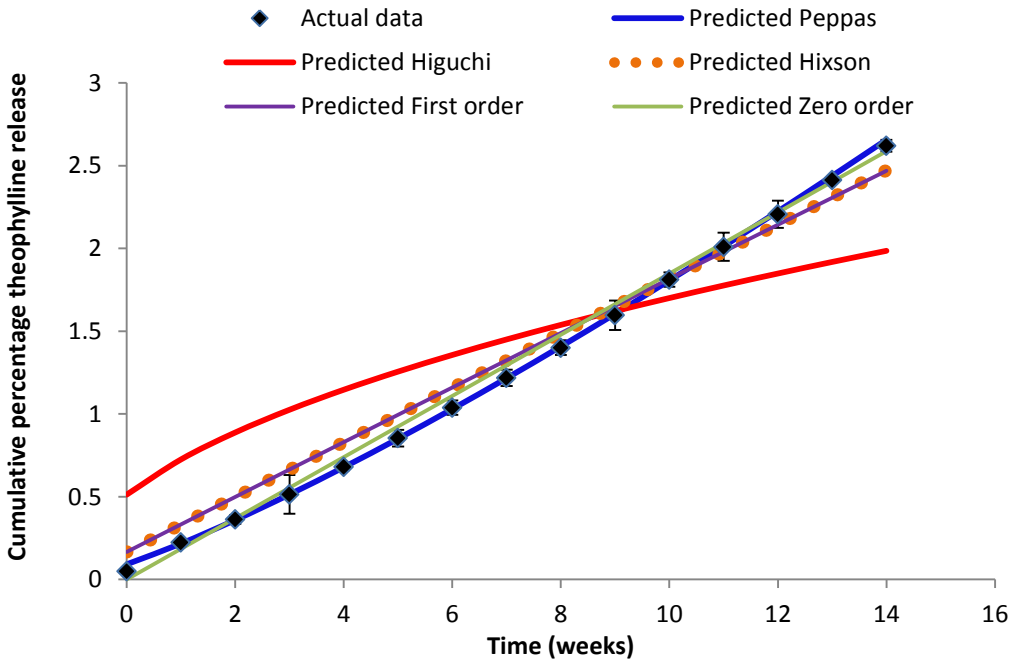

Figure 6.36: *Comparison between actual curcumin release and predicted curcumin release by various models for CPLA films oriented to λ = 4X.*

*The actual data is plotted here as mean of 6 replicates. The errors bars represent the standard deviation.

Although the curcumin release data was within the 95% confidence intervals of the Hixon-Crowell model the overall trend showed a poorer fit than the zero order and Peppas models. Moreover, it was found that the investigated PLA films underwent bulk erosion in water, without losing the weight and geometry for approximately 20 weeks. The Hixson-Crowell model explains drug release from a surface of a drug delivery device, where erosion of the surface causes a change in the geometry. Therefore, this model will be clearly inapplicable to the studied films.

The material investigation studies confirmed that curcumin was present in the solution state within PLA. Importantly, it did not phase separate during cooling, suggesting that its concentration was below its saturation solubility in PLA. In such cases, diffusion is invariably involved in the mass transport of the drug out of the dosage form (Siepmann and Siepmann, 2012). Moreover, the layer by layer diffusion of a solution state drug does not require dissolution of the excess drug in each theoretical layer before the drug in the next layer can

start to diffuse. Despite this, the cumulative curcumin release could not be explained by the Higuchi model, perhaps due to the reasons listed in the beginning of this section. The Higuchi model claims that the drug diffusion rate remains constant at least over the first 60% of drug release. Therefore, it can be assumed that bulk degradation of the PLA films in the course of drug release, did not affect the diffusion rate of theophylline (suspended drug); however, it augmented that of curcumin (drug in the solution state). Increased diffusion of curcumin (along with several unknown factors) may have balanced the reduction in the release rate due to depletion of the concentration gradient. Consequently, a nearly constant release rate was evidenced.

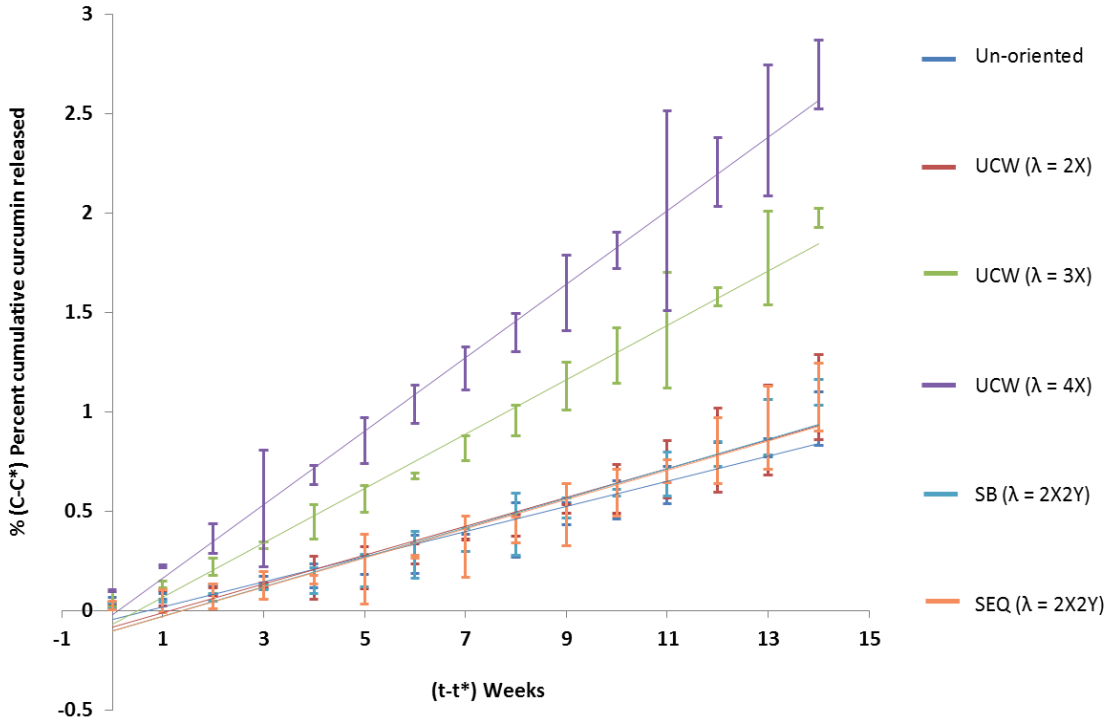

Figure 6.37: *Fraction of curcumin released against time from oriented CPLA films between 2nd and 16th week – zero order kinetics.*

*The graph represents cumulative curcumin release as the mean ± standard deviation; for n = 6

The zero order release profile is usually observed in polymeric drug delivery devices, where the polymer undergoes swelling. As water percolates into the polymer it hydrates the polymer chains, which subsequently swell. A clear boundary separates the swollen outer region and the glassy polymer core. The boundary slowly moves towards the centre. The rate of drug diffusion is faster in the swollen polymer than in the glassy core. Although the diffusion rate in the glassy core reduces gradually due to drug depletion, this can be balanced by the inward movement of the boundary at an appropriate speed. Consequently, the overall drug release rate remains constant. The films studied here neither showed any visible swelling, nor substantial weight gain due to water absorption. Therefore, a mechanism other than swelling must have contributed in the augmentation/ balancing of the diffusion rate. The studied films progressively underwent molecular weight reduction and the resultant oligomers remained entrapped within the bulk of the matrix, this might have contributed in enhancing the diffusivity of curcumin, which may subsequently balance the effect of concentration depletion.

This work highlighted that the release of a solution state drug from PLA substantially varied from that of a suspension state drug. Finding a justification for the observed differences would require significantly more experiments and separate mathematical modelling, which was beyond the scope of this work.

6.9.2.3. The effect of solid-state orientation

Solid-state orientation of the drug loaded PLA films significantly altered the phase II drug release (figure 6.35 & figure 6.37). Theophylline release from TPLA films was suppressed when they were subjected to simultaneous biaxial or sequential biaxial stretching to λ = 2X2Y or UCW stretching to a uniaxial draw ratio of 2X. Further stretching in UCW mode in fact accelerated drug release (figure 6.35). Since only a small percentage of drug was released between 2 – 16 weeks, the difference between individual draw ratios was statistically validated by one-way ANOVA followed by Tukey's test (table 6.20).

The results of statistical analysis confirmed that at selected time-points the cumulative theophylline release from TPLA films was highly significant ($P < 0.001$) between the studied draw ratios. Contrarily, the cumulative curcumin release from CPLA films followed a slightly different trend. At the same time-points, throughout the study duration, the cumulative curcumin release from biaxially oriented CPLA films and those oriented to UCW draw ratio of 2X was statistically equivalent ($P > 0.05$) to that from the un-oriented CPLA films (table 6.19, figure 6.37). This can be attributed to shrinkage of the mentioned films, which resulted in a partial loss of the oriented structure (sec. 6.8.1). Similar to TPLA films, curcumin release was accelerated from CPLA films oriented to UCW draw ratios of 3X and 4X (figure 6.37). These films showed a statistically significant difference in the cumulative drug release compared to un-oriented films and even between themselves (table 6.19).

Orientation of the TPLA films by tensile stretching created several voids, owing to the poor affinity between PLA and suspended theophylline particles (sec 6.4). Theoretically, pore size will increase as films are stretched to a higher draw ratio. A greater pore size may augment water permeation and consequently the theophylline release. However, the faster drug release from UCW oriented ($\lambda \geq 3X$) TPLA films cannot be entirely attributed to void formation; since it fails to justify the following findings. Firstly, biaxial orientation of TPLA films as well as orientation to a UCW draw ratio of 2X also exhibited formation of voids; however, drug release from these films was slower than that from the un-oriented films (figure 6.35). Secondly, such voids were absent in oriented CPLA films. Albeit, curcumin release from the CPLA films was accelerated after orienting them to UCW draw ratios of 3X and 4X (figure 6.37).

The characteristic differences in drug release patterns displayed by oriented PLA films can be correlated with their molecular organisation. It was derived from MDSC and WAXD studies that films oriented to a UCW draw ratio of 2X exhibited no strain induced crystallisation. Strain induced crystallisation in

the biaxially oriented films (λ = 2X2Y) was practically insignificant. These films contained merely amorphous chains oriented in the drawing direction/s. On the contrary, UCW stretching to draw ratios of 3X and above produced a three dimensional α crystalline order. Several studies have previously confirmed that drug elution is faster from crystalline PLA matrices than from the amorphous matrices (Hurrell and Cameron, 2001b; Hurrell and Cameron, 2002; Izumikawa *et al*., 1991; Miyajima *et al*., 1997). A rise in polymer crystallinity increases drug concentration in the polymer's amorphous phase. Consequently, an elevated concentration gradient augments drug release by Fickian diffusion mechanisms (Miyajima *et al*., 1997).

It was earlier confirmed that oriented as well as un-oriented films underwent insertion crystallisation after submersion in the release medium (sec. 6.8.1). The crystallinity of all studied films reached a constant level of about 35% by the 6^{th} week after aqueous submersion. If the percentage crystallinity was the sole influencing factor, the drug release from all of the films should have been similar after 6 weeks. However, a higher drug release from films oriented to UCW draw ratios of 3X and 4X, highlights the importance of structural order rather than mere crystallinity.

Insertion crystallisation is essentially a template crystallisation phenomenon. Therefore, new crystal growth follows the existing crystalline arrangement (Hurrell and Cameron, 2002). Tsuji *et al*. (2000b) reported that insertion crystallisation in a previously amorphous polymer matrix generates largely imperfect crystals (figure 6.38). In such crystals the inter-crystalline and intra-crystalline amorphous phase is loosely arranged (refer sec. 3.8 for lamellar polymer crystals). Contrastingly, the polymer matrices, which have a well-developed crystalline order, already contain the amorphous phase as tie molecules and chain ends interspaced between the crystalline folds. Insertion crystallisation of such a structure may pull the inter/intra- crystalline amorphous chains into the crystalline folds. Consequently, the free (unmasked) chain ends

may create a defect zone (figure 6.38). Since such a defect zone contains hydrophilic chain ends (carboxylic acid groups), they can augment percolation of water and degradation of the surrounding amorphous phase. Subsequently, this region is transformed into a water filled channel. The medium / water present in these channels can dissolve the surrounding drug molecules, and transport them to the outside medium by virtue of the concentration gradient (Miyajima *et al*., 1998; Ritger and Peppas, 1987).

Films oriented to UCW draw ratios of 3X and 4X contained a highly ordered α crystalline phase. This may augment drug release owing to the following possibilities.

A. Due to a greater crystalline order, the oriented α crystalline phase may already contain several chain ends concentrated in the inter / intra-lamellar region. Insertion crystallisation of such matrices will further enhance the number of defect zones, Therefore, formation of water filled channels and associated drug release can be higher from the oriented crystalline films.

B. Presence of an ordered α crystalline form led to a rise in the polar surface energy of oriented PLA films (UCW $\lambda \geq 3X$). This was attributed to a relative increase in the concentration of polar functional groups (hydroxyl) on the film surface. Since such an order is repeated in the bulk of the oriented films (UCW $\lambda \geq 3X$), the overall hydrophilicity of the bulk might be enhanced. This may augment percolation of water and consequently, drug release.

C. The α crystalline form has a lamellar structure; where, the lamellar stacks are aligned in the drawing direction (figure 6.38). Percolation of water might be easier in such a structure in contrast to a spherulitic structure (generated in the previously amorphous matrices, due to insertion crystallisation). Alternatively, it can be said that a continuous channel formed due to permeation of water might be longer/deeper and less tortuous in oriented crystalline films, owing to the regular chain organisation. Consequently, the drug release from such films was higher than from un-oriented films.

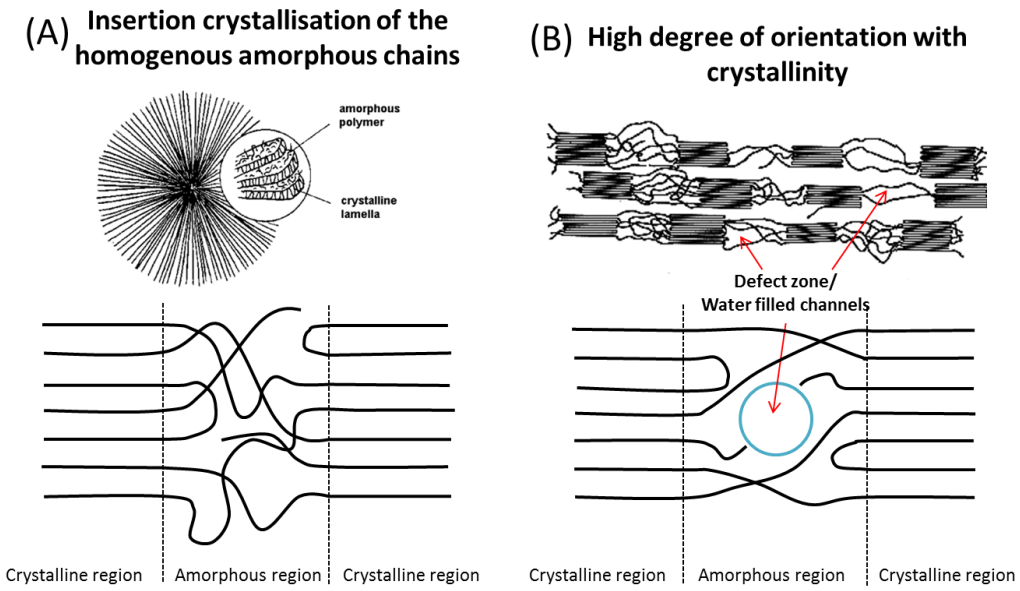

Figure 6.38: *A model explaining concentration of chain defects in the inter-lamellar region of highly oriented PLA films containing a 3-dimensional crystalline order (Tsuji et al., 2000)*

Interestingly, biaxially oriented TPLA films (both SB – 2X2Y and SEQ-2X2Y) and films with a UCW draw ratio of 2X, exhibited slower drug release than the un-oriented films. An important difference in the structure of these films and the films with higher UCW draw ratio was that the former films contained amorphous PLA chains aligned in the drawing direction, with negligible crystallisation. In such films, increased packing of the amorphous chains may reduce the diffusivity of the matrix. Nevertheless, insertion crystallisation in such matrices may occur randomly, resulting into a structure which has fewer defects and highly convoluted fluid filled channels. Therefore, the reduction in the drug release in the mentioned films can be attributed to the increased orientation of the amorphous chains without generation of the α crystalline phase.

Drug release reduced in order from UCW-2X films to SEQ-2X2Y and finally to SB-2X2Y films. This can be correlated with the oriented structure of the mentioned films. As explained in section 6.4, UCW stretching to $\lambda = 2X$, produced uniaxially oriented amorphous chains. The sequential stretching of such films in the perpendicular direction rotated a part of the already oriented

chains; whereas, biaxial orientation generated an oriented orthotropic structure (organisation of the chains almost parallel to the two orthogonal stretch directions but in the film plane). The orthotropic biaxial structure has been found to reduce diffusivity of the polymer matrices to a greater extent (Delpouve *et al*., 2012; Jang and Lee, 2004) by substantially increasing the matrix tortuosity, than that observed with uniaxially oriented matrices (Delpouve *et al*., 2012; McGonigle *et al*., 2001). This may explain the reduction in drug release rate in an order from UCW (λ = 2X) TPLA films, SEQ (λ = 2X2Y) TPLA films and finally SB (λ = 2X2Y) TPLA films.

CPLA films oriented to UCW draw ratio of 2X or biaxial draw ratio of 2X2Y (both SB and SEQ) underwent shrinkage, after incubation (at 37 °C) in the release medium. Consequently, these films showed little difference in the curcumin release profile (figure 6.37) than that obtained from un-oriented CPLA films. This observation further emphasizes the importance of amorphous orientation in reducing drug release rate from oriented films.

6.9.2.4. Effect of orientation of the kinetics of the phase II drug release

The kinetic models explained in the section 6.9.2.2 confirmed that curcumin release from oriented as well as un-oriented CPLA films followed the zero order kinetics. Similarly, theophylline release from TPLA films was confined to the Higuchi model, regardless of the degree and the nature of orientation. Therefore, it is safe to state that solid-state orientation of PLA films did not alter the mechanism of drug release. Despite of this, the slope of the kinetic curves (cumulative drug release Vs time or cumulative drug release Vs time$^{1/2}$) changed after solid-state orientation of PLA films (figure 6.35 and figure 6.37). For theophylline the slope represented the rate of diffusion, while for curcumin it represented the release rate.

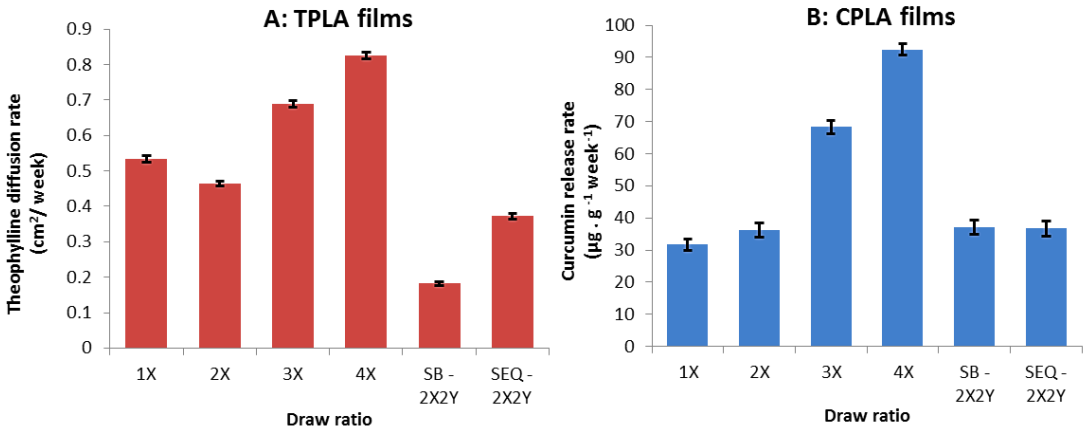

Figure 6.39: *Effect of solid state orientation on kinetics of drug release.*

* The theophylline diffusion rate was calculated from the slope of the cumulative release Vs time$^{1/2}$ curves (regression lines), which were linear in the case of TPLA films. Similarly, the curcumin release rate in µg.g $^{-1}$.week $^{-1}$ units was calculated by plotting cumulative µg of curcumin released per gram of CPLA films against time in weeks. The cumulative curcumin release exhibited a linear relationship with time, instead of with the square root of it. Therefore the slope of such curves represented the curcumin release rate.

**The error bars in both cases represent the standard error obtained by regression analysis of the respective data.

The change in slope with respect to draw ratio is represented in figure 6.39. It is evident that UCW orientation to the draw ratio of 2X led to a slight reduction in the diffusivity; while a larger difference was observed after biaxial orientation to the 2X2Y draw ratio. Contrarily orientation to UCW $\lambda \geq 3X$, progressively increased the diffusivity. A regression analysis of the diffusivities of TPLA-1X, TPLA-3X and TPLA-4X films confirmed that there was a possibly significant ($P = 0.09$, $F = 45.73$) linear ($R^2 = 0.9786$) correlation between the diffusivities and the draw ratios of these films. This relationship is graphically represented in figure 8.4. It is believed that once a drug molecule is released from a polymeric matrix, it still has to diffuse through a thin, unstirred layer of the release medium that immediately surrounds the matrix. This layer therefore contributes to the overall diffusivity of the drug. According to the drug release

study protocol utilised here, the release medium was replaced at weekly intervals. This can potentially disturb the unstirred liquid layer. Consequently, the theophylline diffusivity values obtained from the slope of the Higuchi curves will have a small error. Therefore, it can be assumed that in the absence of such an error, the linear relationship between theophylline diffusivity and draw ratios ($\lambda \geq 3X$) can be highly significant.

In contrast to TPLA films, the biaxially oriented ($\lambda = 2X2Y$) CPLA films and those oriented to UCW draw ratio of 2X, showed release rates comparable to un-oriented CPLA films. As discussed previously, this can be attributed to shrinkage of the mentioned CPLA films, resulting in loss of their orientation. This difference between the CPLA and the TPLA films highlighted that orientation had an influence on drug release. The CPLA films drawn to UCW draw ratios of 3X and 4X displayed enhancement of curcumin release rate, similar to the TPLA films oriented to the same draw ratios. Regression analysis of the release rates from CPLA-1X, CPLA-3X and CPLA-4X films suggested that there existed a statistically significant ($P < 0.05$, $F = 197.02$) linear ($R^2 = 0.9950$) correlation between curcumin release rates and draw ratios of these films. This relationship is graphically represented in figure 8.4.

Overall, the results of kinetic analysis emphasised that control of drug release rate can be imposed by controlling the draw ratio. Nevertheless, retardation of drug release from oriented amorphous matrices was reported here for the first time. The current study also highlighted the importance of the incorporated drug in affecting its elution from the oriented films

6.9.3. Phase 3: Erosion controlled release

The diffusion mediated release phase lasted for approximately 16 weeks, following which the drug release from all the films increased in an exponential manner (figure 6.30, figure 6.31 & figure 6.40). The exponential drug release overlapped with dramatic changes in the film properties that are summarised in section 6.8. By the 20^{th} week molecular weight of the films reduced significantly.

The fall in molecular weight was accompanied by a sharp decline in the polydispersity of the films between the 16th and 20th week (sec. 6.8.4). The mechanical strength of the smaller circular sections was lost by the 20th week and they could be easily crushed between the fingers. Scanning electron microscopy revealed formation of cracks on the transverse surface; while cryo-fractured sections showed a highly porous internal structure (sec. 6.8.5). Moreover, the films exhibited weight loss and the pH of the release medium became more acidic. These changes clearly indicate erosion of the films. Consequently, an exponential upsurge in drug release was evidenced.

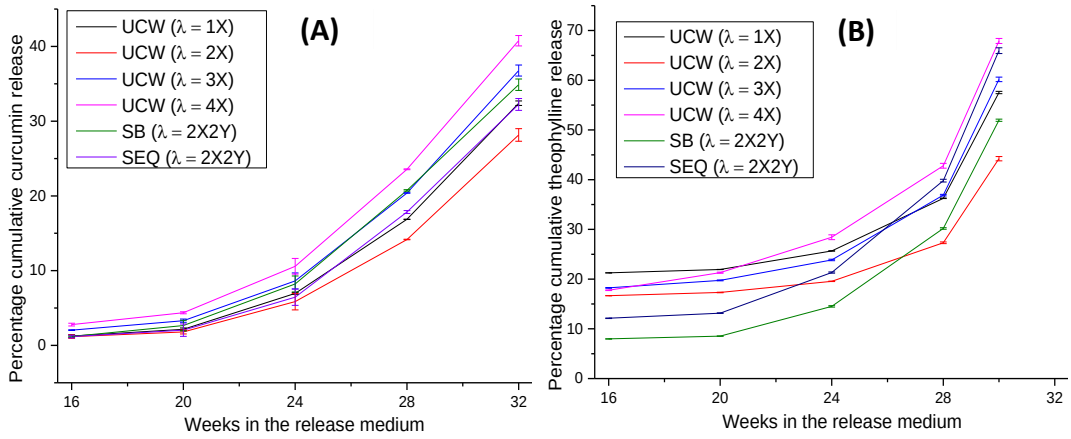

Figure 6.40: *Percentage cumulative drug release during the erosion phase*

(A) Release of curcumin from CPLA films, **(B)** Release of theophylline from TPLA films

*The graph represents cumulative drug release as the mean ± standard deviation; for n = 6

Surprisingly, the onset of the erosion phase was similar for all studied films regardless of whether and how the films were oriented. (The exact onset could not be detected because sampling after the 16th week was carried out every 4 weeks. However the erosion of all studied films started between the 16th and the 20th week). Since the films started falling apart in the erosion phase, drug release occurred in an uncontrolled manner. Consequently, there was not a characteristic correlation between drug release from the studied films and their degree and nature of orientation.

6.10. Summary

This chapter reported changes in the crystalline structure of drug loaded PLA films, with respect to drawing temperature, strain rate, draw ratio and mode of drawing; i.e. uniaxial or biaxial. A comprehensive understanding of the structural changes associated with orientation of drug loaded PLA films, can be later used for creating a design rule for controlled drug delivery through oriented biodegradable polymers.

In the current study, few samples were shortlisted for drug release and related characterisations. The films oriented to a uniaxial constant width (UCW) draw ratio (λ) of 2X (using selected conditions), exhibited anisotropic alignment of amorphous chains with negligible strain induced crystallisation. At λ = 3X an oriented α PLA crystals were generated; whereas, further drawing led to additional improvement in the structural order and crystallinity. Films oriented biaxially to a draw ratio of 2X2Y (in the simultaneous biaxial mode as well sequential biaxial mode), were predominantly amorphous and contained orthotropic organisation of PLA chains. UCW orientation of the films resulted in an overall rise in the surface energy, perhaps due to regular arrangement of the PLA chains. When a rise in draw ratio produced α crystalline order, the polar component of surface energy was enhanced.

The investigated PLA matrices underwent hydrolytic degradation by the bulk erosion mechanism. A monotonous fall in molecular weight was observed after submerging the PLA films in the drug release medium. However, oligomers generated in this process remained entrapped within the bulk of the films for the first 16 weeks. Path followed by the percolating medium was transformed into fluid filled channels, whose size and number increased gradually. Actual erosion of the films started from the 20^{th} week. Withstanding this degradation pattern, all studied films showed biphasic drug release. For the first 16 weeks the model drugs were predominantly released by diffusion through the polymer matrix and transport through fluid filled channels. From the

16th week onwards, drug release was progressively accelerated due to onset of polymer erosion. Orientation of drug loaded PLA films mainly influenced drug release in the prior phase. Oriented films which were predominantly amorphous in nature (UCW λ = 2X & Biaxial λ = 2XY) showed retardation of drug release only when the amorphous orientation was stabilised by the presence of a crystalline drug (i.e. theophylline). Contrarily, oriented amorphous films containing a drug in a glassy solution state (i.e. curcumin), shrunk after submersion into the release medium. Consequently, such films showed a drug release profile similar to un-oriented films. All UCW oriented films, which contained oriented α crystalline form showed acceleration of drug release with respect to draw ratio. A probable mechanism was predicted, according to which augmented formation of fluid filled channels in oriented crystalline films may be held responsible for acceleration of drug release. The proposed mechanism can be confirmed in the future by quantifying porosity of oriented drug releasing matrices and studying changes in their crystalline/ porous structure as they are aged to in the release medium.

7. Directional drug release from oriented rods: results and discussion

The previous chapter systematically reported the effect of the degree and nature of polymer orientation (e.g. uniaxial, biaxial) on drug release, using a simple two dimensional geometry, i.e. films. It was evidenced that the structural organisation within the oriented films significantly influenced the drug release profile. Based on this finding, it was hypothesised that anisotropic structural organisation after uniaxial orientation, may produce a direction specific drug release pattern. This chapter discusses the results that validate this hypothesis. The initial section of the chapter includes WAXD and MDSC results that establish development of the uniaxially oriented anisotropic structure in the die-drawn, paracetamol loaded PLA rods. In the later sections assessment of morphological changes in the oriented rods following aqueous submersion and drug release profiles exhibited by these rods is discussed, with an attempt to identify the directionality in drug release rate and its correlation with draw ratio.

7.1. Uniaxial structure evolution in die-drawn PLA rods

The paracetamol loaded PLA (PPLA) rods studied here were oriented using the die-drawing method. The technique originally invented by Coates *et al.* (1979; 1981), relies upon pulling a heated polymer billet through a heated converging die. The compressive stress exerted by the conical die walls combined with the tensile stress, promotes polymer chain organisation in the drawing direction. Therefore, an anisotropic structure is developed following die drawing (section 3.8.1.2).

7.1.1. Anisotropic structure

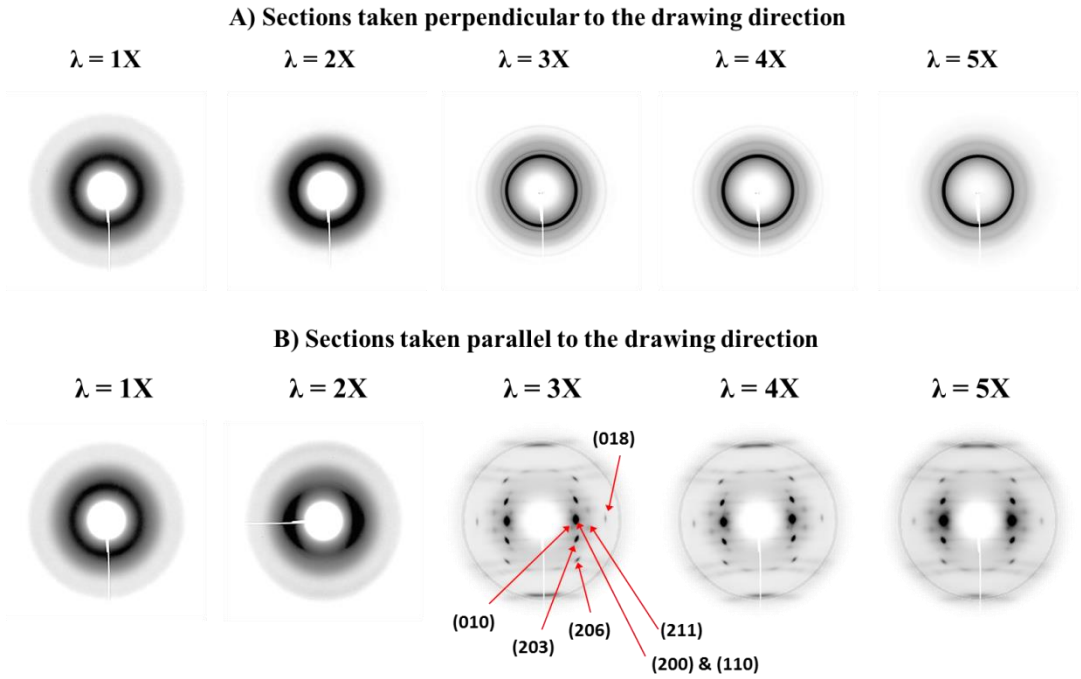

Figure 7.1: *WAXD diffraction patterns of paracetamol loaded rods oriented to different draw ratios.*

(A) Cross section/ transverse section, **(B)** Lateral section

Development of an anisotropic structure in the die drawn PPLA rods is depicted in figure 7.1, through WAXD diffraction patterns. Cross sections of the oriented rods (sectioned perpendicular to the drawing direction) showed homogenous 2D WAXD patterns, indicating an absence of structural anisotropy in the transverse plane. Samples oriented to a draw ratio of 2X exhibited a diffuse isotropic scatter, resembling the un-oriented amorphous rods. Nevertheless, the brightness of the amorphous halo was higher at λ = 2X, indicating densification of the amorphous chains. Further orientation to draw ratios of 3X, 4X and 5X led to strain crystallisation. The cross sections of the mentioned samples showed crystalline reflections in the (200, 110) and (203) crystallographic planes, appearing as a complete azimuthal ring.

In contrary to above observation, the lateral sections (sectioned parallel to the drawing direction) of the PPLA rods exhibited a clear evolution of the anisotropic structure, with respect to the draw ratio. The un-oriented samples

showed an isotropic halo, suggesting existence of a homogenous amorphous matrix. At a draw ratio of 2X, organisation of amorphous chains along the drawing direction resulted in concentration of the amorphous halo towards the equator. A three dimensional crystalline order was developed at λ = 3X. The azimuthal spread of the crystalline reflections ((203) and (200, 110)) progressively reduced on further drawing, signifying further refinement of the structure in the drawing direction. Altogether, the 2D WAXD patterns confirmed that the oriented PPLA rods had an anisotropic structure, where the PLA chains were exclusively oriented in the drawing direction.

7.1.2. Evolution of the oriented structure with respect to draw ratio

The changes in 2D WAXD patterns (sec 7.1.1) of the oriented PPLA rods were closely aligned with the trend in their percentage crystallinity (figure 7.2). The extrusion moulding process involved rapid quenching of the mould in a water bath. Consequently, the un-oriented rods were practically amorphous in nature (figure 7.2).

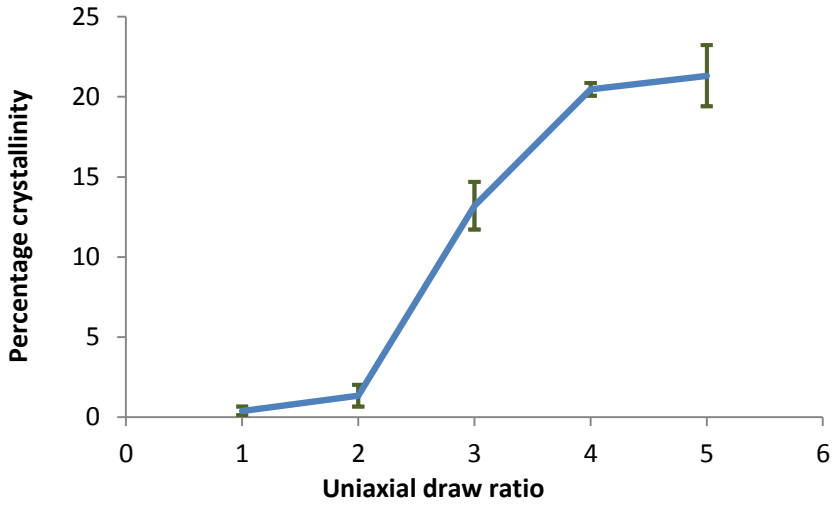

Figure 7.2: *Changes in percentage crystallinity and glass transition temperature of the die-drawn rods, with respect to uniaxial draw ratio.*

*The glass transition temperature and % crystallinity values are expressed as mean ± SD, where n = 6.

Table 7.1: *Statistical comparison of crystallinity of the die drawn rods by paired t-test*

Property	Draw ratio	Paired t-test comparison
% Crystallinity	1X Vs 2X	P = 0.1524, t = 2.259
	2X Vs 3X	P = 0.0112, t = 9.374
	3X Vs 4X	P = 0.0024, t = 20.509
	4X Vs 5X	P = 0.8112, t = 0.2718

Notes: For relevant data refer figure 7.2.

The null hypothesis was that the compared samples were statistically the same

P > 0.05 = The difference between the compared samples is **not statistically significant**

0.05 > P > 0.01 = The difference between the compared samples is **statistically significant**

0.01 > P = The difference between the compared samples is **highly significant**

At a draw ratio of 2X, the crystallinity of the rods remained statistically equivalent to un-oriented rods (table 7.1). This can be attributed to alignment of the amorphous chains, generating a nematic phase (figure 7.1 – λ = 2 & figure 7.4). Further stretching to a draw ratio of 3X results in strain induced crystallisation. The deformation stress aligns the newly generated crystals in the drawing direction. Moreover, such crystals stabilise the remaining amorphous chains in their oriented state. Therefore at λ = 3X, a sharp rise in the crystallinity was observed, along with generation of a WAXD pattern characteristic of an oriented semicrystalline PLA (figure 7.1 – λ = 3X). The crystallinity increased almost linearly between draw ratios of 3X and 4X, suggesting further reinforcement of the oriented structure. The rise in crystallinity at both of these draw ratios was statistically validated by a paired t-test comparison to the preceding draw ratio (table 7.1). On extension to λ = 5X, crystallinity of the oriented PPLA rods remained practically constant (P = 0.8, table 7.1). This can be attributed to fragmentation of the existing crystals, accompanied by orientation of amorphous chains leading to strain crystallisation (Zhang *et al*., 2011). Evolution of an anisotropic chain organisation in the die drawn rods is depicted in figure 7.3

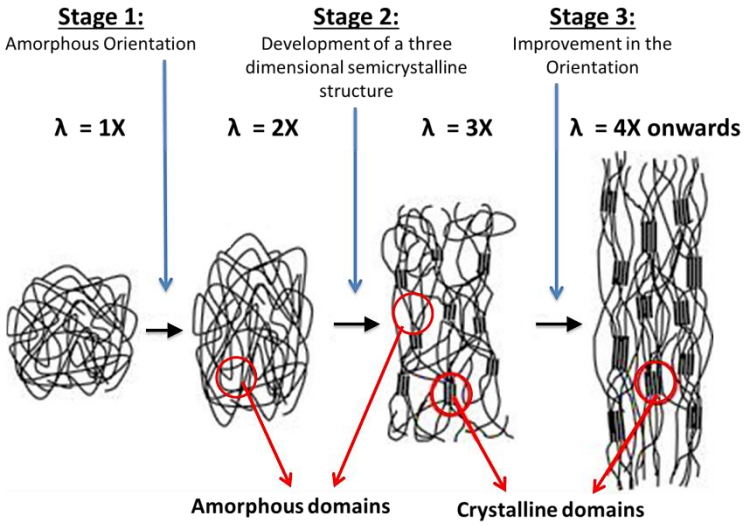

Figure 7.3: *Evolution of an anisotropic chain organisation in the die drawn rods (Adapted from (Ou and Cakmak, 2008))*

Strain induced fragmentation of crystals in the oriented PLA matrices leads to a lateral broadening of the crystalline reflections (Kokturk *et al*., 2002). Nevertheless, such broadening is also associated with the presence of a disordered α crystal form, alternatively known as the α' Form or the δ Form (Wasanasuk and Tashiro, 2011). Similar to the α crystal form observed in oriented PLA films (sec. 6.4), the α' Form has a -10/3 helical conformation and packs into the orthorhombic or pseudo-orthorhombic unit cell (Zhang *et al*., 2008). However, the -10/3 helix of the α Form assumes a 2_1 screw symmetry along the chain axis; while such a symmetry is absent in the α' Form (Wasanasuk and Tashiro, 2011). Consequently, the molecular chains of the α' Form are considerably disordered. This further changes the unit cell parameters of the α' Form as well as the arrangement of the higher order domains (Pan *et al*., 2008; Wasanasuk and Tashiro, 2011).

Due to common fundamental chain organisation, the spectral profiles of both the α and the α' Form look similar. However, in the case of the α' Form, the 2D WAXD bands are thicker and Bragg's angle (2θ) position of certain bands is slightly altered. WAXD patterns of oriented rods showed characteristic reflections at the (200/110), (203), (206) and (018) crystallographic planes

(figure 7.1), corresponding to the Bragg's angle (2θ) of 16.4°, 18.8°, 24.5°, 32.6°. Here the Bragg's position of the (200/110), (203) and (206) reflections was shifted by 0.3° with respect to the α Form. Moreover, the reflection in the (020) plane shown by the α Form was replaced by the (018) reflection, which appeared at 32.6° Bragg's angle in the one dimensional diffractogram. These characteristic features of the WAXD data were consistent with the literature reports on the α' Form of PLA (Chen *et al*., 2011; Pan *et al*., 2008; Wasanasuk and Tashiro, 2011; Zhang *et al*., 2008). Therefore, the results confirmed development of the α' crystalline form of PLA during die drawing of the PPLA rods.

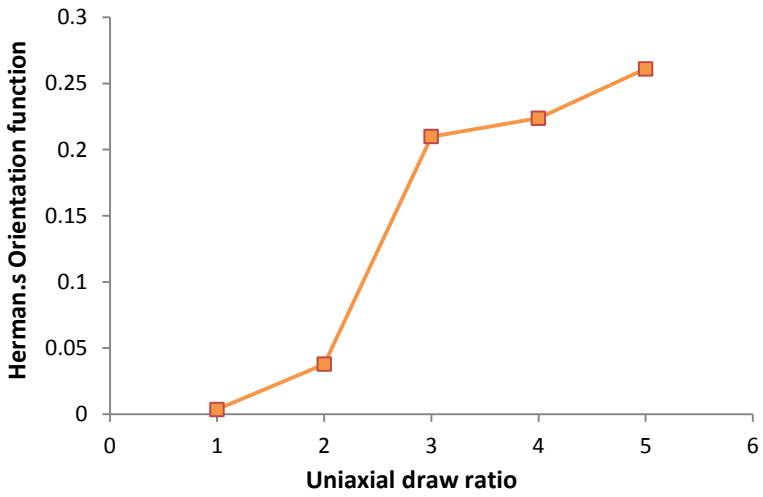

Figure 7.4: *Changes in Herman's orientation function calculated for die-drawn rods, with respect to the uniaxial draw ratio.*

A further insight into the structural organisation of oriented PPLA rods was obtained by deriving Herman's orientation function (sec 4.13 – eqn. 4.5), from the WAXD data. This allows a quantitative expression of the degree of unidirectional orientation. Die drawing of the PPLA rods augmented the orientation function in three distinguishing steps (figure 7.4), coherent with 2D WAXD patterns and the crystallinity data (figure 7.1, figure 7.2). Up to a draw ratio of 2X, plastic deformation of the amorphous chains without strain crystallisation only enhanced the orientation function by a smaller margin. A

major improvement in the structural order occurred between draw ratios of 2X and 3X, due to the onset of strain crystallisation. Following this stage, previously un-oriented chains or chains resulting from the fragmentation of strained crystals are merely inserted in to the existing three dimensional order. Therefore, the orientation function increased gradually between λ = 3X and λ = 5X (Mulligan and Cakmak, 2005, Wong *et al*., 2008). Evolution of an oriented structure in the die-drawn PPLA rods, significantly matched with that observed in UCW orientation of PLA films (sec. 6.4). This suggests a similarity between the mentioned orientation methods under the processing conditions utilised in this study. Nevertheless, it highlights the importance of polymer composition (grade) in affecting the structure development.

7.2. State of the PLA matrix during drug release

Due to a limited number of samples, changes in the molecular weight, crystallinity and microscopic changes in the morphology of the PPLA rods were evaluated only at the end of the drug release study. During the release study, PPLA rods were monitored for the visual alterations. This information is summarised below. In the following section the oriented PPLA rods with draw ratios of λ = 2X, λ = 3X, λ = 4X and λ = 5X are referred as PPLA-2X, PPLA-3X, PPLA-4X and PPLA-5X respectively for simplification.

7.2.1. Visual changes

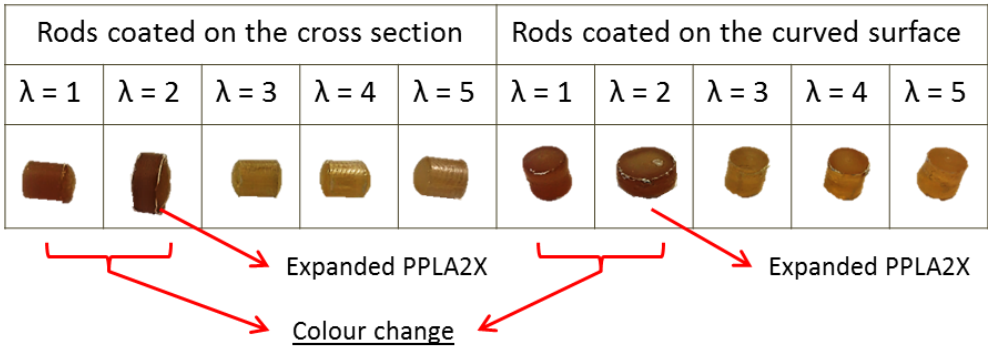

Figure 7.5: *Visual changes in PPLA rods during drug release study*

*(The above representative image was captured at the end of the study; i.e. 16 weeks)

Two prominent visual changes were detected in the PPLA rods during the drug release studies. Firstly, between the 10th and the 20th day, the PPLA-2X rods progressively expanded to 89% of their cross sectional area before die-drawing (i.e. 178% of their cross sectional area after die drawing or equivalent to λ =1.12) (figure 7.5). This signifies that the mentioned rods lost a large proportion of the oriented structure, by the end of the third week, when submerged in the drug release media (at 37 °C). As discussed previously, the PPLA-2X rods contained oriented amorphous chains with a negligible crystallinity. When such rods are submerged in the drug release media, the permeated water plasticises the polymer matrix, allowing the amorphous chains to recoil back to the homogenous state. Here the extent of recovery is limited by insertion crystallisation of the matrix in presence of water.

The second important observation was that the colour of the PPLA rods darkened as the study progressed. The most prominent change was observed with un-oriented and PPLA-2X (expanded) rods, which turned amber brown after about 10 weeks (figure 7.5). This was initially attributed to higher degradation of the un-orientated rods compared to the oriented rods (similar to the PLA films – sec 6.8.3). However, molecular weight determination at the end of the study revealed that the reverse was true. Therefore, the exact reason for such a colour change could not be identified at the present stage.

7.2.2. The molecular weight changes

Un-oriented PPLA rods showed molecular weight degradation (table 7.1) comparable to the un-oriented drug loaded PLA films (sec. 6.8.3), after 16 weeks of aqueous submersion. Surprisingly a monotonous GPC peak was obtained; suggesting that the rods left at the end of the 16th week were homogenously degraded throughout the bulk. The PPLA-2X rods underwent expansion and lost the majority of their oriented structure. Therefore, the degradation profile of PPLA-2X rods matched with that of the un-oriented rods.

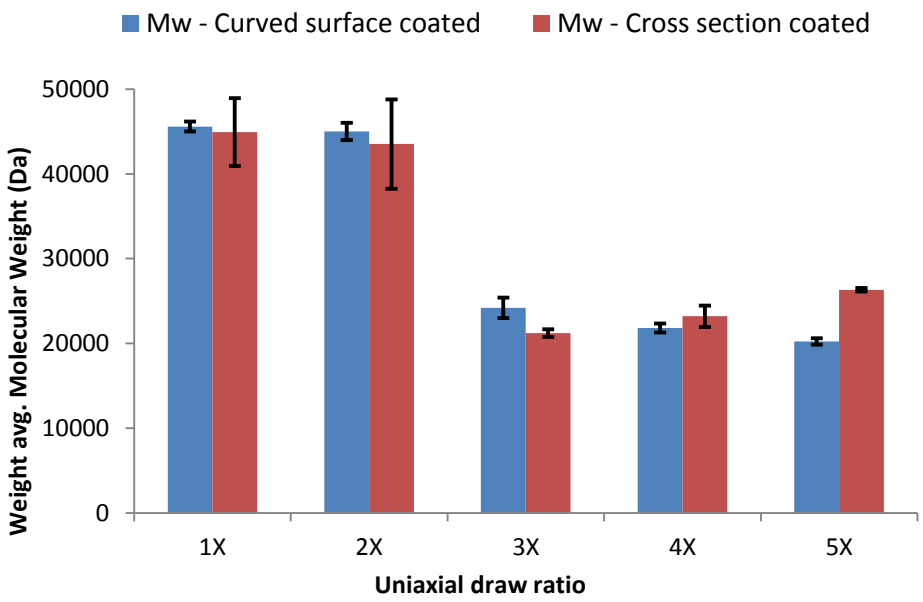

Figure 7.6: *Molecular weight (Mw) of PPLA rods at the end of the drug release studies*

*The values of molecular weight and polydispersity are expressed as mean ± SD, where n = 6.

Table 7.2: *Statistical analysis of the molecular weight at the end of the release study by one-way ANOVA - Tukey's test comparison between draw ratios.*

Comparison	Molecular weight	
	Cross section coated	Curved surface coated
1X vs 2X	P > 0.05, q = 1.77	P > 0.05, q = 1.13
1X vs 3X	P < 0.001, q = 64.41	P < 0.001, q = 19.25
1X vs 4X	P < 0.001, q = 71.58	P < 0.001, q = 17.63
1X vs 5X	P < 0.001, q = 76.34	P < 0.001, q = 15.1
2X vs 3X	P < 0.001, q = 62.64	P < 0.001, q = 18.12
2X vs 4X	P < 0.001, q = 69.81	P < 0.001, q = 16.5
2X vs 5X	P < 0.001, q = 74.57	P < 0.001, q = 13.96
3X vs 4X	P < 0.001, q = 7.17	P > 0.05, q = 1.62
3X vs 5X	P < 0.001, q = 11.93	P > 0.05, q = 1.16
4X vs 5X	P < 0.05, q = 4.76	P > 0.05, q = 2.54

Table 7.3: *Statistical comparison of molecular weights of PPLA rods before and after completion of the release study, by one-way ANOVA followed by Tukey's test.*

Comparison	Molecular weight				
	1X	2X	3X	4X	5X
0 week Vs 16 weeks cross section coated	P < 0.001, q = 86.59	P < 0.001, q = 75	P < 0.001, q = 325	P < 0.001, q = 358	P < 0.001, q = 421
0 week Vs 16 weeks curved surface coated	P < 0.001, q = 87.22	P < 0.001, q = 76.16	P < 0.001, q = 333	P < 0.001, q = 354	P < 0.001, q = 398
16 weeks cross section coated Vs 16 weeks curved surface coated	P > 0.05, q = 0.63	P > 0.05, q = 1.16	P < 0.001, q = 8.46	P < 0.05, q = 4.27	P < 0.001, q = 22.32

The null hypothesis was that the compared samples were statistically the same

P > 0.05 = The difference between the compared samples is **not statistically significant**
0.05 > P > 0.01 = The difference between the compared samples is **statistically significant**
0.01 > P = The difference between the compared samples is **highly significant**

A remarkable difference was found between the hydrolytic degradation of oriented drug loaded PLA films (λ ≥ 3X) and oriented PPLA rods (λ ≥ 3X). Tensile drawing of the PLA films above a draw ratio of 3X hindered their hydrolytic degradation. On the contrary, degradation was significantly higher in the oriented PPLA rods (λ ≥ 3X). It is evident from figure 7.6 that the molecular weight of the PPLA-3X, PPLA-4X and PPLA-5X rods was nearly half as much as the molecular weight of the un-oriented rods, after 16 weeks of submersion. This can perhaps be attributed to formation of macroscopic cracks in the mentioned rods (figure 7.9). The presence of large cracks might have enhanced water uptake by the rods, thereby accelerating their degradation. An augmented degradation of the oriented PPLA rods (λ ≥ 3X), can further enhance the drug release by increasing mass transport by several mechanisms.

The difference between molecular weights of the rods oriented to various draw ratios was statistically validated by one-way ANOVA – Tukey's test (table 7.2). All rods had statistically equivalent molecular weight regardless of the draw ratio, at the beginning of drug release study. At the end of the study un-oriented and PPLA-2X rods displayed comparable (P > 0.05) molecular weight,

which was significantly higher than that of the remaining rods. When the curved surface was coated, the molecular weight of the PPLA-3X, PPLA-4X and PPLA-5X rods showed an absence of any statistically significant difference. Contrarily, when the cross section was coated, the rods oriented to higher draw ratios showed progressively lower degradation (or progressively higher molecular weights). Higher anisotropic orientation may lower water permeation perpendicular to the chain orientation due to increased chain packing. However, this may not greatly affect water permeation in the chain orientation direction (curved surface coated).

Molecular weights of the rods with coated curved surface and coated cross sections were statistically compared at the end of the study. The results of such analysis (table 7.3) confirmed that the un-oriented and PPLA-2X (expanded) rods showed no statistical difference between their molecular weights, regardless of which surface was exposed to the medium. Contrarily, a statistically significant difference was observed between the molecular weights of the curved surface coated and cross section coated rods, whose draw ratio was greater than or equal to 3X. This observation highlighted a possibility that water permeation can be anisotropic in the uniaxially oriented rods. If true, drug release can also be expected to have a directional dependency.

7.2.3. Crystallinity changes

Submersion of the PPLA rods in the release medium resulted in a crystallinity rise due to insertion crystallisation of PLA. All PPLA rods showed substantially higher crystallinity after 16 weeks of aqueous submersion than their original crystallinity (figure 7.7, table 7.5). A statistical comparison between the crystallinity values obtained at the end of the release study revealed the following (table 7.4). When cross-sections of the rods were protected from direct contact with water, all rods oriented to $\lambda \geq 3X$, exhibited the same crystallinity at the end of the release study. Similarly, when the curved surface of the rods was protected from water, the PPLA-3X and PPLA-4X rods exhibited statistically

equivalent crystallinity, but the crystallinity of PPLA-5X rods was slightly lower. Although statistically significant, this difference was unsubstantial; consequently, it was ignored. A highly significant difference existed between the crystallinity values of un-oriented, PPLA-2X rods and the rods oriented to greater draw ratios (λ ≥ 3X) (table 7.4). The expanded PPLA-2X and un-oriented rods, which were initially amorphous, showed progressively lower crystallinity of 24.93% and 14.52% respectively than the λ ≥ 3X rods (figure 7.7).

A similar change in crystallinity was detected while studying drug release from oriented curcumin loaded films (sec. 6.8.2). All curcumin loaded films reached the same level of crystallinity by the 6th week after submersion into the release medium. However, towards 16 weeks the initially amorphous films (i.e. λ = 1X, 2X) exhibited a significantly lower crystallinity than the films which were inherently crystalline (λ = 3X, 4X). As explained previously, this can be attributed to differences in the organisation of the crystalline phase, between the two kinds of matrices mentioned above.

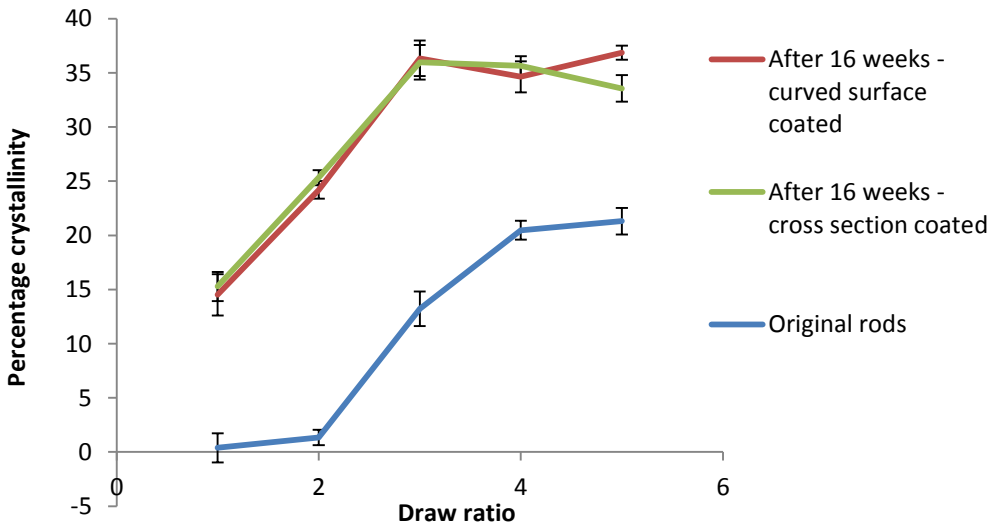

Figure 7.7: *The percentage crystallinity of the PPLA rods before and after the drug release studies.*

*The % crystallinity values are expressed as mean ± SD; where n = 6.

Table 7.4: *Statistical analysis of the percentage crystallinity at the end of the release study by one-way ANOVA - Tukey's test comparison between draw ratios.*

Comparison	% Crystallinity	
	Cross section coated	Curved surface coated
1X vs 2X	P < 0.001 q = 17.26	P < 0.001 q = 20.65
1X vs 3X	P < 0.001 q = 38.93	P < 0.001 q = 42.55
1X vs 4X	P < 0.001 q = 35.88	P < 0.001 q = 41.92
1X vs 5X	P < 0.001 q = 39.14	P < 0.001 q = 37.6
2X vs 3X	P < 0.001 q = 21.67	P < 0.001 q = 21.9
2X vs 4X	P < 0.001 q = 18.62	P < 0.001 q = 21.27
2X vs 5X	P < 0.001 q = 21.88	P < 0.001 q = 16.95
3X vs 4X	P > 0.05 q = 3.05	P > 0.05 q = 0.64
3X vs 5X	P > 0.05 q = 0.21	P < 0.05 q = 4.96
4X vs 5X	P > 0.05 q = 3.26	P < 0.05 q = 4.32

Table 7.5: *Statistical comparison of the percentage crystallinity values before and after completion of the release study, by one-way ANOVA followed by Tukey's test.*

Comparison	% crystallinity				
	1X	2X	3X	4X	5X
0 week Vs 16 weeks cross section coated	P < 0.001, q = 25.69	P < 0.001, q = 90.15	P < 0.001, q = 35.93	P < 0.001, q = 34.92	P < 0.001, q = 27.26
0 week Vs 16 weeks curved surface coated	P < 0.001, q = 27.09	P < 0.001, q = 94.61	P < 0.001, q = 35.36	P < 0.001, q = 37.46	P < 0.001, q = 22.04
16 weeks cross section coated Vs 16 weeks curved surface coated	P > 0.05, q = 1.4	P > 0.05, q = 2.72	P > 0.05, q = 0.57	P > 0.05, q = 2.54	P < 0.05, q = 4.46

The null hypothesis was that the compared samples were statistically the same

P > 0.05 = The difference between the compared samples is **not statistically significant**
0.05 > P > 0.01 = The difference between the compared samples is **statistically significant**
0.01 > P = The difference between the compared samples is **highly significant**

The crystallinity values obtained at the end of the study were regardless of whether the PPLA rods were coated on the curved surface or on the cross section (table 7.5). (PPLA-5X rods showed slightly anomalous behaviour). A difference in diffusion of water from the curved surface (diffusion direction

perpendicular to the orientation direction) and from the cross section (diffusion direction parallel to the orientation direction) may vary crystallisation of oriented PPLA rods. However, such a difference can only be detected in the early stages, before water saturates the entire rod. In the future, the differential movement of the crystallisation front from the curved surface and from the cross section will be traced using an XRD mapping technique.

7.2.4. Microscopic changes

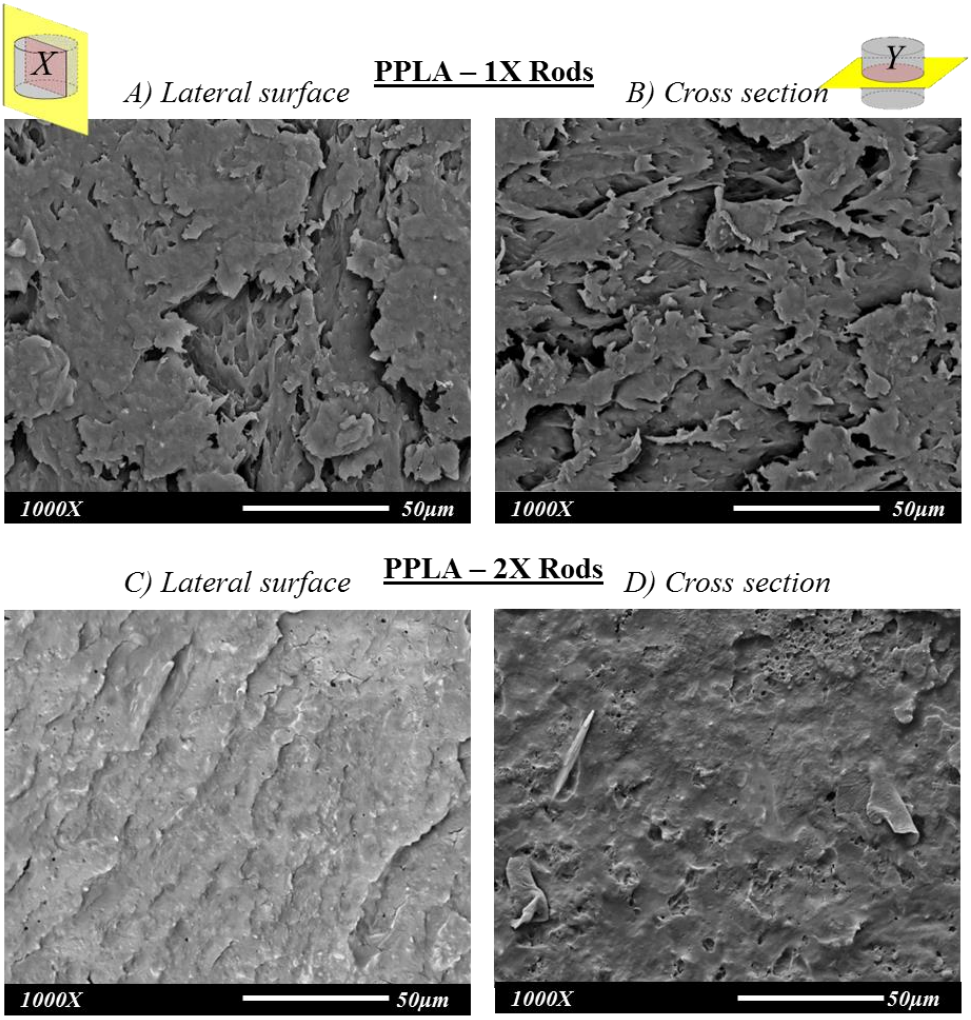

Figure 7.8: *Microscopic changes in the fractured lateral surface* ***(X)*** *and cross section* **(Y)** of un-oriented **(A, B)** and PPLA-2X rods **(C, D)**.

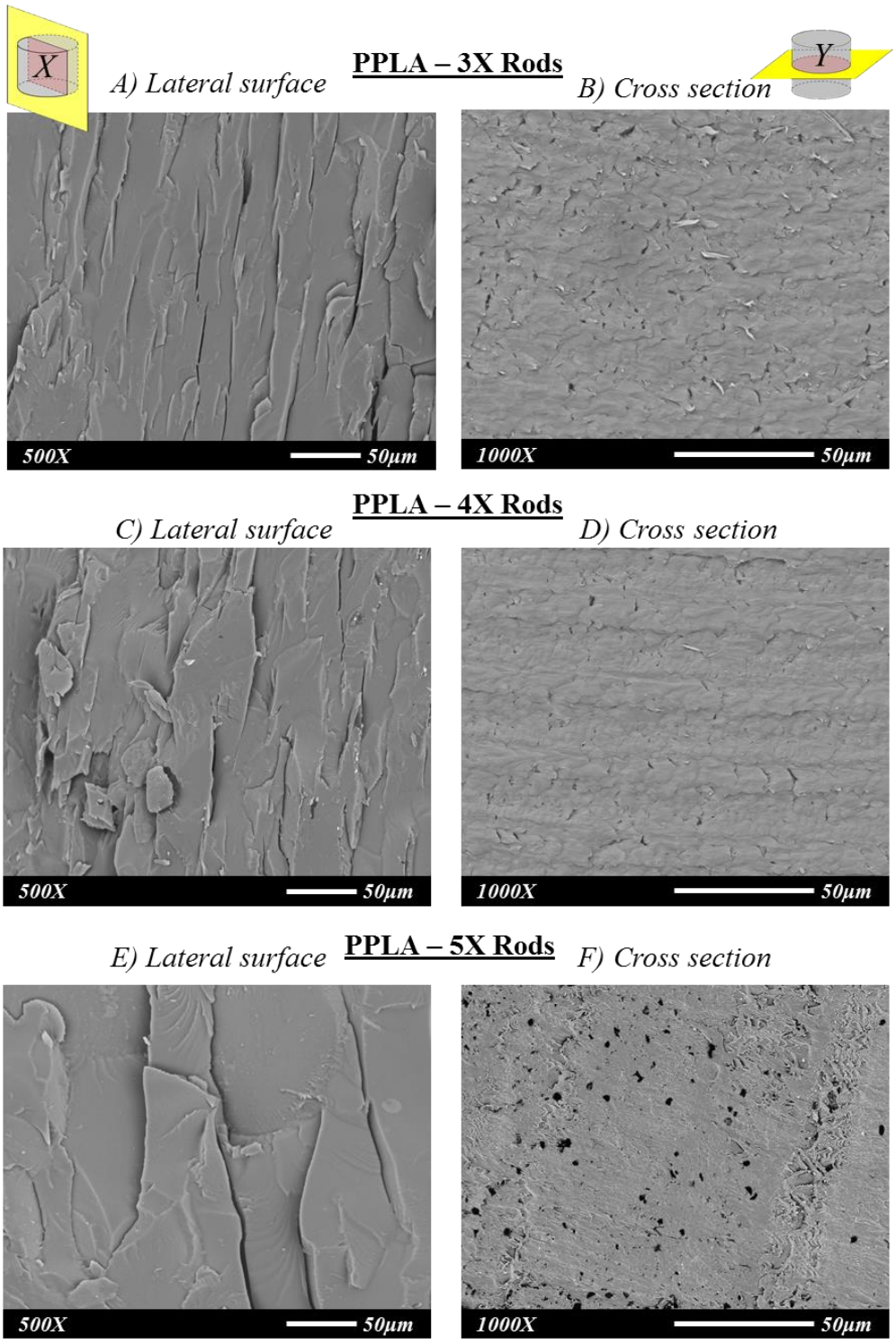

Figure 7.9: *Microscopic changes in the fractured lateral surface* ***(X)*** *and cross section* ***(Y)*** *of PPLA-3X* ***(A, B)****, PPLA-4X* ***(C, D)*** *and PPLA-5X rods* ***(E, F)****.*

In order to understand the microscopic changes in PPLA rods two distinct sections were obtained from samples remaining at the end of the drug release study. A transverse section was obtained by cryo-fracturing the rod parallel to

the base / cross section (figure 7.8 - Y), while a lateral section was obtained by cryo-fracturing the rod parallel to the curved surface (figure 7.8 - X). Irrespective of whether the rods were coated on the curved surface or on the cross section, they showed similar microscopic features at the end of the drug release study. These are represented below in figure 7.8 and figure 7.9

Un-oriented rods exhibited a homogenously degraded structure in both the lateral section and the cross section (figure 7.8 - A & B). The lateral section of PPLA-2X rods showed few striations, which were aligned parallel to the drawing direction (figure 7.8 - C). Since such striations were absent in the cross section (figure 7.8 - D), these might be considered as imprints of the residual orientation, in the expanded PPLA-2X rods. Both the lateral surface and cross section of the un-oriented and the PPLA-2X rods displayed minute cavities (1-2 μm). The presence of such cavities on either of the surfaces suggests that water-filled channels in the isotropic PPLA rods were formed randomly.

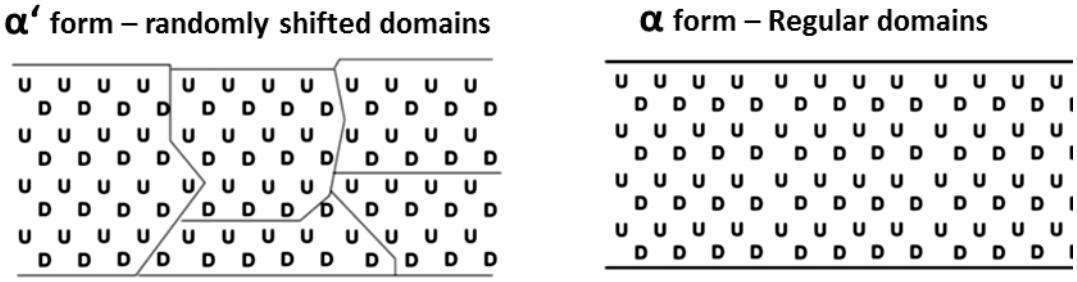

Figure 7.10: *Postulated structural difference between the α' and the α Form of PLA. (Wasanasuk and Tashiro, 2011)*

*(U and D signify up and down arrangement of 5 monomeric units in a 2_1 screw geometry)

Quite contrarily, the lateral sections of PPLA-3X, PPLA-4X and PPLA-5X rods showed formation of large crevices parallel to the drawing direction (figure 7.9). For PPLA-3X rods, the average width of the crevices was less than a micrometre; however their length was over 100 μm. The crevices became wider as the uniaxial draw ratio increased but their number reduced significantly.

WAXD studies on the die-drawn PPLA rods had confirmed that the rods oriented to the draw ratio of 3X and above, contained the α' crystalline form of PLA (sec. 7.1). The α' Form has a structural disorder at the unit cell level as well as between the macroscopic domains (figure 7.10) (Wasanasuk and Tashiro, 2011). Nevertheless, it has a sheaf-like structure in contrast to the lamellar structure of the α Form (Pan *et al*., 2008). All of the above factors clearly justify formation of the large crevices in the PPLA-3X, PPLA-4X and PPLA-5X rods. The crevices observed in the lateral sections were detected as voids in the cross sections. The presence of such morphology can perhaps explain higher degradation of the oriented rods. Nevertheless, it may lead to an extreme enhancement of the drug release, due to easy permeation of the release media.

7.3. Drug release from oriented rods

Uniaxial orientation of the polymeric matrices has been known to produce directionally dependent properties such as mechanical strength, refractive index, thermal conductivity, etc. (Kurabayashi, 2001; Ward, 1997; Ward and Sweeney, 2012). Since drug release from the oriented PLA matrices is influenced by the organisation of the polymer chains (chapter 6), an anisotropic chain orientation may produce a direction specific drug release. In this research, a possibility of obtaining direction specific drug release from the oriented PLA rods was evaluated for the first time.

7.3.1. Differential paracetamol release from the cross section and the curved surface

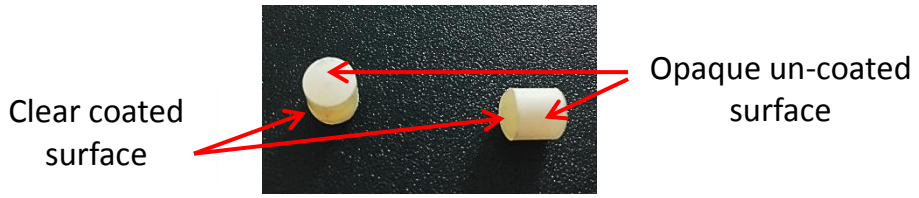

Figure 7.11: *Crystallisation of paracetamol on the uncoated surface of a PPLA rod*
*(When the submerged rod was subjected to drying)

In order to separately evaluate paracetamol release from the cross section, the curved surface of the PPLA rods was coated with a water impermeable epoxy polymer. Similarly, paracetamol release from the curved surface was studied by coating the cross section of the rods. The intactness of the coat was verified at weekly sampling intervals by microscopy. Nevertheless, a thin coat was reapplied at monthly intervals. If a submerged rod was withdrawn and allowed to dry, only the uncoated surface showed crystallisation of the drug, while the coated surface remained clear (figure 7.11). This observation further confirmed that the coated surface was protected from direct contact with water.

Preliminary drug release studies on the oriented films had revealed that the thickness of the films played a significant role by affecting the diffusional path-length and relative concentration gradient per unit film surface area. Therefore, the rods utilised in the drug release study were cut into 6 mm lengths, equivalent to their diameter. This way the diffusional path-length from the centre to the curved surface and from the centre to the cross sectional ends remained constant. However, with this approach the curved surface area became twice as large as the total cross sectional surface area. When drug release was not normalised against the surface area, un-oriented rods showed higher release from the curved surface than from the cross section. Since the un-oriented rods had an isotropic structure, differential release of paracetamol from the cross section and the curved surface can perhaps be attributed the difference in the respective surface areas. In order to avoid this effect, the amount of paracetamol released from the cross section and from the curved surface was divided by the respective surface areas.

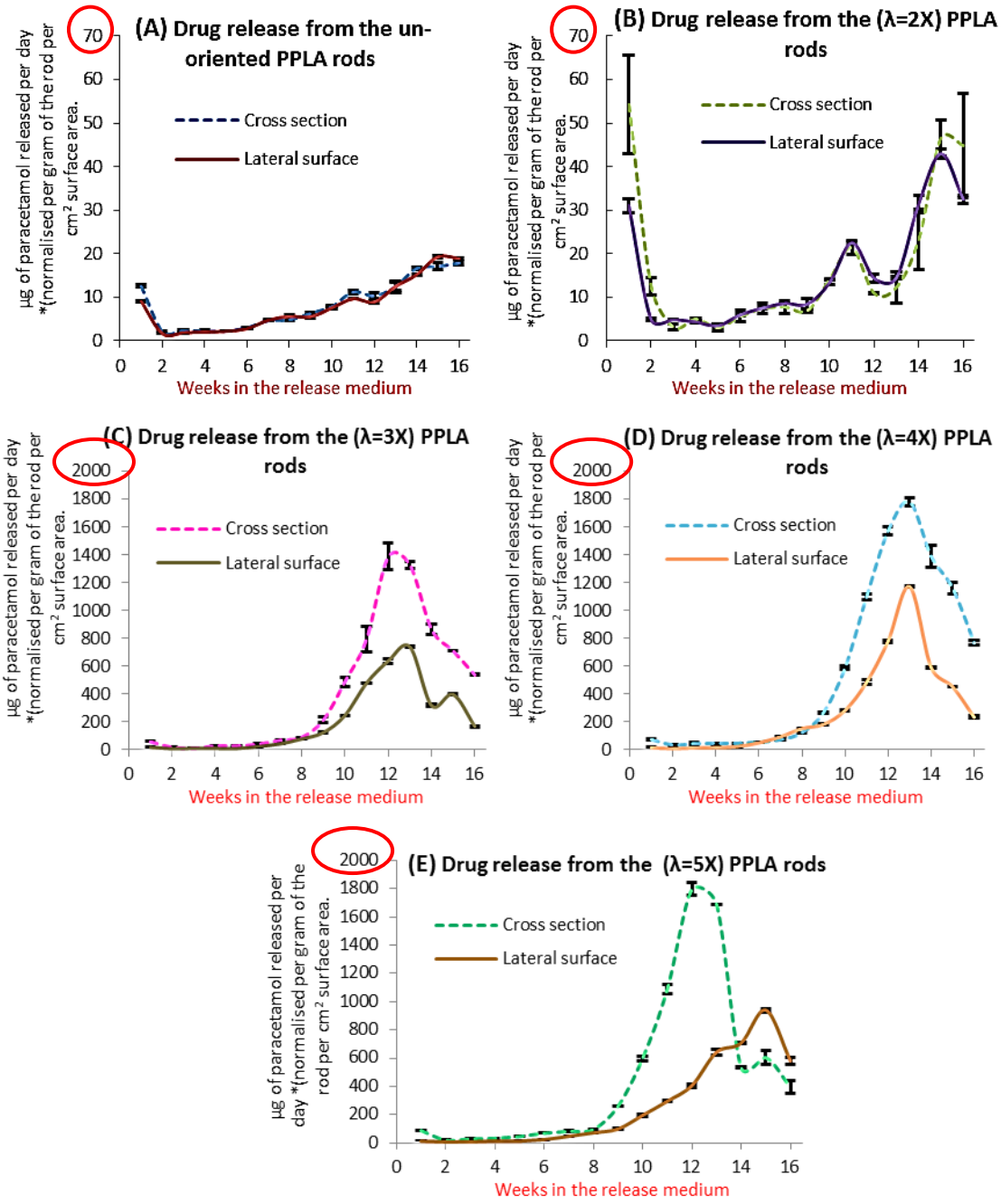

Figure 7.12*:** Comparison of the amount of paracetamol released on individual days per gram of the PPLA rods, from the curved surface and the cross section per cm^2 surface area. (A:*** *λ = 1X,* ***B:*** *λ = 2X,* ***C:*** *λ = 3X,* ***D:*** *λ = 4X,* ***E:*** *λ = 5X)*

*The cumulative drug release data is expressed as mean ± SD; where n = 6.

Table 7.6: *Statistical comparison between paracetamol release ($day^{-1}.g^{-1}.cm^{-1}$) from the cross section and the curved surface of the PPLA rods by paired t-test*

Intervals	Cross section Vs curved surface				
	1X	2X	3X	4X	5X
Week 4	P = 0.2287, t = 1.291	P = 0.1615, t = 1.642	P < 0.0001, t = 57.611	P < 0.0001, t = 48.183	P < 0.0001, t = 43.580
Week 8	P = 0.0472, t = 2.490	P = 0.2587, t = 1.247	P < 0.0001, t = 17.337	P < 0.0001, t = 177.29	P < 0.0001, t = 21.332
Week 12	P = 0.0658, t = 2.093	P = 0.005, t = 4.031	P < 0.0001, t = 18.788	P < 0.0001, t = 64.689	P < 0.0001, t = 70.741
Week 16	P = 0.07, t = 2.201	P = 0.0864, t = 1.924	P < 0.0001, t = 128.66	P < 0.0001, t = 70.534	P < 0.0001, t = 8.605

Notes: For relevant data refer figure 7.12.

The null hypothesis was that the compared samples were statistically the same

P > 0.05 = The difference between the compared samples is **not statistically significant**
0.05 > P > 0.01 = The difference between the compared samples is **statistically significant**
0.01 > P = The difference between the compared samples is **highly significant**

Figure 7.12 displays a comparison between paracetamol release from the cross section and from the curved surface of the oriented PPLA rods. It is evident that un-oriented rods released the same amount of paracetamol from the cross section and from the curved surface, when normalised with respect to the surface area (figure 7.12 - A). A similar drug release profile was shown by rods oriented to a draw ratio of 2X (figure 7.12 - B). This can be attributed to loss of the oriented structure, when the mentioned rods underwent expansion whilst ageing in the release media (sec. 7.2.1, figure 7.5). An absence of a statistical difference between paracetamol release ($day^{-1}.g^{-1}.cm^{-1}$) from the curved surface and the cross section of the un-oriented and PPLA-2X rods was validated by a paired t-test carried out at four different submersion intervals (table 7.6).

Contrary to un-oriented and PPLA-2X rods, the rods oriented to draw ratios of 3X, 4X and 5X exhibited a highly significant ($P < 0.0001$, table 7.6) difference in paracetamol release from the cross section and from the curved surface (figure 7.12 - C, D, E). Such a difference existed at all stages of drug release. However, because the drug release after 8 weeks was substantially higher, the difference before 8 weeks is masked in the overall drug release profile. For all of these samples, paracetamol release from the cross section exceeded that from the curved surface by a margin of 10-20 $\mu g.g^{-1}.cm^{-2}$ for the initial 60 days. From the 60^{th} day till the end of the study (112^{th} day = 16 weeks), paracetamol release from the cross section (per cm^2 surface area) was notably higher than that from the curved surface. Figure 7.12 further highlights that orientation of PPLA rods to $\lambda \geq 3X$ significantly accelerated the overall release. This aspect is discussed separately in a later section. Nevertheless, it is important to note that an augmented drug release from the mentioned rods rapidly depleted the amount of drug remaining in them. This may explain the decline in the drug release observed from the 13^{th} week (91 days) onwards.

Overall, the results suggest that unidirectional orientation of the rods enhanced paracetamol release in the drawing direction as well as in the perpendicular direction. When the drug release was normalised for the surface area, the augmentation effect was found to be more prominent along the PLA chain orientation direction.

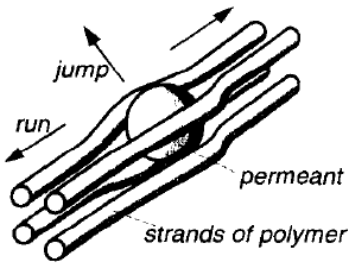

Figure 7.13: *'Run and jump model' explaining diffusion of small molecules through the polymer matrix. (Adapted from (Wesselingh, 1993))*

Diffusion of small molecules through the polymeric matrices can occur either parallel to the chain axis (Brandt, 1955) or perpendicular to it (DiBenedetto, 1963). Pace *et al*. (1979) proposed that the small molecules 'run' along the chain axis, through the tubular surrounding created by the polymer chains (figure 7.13). Once they encounter a region of high entanglement, the molecules have to 'jump' from one tube to another. Contrarily, diffusion perpendicular to the chain axis would require numerous 'jumps' from one surrounding to the adjacent surrounding. Since, jumps require higher energy than the movement through the tubular channels, the latter is favoured.

Considering this theory, uniaxial orientation of the rods should accelerate the drug release through the cross section by aligning the polymer chains in a single direction (sec. 7.1). Contrarily, increased chain packing after orientation should retard the drug diffusion perpendicular to the drawing direction. However, the drug release was enhanced from both the curved surface and the cross section; which suggests that a process in addition to directional diffusion of the drug through the polymer matrix might have played a role here. If the mechanism proposed from the studies on the oriented films was true, this can be attributed to augmented formation of water-filled channels. In order to make a safe conclusion on mechanism behind directional drug release, the changes in the oriented polymer matrix following aqueous submersion must be traced using a technique such as micro-CT.

7.3.2. The effect of uniaxial draw ratio

The cumulative drug release from uniaxially oriented rods displayed a sigmoidal pattern (figure 7.14 & figure 7.15). The initial slow release phase was followed by a rapid release phase, ultimately leading to a plateau. Such a trend was constant, regardless of whether the drug release occurred from the cross section (figure 7.14) or from the curved surface (figure 7.15).

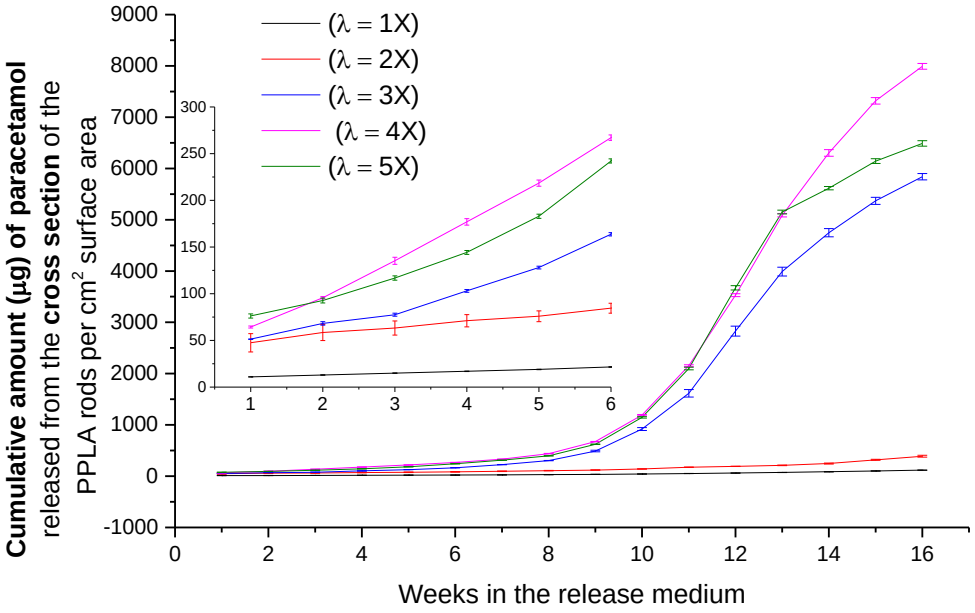

Figure 7.14: *Cumulative paracetamol release from the cross section of oriented PPLA rods per cm² surface area (inset: magnified view between 0 to 6 weeks).*

*The cumulative paracetamol release is expressed as mean ± SD; where n = 6.

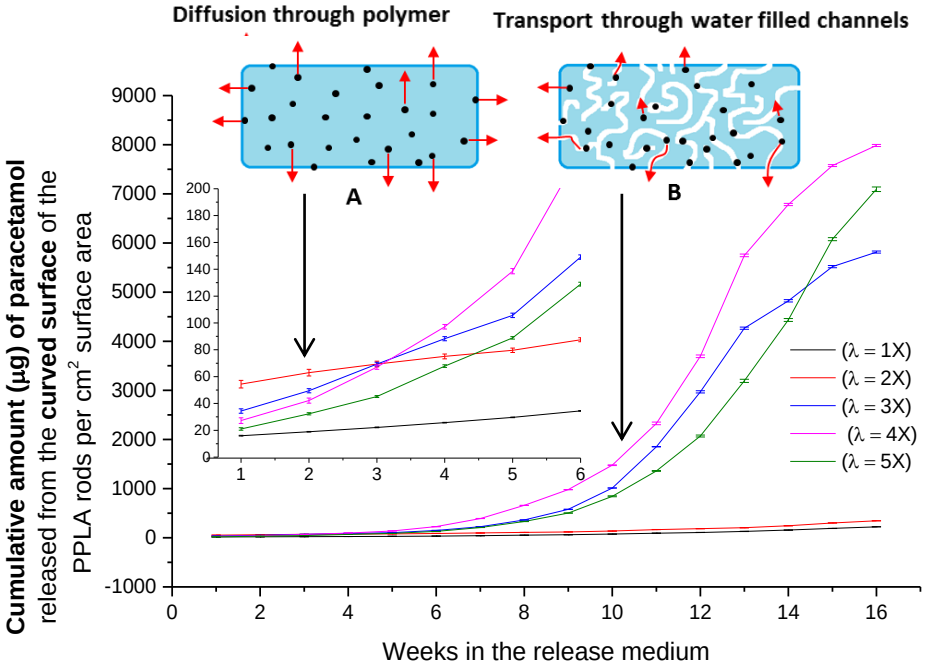

Figure 7.15: *Cumulative paracetamol release from the curved surface of oriented PPLA rods per cm² surface area (inset: magnified view between 0 to 6 weeks).*

*The cumulative paracetamol release is expressed as mean ± SD; where n = 6.

Table 7.7: *Statistical comparison between cumulative paracetamol release (μg.cm^{-1}) from the cross section of the PPLA rods drawn to different draw ratios*

One-way ANOVA followed by Tukey's test				
Comparison	Week 4	Week 8	Week 12	Week 16
1X Vs 2X	P < 0.001, q = 34.11	P < 0.001, q = 46.3	P < 0.05, q = 7.17	P < 0.001, q = 7.04
1X Vs 3X	P < 0.001, q = 60.37	P < 0.001, q = 223.46	P < 0.001, q = 139.25	P < 0.001, q = 316.74
1X Vs 4X	P < 0.001, q = 112.22	P < 0.001, q = 335.2	P < 0.001, q = 174.52	P < 0.001, q = 435.86
1X Vs 5X	P < 0.001, q = 89.3	P < 0.001, q = 299.58	P < 0.001, q = 181.69	P < 0.001, q = 352.66
2X Vs 3X	P < 0.001, q = 26.26	P < 0.001, q = 177.16	P < 0.001, q = 135.63	P < 0.001, q = 309.71
2X Vs 4X	P < 0.001, q = 78.11	P < 0.001, q = 288.9	P < 0.001, q = 170.9	P < 0.001, q = 428.82
2X Vs 5X	P < 0.001, q = 55.19	P < 0.001, q = 253.28	P < 0.001, q = 178.07	P < 0.001, q = 345.62
3X Vs 4X	P < 0.001, q = 51.85	P < 0.001, q = 111.74	P < 0.001, q = 35.27	P < 0.001, q = 119.11
3X Vs 5X	P < 0.001, q = 28.93	P < 0.001, q = 76.12	P < 0.001, q = 42.44	P < 0.001, q = 35.92
4X Vs 5X	P < 0.001, q = 22.93	P < 0.001, q = 35.62	P > 0.05, q = 3.62	P < 0.001, q = 83.2

Notes: The associated release data can be found in figure 7.14

The null hypothesis was that the compared samples were statistically the same

P > 0.05 = The difference between the compared samples is **not statistically significant**
0.05 > P > 0.01 = The difference between the compared samples is **statistically significant**
0.01 > P = The difference between the compared samples is **highly significant**

Table 7.8: *Statistical comparison between cumulative paracetamol release (μg.cm^{-1}) from the curved surface of the PPLA rods drawn to different draw ratios.*

One-way ANOVA followed by Tukey's test				
Comparison	Week 4	Week 8	Week 12	Week 16
1X Vs 2X	P < 0.001, q = 89.92	P < 0.001, q = 73.14	P < 0.001, q = 18.01	P < 0.001, q = 24.37
1X Vs 3X	P < 0.001, q = 105.31	P < 0.001, q = 299.37	P < 0.001, q = 386.71	P < 0.001, q = 526.66
1X Vs 4X	P < 0.001, q = 120.16	P < 0.001, q = 583.29	P < 0.001, q = 483.98	P < 0.001, q = 729.39
1X Vs 5X	P < 0.001, q = 71.1	P < 0.001, q = 271.42	P < 0.001, q = 265.74	P < 0.001, q = 646.17
2X Vs 3X	P < 0.001, q = 15.39	P < 0.001, q = 226.23	P < 0.001, q = 368.7	P < 0.001, q = 502.29
2X Vs 4X	P < 0.001, q = 30.23	P < 0.001, q = 510.16	P < 0.001, q = 465.97	P < 0.001, q = 705.02
2X Vs 5X	P < 0.001, q = 18.82	P < 0.001, q = 198.29	P < 0.001, q = 247.73	P < 0.001, q = 621.8
3X Vs 4X	P < 0.001, q = 14.84	P < 0.001, q = 283.93	P < 0.001, q = 97.27	P < 0.001, q = 202.73
3X Vs 5X	P < 0.001, q = 34.21	P < 0.001, q = 27.95	P < 0.001, q = 120.97	P < 0.001, q = 119.51
4X Vs 5X	P < 0.001, q = 49.05	P < 0.001, q = 311.87	P < 0.001, q = 218.24	P < 0.001, q = 83.22

Notes: The associated release data can be found in figure 7.15

The null hypothesis was that the compared samples were statistically the same

P > 0.05 = The difference between the compared samples is **not statistically significant**
0.05 > P > 0.01 = The difference between the compared samples is **statistically significant**
0.01 > P = The difference between the compared samples is **highly significant**

A sigmoidal release pattern was observed by Miyajima *et al*. (1997) when studying release of papaverine from un-oriented melt compressed PLA rods. They proposed that the initial slower release occurred predominantly by diffusion of the drug through the hydrated polymer matrix. A faster drug release in the second stage was attributed to formation of water filled channels; following which the drug release declined due to a progressive fall in the concentration gradient.

A similar drug release profile was also obtained by Vieranto *et al*. (2002) and Tormala *et al*. (2008) from die drawn PLA matrices containing a drug in a suspension form. Vieranto *et al*. (2002), prepared self-reinforced screws by machining a die drawn PLA billet (M_w = 910 000 g/mol), containing ciprofloxacin. Surprisingly, no mention of the draw ratio or the drug loading was found. The authors observed that less than 10% of the drug was released in the first 9 weeks. Between the 10^{th} and the 20^{th} week a rapid release of about 60% ciprofloxacin occurred, followed by a plateau phase. Tormala *et al*. (2008) compared ciprofloxacin release from isotropic polyester (PLA/PGA) rods and polyester rods die drawn to λ = 4.4X. The initial slow release phase for the isotropic rods lasted for approximately 220 days, whereas that in the case of the die-drawn rods was only about 100 days longer. An early onset of the exponential release phase in the die-drawn rods resulted in greater overall release of ciprofloxacin from such rods.

In the present study, drug release was divided into three distinct phases, namely the slow release phase (until the 5^{th} week), the transition phase (from 5^{th} to the 8^{th} week) and the exponential phase (8^{th} week onwards) (figure 7.14, figure 7.15). During the first two phases, the amount of paracetamol released daily, from the cross section or from the curved surface of an un-oriented PPLA rod did not exceed 1.5 $\mu g.cm^{-2}$. The PPLA-2X rods showed anomalously higher drug release for the initial 2 weeks; however, drug release reduced from the third week onwards. A statistical comparison revealed that there was a significant difference between paracetamol release from un-oriented rods and PPLA-2X rods (both surface and cross section) throughout the drug release study (table 7.7, table 7.8). If the initial anomalous release from PPLA-2X rods was subtracted, the cumulative paracetamol release from the cross section of PPLA-2X rods was 1.5 to 1.7 fold higher than that from the cross-section of the un-oriented rods. Similarly, the cumulative paracetamol release from the curved surface of PPLA-2X rods was 2.0 to 2.2 fold higher than that from the curved surface of the un-oriented rods. These results were surprising as the PPLA-2X

rods underwent expansion (sec. 7.2.1), which can result in loss of the oriented structure. Contrary to shrinkage of the oriented amorphous films, expansion of the PPLA-2X rods may induce substantial changes in the microstructure as well as macrostructure. This needs to be investigated in order to find a logical explanation for higher drug release from PPLA-2X rods. Despite a difference in the amount of drug release, PPLA-2X rods showed a very similar release pattern to that exhibited by un-oriented rods. The overall drug release from these rods continued to be slower and never lead to an exponential phase. Therefore, the maximum amount of paracetamol released from the un-oriented and the PPLA-2X rods merely reached 5 $\mu g.cm^{-2}.day^{-1}$ and 11.5 $\mu g.cm^{-2}.day^{-1}$ respectively.

PPLA rods oriented to $\lambda \geq 3X$, showed a marked enhancement of drug elution, during all three phases mentioned above. Between the 2^{nd} and 5^{th} week, the curved surface of PPLA-3X rods released 5-6 fold higher paracetamol than the curved surface of un-oriented PPLA rods. Similarly, drug release from the cross section of PPLA-3X rods was 10-12 fold higher than the corresponding release from un-oriented rods. The aforementioned difference between the paracetamol release from PPLA- 3X and un-oriented rods almost doubled in the transition phase. Nevertheless, this difference increased exponentially from the 8^{th} week onwards. The maximum amount of paracetamol released per day by the PPLA-3X rods was 184.89 $\mu g.cm^{-2}$ from the curved surface and 346.66 $\mu g.cm^{-2}$ from the cross section. Quite remarkably, this amount was 60 and 134 times higher than the corresponding drug release from un-oriented rods.

PPLA-5X rods exhibited an intermediate drug release between PPLA-3X and PPLA-4X rods during the slow release phase. Drug release from the cross section of PPLA-5X rods increased during the exponential phase, and became comparable to the PPLA-4X rods. Contrarily, drug release from the curved

surface of PPLA-5X rods remained significantly lower than the corresponding release from PPLA-4X and even PPLA-3X rods.

Altogether, drug release from PPLA rods was significantly ($P < 0.001$) enhanced at $\lambda \geq 3X$. A statistical comparison by one-way ANOVA – Tukey's test validated that the difference in the cumulative paracetamol release between the PPLA-3X, PPLA-4X and PPLA-5X rods was highly significant (table 7.7, table 7.8). However, a definite proportionality was not observed between the drug release rate and the draw ratio ($\lambda \geq 3X$); perhaps because the enhancement at $\lambda = 3X$ itself was large. Orientation of the films produced a maximum threefold rise in the drug release, while the maximum acceleration in the case of PPLA rods was 175-fold (PPLA-5X cross section, week 12). Such a difference can be attributed to formation of large cracks (sec. 7.2.4, figure 7.9) in the oriented PPLA rods, after 8-9 weeks of water submersion. These cracks when filled by the bathing medium can accelerate the drug release as well as polymer degradation.

Strain crystallisation of PLA during solid-state orientation enhances the concentration of the drug in the remaining amorphous phase. Nevertheless, drug can also be excluded from the highly organised amorphous sections, where augmented inter-chain interactions may reduce the number of functional groups available for the drug molecules to attach. Both of these factors can generate a higher concentration gradient, thereby enhancing diffusion mediated drug release from the oriented PLA. Based on the hypothesis proposed previously (section 6.9.2.3, figure 6.37), concentration of the chain defects in the inter-lamellar regions of the highly oriented matrices supposedly augments formation of water filled channels. In the case of PPLA rods, even the macroscopic crevices were formed due the presence of the disordered α' crystalline form. Therefore, a higher drug release from the oriented ($\lambda \geq 3X$) PPLA rods in the exponential release phase can be attributed to the abovementioned morphological changes.

7.4. Summary

This is the first study reporting release of a polymer soluble drug from the oriented polymer rods. Nevertheless, directional dependency of drug release was evaluated for the first time. The paracetamol release from oriented PPLA rods followed a sigmoidal pattern. Drug release was divided into three phases as follows; a slower release phase – from the 2nd to the 5th week, a transition phase – from the 5th to the 8th week and an exponential phase - from the 8th week onwards. Uniaxial orientation of the PPLA rods generated an oriented crystalline structure, which significantly enhanced the paracetamol release. The effect of orientation was most prominent in the exponential phase due to formation of the microscopic and then macroscopic water filled-channels. Normalisation of drug release with respect to the surface area confirmed that the augmentation of the drug release was superior along the chain orientation direction than in the perpendicular direction.

8. Comparison of the distinctive findings between drug release from oriented PLA films and die-drawn PLA rods

8.1. The structural distinction between oriented rods and oriented films

The uniaxial constant width (UCW) oriented PLA films and die drawn PLA rods showed analogous changes in their oriented structure with respect to uniaxial draw ratio. At uniaxial λ = 2X, both geometries developed a nematic organisation of the amorphous PLA chains in the drawing direction. Negligible strain crystallisation was observed up to this level of extension. At λ = 3X, PLA films exhibited generation of α PLA crystals with their c-axis oriented parallel to the drawing direction (figure 6.9). Conversely, die-drawn rods showed the presence of α' PLA crystals with similar orientation (figure 7.1). On further extension, an increasing number of PLA chains were recruited into the oriented crystalline arrangement. However, the respective crystalline forms remained the same.

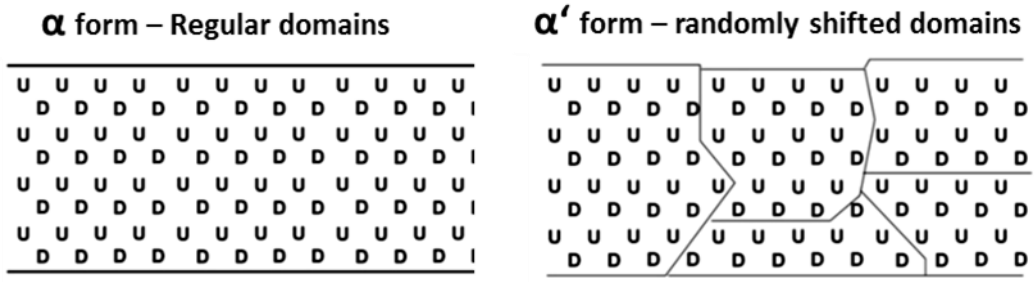

Figure 8.1: *Postulated structural difference between the α' and the α Form of PLA. (Wasanasuk and Tashiro, 2011)*

*(U and D signify up and down arrangement of 5 monomeric units in a 2_1 screw geometry)

The characteristic differences between the α and the α' Form of PLA are summarised in section 7.1.2 and through figure 7.10 (shown here as figure 8.1). In brief, the α' Form possesses slightly disordered molecular chains compared with the α Form (Zhang *et al*., 2008). Such a disorder alters the unit cell parameters of the α' Form and consequently, organisation of the higher order domains becomes imperfect (figure 8.1) (Pan *et al*., 2008; Wasanasuk and Tashiro, 2011). A boundary is created between the disordered crystalline domains, which perhaps possesses crystal defects in the form of chain ends. Such macroscopic defects are absent in the α Form of PLA due to existence of a 2_1 screw symmetry (figure 8.1). The mentioned distinction between the crystalline organisation of PLA in the oriented films and rods, along with the other differences such as that in the geometry, size, model drug and overall chain orientation resulted in largely dissimilar drug release profile from the two systems.

8.2. Difference in the biphasic nature of drug release profiles

If the initial burst release was ignored, the drug loaded PLA films exhibited a biphasic drug release. A similar release profile was displayed by the paracetamol loaded PLA rods following die-drawing (λ ≥ 3X). However, the rods exhibited a plateau towards the end of the drug release testing due to a substantial depletion of the drug concentration (figure 8.2). Although both kinds of systems exhibited a biphasic release pattern, the nature of the two phases was substantially different in the oriented films and the die-drawn rods (λ ≥ 3X). Figure 8.2 summarises these differences through comparison of the drug release profiles of curcumin loaded oriented PLA films (UCW λ = 3X) and paracetamol loaded die drawn rods (λ = 3X).

As displayed in figure 8.2, the slow release phase in the oriented rods relates to diffusion of the drug through the hydrated polymer matrix. This phase lasted approximately for 4-6 weeks, following which there was a smooth transition to the exponential release phase between 6^{th} and the 10^{th} week.

Since, no weight loss (reduction in the dried weight) was detected in the oriented rods for the entire study duration; acceleration of drug release in the exponential phase can be attributed to formation of several microscopic and macroscopic water filled channels. The exponential release phase in the case of oriented rods continued approximately from the 10th week onwards. Due to substantially faster drug release in this phase (sec. 7.3.2), the oriented rods were progressively depleted of the drug. The falling concentration gradient subsequently lowered the release rate.

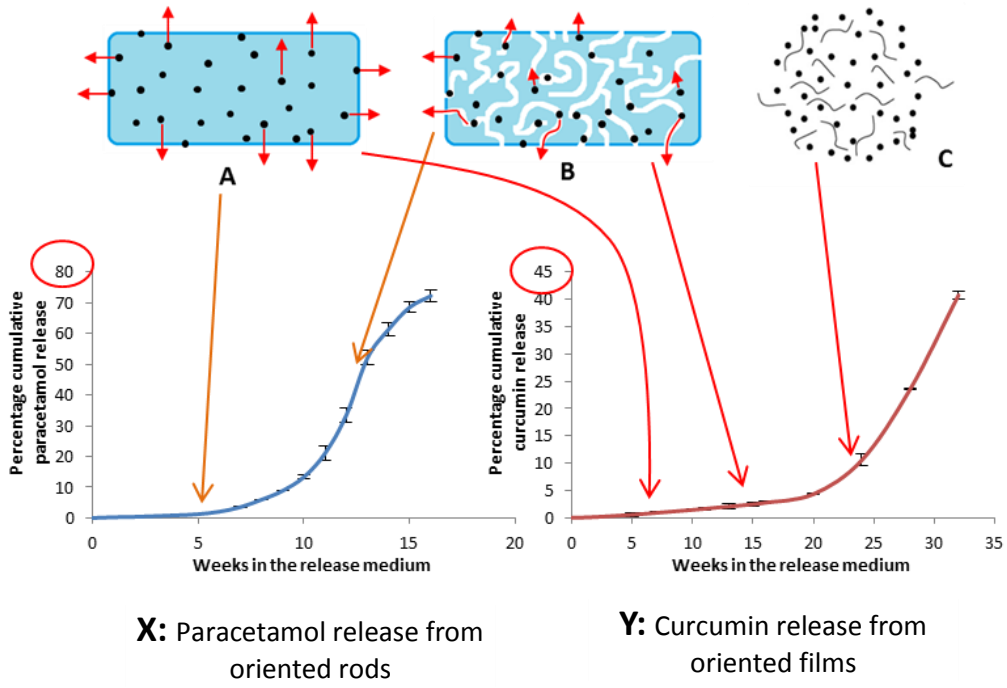

Figure 8.2: *Distinction between biphasic release of **(X)** paracetamol from oriented rods and that of **(Y)** curcumin from the oriented films*

* The cumulative release is represented as Mean ± SD, where n = 6.

The percentage cumulative paracetamol release represented here is the release from the curved surface of the rods, without area normalisation.

Due to the larger size of the rods (6 mm diameter X 6 mm thickness) compared to the films (5 mm diameter X 0.2 mm thickness), percolation of water is extremely slow and requires a longer duration before the rod is

completely saturated by the water. As water starts percolating in the rods, it gradually hydrates numerous successive layers from the periphery towards the centre. Drug present in a hydrated layer diffuses towards the surface of the rods and it is subsequently released in the bathing medium. In parallel to this, the percolated water causes hydrolytic degradation of the surrounding polymer phase and promotes formation of the water filled channels. Drug release is accelerated as the number of channels gradually increases and they are transformed from the microscopic to macroscopic dimensions. Once the matrix is significantly porous, drug release predominantly occurs through such channels (figure 7.9).

Diffusion through the hydrated polymer and through water filled channels could not be distinguished in the drug release profile of the oriented films. Lower thickness of the films can result in faster equilibration by the release medium and an earlier onset of channel formation. Nevertheless, the network of the connected channels can grow faster in the films due to significantly higher surface area to volume ratio compared to the rods. Due to lower thickness of the films (0.2 mm), drug diffusion in the films is virtually one dimensional. Consequently, diffusion through the hydrated polymer phase plays a substantially greater role in drug release from films than from the rods. All these factors perhaps resulted in a monophasic drug release from the oriented PLA films until the 16^{th} week after aqueous submersion.

These mass transport mechanisms play a key role in affecting drug elution from PLA matrices only till the onset of erosion. Study of the molecular weight degradation and morphological changes in the submerged films revealed that the films started to disintegrate from the 20^{th} week onwards. This led to uncontrolled release of the remaining drug from the films. Therefore, the exponential phase observed in the release profile of the PLA films relates to erosion mediated drug release. The erosion of the paracetamol loaded PLA

rods could not be observed in the current study, which was restricted to 16 weeks (due to drug depletion).

8.3. Difference in the effects of solid state orientation

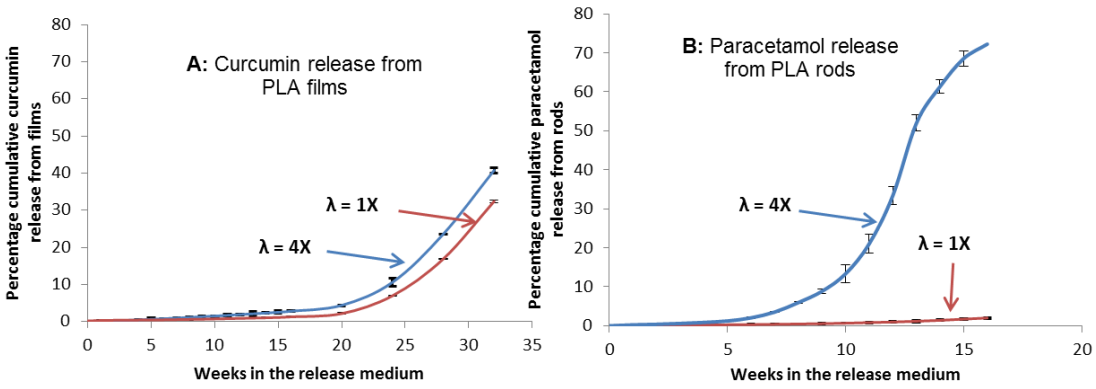

Figure 8.3: *Distinction between the effect of solid state orientation on the biphasic drug release profiles of* ***(A)*** *curcumin and* ***(B)*** *paracetamol from the oriented films and the rods respectively*

* The cumulative release is represented as Mean ± SD, where n = 6.

The percentage cumulative paracetamol release represented here is the release from the curved surface of the rods, without area normalisation.

The effect of solid-state orientation on drug release from the PLA films was quite distinct from that observed in the case of oriented PLA rods (figure 8.3). The biphasic nature of the drug release profile was not altered after solid-state orientation of the PLA films. All PLA films irrespective of their degree of orientation and the compounded model drug exhibited slower drug release until the 16th week, followed by an erosion induced acceleration of drug release. Conversely, the un-oriented PLA rods (and the λ = 2X rods that shrunk after aqueous submersion) exhibited a monophasic drug release for the entire study duration (16 weeks). Orientation of the rods to UCW draw ratios of 3X and above, transformed the drug release profile from monophasic to biphasic. Here the initial phase represented drug release by diffusion through the hydrated polymer; while the later phase represented substantial acceleration of drug

release due to formation of microscopic and macroscopic water filled channels. Importantly, orientation of the films to the draw ratio of 4X produced a maximum two fold rise in the cumulative curcumin release before the onset of erosion (during the first 16 weeks). Contrastingly, the maximum difference between the cumulative paracetamol release from PPLA-4X rods and that from the un-oriented rods was 52-fold (at the end of the 13th week). Such a difference predominantly relates to formation of macroscopic channels in the oriented rods (sec. 7.2.4); along with other factors such as differences in their size, geometry, model drug and oriented morphology.

The presence of macroscopic channels in the oriented rods ($\lambda \geq 3X$) was confirmed by SEM at the end of the release study. For the rods oriented to $\lambda = 3X$, the average width of the channels was less than a micrometre and they were approximately 100 μm long. The width of the channels increased with the draw ratio, but their number reduced significantly. Importantly, all such channels were aligned parallel to the drawing direction. They were absent in the un-oriented and the $\lambda = 2X$ rods. A key difference between the un-oriented (and $\lambda = 2X$) and the oriented ($\lambda \geq 3X$) rods was that the former were amorphous in nature while the latter contained α' crystalline form of PLA. The α' Form has a sheaf like structure where PLA chains are loosely bundled together (Pan *et al*., 2008). Therefore, formation of macroscopic channels quite clearly relates to existence of the α' Form of PLA. This further explains transformation of monophasic drug release profile to a biphasic profile after orientation of the PLA rods ($\lambda \geq 3X$). As explained in section 8.1, oriented PLA films also underwent strain crystallisation at the draw ratio of 3X and above. However, they contained the α crystalline form of PLA. Since the α crystals have lamellar structure and a higher order symmetry than the α' Form (figure 8.1), formation of macroscopic channels was not observed in the case of oriented films. Consequently, the nature of drug release profile remained constant, although the overall drug release was accelerated after orientation of the films.

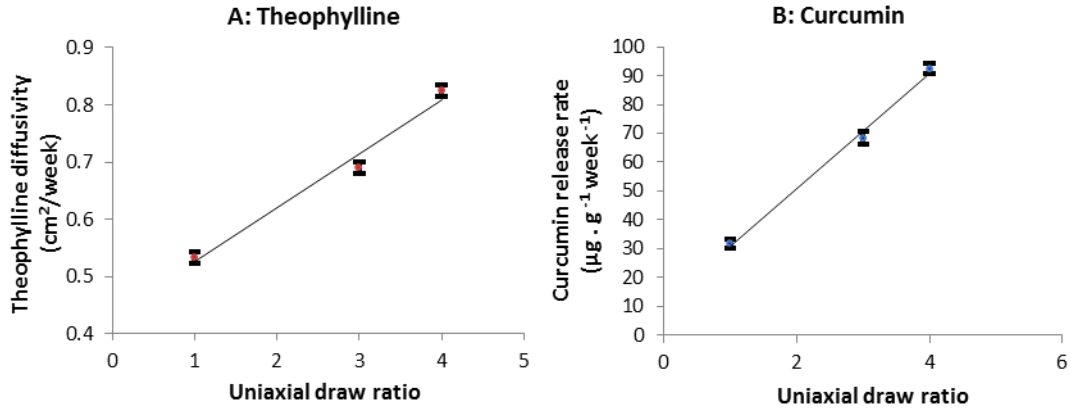

Figure 8.4: *Effect of solid state orientation on kinetics of drug release from oriented films.*

A: Theophylline diffusivity/ diffusion rate, **B:** Curcumin release rate

* The theophylline diffusivity was calculated from the slope of the cumulative release Vs time$^{1/2}$ curves (regression lines), which were linear in the case of TPLA films. Similarly, the curcumin release rate in µg.g $^{-1}$.week $^{-1}$ units was calculated by plotting cumulative µg of curcumin released per gram of CPLA films against time in weeks. The cumulative curcumin release exhibited a linear relationship with time, instead of with the square root of it. Therefore the slope of such curves represented the curcumin release rate.

**The error bars in both cases represent the standard error obtained by regression analysis of the respective data.

Orientation of the films to UCW draw ratios of 3X and 4X resulted in acceleration of the release of both model drugs, despite difference in their release mechanisms. Theophylline was predominantly released by a Fickian diffusion mechanism. This signifies that the rate of theophylline release reduced gradually, in response to the falling concentration gradient; however, the diffusivity remained constant. Here the diffusivity of theophylline was calculated from the slope of the cumulative drug release Vs time$^{1/2}$ curves. A linear (R^2 = 0.9786) rise in the diffusivity of theophylline was observed with respect to UCW draw ratio ≥ 3X (figure 8.4 - A).

It was previously confirmed that curcumin (at 5% w/w loading) formed a solid-solution in PLA. Therefore, hydrolytic degradation of the polymer matrix resulted in a gradual rise in the diffusivity of curcumin as the drug release study progressed. This perhaps balanced the effect of falling concentration gradient and the overall release rate remained constant until the 16^{th} week. The curcumin release rate was therefore obtained from the slope of the cumulative drug release Vs time curves. A linear rise (R^2 = 0.9950) in the release rate of curcumin was observed with respect to UCW draw ratio ≥ 3X (figure 8.4 - B).

In the case of oriented rods (λ ≥ 3X), no proportionality between the draw ratio and the release rate or diffusivity was observed, since neither the release rate nor diffusivity remained constant during the drug release study. Moreover, the enhancement of drug release due to formation of macroscopic channels was so high that it masked the effect of individual draw ratios.

8.4. Summary

In summary, the comparison between the drug release profiles of the oriented films and the oriented rods emphasised the role played by microscopic and macroscopic channels in enhancing drug release from orientated materials. The importance of the crystalline form of PLA in influencing this process was also highlighted. It was confirmed that presence of the α Form can offer a better control over the drug release rate than the α' Form. Since strain crystallisation of PLA generates varied crystalline polymorphs depending upon the drawing temperature, strain rate, draw ratio and the method of drawing; manipulation of these conditions can offer a control over the crystalline form of PLA and consequently drug release from oriented semicrystalline PLA.

9. Conclusions

This study represents the first systematic exploration of polymer orientation as a novel method for controlling drug release from biodegradable polymers. The effect of the degree and nature of polymer orientation (e.g. uniaxial, biaxial) on the release of model drugs was studied, using oriented Poly (lactic acid) – (PLA) films. Importantly, anisotropy in the drug release rate following uniaxial orientation of PLA rods was also evaluated for the first time. From the work performed here the following conclusions could be drawn:

- An efficient melt processing method was developed, which caused minimal thermal degradation of the experimental materials (model drugs & PLA) during melt compounding and during extrusion into sheets or rods. This ensured that the characteristics of drug release from oriented PLA matrices were solely attributable to the structural changes caused by solid-state orientation.

- Changes in the polymorphic and physical state of the experimental materials due to melt processing were identified. When melt compounded with PLA, curcumin and paracetamol at 5% w/w loading formed a solid solution, while theophylline remained in a crystalline suspension state at the same loading.

- The physical state of the model drug critically influenced the stability and consequent drug release profile of the oriented amorphous PLA matrices. When the nematic orientation of amorphous PLA chains was stabilised by the presence of a crystalline model drug, it caused retardation of drug release. Contrarily, oriented amorphous PLA matrices (rods and films) containing a model drug in a solution state lost their oriented structure after submersion in the release medium at 37 °C. Drug release from such matrices became equivalent to that from the un-oriented PLA matrices.

- Morphology of the amorphous and crystalline regions in oriented PLA matrices played a pivotal role in affecting drug release prior to the onset of erosion.

- PLA films oriented to a lower draw ratio (uniaxial constant width λ = 2X, biaxial λ = 2X2Y), which contained a nematic alignment of the amorphous chains and negligible crystallinity (<1%) showed retardation of drug release. Among these, biaxially oriented films exhibited a greater release retardation effect due to higher tortuosity.

- Uniaxial orientation of the PLA matrices (both films and rods) enhanced drug release when accompanied by strain induced crystallisation at draw ratios of 3X and above.

- Generation of α crystalline form with its c-axis parallel to the drawing direction led to enhancement of polarity of the PLA films, which were oriented to uniaxial constant width (UCW) draw ratios of 3X or greater.

- Based on the above finding, a mechanism was proposed for explaining higher drug release from oriented crystalline PLA matrices (films UCW λ ≥ 3X, rods λ ≥ 3X). According to it, augmented formation of water filled channels in such matrices was responsible for acceleration of drug release.

- The polymorphic form of PLA generated during solid-state orientation was of equivalent importance to the degree of orientation, in influencing drug release from oriented PLA matrices. The disordered α' Form of PLA (generated during die drawing of PLA rods; UCW λ ≥ 3X) accelerated drug release to a much greater extent than that exhibited by the α crystalline form (present in the oriented PLA films; UCW λ ≥ 3X). This resulted due to the formation of cracks between disordered domains of the α' Form.

- Importantly, the anisotropic morphology of uniaxially oriented PLA rods resulted in direction specific drug release. Drug release was faster along the polymer chain orientation direction, than that in the perpendicular direction.

- This work provided substantial evidence that the rate of drug release from oriented PLA matrices significantly depends on the morphology of such matrices. Results described in chapter 6 confirmed that various oriented morphologies could be generated by varying the strain rate, drawing temperature, and draw ratio during solid-state orientation of PLA. Therefore, it was established that polymer orientation can serve as a novel method of controlling drug release from biodegradable polymers.

10. Future work

The current findings highlighted the following aspects to be studied in the future

- **Effect of drug concentration:**

  Effect of orientation was studied here keeping the drug loading constant at 5% w/w. As explained in section 3.4.1, different drug loadings may change the distribution of drug in the polymer matrix and drug – polymer interactions. This may subsequently affect solid-state deformation behaviour of PLA and resultant release profile. Nevertheless, increasing the drug loading will enhance the concentration gradient between the polymer phase and the bathing medium. In such a case, correlation between the drug release rate and the degree of orientation may vary. Therefore, it will be interesting to study drug release from PLA matrices oriented to a constant draw ratio but containing varied drug loading.

- **Effect of amorphous orientation:**

  This work confirmed that PLA films oriented to different draw ratios but containing a predominantly amorphous structure can be prepared at lower drawing temperatures (70 °C using the selected grade). Drug elution studies on these films will generate an understanding of whether release retardation observed in the current study was due to amorphous orientation or due to a lower draw ratio.

- **Additional biaxial draw ratios:**

  In the current work, a single biaxial draw ratio of 2X2Y was studied due to technical limitations. In the future, PLA films oriented to higher biaxial draw ratios can be generated. Nevertheless, the films can be oriented to different extents along the perpendicular directions (e.g. λ = 2X3Y, 2X4Y, 3X4Y, etc.) in sequential biaxial mode. Drug release studies on these films will provide further insight into the effect of biaxial orientation on drug release.

❖ **The mechanism by which drug release is altered in oriented PLA:**

A mechanism proposed in this research explained augmented formation of water filled channels as a probable cause of accelerated drug release from oriented crystalline matrices. In order to verify this mechanism, changes in the connected porosity and crystalline structure of the oriented PLA matrices can be studied periodically during drug release studies. The prior can be achieved by a micro-computed tomography measurement, while the latter can be determined by WAXD. Such a study in the case of biaxially oriented PLA films (currently studied λ = 2X2Y) and oriented amorphous films (currently studied UCW λ = 2X) will highlight the cause of drug release retardation exhibited by these films.

❖ **Anisotropic drug release from a cube geometry:**

It was established that drug release from uniaxially oriented rods was anisotropic in nature. Drug release in the drawing direction was studied from a flat cross section, while that in the perpendicular direction was studied from a curved surface. Moreover, oriented rods with equivalent length and diameter were used in the drug release studies, so as to keep the diffusional path-length from the centre to the curved surface and from the centre to the cross section constant. However, with this approach the curved surface area became twice as much as the total cross sectional surface area. In order to eliminate these geometric variables, drug release can be studied from different surfaces of a cube specimen obtained from an oriented square billet.

❖ **Creating a design rule:**

Various oriented morphologies can be generated in PLA and related bulk eroding biodegradable polymers, by varying drawing temperature, strain rate and draw ratios. Drug release studies on such matrices will allow formulation of a design rule for controlling drug release from oriented bulk eroding biodegradable polymers.

11. References

Ahmed, A. R., Dashevsky, A. and Bodmeier, R. (2008) Reduction in burst release of PLGA microparticles by incorporation into cubic phase-forming systems. *European Journal of Pharmaceutics and Biopharmaceutics,* 70 (3)**,** 765-769.

Ajji, A., Cole, K. C., Dumoulin, M. M. and Ward, I. M. (1997) Orientation of amorphous poly(ethylene terephthalate) by tensile drawing, roll-drawing, and die-drawing. *Polymer Engineering & Science,* 37 (11)**,** 1801-1808.

Ak, T. and Gulcin, I. (2008) Antioxidant and radical scavenging properties of curcumin. *Chemico-Biological Interactions,* 174 (1)**,** 27-37.

Alexander, L. (1971) X-ray diffraction methods in polymer science. *Journal of Materials Science,* 6 (1)**,** 93.

Alexis, F. (2005) Factors affecting the degradation and drug-release mechanism of poly(lactic acid) and poly[(lactic acid)-co-(glycolic acid)]. *Polymer International,* 54 (1)**,** 36-46.

Alexis, F., Venkatraman, S., Kumar Rath, S. and Gan, L.-H. (2006) Some insight into hydrolytic scission mechanisms in bioerodible polyesters. *Journal of Applied Polymer Science,* 102 (4)**,** 3111-3117.

Andreopoulos, A. G. (1994) Plasticization of biodegradable polymers for use in controlled release. *Clinical Materials,* 15 (2)**,** 89-92.

Aou, K. and Hsu, S. L. (2006) Trichroic vibrational analysis on the α Form of poly(lactic acid) crystals using highly oriented fibers and spherulites. *Macromolecules,* 39 (9)**,** 3337-3344.

Apicella, A., Cappello, B., Del Nobile, M. A., La Rotonda, M. I., Mensitieri, G. and Nicolais, L. (1993) Poly (ethylene oxide) (PEO) and different molecular weight PEO blends monolithic devices for drug release. *Biomaterials,* 14 (2)**,** 83-90.

Arm, D. M. and Tencer, A. F. (1997) Effects of cyclical mechanical stress on the controlled release of proteins from a biodegradable polymer implant. *Journal of Biomedical Materials Research,* 35 (4)**,** 433-441.

Aso, Y., Yoshioka, S., Li Wan Po, A. and Terao, T. (1994) Effect of temperature on mechanisms of drug release and matrix degradation of poly (D,L-lactide) microspheres. *Journal of Controlled Release,* 31 (1)**,** 33-39.

Auras, R., Harte, B. and Selke, S. (2004) An overview of polylactides as packaging materials. *Macromolecular Bioscience,* 4 (9)**,** 835-864.

Baji, A., Mai, Y.-W., Wong, S.-C., Abtahi, M. and Chen, P. (2010) Electrospinning of polymer nanofibers: Effects on oriented morphology, structures and tensile properties. *Composites Science and Technology,* 70 (5)**,** 703-718.

Bales, J. R., Nicholson, J. K. and Sadler, P. J. (1985) Two-dimensional proton nuclear magnetic resonance "maps" of acetaminophen metabolites in human urine. *Clin Chem,* 31 (5)**,** 757-62.

Barbooti, M. M. and Al-Sammerrai, D. A. (1986) Thermal decomposition of citric acid. *Thermochimica Acta,* 98**,** 119-126.

Barnes, W. J., Luetzel, W. G. and Price, F. P. (1961) Crystallization of poly-(ethylene oxide) in bulk. *The Journal of Physical Chemistry,* 65 (10)**,** 1742-1748.

Barra, J., Pena, M. A. and Bustamante, P. (2000) Proposition of group molar constants for sodium to calculate the partial solubility parameters of sodium salts using the van Krevelen group contribution method. *European Journal of Pharmaceutical Sciences,* 10 (2)**,** 153-161.

Barrer, R. M. (1957) Some properties of diffusion coefficients in polymers. *Journal of Physical Chemistry,* 61 (2)**,** 178-189.

Belbella, A., Vauthier, C., Fessi, H., Devissaguet, J.-P. and Puisieux, F. (1996) *In vitro* degradation of nanospheres from poly (D,L-lactides) of different molecular weights and polydispersities. *International Journal of Pharmaceutics,* 129 (12)**,** 95-102.

Bigg, D. M. (1976) A review of techniques for processing ultra-high modulus polymers. *Polymer Engineering & Science,* 16 (11)**,** 725-734.

Blackburn, R. S., Zhao, X., Farrington, D. W. and Johnson, L. (2006) Effect of D-isomer concentration on the coloration properties of poly (lactic acid). *Dyes and Pigments,* 70 (3)**,** 251-258.

Bodmeier, R. and Chen, H. (1988) Preparation of biodegradable poly (±) lactide microparticles using a spray-drying technique. *Journal of Pharmacy and Pharmacology,* 40 (11)**,** 754-757.

Brabander de, C., Vervaet, C. and Remon, J. P. (2003) Development and evaluation of sustained release mini-matrices prepared via hot melt extrusion. *Journal of Controlled Release,* 89 (2)**,** 235-247.

Brandt, W. (1955) Calculation of the compressibility of polyethylene from the energy of interaction between (-CH_2-) groups. In: *Physical review.* American physical society, Vol. 98, p. 243.

Brostow, W. (2007) Mechanical properties. In: Mark, J. (Ed.) *Physical properties of polymers handbook.* Springer New York, pp. 423-445.

Burg, K. J. L. and Shalaby, S. W. (1998) Physicochemical changes in degrading polylactide films. *Journal of Biomaterials Science, Polymer Edition,* 9 (1)**,** 15-29.

Butrimovitz, G. and Raisys, V. (1979) An improved micromethod for theophylline determination by reversed-phase liquid chromatography. *Clinical Chemistry,* 25 (8)**,** 1461-1464.

Cai, H., Dave, V., Gross, R. A. and McCarthy, S. P. (1996) Effects of physical aging, crystallinity, and orientation on the enzymatic degradation of poly (lactic acid). *Journal of Polymer Science Part B: Polymer Physics,* 34 (16)**,** 2701-2708.

Cam, D., Hyon, S. and Ikada, Y. (1995) Degradation of high molecular weight poly (L-lactide) in alkaline medium. *Biomaterials,* 16 (11)**,** 833-843.

Carrasco, F., Pages, P., Gamez-Perez, J., Santana, O. and Maspoch, M. (2010) Processing of poly (lactic acid): Characterization of chemical structure, thermal stability and mechanical properties. *Polymer Degradation and Stability,* 95 (2)**,** 116-125.

Cava, D., Gavara, R., Lagaron, J. M. and Voelkel, A. (2007) Surface characterization of poly(lactic acid) and polycaprolactone by inverse gas chromatography. *Journal of Chromatography A,* 1148 (1)**,** 86-91.

Cha, Y. and Pitt, C. G. (1989) The acceleration of degradation-controlled drug delivery from polyester microspheres. *Journal of Controlled Release,* 8 (3)**,** 259-265.

Chen, S. X. and Lostritto, R. T. (1996) Diffusion of benzocaine in poly(ethylene-vinyl acetate) membranes: Effects of vehicle ethanol concentration and membrane vinyl acetate content. *Journal of Controlled Release,* 38 (2–3)**,** 185-191.

Chen, X., Kalish, J. and Hsu, S. L. (2011) Structure evolution of α′-phase poly(lactic acid). *Journal of Polymer Science Part B: Polymer Physics,* 49 (20)**,** 1446-1454.

Cheng, S. Z. D., Barley, J. S. and Giusti, P. A. (1990) Spherulite formation in poly(ethylene oxide) mixtures. *Polymer,* 31 (5)**,** 845-849.

Chiang, C.-M. and Tenzel, R. A. (1991) *Solid matrix system for transdermal drug delivery*. Accept.: Mar 9, 1991. WO1991003219 A1.

Cho, D. K., Park, J. W., Kim, S. H., Kim, Y. H. and Im, S. S. (2003) Effect of molecular orientation on biodegradability of poly(glycolide-co-ε-caprolactone). *Polymer Degradation and Stability,* 80 (2)**,** 223-232.

Choi, K. J., Spruiell, J. E. and White, J. L. (1982) Orientation and morphology of high-density polyethylene film produced by the tubular blowing method and its relationship to process conditions. *Journal of Polymer Science: Polymer Physics Edition,* 20 (1)**,** 27-47.

Christopher, V. (1997) Natural silks: archetypal supramolecular assembly of polymer fibres. *Supramolecular Science,* 4 (1-2)**,** 75-81.

Cleary, G. W. (1990) *Diffusion matrix for transdermal drug administration and transdermal drug delivery devices including same*. Appl.: Mar 27, 1990. US4911916 A.

Coates, P., Gibson, A. and Ward, I. (1980) *Polymer processing*. Accept.: 11/12/1980. WO1980002671 A1.

Coates, P. D. and Ward, I. M. (1978) Hydrostatic extrusion of polyoxymethylene. *Journal of Polymer Science: Polymer Physics Edition,* 16 (11)**,** 2031-2047.

Coates, P. D. and Ward, I. M. (1979) Drawing of polymers through a conical die. *Polymer,* 20 (12)**,** 1553-1560.

Coates, P. D. and Ward, I. M. (1981) Die drawing: Solid phase drawing of polymers through a converging die. *Polymer Engineering & Science,* 21 (10)**,** 612-618.

Codari, F., Lazzari, S., Soos, M., Storti, G., Morbidelli, M. and Moscatelli, D. (2012) Kinetics of the hydrolytic degradation of poly(lactic acid). *Polymer Degradation and Stability,* 97 (11)**,** 2460-2466.

Colo di, G., Burgalassi, S., Chetoni, P., Fiaschi, M. P., Zambito, Y. and Saettone, M. F. (2001) Relevance of polymer molecular weight to the *in vitro/in vivo* performances of ocular inserts based on poly(ethylene oxide). *International Journal of Pharmaceutics,* 220 (1–2)**,** 169-177.

Cooper-White, J. J. and Mackay, M. E. (1999) Rheological properties of poly (lactides). Effect of molecular weight and temperature on the viscoelasticity of poly (L-lactic acid). *Journal of Polymer Science Part B: Polymer Physics,* 37 (15)**,** 1803-1814.

Costa, P. and Sousa Lobo, J. M. (2001) Modeling and comparison of dissolution profiles. *European Journal of Pharmaceutical Sciences,* 13 (2)**,** 123-133.

Crowley, M. M., Fredersdorf, A., Schroeder, B., Kucera, S., Prodduturi, S., Repka, M. A. and McGinity, J. W. (2004a) The influence of guaifenesin and ketoprofen on the properties of hot-melt extruded polyethylene oxide films. *European Journal of Pharmaceutical Sciences,* 22 (5)**,** 409-418.

Crowley, M. M., Schroeder, B., Fredersdorf, A., Obara, S., Talarico, M., Kucera, S. and McGinity, J. W. (2004b) Physicochemical properties and mechanism of drug release from ethyl cellulose matrix tablets prepared by direct compression and hot-melt extrusion. *International Journal of Pharmaceutics,* 269 (2)**,** 509-522.

Crowley, M. M., Zhang, F., Repka, M. A., Thumma, S., Upadhye, S. B., Kumar Battu, S., McGinity, J. W. and Martin, C. (2007) Pharmaceutical Applications of Hot-Melt Extrusion: Part I. *Drug Development and Industrial Pharmacy,* 33 (9)**,** 909-926.

Cutrignelli, A., Lopedota, A., Trapani, A., Boghetich, G., Franco, M., Denora, N., Laquintana, V. and Trapani, G. (2008) Relationship between dissolution efficiency of oxazepam carrier blends and drug and carrier molecular descriptors using multivariate regression analysis. *International Journal of Pharmaceutics,* 358 (1–2)**,** 60-68.

Dash, S., Murthy, P. N., Nath, L. and Chowdhury, P. (2010) Kinetic modeling on drug release from controlled drug delivery systems. *Acta Pol Pharm,* 67 (3)**,** 217-223.

Dasmalchi, S., Rashidi, M. and Rassi, M. (1995) Simultaneous determination of the pKa and octanol/water partition coefficient (Pm) of acetaminophen. *Journal of School of Pharmacy, Medical Science University, Tehran,* 4**,** 7-14.

De Vries, A. J., Bonnebat, C. and Beautemps, J. (1977) Uni- and biaxial orientation of polymer films and sheets. *Journal of Polymer Science: Polymer Symposia,* 58 (1)**,** 109-156.

Delpouve, N., Stoclet, G., Saiter, A., Dargent, E. and Marais, S. (2012) Water barrier properties in biaxially drawn poly (lactic acid) films. *The Journal of Physical Chemistry B,* 116 (15)**,** 4615-4625.

Di Colo, G. and Zambito, Y. (2002) A study of release mechanisms of different ophthalmic drugs from erodible ocular inserts based on poly (ethylene oxide). *European Journal of Pharmaceutics and Biopharmaceutics,* 54 (2)**,** 193-199.

Di Martino, P., Palmieri, G. F. and Martelli, S. (2000) Molecular mobility of the paracetamol amorphous form. *Chemical and Pharmaceutical Bulletin,* 48 (8)**,** 1105-8.

DiBenedetto, A. T. (1963) Molecular properties of amorphous high polymers. I. A cell theory for amorphous high polymers. *Journal of Polymer Science Part A: General Papers,* 1 (11)**,** 3459-3476.

Espeau, P., Céolin, R., Tamarit, J.-L., Perrin, M.-A., Gauchi, J.-P. and Leveiller, F. (2005) Polymorphism of paracetamol: Relative stabilities of the monoclinic and orthorhombic phases inferred from topological pressure-temperature and temperature-volume phase diagrams. *Journal of Pharmaceutical Sciences,* 94 (3)**,** 524-539.

Fabien, S. and Isabelle, V. (2009) Curcumin-loaded nanocapsules: Formulation and influence of the nanoencapsulation processes variables on the physico-chemical characteristics of the particles. *International Journal of Chemical Reactor Engineering,* 7 (1).

Fan, Y., Nishida, H., Shirai, Y. and Endo, T. (2004a) Thermal stability of poly (L-lactide): influence of end protection by acetyl group. *Polymer Degradation and Stability,* 84 (1)**,** 143-149.

Fan, Y., Nishida, H., Shirai, Y., Tokiwa, Y. and Endo, T. (2004b) Thermal degradation behaviour of poly(lactic acid) stereocomplex. *Polymer Degradation and Stability,* 86 (2)**,** 197-208.

Flory, P. J. (1962) On the morphology of the crystalline state in polymers. *The journal of the American Chemical Society,* 84 (15)**,** 2857-2867.

Frank, A., Rath, S. K. and Venkatraman, S. S. (2005) Controlled release from bioerodible polymers: Effect of drug type and polymer composition. *Journal of Controlled Release,* 102 (2)**,** 333-344.

Fredenberg, S., Wahlgren, M., Reslow, M. and Axelsson, A. (2011) The mechanisms of drug release in poly (lactic-co-glycolic acid)-based drug delivery systems—A review. *International Journal of Pharmaceutics,* 415 (1–2)**,** 34-52.

Frenkel, S. (2008) Problems of the physics of the oriented state of polymers. In: *Oriented Polymer Materials.* Wiley-VCH Verlag GmbH, pp. 1-37.

Friedman, M. and Golomb, G. (1982) New sustained release dosage form of chlorhexidine for dental use. *Journal of Periodontal Research,* 17 (3)**,** 323-328.

Fu, Y. and Kao, W. J. (2010) Drug release kinetics and transport mechanisms of non-degradable and degradable polymeric delivery systems. *Expert Opinion on Drug Delivery,* 7 (4)**,** 429-444.

Garlotta, D. (2001) A literature review of poly(lactic acid). *Journal of Polymers and the Environment,* 9 (2)**,** 63-84.

Gerlach, K. L. (1993) *In vivo* and clinical evaluations of poly (L-lactide) plates and screws for use in maxillofacial traumatology. *Clinical Materials,* 13 (1–4)**,** 21-28.

Godovsky, Y. K., Slonimsky, G. L. and Garbar, N. M. (1972) Effect of molecular weight on the crystallization and morphology of poly (ethylene oxide) fractions. *Journal of Polymer Science Part C: Polymer Symposia,* 38 (1)**,** 1-21.

Gogolewski, S., Jovanovic, M., Perren, S. M., Dillon, J. G. and Hughes, M. K. (1993) The effect of melt-processing on the degradation of selected polyhydroxyacids: Polylactides, polyhydroxybutyrate, and polyhydroxybutyrate-co-valerates. *Polymer Degradation and Stability,* 40 (3)**,** 313-322.

Gopferich, A. (1996) Mechanisms of polymer degradation and erosion. *Biomaterials,* 17 (2)**,** 103-114.

Gotelli, G. R., Kabra, P. M. and Marton, L. J. (1977) Determination of acetaminophen and phenacetin in plasma by high-pressure liquid chromatography. *Clinical Chemistry,* 23 (6)**,** 957-9.

Granberg, R. and Rasmuson, A. (1999) Solubility of paracetamol in pure solvents. *Journal of Chemical & Engineering Data,* 44 (6)**,** 1391-1395.

Grayson, A. C. R., Choi, I. S., Tyler, B. M., Wang, P. P., Brem, H., Cima, M. J. and Langer, R. (2003) Multi-pulse drug delivery from a resorbable polymeric microchip device. *Nature Materials,* 2 (11)**,** 767-772.

Greenhalgh, D. J., Williams, A. C., Timmins, P. and York, P. (1999) Solubility parameters as predictors of miscibility in solid dispersions. *Journal of Pharmaceutical Sciences,* 88 (11)**,** 1182-1190.

Grizzi, I., Garreau, H., Li, S. and Vert, M. (1995) Hydrolytic degradation of devices based on poly (DL-lactic acid) size-dependence. *Biomaterials,* 16 (4)**,** 305-311.

Gruber, P. and O'Brien, M. (2005) Polylactides “NatureWorks® PLA”. In: *Biopolymers Online.* Wiley-VCH Verlag GmbH & Co. KGaA.

Gruber, P. R., Hall, E. S., Kolstad, J. J., Iwen, M. L., Benson, R. D. and Borchardt, R. L. (1992) *Concentrating lactic acid solution, polymerizing, depolymerizing to form lactide, distilling, polymerizing*. US5142023 A.

Gruber, P. R., Kolstad, J. J., Ryan, C. M., Hall, E. S. and Conn, R. S. E. (1998) *Catalytically polymerizing lactic acid, devolatizing polylactide produced to form solid flowable form, melting and extruding to form a film*. Accept.: 25 Aug 1998. US5798436 A.

Gu, S.-Y., Zou, C.-Y., Zhou, K. and Ren, J. (2009) Structure-rheology responses of polylactide/calcium carbonate composites. *Journal of Applied Polymer Science,* 114 (3)**,** 1648-1655.

Guohua, Z., Ya, L., Cuilan, F., Min, Z., Caiqiong, Z. and Zongdao, C. (2006) Water resistance, mechanical properties and biodegradability of methylated-cornstarch/poly(vinyl alcohol) blend film. *Polymer Degradation and Stability,* 91 (4)**,** 703-711.

Hakkarainen, M., Albertsson, A.-C. and Karlsson, S. (1996) Weight losses and molecular weight changes correlated with the evolution of hydroxyacids in simulated *in vivo* degradation of homo- and copolymers of PLA and PGA. *Polymer Degradation and Stability,* 52 (3)**,** 283-291.

Hansen, C. M. (1969) The universality of the solubility parameter. *Product R&D,* 8 (1)**,** 2-11.

Hansen, C. M. (2004) Polymer additives and solubility parameters. *Progress in organic coatings,* 51 (2)**,** 109-112.

Hansen, F. K. and Rodsrud, G. (1991) Surface tension by pendant drop: I. A fast standard instrument using computer image analysis. *Journal of Colloid and Interface Science,* 141 (1)**,** 1-9.

Higuchi, T. (1963) Mechanism of sustained-action medication. Theoretical analysis of rate of release of solid drugs dispersed in solid matrices. *Journal of Pharmaceutical Sciences,* 52 (12)**,** 1145-1149.

Higuchi, T. and Leeper, H. (1973a) *Drug-delivery device with stretched, rate-controlling membrane*. Appl.: Jan 16, 1973. US3710795 A.

Hinrichsen, G., Eberhardt, A., Lippe, U. and Springer, H. (1981a) Orientation mechanisms during biaxial drawing of polymer films. *Colloid and Polymer Science,* 259 (1)**,** 73-79.

Hixson, A. and Crowell, J. (1931) Dependence of reaction velocity upon surface and agitation. *Industrial & Engineering Chemistry,* 23 (10)**,** 1160-1168.

Hoogsteen, W., Postema, A. R., Pennings, A. J., Ten Brinke, G. and Zugenmaier, P. (1990) Crystal structure, conformation and morphology of solution-spun poly(L-lactide) fibers. *Macromolecules,* 23 (2)**,** 634-642.

Hopfenberg, H. B. (1976) Controlled release from erodible slabs, cylinders, and spheres. In: *Controlled Release Polymeric Formulations.* (ACS Symposium Series) Vol. 33. American Chemical Society, pp. 26-32.

http://www.chem.qmul.ac.uk/surfaces, Q. M. U. (2015) *Miller Indices (hkl).* Miller Indices (hkl). Available from:

http://www.chem.qmul.ac.uk/surfaces/scc/scat1_1b.htm (Accessed 25/03/2015).

Huang, X. and Brazel, C. S. (2001) On the importance and mechanisms of burst release in matrix-controlled drug delivery systems. *Journal of Controlled Release,* 73 (2–3)**,** 121-136.

Hurrell, S. and Cameron, R. (2001a) Polyglycolide: Degradation and drug release. Part I: Changes in morphology during degradation. *Journal of Materials Science: Materials in Medicine,* 12 (9)**,** 811-816.

Hurrell, S. and Cameron, R. (2001b) Polyglycolide: Degradation and drug release. Part II: Drug release. *Journal of Materials Science: Materials in Medicine,* 12 (9)**,** 817-820.

Hurrell, S. and Cameron, R. E. (2002) The effect of initial polymer morphology on the degradation and drug release from polyglycolide. *Biomaterials,* 23 (11)**,** 2401-2409.

Huu-Phuoc, N., Nam-Tran, H., Buchmann, M. and Kesselring, U. W. (1987) Determination of partial and total cohesion parameters of caffeine, theophylline, and methyl p-hydroxybenzoate by gas-solid chromatography. *Journal of Pharmaceutical Sciences,* 76 (5)**,** 406-410.

Izumikawa, S., Yoshioka, S., Aso, Y. and Takeda, Y. (1991) Preparation of poly (L-lactide) microspheres of different crystalline morphology and effect of crystalline morphology on drug release rate. *Journal of Controlled Release,* 15 (2)**,** 133-140.

Jackson, J. K., Smith, J., Letchford, K., Babiuk, K. A., Machan, L., Signore, P., Hunter, W. L., Wang, K. and Burt, H. M. (2004) Characterization of perivascular poly(lactic-co-glycolic acid) films containing paclitaxel. *International Journal of Pharmaceutics,* 283 (1–2)**,** 97-109.

Jamshidi, K., Hyon, S., Nakamura, T., Ikada, Y., Shimizu, Y. and Teramatsu, T. (1986) *In vitro* and *in vivo* degradation of poly-L-lactide fibers. *Biological and Biomechanical Performance of Biomaterials, Elsevier, Amsterdam***,** 227-232.

Jamshidi, K., Hyon, S. H. and Ikada, Y. (1988) Thermal characterization of polylactides. *Polymer,* 29 (12)**,** 2229-2234.

Jang, J. and Lee, D. K. (2004) Oxygen barrier properties of biaxially oriented polypropylene/polyvinyl alcohol blend films. *Polymer,* 45 (5)**,** 1599-1607.

Jarvas, G., Quellet, C. and Dallos, A. (2011) Estimation of Hansen solubility parameters using multivariate nonlinear QSPR modeling with COSMO screening charge density moments. *Fluid Phase Equilibria,* 309 (1)**,** 8-14.

Jones, D. S. and Medlicott, N. J. (1995) Casting solvent controlled release of chlorhexidine from ethylcellulose films prepared by solvent evaporation. *International Journal of Pharmaceutics,* 114 (2)**,** 257-261.

Kader, A. and Jalil, R. (1998) *In vitro* release of theophylline from poly (lactic acid) sustained-release pellets prepared by direct compression. *Drug development and industrial pharmacy,* 24 (6)**,** 527-34.

Kamezawa, M., Yamada, K. and Takayanagi, M. (1979) Preparation of ultrahigh modulus isotactic polypropylene by means of zone drawing. *Journal of Applied Polymer Science,* 24 (5)**,** 1227-1236.

Karasulu, H. Y., Ertan, G. and Köse, T. (2000) Modeling of theophylline release from different geometrical erodible tablets. *European Journal of Pharmaceutics and Biopharmaceutics,* 49 (2)**,** 177-182.

Kawai, T., Rahman, N., Matsuba, G., Nishida, K., Kanaya, T., Nakano, M., Okamoto, H., Kawada, J., Usuki, A., Honma, N., Nakajima, K. and Matsuda, M. (2007) Crystallization and Melting Behavior of Poly (l-lactic Acid). *Macromolecules,* 40 (26)**,** 9463-9469.

Kawakami, D., Burger, C., Ran, S., Avila-Orta, C., Sics, I., Chu, B., Chiao, S.-M., Hsiao, B. S. and Kikutani, T. (2008) New insights into lamellar structure development and saxs/waxd sequence appearance during uniaxial stretching of amorphous poly(ethylene terephthalate) above glass transition temperature. *Macromolecules,* 41 (8)**,** 2859-2867.

Keller, A. (1992) Morphology of polymers. *Pure & Applied Chemistry,* 64 (2)**,** 193-204.

Khamar, D., Pritchard, R. G., Bradshaw, I. J., Hutcheon, G. A. and Seton, L. (2011) Polymorphs of anhydrous theophylline: Stable Form IV consists of dimer pairs and metastable Form I consists of hydrogen-bonded chains. *Acta Crystallographica Section C: Crystal Structure Communications,* 67 (12)**,** o496-o499.

Kim, H. S., Park, B. H., Choi, J. H. and Yoon, J. S. (2008) Mechanical properties and thermal stability of poly(L-lactide)/calcium carbonate composites. *Journal of Applied Polymer Science,* 109 (5)**,** 3087-3092.

Kokturk, G., Piskin, E., Serhatkulu, T. F. and Cakmak, M. (2002) Evolution of phase behavior and orientation in uniaxially deformed polylactic acid films. *Polymer Engineering & Science,* 42 (8)**,** 1619-1628.

Kolstad, J. J. (1996) Crystallization kinetics of poly(L-lactide-co-meso-lactide). *Journal of Applied Polymer Science,* 62 (7)**,** 1079-1091.

Kopinke, F. D., Remmler, M., Mackenzie, K., Möder, M. and Wachsen, O. (1996) Thermal decomposition of biodegradable polyesters—II. Poly(lactic acid). *Polymer Degradation and Stability,* 53 (3)**,** 329-342.

Korsmeyer, R. W., Gurny, R., Doelker, E., Buri, P. and Peppas, N. A. (1983) Mechanisms of solute release from porous hydrophilic polymers. *International Journal of Pharmaceutics,* 15 (1)**,** 25-35.

Kranz, H., Ubrich, N., Maincent, P. and Bodmeier, R. (2000) Physicomechanical properties of biodegradable poly(D,L-lactide) and poly(D,L-lactide-co-glycolide) films in the dry and wet states. *Journal of Pharmaceutical Sciences,* 89 (12)**,** 1558-1566.

Kulkarni, C. S. (2013) *Novel formulations of a poorly soluble drug using the extrusion process*. PhD. University of Bradford.

Kurabayashi, K. (2001) Anisotropic thermal properties of solid polymers. *International Journal of Thermophysics,* 22 (1)**,** 277-288.

Kwack, T. H., Han, C. D. and Vickers, M. E. (1988) Development of crystalline structure during tubular film blowing of low-density polyethylene. *Journal of Applied Polymer Science,* 35 (2)**,** 363-389.

Lakshman, J. P., Cao, Y., Kowalski, J. and Serajuddin, A. T. M. (2008) Application of melt extrusion in the development of a physically and chemically stable high-energy amorphous solid dispersion of a poorly water-soluble drug. *Molecular Pharmaceutics,* 5 (6)**,** 994-1002.

Lee, H. S., Park, S. C. and Kim, Y. H. (2000) Structural changes of poly(trimethylene terephthalate) film upon uniaxial and biaxial drawing. *Macromolecules,* 33 (21)**,** 7994-8001.

Lee, J. K., Lee, K. H. and Jin, B. S. (2001a) Structure development and biodegradability of uniaxially stretched poly (L-lactide). *European Polymer Journal,* 37 (5)**,** 907-914.

Lee, J. K., Lee, K. H. and Jin, B. S. (2001b) Structure development and biodegradability of uniaxially stretched poly(l-lactide). *European Polymer Journal,* 37 (5)**,** 907-914.

Lee, S. H., Lee, K. H. and Hong, S. K. (1997) Effect of orientation on the biodegradability of uniaxially stretched aliphatic copolyester films. *Journal of Applied Polymer Science,* 64 (10)**,** 1999-2006.

Legras, R., Mercier, J. P. and Nield, E. (1983) Polymer crystallization by chemical nucleation. *Nature,* 304 (5925)**,** 432-434.

Lewis, D. (1990) Controlled release of bioactive agents from lactide/glycolide polymers, . In: Chasin M., L. R. (Ed.) *Biodegradable Polymers as Drug Delivery Systems.* Vol. 45. New York: Marcel Dekker, New York, pp. 1-41.

Li, H. and Huneault, M. A. (2007) Effect of nucleation and plasticization on the crystallization of poly(lactic acid). *Polymer,* 48 (23)**,** 6855-6866.

Li, J. and Lee, Y.-W. (1993) Evolution of morphology in high molecular weight polyethylene during die drawing. *Journal of Materials Science,* 28 (23)**,** 6496-6502.

Li, S. (1999) Hydrolytic degradation characteristics of aliphatic polyesters derived from lactic and glycolic acids. *Journal of Biomedical Materials Research,* 48 (3)**,** 342-353.

Li, S., Garreau, H. and Vert, M. (1990) Structure-property relationships in the case of the degradation of massive poly(α-hydroxy acids) in aqueous media. *Journal of Materials Science: Materials in Medicine,* 1 (4)**,** 198-206.

Li, S., Girard, A., Garreau, H. and Vert, M. (2000) Enzymatic degradation of polylactide stereocopolymers with predominant D-lactyl contents. *Polymer Degradation and Stability,* 71 (1)**,** 61-67.

Li, S., Girod-Holland, S. and Vert, M. (1996) Hydrolytic degradation of poly (DL-lactic acid) in the presence of caffeine base. *Journal of Controlled Release,* 40 (1–2)**,** 41-53.

Lim, L. T., Auras, R. and Rubino, M. (2008) Processing technologies for poly(lactic acid). *Progress in Polymer Science,* 33 (8)**,** 820-852.

Liu, J., Xiao, Y. and Allen, C. (2004) Polymer–drug compatibility: A guide to the development of delivery systems for the anticancer agent, ellipticine. *Journal of Pharmaceutical Sciences,* 93 (1)**,** 132-143.

Liu, R. Y. F., Schiraldi, D. A., Hiltner, A. and Baer, E. (2002) Oxygen-barrier properties of cold-drawn polyesters. *Journal of Polymer Science Part B: Polymer Physics,* 40 (9)**,** 862-877.

Ljungberg, N. and Wesslen, B. (2002) The effects of plasticizers on the dynamic mechanical and thermal properties of poly(lactic acid). *Journal of Applied Polymer Science,* 86 (5)**,** 1227-1234.

Lu, L., Garcia, C. A. and Mikos, A. G. (1999) *In vitro* degradation of thin poly (DL-lactic-co-glycolic acid) films. *Journal of Biomedical Materials Research,* 46 (2)**,** 236-244.

Luderwald, I. (1979) Thermal degradation of polyesters in the mass spectrometer. In: Grassie, N. (Ed.) *Developments in Polymer Degradation.* Vol. 2. Applied Science Publishers, p. 77.

Luong-Van, E., Grøndahl, L., Chua, K. N., Leong, K. W., Nurcombe, V. and Cool, S. M. (2006) Controlled release of heparin from poly(ε-caprolactone) electrospun fibers. *Biomaterials,* 27 (9)**,** 2042-2050.

Maharana, T., Mohanty, B. and Negi, Y. S. (2009) Melt–solid polycondensation of lactic acid and its biodegradability. *Progress in Polymer Science,* 34 (1)**,** 99-124.

Mahendrasingam, A., Blundell, D. J., Parton, M., Wright, A. K., Rasburn, J., Narayanan, T. and Fuller, W. (2005) Time resolved study of oriented crystallisation of poly(lactic acid) during rapid tensile deformation. *Polymer,* 46 (16)**,** 6009-6015.

Makino, K., Ohshima, H. and Kondo, T. (1986) Mechanism of hydrolytic degradation of poly (L-lactide) microcapsules: Effects of pH, ionic strength and buffer concentration. *Journal of Microencapsulation,* 3 (3)**,** 203-212.

Manas-Zloczower, I. (2012) *Mixing and compounding of polymers: theory and practice.* Carl Hanser Verlag GmbH Co KG.

Mandelkern, L. (2002) *Crystallization of polymers.* Cambridge ; New York: Cambridge University Press.

Maniruzzaman, M., Boateng, J. S., Bonnefille, M., Aranyos, A., Mitchell, J. C. and Douroumis, D. (2012) Taste masking of paracetamol by hot-melt extrusion: An *in vitro* and *in vivo* evaluation. *European Journal of Pharmaceutics and Biopharmaceutics,* 80 (2)**,** 433-442.

Mauduit, J., Bukh, N. and Vert, M. (1993) Gentamycin/poly(lactic acid) blends aimed at sustained release local antibiotic therapy administered per-operatively. I. The case of gentamycin base and gentamycin sulfate in poly(dl-lactic acid) oligomers. *Journal of Controlled Release,* 23 (3)**,** 209-220.

McGonigle, E. A., Liggat, J. J., Pethrick, R. A., Jenkins, S. D., Daly, J. H. and Hayward, D. (2001) Permeability of N_2, Ar, He, O_2 and CO_2 through biaxially oriented polyester films — dependence on free volume. *Polymer,* 42 (6)**,** 2413-2426.

McNeill, I. C. and Leiper, H. A. (1985) Degradation studies of some polyesters and polycarbonates—2. Polylactide: Degradation under isothermal conditions, thermal degradation mechanism and photolysis of the polymer. *Polymer Degradation and Stability,* 11 (4)**,** 309-326.

Mead, W. T., Zachariades, A. E., Shimada, T. and Porter, R. S. (1979) Solid state extrusion of poly(vinylidene fluoride). 1. Ram and hydrostatic extrusion. *Macromolecules,* 12 (3)**,** 473-478.

Meijer-Han, E. H. (1997) *Processing of polymers.* (Materials Science and Technology) Vol. 18 New York: Wiley-VCH.

Men, Y., Rieger, J. and Strobl, G. (2003) Role of the entangled amorphous network in tensile deformation of semicrystalline polymers. *Physical Review Letters,* 91 (9)**,** 095502.

Mikkonen, J., Uurto, I., Isotalo, T., Kotsar, A., Tammela, T. L. J., Talja, M., Salenius, J. P., Tormala, P. and Kellomaki, M. (2009) Drug-eluting bioabsorbable stents: an *in vitro* study. *Acta Biomaterialia,* 5 (8)**,** 2894-2900.

Miyajima, M., Koshika, A., Okada, J. i., Ikeda, M. and Nishimura, K. (1997) Effect of polymer crystallinity on papaverine release from poly (L-lactic acid) matrix. *Journal of Controlled Release,* 49 (2-3)**,** 207-215.

Miyajima, M., Koshika, A., Okada, J. i., Kusai, A. and Ikeda, M. (1998) The effects of drug physico-chemical properties on release from copoly (lactic/glycolic acid) matrix. *International Journal of Pharmaceutics,* 169 (2)**,** 255-263.

Mohanraj, J., Bonner, M. J., Barton, D. C. and Ward, I. M. (2006) Physical and mechanical characterization of oriented polyoxymethylene produced by die-drawing and hydrostatic extrusion. *Polymer,* 47 (16)**,** 5897-5908.

Morath, C., Taraiya, A., Richardson, A., Craggs, G. and Ward, I. (1993) The development of continuous large-scale die drawing for the production of oriented polymer rods and tubes. *Plastics rubber and composites processing and applications,* 19 (1)**,** 55-62.

Moynihan, H. A. and O'Hare, I. P. (2002) Spectroscopic characterisation of the monoclinic and orthorhombic forms of paracetamol. *International Journal of Pharmaceutics,* 247 (1–2)**,** 179-185.

Mulligan, J. and Cakmak, M. (2005) Nonlinear mechanooptical behavior of uniaxially stretched poly(lactic acid): dynamic phase behavior. *Macromolecules,* 38 (6)**,** 2333-2344.

Nakamura, K., Nagai, M., Kanamoto, T., Takahashi, Y. and Furukawa, T. (2001) Development of oriented structure and properties on drawing of poly(vinylidene fluoride) by solid-state coextrusion. *Journal of Polymer Science Part B: Polymer Physics,* 39 (12)**,** 1371-1380.

Nakayama, K. and Kanetsuna, H. (1977) Hydrostatic extrusion of solid polymers. *Journal of Materials Science,* 12 (7)**,** 1477-1483.

Nam, J. Y., Okamoto, M., Okamoto, H., Nakano, M., Usuki, A. and Matsuda, M. (2006) Morphology and crystallization kinetics in a mixture of low-molecular weight aliphatic amide and polylactide. *Polymer,* 47 (4)**,** 1340-1347.

Naraharisetti, P. K., Guan Lee, H. C., Fu, Y.-C., Lee, D.-J. and Wang, C.-H. (2006) *In vitro* and *in vivo* release of gentamicin from biodegradable

discs. *Journal of Biomedical Materials Research Part B: Applied Biomaterials,* 77B (2)**,** 329-337.

Narasimhan, B. and Peppas, N. A. (1997) Molecular analysis of drug delivery systems controlled by dissolution of the polymer carrier. *Journal of Pharmaceutical Sciences,* 86 (3)**,** 297-304.

Ng, C. S., Teoh, S. H., Chung, T. S. and Hutmacher, D. W. (2000) Simultaneous biaxial drawing of poly (e-caprolactone) films. *Polymer,* 41 (15)**,** 5855-5864.

Nikkola, L., Viitanen, P. and Ashammakhi, N. (2009) Temporal control of drug release from biodegradable polymer: Multicomponent diclofenac sodium releasing PLGA 80/20 rod. *Journal of Biomedical Materials Research Part B: Applied Biomaterials,* 89B (2)**,** 518-526.

Nikolic, L., Ristic, I., Adnadjevic, B., Nikolic, V., Jovanovic, J. and Stankovic, M. (2010) Novel microwave-assisted synthesis of poly (D,L-lactide): The influence of monomer/initiator molar ratio on the product properties. *Sensors,* 10 (5)**,** 5063-5073.

Nordstrom, P., Pohjonen, T., Tormala, P. and Rokkanen, P. (2001) Shear-load carrying capacity of cancellous bone after implantation of self-reinforced polyglycolic acid and poly-l-lactic acid pins: Experimental study on rats. *Biomaterials,* 22 (18)**,** 2557-2561.

Okada, M. (2002) Chemical syntheses of biodegradable polymers. *Progress in Polymer Science,* 27 (1)**,** 87-133.

Omelczuk, M. and McGinity, J. (1992) The influence of polymer glass transition temperature and molecular weight on drug release from tablets containing poly (DL-lactic acid). *Pharmaceutical Research,* 9 (1)**,** 26-32.

Ou, X. and Cakmak, M. (2008) Influence of biaxial stretching mode on the crystalline texture in polylactic acid films. *Polymer,* 49 (24)**,** 5344-5352.

Owens, D. K. and Wendt, R. C. (1969) Estimation of the surface free energy of polymers. *Journal of Applied Polymer Science,* 13 (8)**,** 1741-1747.

Pace, R. J. and Datyner, A. (1979) Statistical mechanical model for diffusion of simple penetrants in polymers. I. Theory. *Journal of Polymer Science: Polymer Physics Edition,* 17 (3)**,** 437-451.

Pan, C. J., Tang, J. J., Weng, Y. J., Wang, J. and Huang, N. (2006) Preparation, characterization and anticoagulation of curcumin-eluting controlled biodegradable coating stents. *Journal of Controlled Release,* 116 (1)**,** 42-49.

Pan, P., Zhu, B., Kai, W., Dong, T. and Inoue, Y. (2008) Effect of crystallization temperature on crystal modifications and crystallization kinetics of poly(L-lactide). *Journal of Applied Polymer Science,* 107 (1)**,** 54-62.

Pan, S. J., Tang, H. I., Hiltner, A. and Baer, E. (1987) Biaxial orientation of polypropylene by hydrostatic solid state extrusion. Part II: Morphology and properties. *Polymer Engineering & Science,* 27 (12)**,** 869-875.

Park, J. W., Lee, D. J., Yoo, E. S., IM, S. S., Kim, S. h. and Kim, Y. H. (1999) Biodegradable Polymer Blends of Poly(lactic acid) and Starch. *Korea Polymer Journal,* 7 (2)**,** 93-101.

Park, T. G. (1994) Degradation of poly (DL-lactic acid) microspheres: effect of molecular weight. *Journal of Controlled Release,* 30 (2)**,** 161-173.

Pawar, Y. B., Shete, G., Popat, D. and Bansal, A. K. (2012) Phase behavior and oral bioavailability of amorphous curcumin. *European Journal of Pharmaceutical Sciences,* 47 (1)**,** 56-64.

Penel-Pierron, L., Seguela, R., Lefebvre, J. M., Miri, V., Depecker, C., Jutigny, M. and Pabiot, J. (2001) Structural and mechanical behavior of nylon-6 films. II. Uniaxial and biaxial drawing. *Journal of Polymer Science Part B: Polymer Physics,* 39 (11)**,** 1224-1236.

Pennings, A. J. (1967) Fractionation of polymers by crystallization from solutions. II. *Journal of Polymer Science Part C: Polymer Symposia,* 16 (3)**,** 1799-1812.

Petas, A., Talja, M., Tammela, T., Taari, K., Lehtoranta, K., Valimaa, T. and Tormala, P. (1997) A randomized study to compare biodegradable self-reinforced polyglycolic acid spiral stents to suprapubic and indwelling catheters after visual laser ablation of the prostate. *The Journal of Urology,* 157 (1)**,** 173-176.

Peterlin, A. (1965) Crystalline character in polymers. *Journal of Polymer Science Part C: Polymer Symposia,* 9 (1)**,** 61-89.

Peterlin, A. (1975) Structural model of mechanical properties and failure of crystalline polymer solids with fibrous structure. *International Journal of Fracture,* 11 (5)**,** 761-780.

Peterlin, A. (1979) Transport phenomena and polymer morphology. *Die Makromolekulare Chemie,* 3 (S19791)**,** 215-232.

Pillin, I., Montrelay, N. and Grohens, Y. (2006) Thermo-mechanical characterization of plasticized PLA: is the miscibility the only significant factor ? *Polymer,* 47 (13)**,** 4676-4682.

Pistner, H., Gutwald, R., Ordung, R., Reuther, J. and Mühling, J. (1993) Poly (L-lactide): A long-term degradation study *in vivo:* I. Biological results. *Biomaterials,* 14 (9)**,** 671-677.

Pluta, M., Jeszka, J. K. and Boiteux, G. (2007) Polylactide/montmorillonite nanocomposites: Structure, dielectric, viscoelastic and thermal properties. *European Polymer Journal,* 43 (7)**,** 2819-2835.

Pohjonen, T., Helevirta, P., Tormala, P., Koskikare, K., Patiala, H. and Rokkanen, P. (1997) Strength retention of self-reinforced poly-L-lactide screws. A comparison of compression moulded and machine cut screws. *Journal of Materials Science: Materials in Medicine,* 8 (5)**,** 311-320.

Pornnimit, B. and Ehrenstein, G. W. (1991) Extrusion of self-reinforced polyethylene. *Advances in Polymer Technology,* 11 (2)**,** 91-98.

Price, F. D. (1961) A theory of spherulite shape. *Journal of Polymer Science,* 54 (160)**,** S40-S46.

Price, F. P. and Kilb, R. W. (1962) The morphology and internal structure of poly(ethylene oxide) spherulites. *Journal of Polymer Science,* 57 (165)**,** 395-403.

Prodduturi, S., Manek, R. V., Kolling, W. M., Stodghill, S. P. and Repka, M. A. (2005) Solid-state stability and characterization of hot-melt extruded poly(ethylene oxide) films. *Journal of Pharmaceutical Sciences,* 94 (10)**,** 2232-2245.

Pukanszky, B. (1990) Influence of interface interaction on the ultimate tensile properties of polymer composites. *Composites,* 21 (3)**,** 255-262.

Pyda, M., Bopp, R. C. and Wunderlich, B. (2004) Heat capacity of poly(lactic acid). *The Journal of Chemical Thermodynamics,* 36 (9)**,** 731-742.

Qi, S., Gryczke, A., Belton, P. and Craig, D. Q. M. (2008) Characterisation of solid dispersions of paracetamol and EUDRAGIT® E prepared by hot-melt extrusion using thermal, microthermal and spectroscopic analysis. *International Journal of Pharmaceutics,* 354 (1–2)**,** 158-167.

Qureshi, N., Stepanov, E. V., Schiraldi, D., Hiltner, A. and Baer, E. (2000) Oxygen-barrier properties of oriented and heat-set poly(ethylene terephthalate). *Journal of Polymer Science Part B: Polymer Physics,* 38 (13)**,** 1679-1686.

Rahman, S. M. H., Telny, T. C., Ravi, T. K. and Kuppusamy, S. (2009) Role of surfactant and pH in dissolution of curcumin. *Indian Journal of Pharmaceutical Sciences,* 71 (2)**,** 149-142.

Ribeiro, Y. A., Caires, A. C. F., Boralle, N. and Ionashiro, M. (1996) Thermal decomposition of acetylsalicylic acid (aspirin). *Thermochimica Acta,* 279 (0)**,** 177-181.

Riluson, C. (1999) So you want to measure surface energy? *Technical note 306* [Technical note], 1-16. Available from https://cmi.epfl.ch/metrology/files/Kruss-DSA30/kruss-tn306-en.pdf (Accessed 14/11/2014)

Ritger, P. L. and Peppas, N. A. (1987) A simple equation for description of solute release I. Fickian and non-fickian release from non-swellable devices in the form of slabs, spheres, cylinders or discs. *Journal of Controlled Release,* 5 (1)**,** 23-36.

Roberts, R. J., Rowe, R. C. and York, P. (1991) The relationship between Young's modulus of elasticity of organic solids and their molecular structure. *Powder Technology,* 65 (1–3)**,** 139-146.

Roseman, T. J. and Higuchi, W. I. (1970) Release of medroxyprogesterone acetate from a silicone polymer. *Journal of Pharmaceutical Sciences,* 59 (3)**,** 353-357.

Rothen-Weinhold, A., Besseghir, K., Vuaridel, E., Sublet, E., Oudry, N., Kubel, F. and Gurny, R. (1999) Injection-molding versus extrusion as manufacturing technique for the preparation of biodegradable implants. *European Journal of Pharmaceutics and Biopharmaceutics,* 48 (2)**,** 113-121.

Rothstein, S. N., Federspiel, W. J. and Little, S. R. (2009) A unified mathematical model for the prediction of controlled release from surface and bulk eroding polymer matrices. *Biomaterials,* 30 (8)**,** 1657-1664.

Saikku-Backstrom, A., Tulamo, R. M., Raiha, J. E., Kellomaki, M., Toivonen, T., Tormala, P. and Rokkanen, P. (2000) Intramedullary fixation of cortical bone osteotomies with absorbable self-reinforced fibrillated poly-96L/4D-lactide (SR-PLA96) rods in rabbits. *Biomaterials,* 22 (1)**,** 33-43.

Salari, A. and Young, R. E. (1998) Application of attenuated total reflectance FTIR spectroscopy to the analysis of mixtures of pharmaceutical polymorphs. *International Journal of Pharmaceutics,* 163 (1–2)**,** 157-166.

Salmeron Sanchez, M., Mathot, V. B. F., Vanden Poel, G. and Gomez Ribelles, J. L. (2007) Effect of the Cooling Rate on the Nucleation Kinetics of Poly(l-Lactic Acid) and Its Influence on Morphology. *Macromolecules,* 40 (22)**,** 7989-7997.

Sampath, S. S., Garvin, K. and Robinson, D. H. (1992) Preparation and characterization of biodegradable poly(l-lactic acid) gentamicin delivery systems. *International Journal of Pharmaceutics,* 78 (1–3)**,** 165-174.

Sanphui, P. (2012) *Physicochemical property improvement of a few active pharmaceutical ingredients by solid form screening*. PhD. University of Hyderabad.

Sanphui, P., Goud, N. R., Khandavilli, U. B. R., Bhanoth, S. and Nangia, A. (2011) New polymorphs of curcumin. *Chemical Communications,* 47 (17)**,** 5013-5015.

Schierholz, J. M., Steinhauser, H., Rump, A. F. E., Berkels, R. and Pulverer, G. (1997) Controlled release of antibiotics from biomedical polyurethanes: morphological and structural features. *Biomaterials,* 18 (12)**,** 839-844.

Schmitt, E. E. and Polistina, R. A. (1976) *Controlled release of medicaments using polymers from glycolic acid*. Appl.: 16 Nov 1976. Accept.: 16 Nov 1976. US3991766 A.

Schultz, J. M., Hsiao, B. S. and Samon, J. M. (2000) Structural development during the early stages of polymer melt spinning by *in-situ* synchrotron X-ray techniques. *Polymer,* 41 (25)**,** 8887-8895.

Seton, L., Khamar, D., Bradshaw, I. J. and Hutcheon, G. A. (2010) Solid state forms of theophylline: Presenting a new anhydrous polymorph. *Crystal Growth & Design,* 10 (9)**,** 3879-3886.

Shah, S. S., Cha, Y. and Pitt, C. G. (1992) Poly (glycolic acid-co-DL-lactic acid): diffusion or degradation controlled drug delivery. *Journal of Controlled Release,* 18 (3)**,** 261-270.

Sharples, A. (1966) *Introduction to polymer crystallization.* New York: St. Martin's Press.

Shin, S.-C. and Byun, S.-Y. (1996) Controlled release of ethinylestradiol from ethylene-vinyl acetate membrane. *International Journal of Pharmaceutics,* 137 (1)**,** 95-102.

Shin, S.-C. and Lee, H.-J. (2002) Controlled release of triprolidine using ethylene-vinyl acetate membrane and matrix systems. *European Journal of Pharmaceutics and Biopharmaceutics,* 54 (2)**,** 201-206.

Sibik, J., Sargent, M. J., Franklin, M. and Zeitler, J. A. (2014) Crystallization and phase changes in paracetamol from the amorphous solid to the liquid phase. *Molecular Pharmaceutics,* 11 (4)**,** 1326-1334.

Siepmann, J. and Siepmann, F. (2012) Modeling of diffusion controlled drug delivery. *Journal of Controlled Release,* 161 (2)**,** 351-362.

Silvestre C, Cimmino S and E, D. P. (2000) Morphology of polyolefins. In: Vasile, C. (Ed.) *Handbook of polyolefins.* 2 ed. New York: Marcel Dekker, Inc., p. 175.

Singh, L., Kumar, V. and Ratner, B. D. (2004) Generation of porous microcellular 85/15 poly (DL-lactide-co-glycolide) foams for biomedical applications. *Biomaterials,* 25 (13)**,** 2611-2617.

Sodergard, A. and Nasman, J. H. (1994) Stabilization of poly (L-lactide) in the melt. *Polymer Degradation and Stability,* 46 (1)**,** 25-30.

Sodergard, A. and Stolt, M. (2002) Properties of lactic acid based polymers and their correlation with composition. *Progress in Polymer Science,* 27 (6)**,** 1123-1163.

Somani, R. H., Yang, L., Zhu, L. and Hsiao, B. S. (2005) Flow-induced shish-kebab precursor structures in entangled polymer melts. *Polymer,* 46 (20)**,** 8587-8623.

Sreenivas, K., Basargekar, R. and Kumaraswamy, G. (2011a) Phase separation of dmdbs from pp: Effect of polymer molecular weight and tacticity. *Macromolecules,* 44 (7)**,** 2358-2364.

Sreenivas, K., Pol, H. V. and Kumaraswamy, G. (2011b) The influence of DMDBS on the morphology and mechanical properties of polypropylene cast films. *Polymer Engineering & Science,* 51 (10)**,** 2013-2023.

Stachewicz, U., Li, S., Bilotti, E. and Barber, A. H. (2012) Dependence of surface free energy on molecular orientation in polymer films. *Applied Physics Letters,* 100 (9)**,** 094104.

Stankovic, I. (2004) *Curcumin - Chemical and Technical Assessment (CTA)* Food and Agriculture Organisation of united nation.

Sternberg, K., Kramer, S., Nischan, C., Grabow, N., Langer, T., Hennighausen, G. and Schmitz, K.-P. (2007) *In vitro* study of drug-eluting stent coatings based on poly (L-lactide) incorporating cyclosporine A – drug release, polymer degradation and mechanical integrity. *Journal of Materials Science: Materials in Medicine,* 18 (7)**,** 1423-1432.

Takagi, J., Nemoto, T., Takahashi, T., Taniguchi, T. and Koyama, K. (2004) Improvement of mechanical properties for poly (L-lactic acid) film through drawing process optimization. *Seni Gakkaishi,* 60 (7)**,** 230-234.

Tang, H., Chen, J.-B., Wang, Y., Xu, J.-Z., Hsiao, B. S., Zhong, G.-J. and Li, Z.-M. (2012) Shear Flow and Carbon Nanotubes Synergistically Induced Nonisothermal Crystallization of Poly(lactic acid) and Its Application in Injection Molding. *Biomacromolecules,* 13 (11)**,** 3858-3867.

Taubner, V. and Shishoo, R. (2001) Influence of processing parameters on the degradation of poly(L-lactide) during extrusion. *Journal of Applied Polymer Science,* 79 (12)**,** 2128-2135.

Termonia, Y. (1994) Molecular modeling of spider silk elasticity. *Macromolecules,* 27 (25)**,** 7378-7381.

Teupe, C., Meffert, R., Winckler, S., Ritzerfeld, W., Tormala, P. and Brug, E. (1992) Ciprofloxacin-impregnated poly-L-lactic acid drug carrier. *Archives of Orthopaedic and Trauma Surgery,* 112 (1)**,** 33-35.

Thi Thu Trang, M., Thi Thu Thuy, N., Quang Duong, L., Thi Ngoan, N., Thi Cham, B., Hai Binh, N., Thi Bich Hoa, P., Dai Lam, T., Xuan Phuc, N.

and Jun Seo, P. (2012) A novel nanofiber curcumin-loaded polylactic acid constructed by electrospinning. *Advances in Natural Sciences: Nanoscience and Nanotechnology,* 3 (2)**,** 025014.

Tormala, P. (1992) Biodegradable self-reinforced composite materials; Manufacturing structure and mechanical properties. *Clinical Materials,* 10 (1–2)**,** 29-34.

Tormala, P. (1993) Ultra-high strength, self-reinforced absorbable polymeric composites for applications in different disciplines of surgery. *Clinical Materials,* 13 (1–4)**,** 35-40.

Tormala, P., Suokas, E., Aro, H. and Koort, J. (2003) *Bioabsorbable drug delivery system for local treatment and prevention of infections*. Accept.: 17/06/03. US6579533 B1.

Tormala, P., Suokas, E., Veiranto, M. and Ashammakhi, N. (2008) *Method to enhance drug release from a drug-releasing material*. 7,419,681.

Trieu, H. (2006) *Oriented polymeric spinal implants*. Appl.: 26/10/2006. Accept.: 26/10/2006. US20060241759 A1.

Tsuji, H. and Ikada, Y. (1996) Crystallization from the melt of poly(lactide)s with different optical purities and their blends. *Macromolecular Chemistry and Physics,* 197 (10)**,** 3483-3499.

Tsuji, H. and Ikada, Y. (1997) Blends of crystalline and amorphous poly(lactide). III. Hydrolysis of solution-cast blend films. *Journal of Applied Polymer Science,* 63 (7)**,** 855-863.

Tsuji, H. and Ikada, Y. (1998) Properties and morphology of poly(L-lactide). II. Hydrolysis in alkaline solution. *Journal of Polymer Science Part A: Polymer Chemistry,* 36 (1)**,** 59-66.

Tsuji, H. and Ikada, Y. (2000b) Properties and morphology of poly (L-lactide) 4. Effects of structural parameters on long-term hydrolysis of poly(l-lactide) in phosphate-buffered solution. *Polymer Degradation and Stability,* 67 (1)**,** 179-189.

Tsuji, H. and Ikarashi, K. (2004) *In vitro* hydrolysis of poly (L-lactide) crystalline residues as extended-chain crystallites. Part I: long-term hydrolysis in phosphate-buffered solution at 37°C. *Biomaterials,* 25 (24)**,** 5449-5455.

Tsuji, H., Mizuno, A. and Ikada, Y. (2000) Properties and morphology of poly(L-lactide). III. Effects of initial crystallinity on long-term *in vitro* hydrolysis of high molecular weight poly(L-lactide) film in phosphate-buffered solution. *Journal of Applied Polymer Science,* 77 (7)**,** 1452-1464.

Tsuji, H., Ogiwara, M., Saha, S. K. and Sakaki, T. (2005) Enzymatic, alkaline, and autocatalytic degradation of poly (L-lactic acid): Effects of biaxial orientation. *Biomacromolecules,* 7 (1)**,** 380-387.

Tsuji, H., Takai, H. and Saha, S. K. (2006) Isothermal and non-isothermal crystallization behavior of poly (L-lactic acid): Effects of stereocomplex as nucleating agent. *Polymer,* 47 (11)**,** 3826-3837.

Tsukada, M., Freddi, G. and Crighton, J. S. (1994) Structure and compatibility of poly(vinyl alcohol)-silk fibroin (PVA/SA) blend films. *Journal of Polymer Science Part B: Polymer Physics,* 32 (2)**,** 243-248.

Tung, L. J. and Buckser, S. (1958) The effects of molecular weight on the crystallinity of polyethylene. *The Journal of Physical Chemistry,* 62 (12)**,** 1530-1534.

Tzafriri, A. R. (2000) Mathematical modeling of diffusion-mediated release from bulk degrading matrices. *Journal of Controlled Release,* 63 (1–2)**,** 69-79.

Uhrich, K. E., Cannizzaro, S. M., Langer, R. S. and Shakesheff, K. M. (1999) Polymeric systems for controlled drug release. *Chemical Reviews,* 99 (11)**,** 3181-3198.

Vargas, C. I. and Ghaly, E. S. (1999) Kinetic release of theophylline from hydrophilic swellable matrices. *Drug Development and Industrial Pharmacy,* 25 (9)**,** 1045-1050.

Vasile, C. (2002) *Handbook of polyolefins.* CRC Press.

Veiranto, M., Tormala, P. and Suokas, E. (2002) *In vitro* mechanical and drug release properties of bioabsorbable ciprofloxacin containing and neat self-reinforced P(L/DL)LA 70/30 fixation screws. *Journal of Materials Science: Materials in Medicine,* 13 (12)**,** 1259-1264.

Vert, M., Li, S. and Garreau, H. (1991) More about the degradation of LA/GA-derived matrices in aqueous media. *Journal of Controlled Release,* 16 (1–2)**,** 15-26.

Vgenopoulos, D. (2012) *An investigation of oriented polymers for power transmission applications*. PhD. University of Bradford.

Vroman, I. and Tighzert, L. (2009) Biodegradable polymers. *Materials,* 2 (2)**,** 307-344.

Wada, R., Hyon, S.-h. and Ikada, Y. (1991) Salt formation of lactic acid oligomers as matrix for sustained release of drugs. *Journal of pharmacy and pharmacology,* 43 (9)**,** 605-608.

Wada, R., Hyon, S. H. and Ikada, Y. (1990) Lactic acid oligomer microspheres containing hydrophilic drugs. *Journal of Pharmaceutical Sciences,* 79 (10)**,** 919-924.

Wan, L. S. C. and Lim, L. Y. (1992) Drug release from heat-treated polyvinyl alcohol films. *Drug Development and Industrial Pharmacy,* 18 (17)**,** 1895-1906.

Wang, I.-C., Lee, M.-J., Seo, D.-Y., Lee, H.-E., Choi, Y., Kim, W.-S., Kim, C.-S., Jeong, M.-Y. and Choi, G. (2011) Polymorph transformation in paracetamol monitored by in-line NIR spectroscopy during a cooling crystallization process. *AAPS PharmSciTech,* 12 (2)**,** 764-770.

Wang, Y.-J., Pan, M.-H., Cheng, A.-L., Lin, L.-I., Ho, Y.-S., Hsieh, C.-Y. and Lin, J.-K. (1997) Stability of curcumin in buffer solutions and characterization of its degradation products. *Journal of Pharmaceutical and Biomedical Analysis,* 15 (12)**,** 1867-1876.

Wang, Y., Jiang, Z., Fu, L., Lu, Y. and Men, Y. (2014) Lamellar thickness and stretching temperature dependency of cavitation in semicrystalline polymers. *PLoS One,* 9 (5)**,** e97234.

Wang, Y., Na, B., Fu, Q. and Men, Y. (2004) Shear induced shish–kebab structure in PP and its blends with LLDPE. *Polymer,* 45 (1)**,** 207-215.

Wang, Y., Steinhoff, B., Brinkmann, C. and Alig, I. (2008) In-line monitoring of the thermal degradation of poly (L-lactic acid) during melt extrusion by UV–vis spectroscopy. *Polymer,* 49 (5)**,** 1257-1265.

Ward, I. M. (1997) *Structure and properties of oriented polymers.* Springer Science & Business Media.

Ward, I. M. and Sweeney, J. (2012) The mechanical properties of polymers: General considerations. In: *Mechanical Properties of Solid Polymers.* John Wiley & Sons, Ltd, pp. 19-29.

Waris, E., Ashammakhi, N., Happonen, H., Raatikainen, T., Kaarela, O., Törmälä, P., Santavirta, S. and Konttinen, Y. T. (2003) Bioabsorbable Miniplating Versus Metallic Fixation for Metacarpal Fractures. *Clinical Orthopaedics and Related Research,* 410**,** 310-319.

Wasanasuk, K. and Tashiro, K. (2011) Crystal structure and disorder in Poly (L-lactic acid) δ Form (α′ Form) and the phase transition mechanism to the ordered α Form. *Polymer,* 52 (26)**,** 6097-6109.

Wasanasuk, K., Tashiro, K., Hanesaka, M., Ohhara, T., Kurihara, K., Kuroki, R., Tamada, T., Ozeki, T. and Kanamoto, T. (2011) Crystal structure analysis of poly (L-lactic acid) α Form on the basis of the 2-dimensional wide-angle synchrotron X-ray and neutron diffraction measurements. *Macromolecules,* 44 (16)**,** 6441-6452.

Wegiel, L. A., Zhao, Y., Mauer, L. J., Edgar, K. J. and Taylor, L. S. (2014) Curcumin amorphous solid dispersions: the influence of intra and intermolecular bonding on physical stability. *Pharmaceutical Development and Technology,* 19 (8)**,** 976-986.

Wenderoth, K., Karbach, A. and Petermann, J. (1985) Characterization of the matrix of polybutene-1 films containing needle crystals. *Colloid and Polymer Science,* 263 (4)**,** 301-305.

Wesselingh, J. A. (1993) Controlling diffusion. *Journal of Controlled Release,* 24 (1–3)**,** 47-60.

Wilchinsky, Z. W. (1963) Orientation in cold-rolled polypropylene. *Journal of Applied Polymer Science,* 7 (3)**,** 923-933.

Witt, C. and Kissel, T. (2001) Morphological characterization of microspheres, films and implants prepared from poly (Lactide-co-glycolide) and ABA triblock copolymers: Is the erosion controlled by degradation, swelling or diffusion? *European Journal of Pharmaceutics and Biopharmaceutics,* 51 (3)**,** 171-181.

Wong, Y. S., Stachurski, Z. H. and Venkatraman, S. S. (2008) Orientation and structure development in poly(lactide) under uniaxial deformation. *Acta Materialia,* 56 (18)**,** 5083-5090.

Wu, N., Wang, L.-S., Tan, D. C.-W., Moochhala, S. M. and Yang, Y.-Y. (2005) Mathematical modeling and *in vitro* study of controlled drug release via a highly swellable and dissoluble polymer matrix: Polyethylene oxide with high molecular weights. *Journal of Controlled Release,* 102 (3)**,** 569-581.

Wu, X. S. and Wang, N. (2001) Synthesis, characterization, biodegradation, and drug delivery application of biodegradable lactic/glycolic acid polymers. Part II: Biodegradation. *Journal of Biomaterials Science, Polymer Edition,* 12 (1)**,** 21-34.

Xu, H., Zhong, G.-J., Fu, Q., Lei, J., Jiang, W., Hsiao, B. S. and Li, Z.-M. (2012) Formation of Shish-Kebabs in Injection-Molded Poly(l-lactic acid) by Application of an Intense Flow Field. *ACS Applied Materials & Interfaces,* 4 (12)**,** 6774-6784.

Yamazaki, S., Itoh, M., Oka, T. and Kimura, K. (2010) Formation and morphology of “shish-like” fibril crystals of aliphatic polyesters from the sheared melt. *European Polymer Journal,* 46 (1)**,** 58-68.

Yang, M., Wang, P., Huang, C.-Y., Ku, M. S., Liu, H. and Gogos, C. (2010) Solid dispersion of acetaminophen and poly(ethylene oxide) prepared by hot-melt mixing. *International Journal of Pharmaceutics,* 395 (1–2)**,** 53-61.

Yasuniwa, M., Tsubakihara, S., Iura, K., Ono, Y., Dan, Y. and Takahashi, K. (2006) Crystallization behavior of poly(l-lactic acid). *Polymer,* 47 (21)**,** 7554-7563.

Ylikontiola, L., Sundqvuist, K., Sàndor, G. K. B., Törmälä, P. and Ashammakhi, N. (2004) Self-reinforced bioresorbable poly-L/DL-Lactide [SR-P(L/DL)LA] 70/30 miniplates and miniscrews are reliable for fixation of anterior mandibular fractures: A pilot study. *Oral Surgery, Oral Medicine, Oral Pathology, Oral Radiology, and Endodontology,* 97 (3)**,** 312-317.

Yu, L., Liu, H., Xie, F., Chen, L. and Li, X. (2008) Effect of annealing and orientation on microstructures and mechanical properties of polylactic acid. *Polymer Engineering & Science,* 48 (4)**,** 634-641.

Zaffaroni, A. U. (1980) *Selective administration of drug with ocular therapeutic system*. Appl.: 23/04/1979. US4186184 A.

Zaki, H. M. (2011) *Spectroscopy surface analysis of paracetamol and paracetamol and excipient systems*. PhD. University of Manchester.

Zhang, F. and McGinity, J. W. (1999) Properties of sustained-release tablets prepared by hot-melt extrusion. *Pharmaceutical Development and Technology,* 4 (2)**,** 241-250.

Zhang, F. and McGinity, J. W. (2000) Properties of hot-melt extruded theophylline tablets containing poly(vinyl acetate). *Drug Development and Industrial Pharmacy,* 26 (9)**,** 931-942.

Zhang, J. (2004) Effective nucleating chemical agents for the crystallization of poly(trimethylene terephthalate). *Journal of Applied Polymer Science,* 93 (2)**,** 590-601.

Zhang, J., Tashiro, K., Domb, A. J. and Tsuji, H. (2006) Confirmation of disorder α Form of poly(L-lactic acid) by the x-ray fiber pattern and polarized ir/raman spectra measured for uniaxially-oriented samples. *Macromolecular Symposia,* 242 (1)**,** 274-278.

Zhang, J., Tashiro, K., Tsuji, H. and Domb, A. J. (2008) Disorder-to-order phase transition and multiple melting behavior of poly (L-lactide) investigated by simultaneous measurements of waxd and dsc. *Macromolecules,* 41 (4)**,** 1352-1357.

Zhang, X., Schneider, K., Liu, G., Chen, J., Brüning, K., Wang, D. and Stamm, M. (2011) Structure variation of tensile-deformed amorphous poly (L-lactic acid): Effects of deformation rate and strain. Polymer, 52 (18), 4141-4149.

Zilberman, M. (2005) Dexamethasone loaded bioresorbable films used in medical support devices: Structure, degradation, crystallinity and drug release. Acta Biomaterialia, 1 (6), 615-624.

Zimmermann, B. and Baranovic, G. (2011) Thermal analysis of paracetamol polymorphs by FT-IR spectroscopies. Journal of Pharmaceutical and Biomedical Analysis, 54 (2), 295-302.

12. Appendix

12.1. Brief description of 2D-WAXD analysis

A crystal is made up of a periodic, symmetrical arrangement of individual atoms or groups of atoms. Such an arrangement is referred to as a crystal lattice. Depending upon the relative lengths of the unit vectors connecting such atoms and angles between them, a unit cell of the lattice may exhibit 14 different geometries. These are known as the Bravais lattices. The principle geometries are monoclinic, triclinic, orthorhombic, rhombohedral, tetragonal, hexagonal and cubic, which further have their own variants.

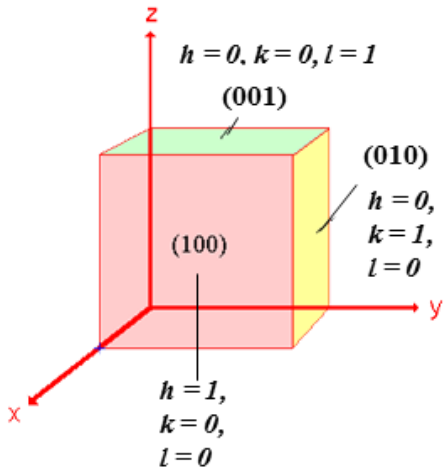

Figure 12.1: *Typical crystallographic planes in a cubic crystal lattice.*
Adapted from: (http://www.chem.qmul.ac.uk/surfaces, 2015)

A crystal lattice can be divided into several lattice planes. The orientation of a lattice plane is usually denoted by the Miller indices. These relate to how the lattice plane intersects the main crystallographic axes of that solid. Figure 12.1 displays the most common planes in a cubic crystal and corresponding Miller indices. When irradiated by X-rays, each crystal plane scatters the X-rays at a unique Bragg's angle. If the sample is rotated in a complete azimuthal circle the scattered rays can be detected on a 2D detector, giving rise to a 2D X-ray pattern. Depending upon the crystal plane orientation, these appear on

characteristic locations within the 2D X-ray pattern. Therefore, their positions help in identification of the crystal type (Alexander, 1971).

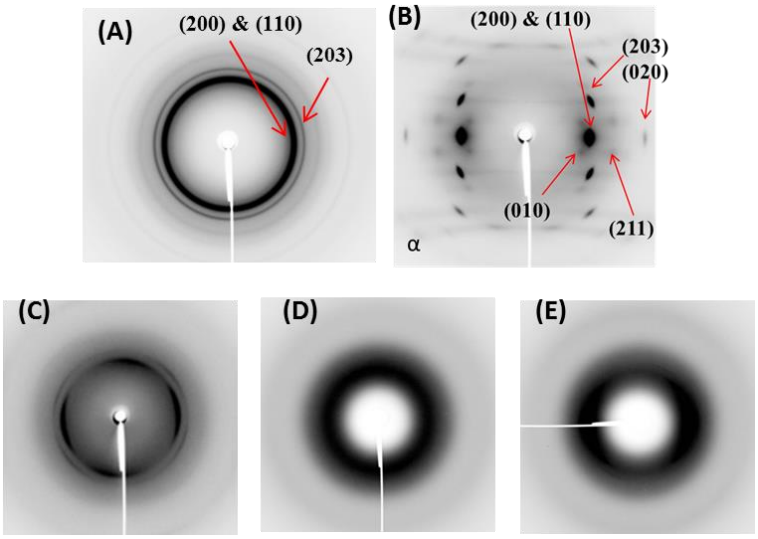

Figure 12.2: *Prototype 2D-WAXD patterns of the oriented and un-oriented PLA films*

In figure 12.2 (A & B), the characteristic reflections for α crystals of PLA are identified. When the crystalline reflections of a polymeric sample are present as a complete azimuthal circle (figure 12.2 - A), they signify that the crystalline phase is isotropic. If the crystals are oriented uniaxially along the meridian, the azimuthal spread of the crystalline reflections reduces and they appear as concentrated spots near the equator (figure 12.2 - B). Biaxially oriented crystalline polymeric matrices contain the crystalline phase aligned in two orthogonal directions. Consequently, crystalline reflections appear on meridian as well as equator (figure 12.2 - C). In an amorphous polymer, the scattered X-rays appear as a diffuse halo (figure 12.2 - D, E). When such a pattern is translated to an 'intensity Vs Brag's angle' diffractogram, no crystalline peaks are observed. The presence of an amorphous halo as a complete azimuthal circle signifies isotropic organisation of the amorphous phase (figure 12.2 - D). Similar to the crystalline pattern, orientation of the amorphous phase results in concentration of the halo along the perpendicular axis (figure 12.2 - E).